



FRIEDRICH-SCHILLER-  
UNIVERSITÄT  
JENA

*Signals or resources?*

Biosynthesis and accumulation of zwitterionic compatible solutes in marine phytoplankton and their role in environmental stress responses

Dissertation  
(kumulativ)

zur Erlangung des akademischen Grades  
Doctor rerum naturalium (Dr. rer. nat.)

vorgelegt dem Rat der Chemisch-Geowissenschaftlichen Fakultät  
der  
Friedrich-Schiller-Universität Jena

von M.Sc. Simona Fenizia  
Geboren am 01.03.1989 in Atripalda (IT)



Gutachter:

1. Prof. Dr. Georg Pohnert
2. Prof. Jonathan Gershenzon

Tag der öffentlichen Verteidigung: 14/06/2023



*To my beloved family,  
who always support and sustained me  
through their unconditional love.*

*Thank you!*



*“Like light rays in the spectrum,  
the different components of a pigment mixture, obeying a law,  
are resolved on the calcium carbonate column  
and then can be qualitatively and quantitatively determined.  
I call such a preparation a chromatogram  
and the corresponding method  
the chromatographic method.”*

**Mikhail Semenovitch Tswett** (botanist, 1872-1919)





# Table of contents

<b>List of abbreviations</b>	<b>I</b>
<b>Zusammenfassung</b>	<b>III</b>
<b>Summary</b>	<b>VII</b>
<b>1 Introduction</b>	<b>1</b>
1.1 Why is the ocean salty? – Seawater salinity and its effects on the ecosystem	1
1.2 Marine algae and compatible solutes	4
1.2.1 Synthesis and accumulation of compatible solutes	7
1.3 Organic sulfur compounds in the environment	8
1.3.1 Methylsulfur compounds and the Sulfur Cycle	8
1.3.2 DMSP biosynthesis	10
1.3.3 Biochemical pathways for DMSP catabolism	13
1.4 Marine sulfonates	15
1.5 Metabolomic analysis of marine compatible solutes	16
1.5.1 Analysis of zwitterionic metabolites	18
1.5.2 Insights on HILIC chromatography and ZIC-HILIC column	19
1.6 Thesis objectives	21
<b>2 Publications</b>	<b>23</b>
2.1 Publication 1	23
2.2 Publication 2	73
2.3 Publication 3	91
2.4 Publication 4	107
2.5 Publication 5	119
<b>3 Discussion</b>	<b>137</b>
<b>4 Conclusions and Outlook</b>	<b>153</b>
<b>5 References</b>	<b>155</b>
<b>Erklärungen</b>	<b>VIII</b>
<b>Curriculum vitae</b>	<b>XII</b>
<b>Acknowledgements</b>	<b>XVI</b>



## List of abbreviations

AGMPFs	algal growth and morphogenesis promoting actors
CCN	cloud condensation nuclei
DHPS	sulfopropanediol
DMS	dimethylsulfide
DMSA	dimethylsulfonioacetate
DMSHB	4-dimethylsulphonio-2-hydroxybutyrate
DMSO	dimethylsulfoxide
DMSP	dimethylsulfoniopropionate
DMSOP	dimethylsulfoxoniumpropionate
GBT	glycine betaine
GC	gas chromatography
HILIC	hydrophobic interaction liquid chromatography
HRMS	high-resolution mass spectrometry
LC	liquid chromatography
MS	mass spectrometry
MS/MS	tandem mass spectrometry
NMR	nuclear magnetic resonance
PSU	practical salinity units
RPLC	reversed-phase liquid chromatography
TIC	total ion current
UHPLC	ultra-high performance liquid chromatography
ZIC-HILIC	zwitterionic-hydrophilic interaction liquid chromatography



## Zusammenfassung

Die Luft, die wir atmen und das Wasser, das wir trinken sind mit dem Meer verbunden. Das Leben auf unserem Planeten hängt vom Wohlergehen der Ozeane ab. Angesichts des Klimawandels ist das Verständnis und die Vorhersage der Auswirkungen verschiedener Stressfaktoren auf die Umwelt eine dringende Herausforderung. Die Erwärmung des Klimas wirkt sich auf den Salzgehalt der Ozeane aus und verändert den globalen Elementkreislauf: Diese Beziehung ist gut dokumentiert, wie die potenzielle Rückkopplungsschleife zwischen Klima und Abkühlung (bekannt als "CLAW-Hypothese"), an der die zwitterionische Schwefelverbindung Dimethylsulfoniopropionat (DMSP), ihr Abbauprodukt Dimethylsulfid (DMS) und andere schwefelhaltige flüchtige Stoffwechselprodukte beteiligt sind. In den letzten Jahrzehnten wurde festgestellt, dass marines Phytoplankton eine der Hauptquellen für DMSP ist und die verschiedenen Eigenschaften dieses Metaboliten gegenüber Meeresalgen wurden weitgehend nachgewiesen. Dennoch fehlte bisher das Wissen über die umweltbedingten Faktoren des DMSP-Abbaus. In dieser Arbeit werden analytische und physiologische Untersuchungen vorgestellt, um die Bedingungen des DMSP-Abbaus und seiner Umwandlung in DMS weiter zu verstehen. Insbesondere haben wir gezeigt, dass die DMSP-Konzentrationen in mikroskaligen Hotspots nahe der Oberfläche von Algenzellen diejenigen sind, die die bakterielle Produktion von DMS fördern und daher für den globalen Schwefelkreislauf von größerer Bedeutung sind. In diesem Zusammenhang sind Salzgehalt und Temperatur zwei wichtige Stressfaktoren in der Meeresumwelt, die sich erheblich auf wichtige biotische Interaktionen und biologische Komponenten auswirken: Ihre Veränderungen, so gering sie auch erscheinen mögen, haben weitreichende Auswirkungen auf die Gesundheit der Erde. Um ungünstige Umweltbedingungen wie Hitze- und Salzstress abzumildern, hat das marine Phytoplankton mehrere Strategien entwickelt: Dazu gehören die Synthese und Akkumulation einer Vielzahl niedermolekularer organischer, wahrscheinlich zwitterionischer Metaboliten, die an der Osmoadaptation und Thermotoleranz mariner Ökosysteme beteiligt zu sein scheinen, darunter das bereits erwähnte DMSP. In Anbetracht dieses breiteren Szenarios haben wir weitere Untersuchungen durchgeführt und unter Nutzung der Ultra-Hochleistungs-Flüssigkeitschromatographie und der hochauflösenden Massenspektrometrie, die Gruppe der Phytoplankton-

Osmolyte um Cysteinolsäure und Ectoin erweitert. Diese beiden Moleküle sind unter den Mikroalgen weit verbreitet: Ihre Identität wurde durch MS/MS-Experimente und Co-Elution mit den entsprechenden synthetischen Standards bestätigt, während ihre osmoregulatorischen Eigenschaften durch Untersuchung der Algenzellen bei physiologischen (35 PSU) und hohen (50 PSU) Salzgehalten überprüft wurden. Vor unserer Arbeit war Ectoin ausschließlich als bakterieller Osmolyt bekannt und über seine Produktion in Meeresalgen wurde noch nie berichtet, während Cysteinolsäure bereits unter den aus Algen gewonnenen Produkten aufgeführt war, aber über ihre osmoregulatorischen Eigenschaften waren nicht bekannt. Aufgrund der höheren intrazellulären Konzentrationen von Ectoin und Cysteinolsäure, die in den Kulturen der Diatomee *T. weissflogii* mit hohem Salzgehalt gefunden wurden, konnten wir diesen beiden Metaboliten osmoregulatorische und osmoadaptive Eigenschaften zuschreiben. Die Quantifizierung von Ectoin in axenischen Kulturen derselben Diatomee veranlasste uns zu weiteren Untersuchungen über dessen Ursprung. Mit unseren Ergebnissen konnten wir den Ursprung dieses Metaboliten, sowohl aus Meeresbakterien als auch aus Algen beweisen. In Anbetracht des höheren Ectoin-Gehalts in xenischen Algenkulturen und der Fähigkeit von Mikroalgen, Metaboliten aus der äußeren Umgebung aufzunehmen, haben wir in unserer Arbeit außerdem gezeigt, dass extern verfügbares Ectoin von Meeresalgen leicht aufgenommen werden kann, um den osmotischen Stress effizient zu kompensieren. Um die Verteilung von Ectoin und Cysteinolsäure im marinen Phytoplankton zu bewerten, haben wir mehrere Mikroalgenarten untersucht und diesen Metaboliten in verschiedenen Taxa nachgewiesen, darunter Diatomeen, Dinoflagellaten, Coccolithophoren und Haptophyten. Ectoin und Cysteinolsäure wurden in allen untersuchten Algenarten nachgewiesen, mit intrazellulären Konzentrationen im gleichen femtomolaren Bereich wie DMSP, dem wichtigsten Metaboliten im marinen Ökosystem, was auf den entscheidenden Beitrag von Ectoin zu den Osmoadaptationsstrategien des Phytoplanktons hinweist. Darüber hinaus haben wir unsere Untersuchungen zur Verbreitung von Ectoin und Cysteinolsäure auf marine Makroalgen ausgeweitet, indem wir die Grünalge *Ulva* sp. in unser Screening einbezogen und die kryoprotektiven Eigenschaften von Ectoin und Cysteinolsäure in dieser Arte untersucht haben. Interessanterweise zeigten unsere Ergebnisse, dass diese beiden Metaboliten in *U. mutabilis* nach einem Temperaturwechsel von warm zu

kalt hochreguliert wurden, was auch ihre Rolle bei der Wärmeverträglichkeit belegt. Mit unserer Arbeit haben wir daher Ectoin und Cysteinolsäure in die Familie der wichtigsten kompatiblen Solute aufgenommen, die von marinem Phytoplankton und Makroalgen produziert werden und neue Einblicke in die molekularen Reaktionen von Meeresalgen auf Umweltstressoren erhalten.





## Summary

The air we breathe, as the water we drink, are linked to the ocean. Life on our planet relies on the wellness of the oceans. In light of climate changes, understanding and predicting the effects of multiple stressors on the environment is a pressing challenge. The warmer climate is affecting the salinity of the oceans and altering the global element cycles: this relationship is well documented, as well documented is the positive feedback loop (known as “CLAW Hypothesis”) that involves the zwitterionic sulfur compound dimethylsulfoniopropionate (DMSP), its breakdown product dimethylsulfide (DMS) and other sulfur-derived volatile metabolites.

Over the last decades, it has been clearly established that marine phytoplankton are among the main source of DMSP. Although the several functions of this metabolite in marine algae have largely been demonstrated, knowledge related to the environmental drivers of DMSP catabolism were still missing. In this work, the application of analytical and physiological methods enables to further explore the conditions involved in DMSP degradation and its conversion into DMS. In particular, we demonstrated that the concentrations of DMSP existing in microscale hotspots, near the surface of algal cells, are those enhancing the bacterial production of DMS, being, therefore, relevant for the global sulfur cycle.

Salinity and temperature are two key stressors in marine environment that significantly effect key biotic interactions and living organisms: their changes, as small as they might seem, have large-scale effects on Earth’s health. To mitigate adverse environmental conditions, like thermal and salinity stress, marine phytoplankton have developed several strategies: among them, the synthesis and accumulation of a small organic, likely zwitterionic metabolites. These compounds, including the afore mentioned DMSP, seem to be involved in the osmoadaptation and thermotolerance of marine ecosystems. Recent metabolomic studies on marine phytoplankton revealed a plethora of metabolites, most likely with osmoregulatory properties, which have not yet been characterized. Taking advantage of refined analytical methods based on ultra-high-performance-liquid chromatography (UHPLC) and high-resolution-mass spectrometry (HRMS), in our work we investigated further and expanded the group of phytoplankton osmolytes by adding cysteinolic acid and ectoine. Both these

molecules are widespread among microalgae: their identities were confirmed through MS/MS experiments and co-elution with the corresponding synthetic standards. In addition, their osmoregulatory properties were verified by investigating the algal cells at physiological (35 PSU) and high (50 PSU) salinities conditions.

Prior to our work, ectoine was exclusively known as bacterial osmolyte but its production has never been reported in marine algae, while cysteinolic acid was already listed among the algal-derived metabolites, although its osmoregulatory properties had never been reported. Due to the higher intracellular concentrations of ectoine and cysteinolic acid found in the high-salinity cultures of the diatom *T. weissflogii*, we could attribute to these two metabolites osmoregulatory and osmoadaptive properties. Quantification of ectoine in axenic cultures of the same diatom led us to further investigate on its origin. With our results we could demonstrate the dual origin of this metabolite, synthesized by both marine bacteria and algae. Moreover, given the higher amount of ectoine found in xenic algal cultures and the ability of microalgae to take up metabolites from the external environment, in our work we demonstrated that externally available ectoine can be readily taken up by marine algae to efficiently compensate for the osmotic stress. To evaluate the distribution of ectoine and cysteinolic acid among marine phytoplankton, we screened several microalgal species and detected this metabolite in different taxa, including diatoms, dinoflagellates, coccolithophores and haptophytes. In all the analyzed algal species, intracellular concentrations of ectoine and cysteinolic acid were in the same femtomolar range as DMSP, a key player metabolite in marine ecosystem. This result points toward the pivotal contribution of both these molecules in the phytoplankton osmoadaptation strategies. In addition, we expanded our investigation on ectoine and cysteinolic acid distribution to the class of marine macroalgae by including in our screening the green seaweed *Ulva* sp. We investigated the cryoprotectant properties of ectoine and cysteinolic acid in these species. Interestingly, our results showed that both these metabolites were upregulated in *U. mutabilis* after a warm to cold temperature shift, thus demonstrating also their role in thermotolerance. With our work, we therefore added ectoine and cysteinolic acid to the family of key compatible solutes produced by marine phytoplankton, and provided new insights into the molecular responses of marine algae to environmental stressors.

# 1 Introduction

## 1.1 Why is the ocean salty? – Seawater salinity and its effects on the ecosystem

Oceans are classified among humanity's most important natural resources<sup>1</sup>, covering more than 70% of the earth's surface, providing almost 99% of the "living space" on the planet, and being responsible for more than 35% of the primary planet production<sup>1,2</sup>. In the aquatic ecosystem, salt is an essential component that spreads through the environment, driving currents that preserve the climate and contributing to global ocean circulation<sup>3,4</sup>. Next to light, temperature and nutrients, the concentration of dissolved salts in the ocean, known as "salinity", is one of the major abiotic factors affecting the growth and distribution of living organisms in marine habitats<sup>5</sup>. Thus, it is considered an environmental master factor for aquatic organisms, playing a primary role in the global climate functioning<sup>4,6</sup>. Open ocean salinity is expressed in Practical Salinity Unit (PSU, grams of salt per liter of water)<sup>7,8</sup> and its levels are rather stable, ranging from about 34 to 37 PSU, and resulting from a constant equilibrium between different ionic species, including chloride ( $\text{Cl}^-$ ), sodium ( $\text{Na}^+$ ), sulfate ( $\text{SO}_4^{2-}$ ), magnesium ( $\text{Mg}^{2+}$ ), calcium ( $\text{Ca}^{2+}$ ) and potassium ( $\text{K}^+$ )<sup>9</sup>. Hence, much of the open ocean has an average salinity concentration of 35 PSU<sup>7-9</sup>, but variations in salinity levels naturally occur and affect water cycle and ocean circulation (Fig. 1).

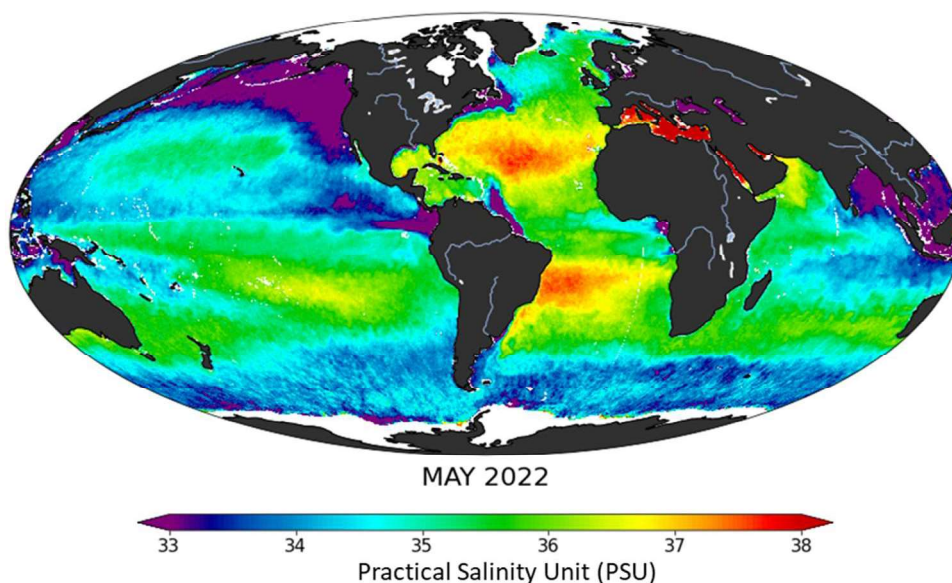


**Figure 1:** Global map of sea surface salinity, updated May 2022.  
Adapted from: <https://salinity.oceansciences.org/smap-salinity.htm>

As schematically depicted below (Fig. 2), some processes (e.g., the weathering of rocks that delivers minerals; the evaporation of ocean water due to temperatures' increase; the formation of sea ice) have served to locally increase the salinity of the ocean<sup>6</sup>. As a consequence, whereas the Baltic Sea (a semi- enclosed sea with many river inputs) has a low surface salinity (10 PSU), the Red Sea is highly salty (40 PSU), due to the warmer temperatures and lack of precipitations that determine high levels of evaporation<sup>9</sup>. Nevertheless, these environmental phenomena are continually counterbalanced by other events that decrease salinity levels, like the continuous input of fresh water from rivers, precipitation of rain and snow, melting of ice<sup>9,10</sup> (Fig. 2).

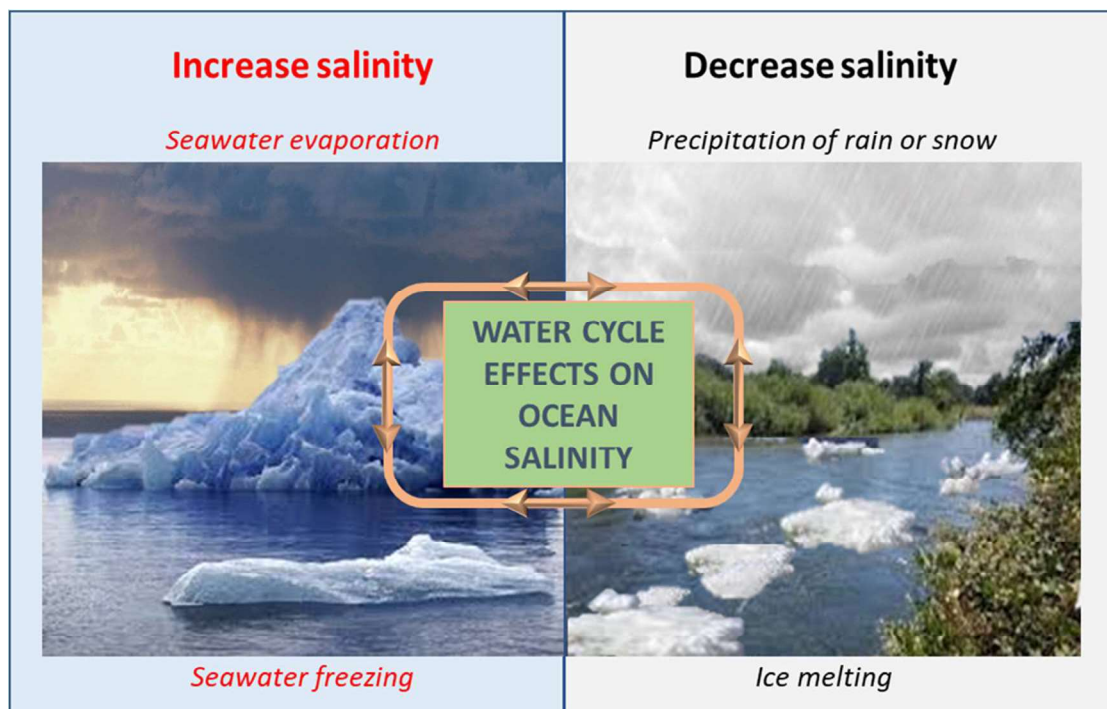


**Figure 2:** The Water Cycle: how water moves from the land into the atmosphere, and then back to the land and ocean. It consists of different steps, mainly driven by the sun.

Changes in this balance will not only influence the local ecology and the structure of biological communities, but will also affect the ability of living organisms to survive and adapt to the new context. Monitoring sea surface salinity patterns provides important clues about climate change and global ocean dynamics<sup>6</sup>.

In this view, homeostasis of ionic composition, also referred to as “osmoregulation”, is an important prerequisite for aquatic organisms and their ability to adapt to different types of stress is necessary for the

successful growth, development, and persistence of the species<sup>11</sup>. Because marine invertebrates are mainly iso-osmotic (30-35 PSU), deviations from the ionic equilibrium, together with ocean warming, have detrimental effects on the physiology of these organisms, as, indeed, they do not possess, on their own, proper mechanism to overcome the related cellular stress<sup>12-15</sup>. Several marine species have, however, developed a variety of strategies to survive these unbalanced conditions: among the strategies implemented, the acclimation enables halophilic Archaea to counteract the high salinity of external environments<sup>16</sup>.

Mechanisms of acclimation are based either on the efflux of water from the cell through water channels that enhance the restoration of cellular turgor and volume, or on the influx of ions ( $K^+$ ,  $Na^+$ ,  $Cl^-$ ) according to the osmotic gradients, through ion transport systems, including membrane-bound ion regulatory pumps and ionic channels (e.g.,  $Na^+/K^+$ -ATPases,  $Cl^-$ /bicarbonate exchangers,  $K^+/Na^+/Cl^-$  channels)<sup>11</sup>. Thanks to this strategy, extremely halophilic Archaea can accumulate inorganic salts up to molar intracellular concentrations to counteract the osmotic pressure of the environment<sup>16</sup>. Species that use ion transport systems are commonly referred to as osmoregulators, which, however, show a relatively narrow range of osmoadaptation and are structurally unstable outside a limited range of salinities<sup>16</sup>. In aquatic environments, osmoregulators include both marine fish and freshwater organisms, species typically characterized by regulatory organs (e.g., kidneys) that, through ion channels, keep their internal body fluids at osmotic concentrations around 400 milliosmoles per liter (mOsm)<sup>17</sup>, unit of measurement of osmolarity that refers to the number of particles (osmoles) per unit volume (liter) of solvent<sup>18</sup>.

On the other hand, most marine invertebrates and algae, including diatoms, belong to the class of osmoconformers<sup>19</sup>. Instead of taking up NaCl, which is dominant in the extracellular fluids, osmoconformer organisms rather keep the environmental ionic homeostasis through the synthesis and accumulation of small organic osmolytes. These intracellular osmoregulatory components can be up- or down-regulated according to the extracellular osmotic pressure and can protect, regenerate and restore proteins and membranes that might have been damaged by the salinity shift<sup>6,17,20</sup>.

In addition to the seawater ionic composition, environmental adverse conditions may also derive from changes in sea surface temperature, which affect the distribution, phenology and metabolism of many marine

organisms (www.eea.com). Global warming, indeed, leads to increases in water vapour over the seas, influencing the living systems at all levels of the organization. Therefore, investigations on the effects of ocean temperature on marine ecosystems are necessary to understand the related consequences of global climate change<sup>12</sup>.

Surface temperature in the ocean varies according to the amount of solar energy absorbed, meaning that ocean surface temperatures cover a range from 30 °C, in tropical regions, to -2 °C, the temperature detected near the poles. In addition, these values change from top to bottom, resulting in a vertical temperature structure, where the upper water layer (0-200 meters deep) receives direct sun radiations, resulting in warmer temperatures, while the below layers have colder temperatures<sup>21</sup>.

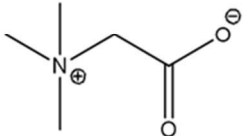
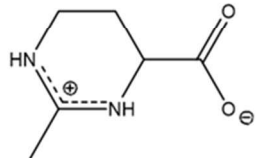
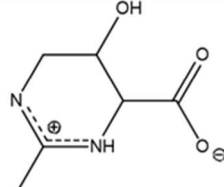
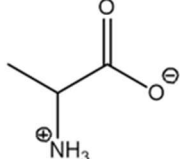
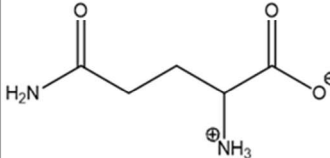
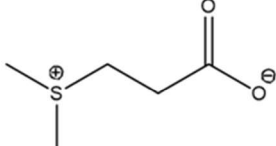
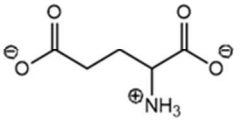
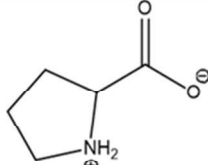
Important temperature changes lead to physiological stress in marine inhabitants, and, in addition to their osmotic function, which provides cellular protection against detrimental effects of high osmotic pressure, compatible solutes show also other intracellular functions, including the increase of thermotolerance, membrane stabilizers and protein protection.

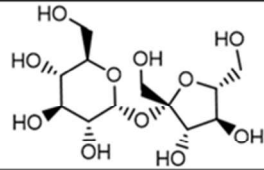
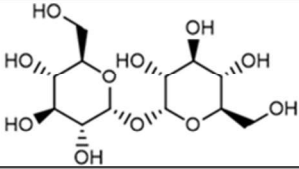
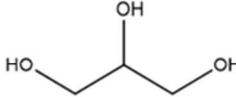
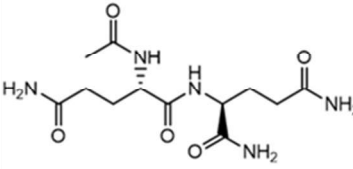
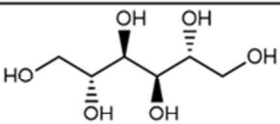
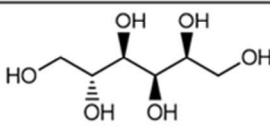
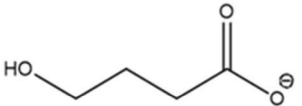
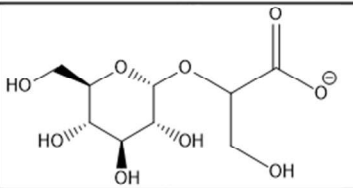
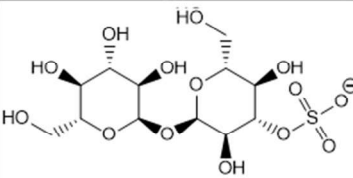
Among marine organisms, algae are the principal primary producers of waterbodies and they often run into extreme stress scenarios, reflecting their ability to adapt to different types of stress. Due to their primary contribution to aquatic systems, their mechanisms of adaptation and tolerance against these hostile conditions assume a high relevance from an ecological point of view<sup>22,23</sup>.

## 1.2 Marine algae and compatible solutes

Seawater salinity directly influences marine species by exerting, among others, an osmotic stress<sup>24</sup>. To counteract this stress and avoid any negative consequence, living organisms have developed a wide range of adaptation mechanisms<sup>25,26</sup>. In particular, as osmoconformers, marine algae accumulate, within the cells, organic osmolytes that neutralize the detrimental effects that salinity shifts may exert at molecular and cellular levels<sup>27</sup>. These organic osmolytes are hydrophilic metabolites and, in many cases, principal photosynthetic derived products<sup>5</sup>, such as sugars, polyols, free amino acids and derivatives, but also compounds not directly linked with the photosynthesis, like quaternary ammonium (proline, betaines) and tertiary sulfonium compounds (dimethylsulfoniopropionate and its derivatives)<sup>5,16,20,24,28</sup>. Based on their ionization, organic osmolytes are

classified into (i) zwitterionic, (ii) uncharged and (iii) anionic molecules<sup>29</sup> (Table 1).

Chemical category	Compound	Structure
<b>Zwitterions</b>	Glycine betaine	
	Ectoine	
	Hydroxyectoine	
	Alanine	
	Glutamine	
	Dimethylsulfoniopropionate	
	Glutamate	
	Proline	

Chemical category	Compound	Structure
Uncharged	Sucrose	
	Trehalose	
	Glycerol	
	N-Acetylglutaminylglutamine amide	
	Mannitol	
	Sorbitol	
Anions	Hydroxybutyrate	
	$\alpha$ -Glucosylglycerate	
	Sulfotrehalose	

**Table 1:** Predominant compatible solutes accumulated by algae and bacteria, adapted from Welsh<sup>16</sup> and Roberts<sup>29</sup>.

Despite the different chemical categories to which they belong, compatible solutes share many relevant characteristics: first of all, they are highly soluble compounds, without a net charge at physiological pH and, from a physiological point of view, they do not interfere at all with intracellular and metabolic processes despite the high intracellular concentrations they can



reach<sup>28,30</sup>. Hence, they are collectively named “compatible solutes”, to express and highlight their full compatibility with biological and physiological cellular functions<sup>16</sup>.

### 1.2.1 Biosynthesis and accumulation of compatible solutes

Biosynthesis and accumulation, as well as degradation of compatible solutes, are physiological mechanisms involved in the balance of intra- and extra-cellular osmotic pressure and, therefore, of the related cellular turgor<sup>16</sup>. Marine algae can tolerate sudden changes in salinity through rapid water fluxes. Nevertheless, this fast and immediate response causes severe metabolic perturbations and can be therefore replaced by uptake of ions (mainly  $K^+$ ,  $Na^+$ ,  $Cl^-$ ) and biosynthesis and accumulation of low molecular weight compatible solutes<sup>5</sup>.

Due to the high cellular concentrations that are needed to balance the osmotic pressure, ionic species may exert secondary negative effects on other physiological cellular functions. To avoid this drawback issue, ions are mainly sequestered in the vacuole, and only small amounts are stored in the cytoplasm, together with the compatible, in name and deed, solutes<sup>5</sup>. Intracellular accumulation of compatible solutes in marine algae may occur either by “*de novo*” biosynthesis or by transport into the cell<sup>30</sup>. Both these mechanisms are energetically costly for the organism, requiring the assimilation and reduction of sulfate and/or nitrate. The uptake of sulfate and nitrogen ions, instead, is energetically favourable, highly regulated and takes place at high rates in phytoplankton<sup>31,32</sup>.

Once synthesized or acquired, these small organic molecules carry out their physiological duties through different mechanisms. Notably, some of them bind to macromolecules (proteins), replacing water from their surface while still ensuring cell viability. Others, like proline, adopt a second strategy and behave as amphiphilic compounds, stabilizing the hydrophilic layer of proteins. Furthermore, through a mechanism referred as “preferential exclusion”, compatible solutes do not link proteins, but rather facilitate intracellular  $Na^+$  and  $Cl^-$  exclusion and the replacement of  $K^+$  and glutamate within the cell, restoring the cell water content<sup>5,16,33</sup>.

Intracellular accumulation of a specific compatible solute instead of others may depend on the specific requirement of an organism<sup>16</sup>. Due to the high intracellular amounts (up to molar concentrations), these compounds accomplish also other tasks, acting, for example, as intracellular reservoirs of carbon and nitrogen: when needed, compatible solutes will be released

into the environment through passive diffusion across the cell membranes, upon cell damage, death or lysis, and will exert their multiple functions. In this way, they also help living organisms to reduce energetically costly biosynthesis of this class of compounds, especially for N-derived compatible solutes<sup>16</sup>.

### 1.3 Organic sulfur compounds in the environment

Sulfur is an essential component for living organisms and the 10<sup>th</sup> most abundant element in the universe, according to the Jefferson National Linear Accelerator Laboratory ([www.jlab.org](http://www.jlab.org)).

In the ocean, sulfur is available mainly as inorganic sulfate<sup>34,35</sup>, which is assimilated by marine phytoplankton and bacteria to be transformed into organic matter, including amino acids, proteins, sulfate esters and sulfolipids, heightening the levels of organic sulfur in the ocean. Dissolved and particulate organosulfur compounds constitute the major source of sulfur in marine environment<sup>36,37</sup>. Chemically, sulfur has several oxidation states, from -2 to +6, characterized by different redox properties that ensure vital cellular functions. In particular, metabolites containing sulfur in the most reduced state (-2), such as the amino acids cysteine and methionine and the methyl-sulfur compounds dimethylsulfoniopropionate (DMSP) and dimethylsulfide (DMS), have mainly antioxidant properties. In addition to these metabolites, dimethylsulfoxide (DMSO), whose sulfur atom has an oxidation state of 0, and taurine (oxidation state of +4), are among the antioxidant compounds as well<sup>34,38</sup>. Sulfur-derived metabolites constitute a bargaining chip between marine bacteria and algal species, establishing a metabolic network where heterotrophs and photoautotrophs intimately interact<sup>39</sup>. In this network, phytoplankton plays an essential role, generating organic sulfur compounds, in form of DMSP and other molecules like dihydroxypropanesulfonate (DHPS), acting as growth factors for marine bacteria, supporting their nutrients requirements and stimulating their chemotaxis. On the other hand, for their part, marine bacteria produce secondary metabolites that promote algal growth and distribution<sup>34,40</sup>.

#### 1.3.1 Methylsulfur compounds and the Sulfur Cycle

Structural and functional diversities of sulfur compounds make studies to decipher the mechanisms involved in their biochemical and ecological interactions challenging, but of high interest. One of the main reasons for

the global interest in sulfur and its derived metabolites is related to the impact they have on climate change and global warming.

Among the natural sources of sulfur-derived metabolites, marine phytoplankton species are the main producers of the tertiary sulfonium compound dimethylsulfoniopropionate (DMSP), a major dimethylsulfide (DMS) precursor. Scientific attention towards DMS goes back to 1935, when Haas<sup>41</sup> described, for the first time, the production of this volatile compound in the marine red macroalga *Polysiphonia fastigiata* when exposed to air. Performing further studies on the same alga, 13 years later, in 1948, the chemists Frederick Challenger and Margaret Isabel Simpson (later Dr. Whitaker) detected and identified the sulfur metabolite DMSP as the precursor of the gaseous molecule DMS<sup>42</sup>. Based on these findings, in 1972, the British environmental scientist James Lovelock investigated further the marine-derived DMS and, during a cruise over the Atlantic Ocean, from Montevideo (Uruguay) to the United Kingdom, detected DMS in surface ocean waters. The low DMS concentrations detected<sup>43</sup> suggested to Lovelock that DMSP might be the main carrier of sulfur from the seas, through the atmosphere, to the land, explaining the global budget of environmental sulfur, which could not be balanced without such transport, thus highlighting the importance of this compound in climate regulation<sup>44</sup>. Deepening this topic, in 1987 Lovelock, together with the climate scientist Robert Jay Charlson, the biogeochemist Meinrat Andrea and the astronomer Stephen G. Warren, demonstrated that DMS acts as an Earth's thermostat and, by enhancing cloud formation, prevents its overheating<sup>45</sup>. The theory behind these considerations became known as CLAW hypothesis (acronym of its authors' names) and shed new light on the environmental contribution of marine microalgae to climate regulation<sup>45,46</sup>. Hence, according to the CLAW hypothesis, changes in solar radiation, as well as in Earth and oceanic conditions, depend on a negative feedback mechanism that involves the production of DMS by marine phytoplankton, its emission into the atmosphere and its subsequent oxidation to sulfate aerosols. Once formed, these sulfate aerosols mitigate solar radiation directed to the Earth, not only by spreading their energy, but also by enhancing the formation of cloud condensation nuclei (CCN) and shaping the cloud albedo (amount of sunlight reflected into space)<sup>47</sup>. Changes in the way the earth reflects sunlight (the aforementioned "albedo") determine temperature and solar radiation shifts, which affect

the marine physiological processes. As a consequence, the biosphere and its productivity and the abundance of marine-derived DMS are altered. Hence, in line with the CLAW hypothesis, warmer temperatures would enhance phytoplankton productivity, thus increasing the synthesis, accumulation and excretion of sulfur metabolites, which contribute to the pool of DMSP. Increased amounts of DMSP determine also higher levels of its breakdown form DMS. As volatile metabolite, DMS leaves the oceans and enters into the atmosphere, raising the concentrations of sulfate aerosols and, in turn, of the CCN, making clouds brighter and reflecting more sunlight, while cooling down the Earth. Less solar radiation reaching the Earth and oceans decreases the productivity of marine organisms, establishing a negative feedback loop<sup>48</sup>. Despite years of observations and studies, compelling and strong evidence of the accuracy of the CLAW hypothesis is still missing. Before his theory, hydrogen sulfide (H<sub>2</sub>S) was considered the gas responsible for this active exchange, although never found in oceanic surface waters. After decades of research, the global emissions of DMS from the ocean to the atmosphere are estimated to be between 13-37 teragrams of sulfur (TgS)/year, impacting Earth's climate<sup>43,49-51</sup>. Moreover, beside DMS and its derivatives, most recent results suggest a more complex scenario behind the climate change and ocean-derived aerosols, where other sources of CCN are involved<sup>46</sup>. Nevertheless, the exploration of the ecological and physiological roles of DMSP in the marine environment are topics of social and scientific interest and several unanswered questions are the focus of ongoing research, feeding the scientific interest in this research area.

### 1.3.2 DMSP biosynthesis

Since its discovery, DMSP turned out to be abundant and widespread among marine organisms<sup>5,52,53</sup> and the elucidation of its biosynthetic pathway and its metabolism became a central topic of many studies. Methionine is considered the immediate precursor in DMSP biosynthesis and its environmental availability will determine the reaction yield of DMSP biosynthesis. Hence, stress conditions and nitrogen starvation enhance protein degradation and, as a consequence, increase the availability of amino acids such as cysteine and methionine for DMSP synthesis.<sup>54-56</sup> Intracellular synthesis of DMSP (Fig. 3) is initiated by a transamination reaction, where methionine is converted into an unstable 2-ketoacid, the 4-methylthio-2-oxobutyrate (MTOB)<sup>55</sup>. This intermediate reaction product forms, through a reduction, the hydroxy-derivative 4-methylthio-2-

hydroxybutyrate (MTHB). The following methylation yields the sulphonium compound 4-dimethylsulphonio-2-hydroxybutyrate (DMSHB), a metabolite only detected in species able to synthesize DMSP and proposed to be the functional and evolutionary precursor of DMSP, as its oxidative decarboxylation yields DMSP as final reaction product<sup>55,57</sup> (Fig. 3).

Recently, Curson et al.<sup>58</sup> identified the eukaryotic DSYB gene, an analogue of the bacterial *dsyB*, encoding key methylthiohydroxybutyrate methyltransferase enzyme which transforms MTHB in DMSHB<sup>59</sup>, providing a molecular tool to predict the relative contributions of eukaryotic and prokaryotic organisms to environmental DMSP production. Moreover, through an evolutionary analysis, the authors suggest that the eukaryotic DSYB gene originated, indeed, in bacteria and then was transferred to eukaryotic species either through endosymbiosis or by horizontal gene transfer<sup>48,58</sup> (Fig. 3).

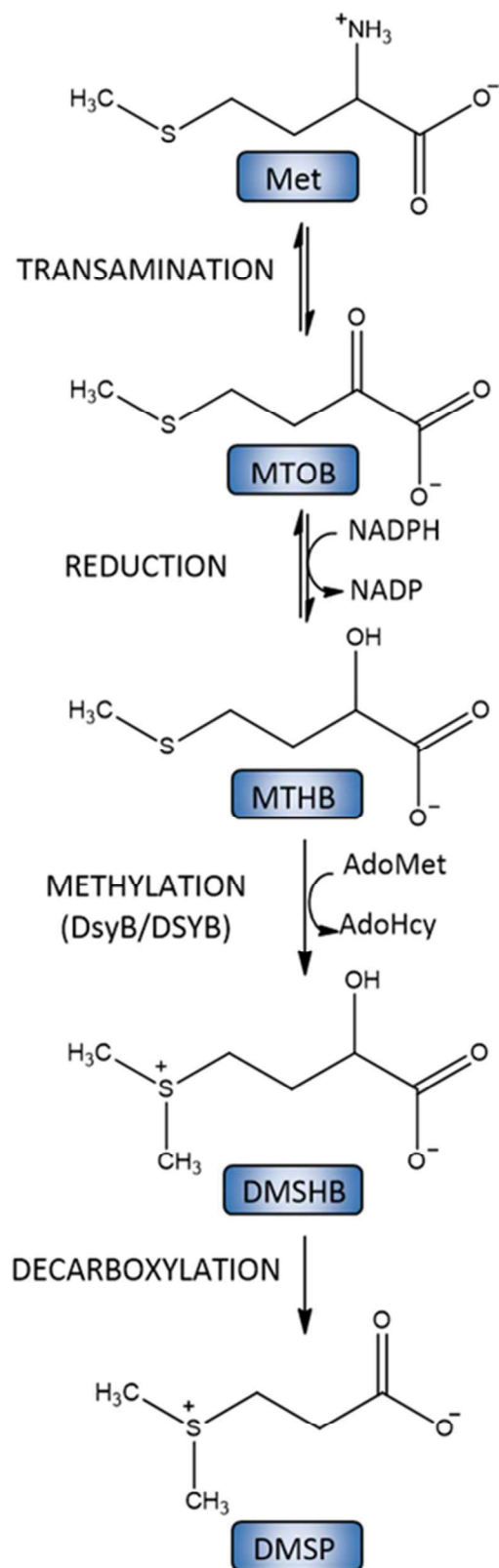


**Figure 3:** Pathway for DMSP biosynthesis in bacteria and marine algae. Met, methionine; MTOB, 4-methylthio-2-oxobutyrate; MTHB, 4-methylthio-2-hydroxybutyrate; AdoMet, Adenosylmethionine; AdoHcy, Adenosylhomocysteine; DMSHB, 4-dimethylsulfonio-2-hydroxybutyrate; DMSP, dimethylsulfoniopropionate. Adapted from Curson et al., 2018.<sup>58</sup>

### 1.3.3 Biochemical pathways for DMSP catabolism

After its biosynthesis, the majority of DMSP is released into the marine environment as dissolved DMSP (DMSPd), where it is available for living organisms, mainly bacteria, which take DMSP up and catabolise it through different competing pathways: the demethylation, the cleavage pathway and the most recent discovered oxidation pathway<sup>48,60-62</sup>, schematically depicted below (Fig. 4).

#### Demethylation pathway for DMSP catabolism

The demethylation pathway does not liberate DMS, but rather leads to the production of methylmercaptopropionic acid (MMPA) and, subsequently, to the volatile compound methanethiol (MeSH), which provides energy, organic carbon and reduced sulfur to the microbial food web<sup>61</sup>. The first step of this catabolic mechanism is mediated by the DmdA enzyme, member of the glycine cleavage T-protein (GcvT) superfamily and first gene to be associated with DMSP catabolism. The activity of the DmdA enzyme yields MMPA, using tetrahydrofolic acid as methyl-acceptor; MMPA is then further degraded into acetaldehyde, carbon dioxide, Coenzyme A (CoA) and MeSH, passing through the intermediates MMPA-CoA and methylthioacryloyl-CoA (MTA-CoA), where DmdB, DmdC and DmdD enzymes are respectively involved in each step of the biochemical pathway (Fig 4)<sup>60,63-65</sup>.

#### DMSP cleavage and oxidation pathways

While the demethylation pathway degrades almost 80% of DMSP, only a small percentage, between 2% and 21%, of DMSP is catabolized through the cleavage pathway to form the climate-active metabolite DMS<sup>64</sup>.

The catabolic pathway leading to the formation of the volatile dimethylsulfide (DMS) is the result of DMSP cleavage by enzymes known as DMSP lyases<sup>60</sup> that lead to the production of around 300 teragrams (Tg)/year of DMS, of which about 10% is transferred to the atmosphere via ocean-atmosphere sulfur flux<sup>37,60</sup>.

In addition to DMS, this catabolic pathway leads to the formation of acrylate, which is further converted into 3-hydroxypropionic acid (3HP) by the action of AcuNK. Five different types of DMSP lyases (Ddd-L, -P, -Q, -W, -Y) catalyse the cleavage of DMSP into acrylate and DMS, while the Ddd-D is the only DMSP lyase that does not directly generate acrylate, but rather 3HP, likely through the formation of a DMSP-CoA intermediate, rapidly converted to 3-HP. Acrylate is further converted, by the action of AcuNK, to

3-HP, which then is catabolized to malonate semi-aldehyde (Mal-SA) and then acetyl-CoA by DddA and DddC, respectively<sup>60</sup> (Fig. 4).

Although most of the cleavage of DMSP into DMS is made by marine bacteria and the enzymes involved in this transformation have been known for many years, the eukaryotic DMSP lyase gene, Alma1, responsible for this conversion was only recently identified in the haptophyte *Emiliana huxleyi* by Alcolombri et al. (2015)<sup>63,66</sup>. Alma1 belongs to the aspartate racemase superfamily and converts DMSP into DMS and acrylate in a way similar to the bacterial Ddd lyases. Moreover, orthologues and paralogues of Alma1 have been found in a wide range of eukaryotes, including dinoflagellates and haptophytes, revealing its wide distribution among marine eukaryotes<sup>48,66,67</sup>.

In addition to the previously described pathways, a third catabolic mechanism, the oxidation pathway, has been recently highlighted. In this pathway, DMSP is oxidized in marine microalgae and bacteria to form dimethylsulfonium propionate (DMSOP)<sup>62</sup>, a new DMSP derivative which is further transformed, contributing to the marine DMSO pool. Due to its recent discovery, the enzymes involved in this pathway haven't yet been elucidated<sup>62</sup> (Fig. 4).



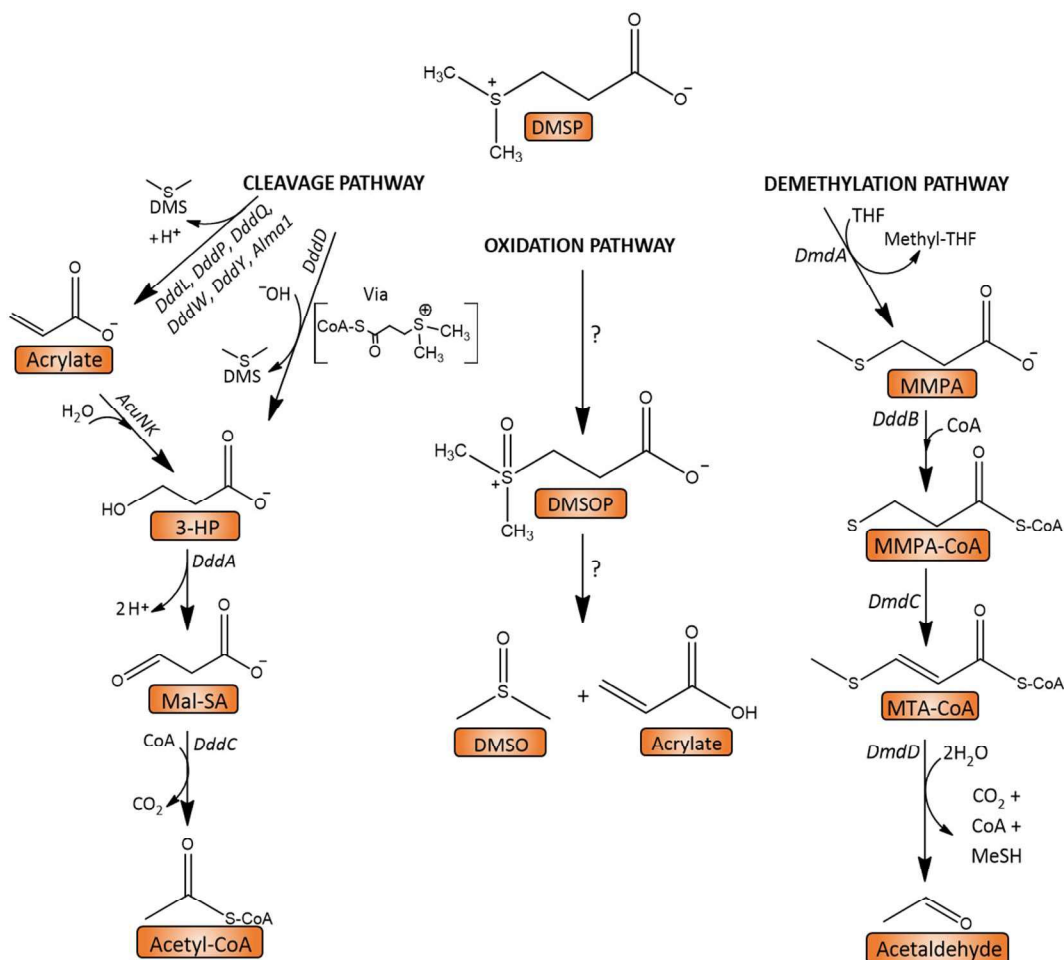


**Figure 4:** Pathway for DMSP degradation and enzymes involved. DMSP, dimethylsulfoniopropionate; DMS, dimethylsulfide; DddL/P/Q/W/Y, DMSP lyases; 3HP, 3-hydroxypropionate; Mal-SA, malonate semi-aldehyde; DddA, alcohol dehydrogenase; DddC, aldehyde dehydrogenase; DMSOP, dimethylsulfoxoniopropionate; DMSO, dimethylsulfoxide; MMPA, methylmercaptopropionic acid; THF, tetrahydrofuran; Methyl-THF, methyl-tetrahydrofuran; DmdA/C/D, DMSP-demethylase; DdB, iron-containing dehydrogenase; MMPA-CoA, methylmercaptopropionic acid-CoA; MTA-CoA, methylthioacryloyl-CoA. Adapted from Curson et al., 2011.<sup>60</sup>

## 1.4 Marine sulfonates

As phytoplankton species can accumulate DMSP in high concentrations, the same is true for sulfonate metabolites, another class of sulfur-derived molecules characterized by a direct carbon-sulfur bond ( $R-SO_3^-$ )<sup>39,68</sup>.

These metabolites are abundant in terrestrial ecosystems, where they constitute up to 95% of sulfur in soil<sup>69</sup>, but, while sulfonates were detected at very low concentrations in heterotrophic bacteria, phytoplankton turned out to produce sulfonates at millimolar intracellular concentrations, on a scale comparable with that of DMSP<sup>34,68</sup>. A diel cycle-linked production and

release of sulfonate by marine phytoplankton has recently been described by Durham and co-workers<sup>68</sup>. During the night, marine phytoplankton releases a percentage of the intracellular sulfonates, which are then taken up and imported by marine bacteria and catabolized to produce further metabolites, such as pyruvate and acetyl-CoA, to fulfill cellular requirements<sup>39,68</sup>. Among these compounds, C2-sulfonates (taurine and isethionate) are more abundant in phytoplankton species, while C3-sulfonates (2,3-dihydroxypropane-1-sulfonate (DHPS), sulfolactate and cysteate) are widespread among diatoms and haptophytes, suggesting a taxon-specific production<sup>68</sup>. Furthermore, a DHPS salinity-dependent accumulation by *Thalassiosira pseudonana* has been observed, suggesting an osmoregulatory function of this metabolite and, likely, of the entire class as well<sup>68</sup>.

Taken together, these evidences confirm diatoms and other phytoplankton species as the main source of sulfonates and highlight the presence of a tight network between eukaryotic phytoplankton (sulfonate producers) and heterotrophic bacteria (sulfonate consumers) in marine environments<sup>39</sup>.

Nevertheless, to date, studies on phytoplankton sulfonate-production and their physiological function are still missing and several other questions related to their biosynthetic pathway and their release into the ocean are still open.

## 1.5 Metabolomic analysis of marine compatible solutes

In the era of precision medicine, modern molecular high-throughput techniques enable to increase the amount and quality of data, helping to improve knowledge in several biological and medical fields<sup>70</sup>. These new technologies are referred to as “omics” (from the Sanskrit “OM”, “completeness”), denoting a universal detection of genes (genomics), proteins (proteomics), RNAs (transcriptomics) and metabolites (metabolomics) in specific biological samples<sup>71</sup>. Genomics was the first omics technology to appear, introduced in 1987 by Victor McKusick and Frank Ruddle as the name of the journal they were starting, but since then it became the way to refer to the study of the entire genome of an organism, until nowadays, where the term defines the determination of an entire DNA sequence of a specific organism<sup>72</sup>. While traditional research methods result to be often time-consuming and quite restrictive, omics

technologies provide simultaneous multiple target analysis in a time-efficient way<sup>73</sup>.

Further research produced new omics technologies, which, together with the most recent bioinformatic and computational tools, allow the investigation and detection of physiological mechanisms and interactions at molecular levels in different biological systems<sup>71,73</sup>. Among the latter developed “omics”, together with proteomics and transcriptomics, which respectively focus on protein expression and genome-wide studies of mRNA, metabolomics has been labeled as the new “omics”, joining the others to study the global metabolite profiles in cells, tissues, and organisms<sup>74,75</sup>. The word “metabolome” was introduced by Oliver et al.<sup>76</sup> to define a complete set of low-molecular-weight molecules (metabolites) present within a cell and involved in vital cellular functions<sup>76,77</sup>. The importance of metabolomic analysis appeared to be significant soon, showing “the potential to revolutionize an entire field of scientific endeavour”, as Mitchell and colleagues stated<sup>78</sup>, highlighting that “It is now within our grasp to be able to detect subtle perturbations within the phenomenally complex biochemical matrix of living organisms” through an “all-encompassing approach to understanding total, yet fundamental, changes occurring in disease processes, drug toxicity and cell function”<sup>74,78</sup>. Although scientists have been using metabolomics for decades, since the first metabolite profile appeared in the 1950s, it has developed slowly, becoming one of the scientific areas of major interest only recently. Metabolomic analysis generates sample-specific metabolite profiles through the use of high-performance analytical techniques, in particular high-throughput nuclear magnetic resonance (NMR) spectroscopy and/or mass spectrometry (MS), obtaining analytical spectra that are analyzed and compared using statistical approaches<sup>74,75</sup>.

Metabolomic applications are increasing in many different fields, from food science, (e.g., to monitor component analysis), to medicine (e.g., in drug research), to ecology, where metabolites can reflect the state of the surrounding environment and reveal potential interaction mechanisms between different organisms and the environment<sup>79-81</sup>. Among the ecological sciences, marine chemical ecology is the field where metabolomics has been very powerful, enabling studies on interactions within and between different marine organisms mediated by chemical compounds, like defense mechanisms and allelopathic interaction<sup>82</sup>.

Moreover, metabolomics analysis of marine organisms led to the discovery of new active compounds, unraveling their mechanism of action and their importance in the entire ecosystem<sup>83,84</sup>. Despite being a promising analytical tool, metabolomics applied to the study of marine organisms is not devoid of complications, mainly due to the extremely low availability of organisms, their remote collection sites, and the high concentrations of salts and lipids present in the collected samples, requiring special treatments to be removed and become ready for a metabolomic analysis<sup>82</sup>. Moreover, the physical and chemical properties of the metabolites produced in marine environments range from highly polar metabolites to hydrophobic compounds, thus requiring powerful and particular extraction and analytical techniques<sup>84</sup>.

### **1.5.1 Analysis of zwitterionic metabolites**

In the present Ph.D. thesis, the metabolomic analysis of algal-derived metabolites focused mainly on zwitterionic metabolites, taking advantage of a refined analytical method based on Ultra-High-Performance Liquid Chromatography (UHPLC) coupled with High-Resolution Mass Spectrometry (HRMS) developed by Spielmeyer and Pohnert<sup>85</sup> to achieve a chromatographic separation and direct determination of zwitterionic compounds.

Before the development of this method, scientific interest towards the sulfur metabolite DMSP and its related products led to the development of analytical methods to identify and quantify these compounds. Therefore, an indirect method based on the cleavage of DMSP to DMS and acrylate and on the quantification of the released DMS via gas chromatography was established<sup>86,87</sup>. Nevertheless, the main disadvantage this indirect quantification method had was that other DMS precursors were not taken into account, resulting in an overestimation of actual DMSP concentrations<sup>85</sup>. To avoid this inaccuracy, other methods, based on direct detection and quantification of these metabolites, were investigated. Thus, analysis of zwitterionic metabolites was performed, among other techniques, through ion chromatography<sup>88</sup> and capillary electrophoresis<sup>89,90</sup>, but significant improvements have been achieved through the combination of liquid chromatography and mass spectrometry. The first method based on LC-MS system was introduced in 2007 by Wiesemeier and Pohnert<sup>91</sup>, strengthening the retention of the polar metabolite DMSP on a C-18 reversed phase column, through a

derivatization reaction with pyrenyldiazomethane (PDAM), resulting in a DMSP-PDAM ester, both UV-visible and MS-detectable.

This method was further developed in 2010 by Li and colleagues<sup>92</sup>, who increased the sensibility and the detection limit of DMSP by using a pentafluorophenyl column, achieving a chromatographic separation of a pool of several other zwitterionic metabolites, including glycine betaine and proline from coral tissue<sup>92</sup>.

In the same year, Spielmeyer and Pohnert<sup>85</sup> described the use of ultra-performance liquid chromatography and mass spectrometry, together with a zwitterionic (ZIC-HILIC) stationary phase column, as a promising and suitable combination for the direct quantification of DMSP and other small organic polar metabolites from aqueous samples and microalgal extracts. Besides the reduced sample preparation steps and the small volumes required, the analytical method allows a direct determination of DMSP and other polar metabolites in aqueous extracts<sup>85</sup>.

### 1.5.2 HILIC chromatography and the ZIC-HILIC® column

Hydrophobic Interaction Liquid Chromatography (HILIC) is a complementary alternative to reversed-phase liquid chromatography (RPLC): it combines polar stationary phases generally used for Normal Phase (NP) chromatography with highly organic mobile phases, typical of a Reversed Phase, with a small percentage of water<sup>93-95</sup>. The small amount of water characterizing the HILIC mobile phase is adsorbed on the column surfaces (made either of silica or other polar adsorbents), thus creating a water-enriched stationary phase<sup>96</sup>: the retention mechanism is considered to be due to the separation of polar metabolites between the aqueous stationary phase, which immobilizes the polar metabolites, and the highly organic mobile phase<sup>93</sup>. During the partitioning, the formation of hydrogen bonds enhances the separation, while electrostatic interactions are responsible for differences in the metabolite's retention, which depend on the strength of this interaction, thus on the type of stationary phase, the ionic composition of the mobile phase and the ionization degree of the compound.

In ZIC-HILIC columns, the stationary phase is made up of silica, where an active layer or polymeric support contains a permanent, covalently bonded hydrophilic zwitterionic functional group, where strongly acidic sulfonic acid groups and highly basic quaternary ammonium groups are in a 1:1 ratio and separated by an alkyl chain. As a consequence, the positive charge of

the quaternary ammonium group is closer to the silica stationary phase and more accessible to interact with the analytes than the negative (Fig. 5)<sup>93</sup>.

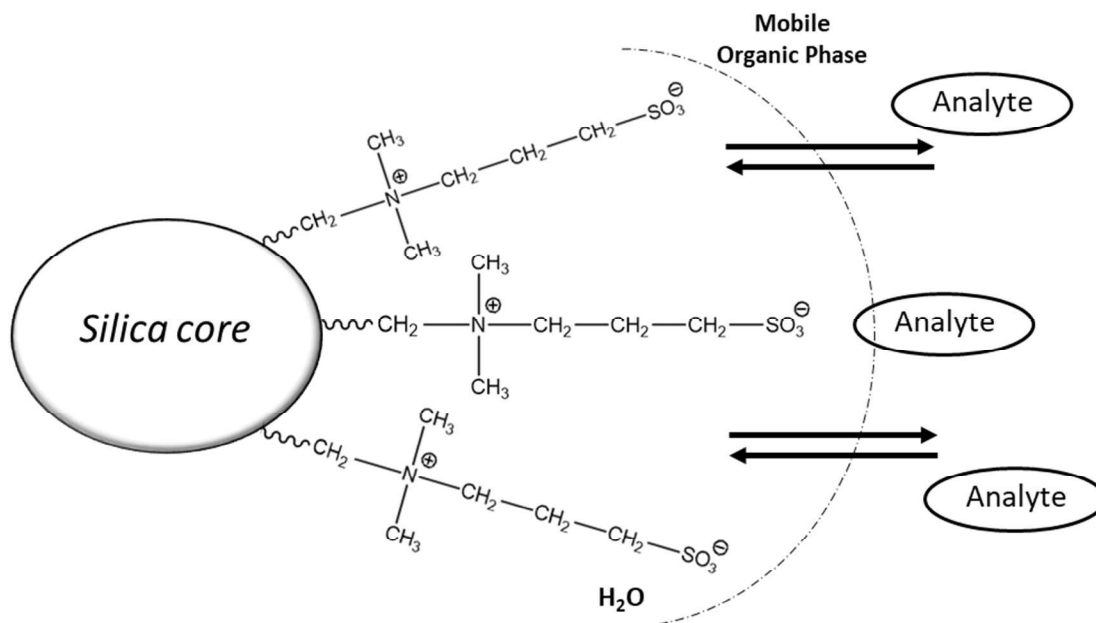


**Figure 5:** The core architecture of a ZIC-HILIC column.

In HILIC separations, acetonitrile is usually used as a weak eluent, while water and other aqueous buffers are considered strong eluents. At least 3% of the strong eluent is necessary for the elution to guarantee the formation of the aqueous layer characterizing the HILIC stationary phase, necessary for a proper separation and analytes' retention. On the other hand, because of its chemical structure, acetonitrile does not interact with the stationary phase as it does not form hydrogen bonds, thus avoiding competition with water molecules for the stationary-phase interaction sites<sup>97</sup>. Thanks to these characteristics, this column provides ionic interactions with the analyte suitable for the analysis of polar and hydrophilic compounds.

## 1.6 Thesis objectives

Marine phytoplankton-bacterial interactions represent, indeed, a major ecological link in aquatic ecosystems, driving the ocean sulfur cycle and regulating climatic processes through the production and exchange of a key compound: dimethylsulfoniopropionate (DMSP).

*Considering the large-scale ecological implications that the fate of this compound can have, and given the lack of information on the microbial catabolism of DMSP, in this work I aim to investigate further on this aspect and elucidate the environmental factors behind the release of DMS into the atmosphere and, therefore, decipher the link between phytoplankton-microbial processes and the carbon and sulfur biogeochemical cycles (**Publication 1**).*

Besides DMSP, several other metabolites, yet unknown, are involved in networks between eukaryotic phytoplankton and heterotrophic bacteria. Their elucidation and chemical characterization represent an important step in linking microbial communities with phytoplankton species.

*Thus, in this work, I aim to broaden the current knowledge on the inter- and intraspecific interactions between marine species and the biochemical mechanisms underlying ocean functioning (**Publication 2**).*

Salinity and temperature are recognized as environmental master factors, playing an active role in the ecological distribution, growth and development of aquatic species. Variations in these key abiotic stressors provide a frame how the ocean works, how it is linked to climate and how it may respond to environmental changes. Marine organisms, therefore, have developed physiological mechanisms to adapt to naturally occurring salinity and temperature changes in the seawater, by intracellular biosynthesis, or up-take from the extracellular environment, of organic compatible solutes to adjust the osmolality of the cells. Osmotic and thermal adaptation of marine species relies, therefore, on small organic

metabolites, whose identities and chemical structures have been partially characterized during the last decades. Nevertheless, in-depth chromatographic analyses revealed that till now only a limited fraction of polar metabolites produced by marine algae has been structurally and functionally characterized, while several others, most likely zwitterions with compatible solute properties, are still uncharacterized.

*In this thesis, taking advantage of highly advanced analytical technologies and developing instrumental methods and ecological bioassays, I aim to identify such uncharacterized metabolites produced by marine algae and investigate the molecular mechanisms behind the responses of marine organisms to different environmental stressors and climate changes factors, like seawater salinity changes and cold temperature adaptations (Publication 3, Publication 4, Publication 5).*



## 2 Publications

### 2.1 Publication 1

“Single-cell bacterial transcription measurements reveal importance of dimethylsulfoniopropionate (DMSP) hotspots in ocean sulfur cycling.”

Cherry Gao, Vicente I. Fernandez, Kang Soo Lee, Simona Fenizia, Georg Pohnert, Justin R. Seymour, Jean-Baptiste Raina, Roman Stocker

*Nature Communications*, Vol. 11(1942), 1-11, 2020

DOI: 10.1038/s41467-020-15693-z

**Open Access** This article is licensed under a Creative Commons Attribution 4.0 International License

Gao C.<sup>1</sup>, Fernandez V.I.<sup>2</sup>, Lee K.S.<sup>3</sup>, Fenizia S.<sup>4</sup>, Pohnert G.<sup>5</sup>, Seymour J.R.<sup>6</sup>, Raina J.B.<sup>7</sup>, Stocker R.<sup>8</sup> Single-cell bacterial transcription measurements reveal importance of dimethylsulfoniopropionate (DMSP) hotspots in ocean sulfur cycling. *Nature Communications*, 2020 11, 1942. 10.1038/s41467-020-15693-z

Author	1	2	3	4	5	6	7	8
Development of concept						x	x	x
Planning of research	x	x				x	x	x
Data collection	x		x					
Data analysis	x	x	x	x	x			x
Preparation of the manuscript	x	x				x	x	x
Correction of the manuscript	x	x	x	x	x	x	x	x
Proposed publication equivalent				0.5				

Authors contribution:

Cherry Gao	Experiment preparation and implementation, data analysis, software development, writing-original draft, writing-review, editing
Vicente I. Fernandez	Software development, writing-original draft, writing-review, editing
Kang Soo Lee	Experiment preparation and implementation, writing-review, editing
Simona Fenizia	Data collection and Data analysis, writing-review, editing
Georg Pohnert	Data analysis, writing-review, editing, supervision
Justin R. Seymour	Conceptualization, research planning, writing-review, editing, supervision
Jean-Baptiste Raina	Conceptualization, research planning, writing-original draft, writing-review, editing, supervision
Roman Stocker	Conceptualization, research planning, software development, writing-original draft, writing-review, editing, supervision



# Single-cell bacterial transcription measurements reveal the importance of dimethylsulfoniopropionate (DMSP) hotspots in ocean sulfur cycling

Cherry Gao <sup>1,2,3</sup>, Vicente I. Fernandez<sup>3</sup>, Kang Soo Lee <sup>2,3</sup>, Simona Fenizia <sup>4</sup>, Georg Pohnert <sup>4</sup>, Justin R. Seymour<sup>5</sup>, Jean-Baptiste Raina <sup>5</sup>✉ & Roman Stocker <sup>3</sup>✉

Dimethylsulfoniopropionate (DMSP) is a pivotal compound in marine biogeochemical cycles and a key chemical currency in microbial interactions. Marine bacteria transform DMSP via two competing pathways with considerably different biogeochemical implications: demethylation channels sulfur into the microbial food web, whereas cleavage releases sulfur into the atmosphere. Here, we present single-cell measurements of the expression of these two pathways using engineered fluorescent reporter strains of *Ruegeria pomeroyi* DSS-3, and find that external DMSP concentration dictates the relative expression of the two pathways. DMSP induces an upregulation of both pathways, but only at high concentrations (>1  $\mu\text{M}$  for demethylation; >35 nM for cleavage), characteristic of microscale hotspots such as the vicinity of phytoplankton cells. Co-incubations between DMSP-producing microalgae and bacteria revealed an increase in cleavage pathway expression close to the microalgae's surface. These results indicate that bacterial utilization of microscale DMSP hotspots is an important determinant of the fate of sulfur in the ocean.

<sup>1</sup>Department of Biological Engineering, Massachusetts Institute of Technology, Cambridge, MA 02139, USA. <sup>2</sup>Department of Civil and Environmental Engineering, Ralph M. Parsons Laboratory, Massachusetts Institute of Technology, Cambridge, MA 02139, USA. <sup>3</sup>Department of Civil, Environmental and Geomatic Engineering, Institute for Environmental Engineering, ETH Zurich, 8093 Zurich, Switzerland. <sup>4</sup>Friedrich Schiller University, Institute of Inorganic and Analytical Chemistry, Jena D-07743, Germany. <sup>5</sup>Climate Change Cluster (C3), University of Technology Sydney, Ultimo, NSW 2007, Australia. ✉email: [jean-baptiste.raina@uts.edu.au](mailto:jean-baptiste.raina@uts.edu.au); [romanstocker@ethz.ch](mailto:romanstocker@ethz.ch)

Up to 10% of the carbon fixed by phytoplankton cells in the ocean is converted to dimethylsulfoniopropionate (DMSP)<sup>1</sup>, resulting in a global production of this compound that exceeds one billion tons per year<sup>2</sup>. DMSP is an important currency in the ecological and metabolic exchanges between phytoplankton and heterotrophic bacteria<sup>3</sup>, as it represents a major nutrient source that contributes significantly to the sulfur and carbon demand of bacteria (up to 95% and 15%, respectively<sup>4,5</sup>). DMSP is utilized by marine bacteria via two competing catabolic pathways<sup>6</sup>: the demethylation pathway leads to the incorporation of both carbon and sulfur into bacterial biomass, whereas the cleavage pathway results in the utilization of carbon but the release of sulfur in the form of the climatically active gas dimethylsulfide (DMS). The environmental factors that govern the utilization of one pathway over the other, and ultimately the production and release of DMS to the atmosphere, have remained elusive, marking a major gap in the mechanistic link between microbial processes and global-scale carbon and sulfur biogeochemical cycles.

The water-column concentration of DMSP has been hypothesized to be an important factor regulating the choice of degradation pathway by bacteria (DMSP Availability Hypothesis<sup>6</sup>) and it has been speculated that bacteria control the fate of sulfur from DMSP by adjusting the relative expression of the demethylation and cleavage pathways (Bacterial Switch Hypothesis<sup>7</sup>). Concentrations of DMSP in bulk seawater are typically low, ranging from a few nanomolar (global oceanic average:  $16.91 \pm 22.17$  nM<sup>8</sup>) up to 200 nM during phytoplankton blooms<sup>9</sup>. However, much higher DMSP concentrations are expected to occur in the vicinity of individual DMSP-producing organisms, such as phytoplankton cells, which can have intracellular DMSP concentrations of hundreds of millimolar<sup>10</sup>. Efforts to elucidate the environmental drivers of microbial catabolism of DMSP have to date been limited to measurements in large-volume batch cultures<sup>11,12</sup> and seawater samples<sup>13</sup>. As a consequence, an understanding of the influence of microscale heterogeneity in DMSP concentrations on the microbial choice of degradation pathway is lacking.

Here, we report that the external concentrations of DMSP that are relevant for controlling the expression of degradation pathways by a model copiotrophic bacterium are unexpectedly high, and are characteristic of DMSP hotspots. This finding was enabled by the development of the first single-cell, time-resolved measurements of DMSP degradation pathway expression and their application to study the response of bacteria to different concentrations of DMSP.

## Results and discussion

### Construction and validation of fluorescent reporter bacteria.

To examine the relative expression of bacterial DMSP catabolism genes at the single-cell level, we genetically transformed *Ruegeria pomeroyi* DSS-3, a model Alphaproteobacterium from the Roseobacter clade. Like many members of the Roseobacter clade, which plays a central role in DMSP cycling<sup>14</sup>, *R. pomeroyi* harbors both DMSP catabolic pathways<sup>15</sup>. We transformed *R. pomeroyi* cells with a custom-built tricolor promoter-fusion plasmid designed to simultaneously report metabolic activity and the expression of the genes encoding the two DMSP degradation pathway enzymes through different fluorescence emission (Fig. 1a, b). In the engineered plasmid, the promoter regions of DMSP-dependent demethylase (DmdA) and DMSP lyase (DddW), which catalyze the first steps of the demethylation and cleavage pathways, respectively, control the expression of fluorescent proteins (Methods). Out of the three functional DMSP lyases (DddP, DddQ, and DddW)<sup>16</sup> encoded in the *R. pomeroyi*

DSS-3 genome, DddW was chosen in this study due to its strong upregulation response to DMSP reported in previous transcriptomic studies<sup>11,17</sup>, which suggests that it is the primary DMSP lyase in this bacterium. However, some of the cleavage dynamics, controlled by DddP and DddQ, may be missed by our approach.

Construction of promoter-fusion reporter strains, followed by quantitative single-cell time-lapse microscopy, has been commonly adopted to utilize fluorescence signal dynamics as a proxy for native gene expression behaviors<sup>18–20</sup>. To control for signal bias caused by the choice of fluorescent protein fused to each promoter region, we constructed two *R. pomeroyi* reporter strains (Goofy and Regular), for which we interchanged the color of fluorescent proteins fused to the *dmdA* and *dddW* promoter regions (Fig. 1a, b and Supplementary Fig. 1). The choice of fluorescent protein led to some differences in the temporal evolution of fluorescence signal, but did not affect our overall conclusions (Supplementary Fig. 2). A comparison of fluorescence signal output by tricolor and single-color reporter strains confirmed that promoter fusion cassettes induce fluorescent protein expression whether encoded alone or together (Supplementary Fig. 2).

To confirm that the strains specifically report *dmdA* and *dddW* gene expression, and to test for non-specific responses, the engineered bacteria were incubated with seven different carbon sources. Rich medium (5% 1/2 YTSS), propionate, acetate, succinate, and glucose did not elicit any fluorescence response (Supplementary Fig. 3). Glucose was chosen as the most suitable negative control for subsequent experiments for the following reasons: it elicited no non-specific DMSP gene transcription responses (Supplementary Fig. 3); its molecular weight is similar to DMSP; and the metabolic pathways of glucose and organosulfur compounds are distinct. The only carbon sources that led to an increase in cell fluorescence were DMSP (activating both *dmdA* and *dddW* promoters) and acrylate, a known *dmdA* inducer<sup>21</sup> (activating only *dmdA*, but not *dddW*), thus confirming the validity of our reporter construct design (Supplementary Fig. 3).

### Time-lapse DMSP incubation experiments in microfluidic chips.

A custom microfluidic chip containing nine observation chambers was employed for the simultaneous incubation of an engineered reporter strain with a range of concentrations of DMSP as a sole amended carbon source (Fig. 1c). The absence of fluid flow in the observation chambers enabled us to monitor the expression of DMSP degradation pathways in a time-resolved manner at the single-cell level (Fig. 1d). Images in phase contrast and fluorescence (in red, yellow, and teal channels) were acquired every 45 min for 24 h at six or seven positions per observation chamber (Fig. 2), encompassing  $218 \pm 120$  (mean  $\pm$  s.d.) cells per field of view (at  $t = 45$  min) per condition (Supplementary Fig. 4). Microscope and camera settings were optimized to minimize phototoxicity and photobleaching while maximizing fluorescence signal capture.

Low levels of expression of both pathways occurred even in the absence of DMSP (Supplementary Fig. 5 and Supplementary Note 1), with baseline *dmdA* expression 1.0–6.7 times higher than *dddW* expression (Fig. 3). High variability of fluorescence output among replicate experiments at  $\geq 10$   $\mu$ M DMSP (Supplementary Fig. 6), likely caused by slight differences in subculture growth phase, prevented the comparison of pathway reporters within each color (Supplementary Fig. 5). Thus, across-color ratio calculation, which enabled comparisons of pathway expression within the same experiment, was employed in our study (Fig. 3). Importantly, the across-color ratios (0.15–1.0; Fig. 3) and

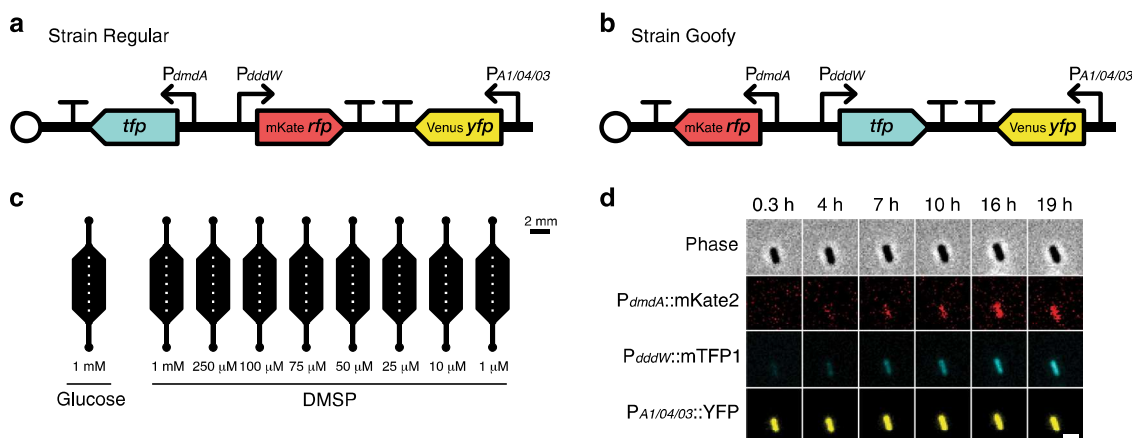


**Fig. 1** Single-cell measurements of DMSP degradation pathway expression. **a, b** Plasmids transformed into *R. pomeroyi* DSS-3 contain three components: *dmdA* reporter (222 bp promoter region); *dddW* reporter (500 bp promoter region); and constitutive *yfp* expression (strong, synthetic promoter  $P_{A1/04/03}$ ). YFP signal was used as a proxy for plasmid copy number and metabolic activity. Transcriptional terminators (represented by T) were placed between promoter fusion cassettes to prevent transcriptional read-through. To control for spectral bias caused by fluorescent protein choice (RFP or TFP), we constructed two *R. pomeroyi* reporter strains—Regular (**a**) and Goofy (**b**)—in which the colors of fluorescent proteins fused to *dmdA* and *dddW* promoter regions were interchanged. Vector backbone: pBBR1MCS-2 with origin of replication pBBR1 (open circles). **c** Schematic of a single microfluidic device used for time-lapse DMSP experiments. Each time-lapse DMSP experiment used one microfluidic device containing nine observation chambers for parallel incubation of a single reporter strain (Regular or Goofy; **a, b**) with different concentrations of DMSP. Glucose was used as negative control. White squares in each observation chamber represent the seven fields of view ( $200\ \mu\text{m} \times 200\ \mu\text{m}$ ) imaged at each time point. **d** Representative phase contrast and fluorescence images of a single cell (strain Goofy) over time in the presence of 1 mM DMSP. Scale bar,  $2\ \mu\text{m}$ .

within-color ratios (0.3–0.5; Supplementary Fig. 5) in glucose showed consistent results.

No significant upregulation beyond these baseline levels of either pathway was detected at DMSP concentrations below  $1\ \mu\text{M}$  (i.e.,  $100\ \text{nM}$  and  $500\ \text{nM}$ ) compared to negative controls (two-tailed *t*-tests,  $n = 259$ – $2125$  cells,  $p > 0.01$ ) (Supplementary Fig. 7). At  $1\ \mu\text{M}$  DMSP, significant upregulation was only observed in some replicate experiments (Supplementary Fig. 8). Only one out of six replicate experiments of the demethylation pathway (*dmdA*) was upregulated at  $1\ \mu\text{M}$  DMSP, while the cleavage pathway (*dddW*) showed more consistent significant upregulation (four out of six replicate experiments) at  $1\ \mu\text{M}$  DMSP compared to glucose negative controls (two-tailed *t*-tests,  $n = 1284$ – $9362$  cells,  $p < 0.01$ ) (Supplementary Fig. 8). At higher concentrations ( $\geq 10\ \mu\text{M}$ ), all replicate experiments exhibited upregulation (Supplementary Fig. 6). These results suggest that  $1\ \mu\text{M}$  approximates the threshold DMSP concentration above which bacteria start to increase *dmdA* gene expression beyond baseline levels. Consistent with existing evidence that points to demethylation as the major fate of DMSP in seawater<sup>22</sup>, our results also suggest that DMSP at typical bulk seawater concentrations ( $16.91 \pm 22.17\ \text{nM}$ <sup>8</sup>) is primarily degraded through the higher baseline expression levels of the demethylation pathway by Roseobacters (such as *R. pomeroyi*), which are major players in marine organic sulfur cycling<sup>14</sup>.

Both pathways were consistently and significantly upregulated compared to negative controls upon incubation with DMSP concentrations between  $10\ \mu\text{M}$  and  $1\ \text{mM}$ , which led to upregulation of 1.6–6.0-fold (*dmdA*) and 8.0–112.6-fold (*dddW*) compared to glucose at 24 h (Fig. 2a, b and Supplementary Figs. 6, 9; averages of  $n = 6$  replicates). The rates of upregulation, expressed as the slope of the exponential phase of the fluorescence kinetics curves, were similar across different DMSP concentrations ( $10\ \mu\text{M}$ – $1\ \text{mM}$ , Fig. 2a, b and Supplementary Fig. 6), suggesting that upon exposure to DMSP concentrations at or above  $10\ \mu\text{M}$ , cells are stimulated to initially increase the expression of both demethylation and cleavage pathways at a conserved rate.

While the rate of upregulation was conserved across DMSP concentrations, maximum gene expression levels of *dddW* and *dmdA* increased with DMSP concentration (Fig. 2c, d). Due to the stability of fluorescent proteins (half-lives of hours to more than a day<sup>23</sup>), the fluorescence signal is expected to persist even after gene expression returns to baseline levels. We therefore used the magnitude of the end-point fluorescence signal (averaged over the last five time points, i.e., 20.4–24 h) as a proxy for maximum gene expression levels of *dddW* and *dmdA*. Normalized maximum gene expression levels of both pathways increased approximately linearly with DMSP concentration between 1 and  $75\ \mu\text{M}$  DMSP (0.07–0.77 a.u. for *dmdA*; 0.02–0.62 a.u. for *dddW*; Fig. 2c, d). This increase plateaued above  $100\ \mu\text{M}$  (Fig. 2c, d), possibly as a result of the gene expression machinery becoming saturated and unable to respond as sensitively to DMSP at these high concentrations (Supplementary Note 2).

To determine how consumption of DMSP in the chambers may have affected our conclusions, we performed a larger-volume (8 ml) experiment in which we directly measured DMSP concentration and cell fluorescence, for selected timepoints (0, 2, 8, 24 h) and initial DMSP concentrations ( $1\ \mu\text{M}$ ,  $75\ \mu\text{M}$ ,  $1\ \text{mM}$ ). DMSP concentration decreased over time, due to uptake by bacteria (Supplementary Fig. 10). Consistent with results from the microfluidic chip experiments (Fig. 2), the initial rate of increase in the fluorescent signal was conserved between the  $75\ \mu\text{M}$  and  $1\ \text{mM}$  conditions, but decreased as the DMSP concentration diminished due to bacterial uptake (Supplementary Fig. 10). The saturation of the fluorescence signal coincided temporally with the depletion of DMSP (at 8 h, for the  $75\ \mu\text{M}$  condition; Supplementary Fig. 10). These results suggest that cells initially increase gene expression at a rate that is independent of DMSP concentration, but halt their gene upregulation when the DMSP supply is exhausted.

Rather than expressing only one pathway at any given DMSP concentration, as implied by the Bacterial Switch Hypothesis<sup>7</sup>, we observed that bacteria express both pathways simultaneously, but modulate the ratio of cleavage and demethylation according to DMSP concentration (Fig. 3). Overall, the cleavage-to-

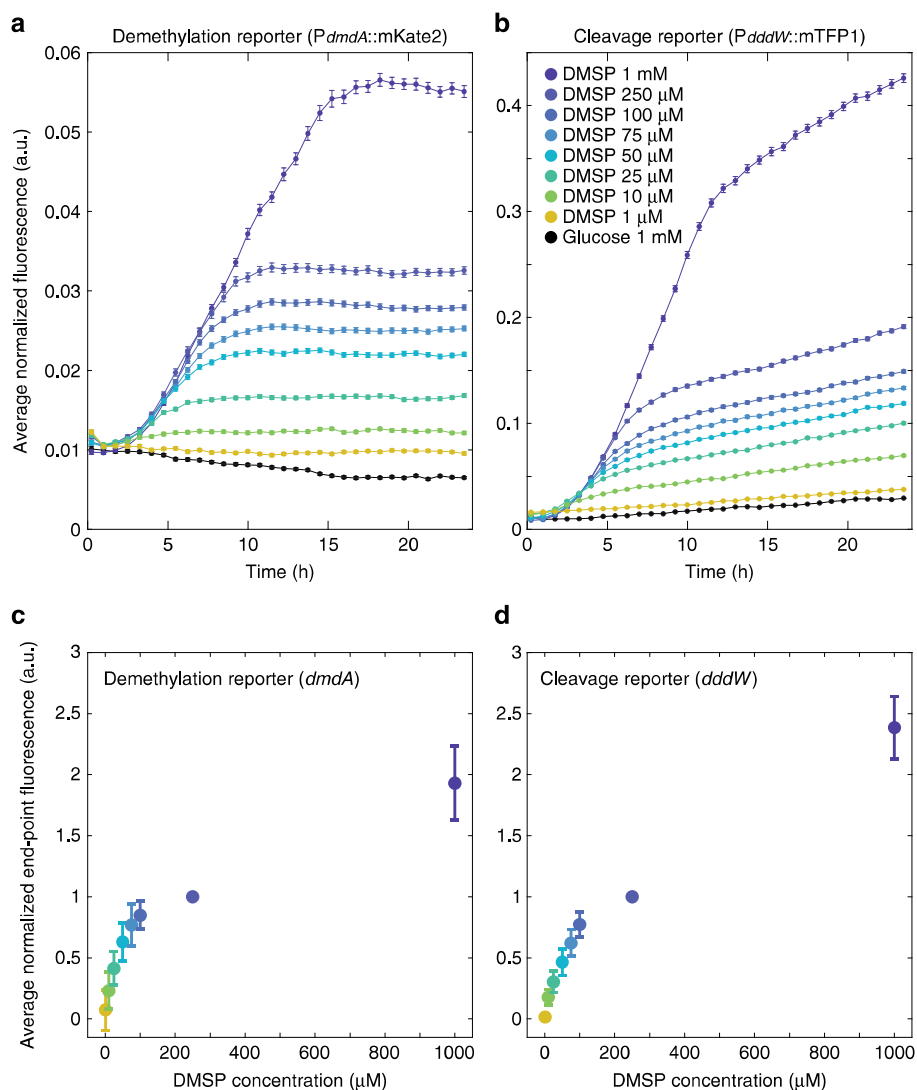


**Fig. 2** DMSP concentration-dependent upregulation of *dmdA* and *dddW*. **a, b** Mean fluorescence signals of *dmdA* (demethylation) (**a**) and *dddW* (cleavage) (**b**) reporters in response to different concentrations of DMSP. One representative replicate experiment of reporter strain Goofy is shown (data from additional replicate experiments ( $n = 3$  for each reporter strain) are shown in Supplementary Fig. 6). Spectral leakage correction, background subtraction, and a threshold on YFP intensity were applied (see Methods and Supplementary Note 1). RFP and TFP signals of each cell were normalized by the mean YFP signal at each time point of each experimental condition. Data points and error bars represent means  $\pm$  s.e.m. of cells (error bars may be smaller than markers). **c, d** Average end-point fluorescence levels of *dmdA* (**c**) and *dddW* (**d**) reporters. For each replicate experiment, baseline signal (glucose) was subtracted at each time point, fluorescence signals over the final five time points ( $\sim 20.4$ – $24$  h) were averaged, then normalized by the corresponding end-point fluorescence signal at  $250 \mu\text{M}$  DMSP. Data points and error bars represent means  $\pm$  s.d. of six total replicates ( $n = 3$  for strain Regular and  $n = 3$  for strain Goofy combined).

demethylation expression ratio increased with DMSP concentration up to  $100 \mu\text{M}$ , above which it started to plateau (Fig. 3b). Baseline expression levels that are biased towards demethylation were represented by cleavage-to-demethylation ratios of  $0.15$ – $1.0$  in the glucose negative controls (Fig. 3). At high DMSP concentrations between  $10 \mu\text{M}$  and  $1 \text{mM}$ , bacteria gradually skewed their gene expression towards the cleavage pathway, with the cleavage-to-demethylation ratio increasing from  $1.89 \pm 0.29$  at  $10 \mu\text{M}$  to  $8.10 \pm 0.60$  at  $1 \text{mM}$  (Fig. 3, strain Regular). Similar ratio values were obtained with strain Goofy (Fig. 3). These results indicate that the cleavage pathway becomes more strongly expressed than the demethylation pathway above a transitional concentration of DMSP that lies between  $1$  and  $10 \mu\text{M}$ . We propose that at this transitional concentration, the sulfur needs of the bacteria are completely met through the demethylation

pathway, and excess organic sulfur at higher DMSP concentrations is released as DMS via cleavage.

**Raman microspectroscopy.** The effect of sulfur satiation on cleavage pathway expression was more directly observed via single-cell Raman microspectroscopy. Measurements with deuterium-labeled DMSP revealed that bacteria that were satiated in sulfur through prior exposure to methionine (also an organic sulfur source) maintained uptake of DMSP but skewed gene expression toward the cleavage pathway (Supplementary Fig. 11). Bacterial sulfur demand has been proposed as a factor that regulates the fate of DMSP<sup>6,7,12</sup>. Since different elements of the DMSP molecule are harvested by the bacteria through demethylation (both carbon and sulfur) and cleavage (carbon

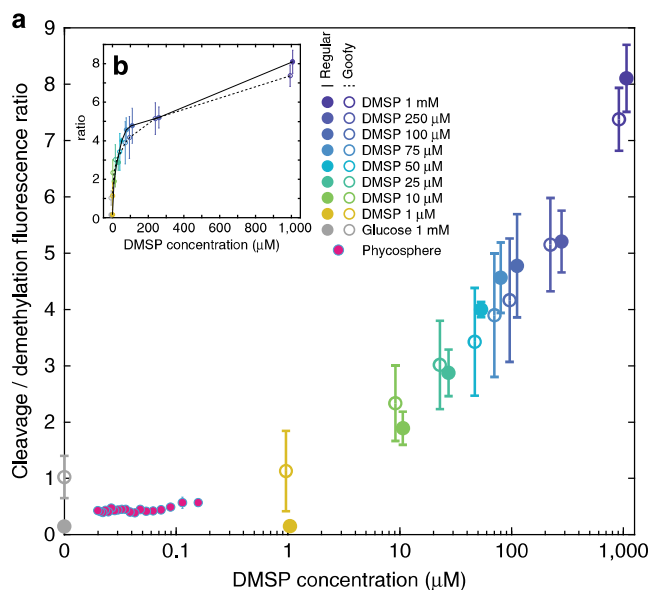


**Fig. 3 DMSP concentration modulates relative expression of *dddW* and *dmdA*.** **a** Cleavage-to-demethylation pathway ratio was calculated at each DMSP concentration for strains Regular (RFP/TFP) and Goofy (TFP/RFP). High variability of fluorescence output amongst replicate experiments at  $\geq 10 \mu\text{M}$  DMSP prevented the comparison of pathway reporters within each color (Supplementary Fig. 5). Average fluorescence signals at time points at which *dmdA* expression is mid-exponential for each DMSP concentration (shown in Supplementary Fig. 6), or at the second time point for glucose and  $1 \mu\text{M}$  DMSP conditions, were used for ratio calculation. Close agreement between strains Regular and Goofy at  $\geq 10 \mu\text{M}$  DMSP suggests that fluorescence ratios are close to true pathway expression ratios. The deviation between strains Regular and Goofy of ratios in glucose and  $1 \mu\text{M}$  DMSP may be due to low fluorescence signals; importantly, ratios calculated within-color (0.3–0.5; Supplementary Fig. 5) and across-color (0.15–1.0; Fig. 3) in glucose showed consistent results (similar values at  $1 \mu\text{M}$  DMSP). Pathway ratios from the phycosphere experiment (also shown in Fig. 4f) were calculated using TFP signals of reporter strains (reporting either *dmdA* or *dddW* expression in strains Regular or Goofy, respectively) normalized by constitutive YFP signals, and were plotted against modeled phycosphere DMSP concentrations (Supplementary Fig. 13). Data points and error bars of DMSP concentration experiments are slightly offset in the x-direction for presentation clarity, and represent means  $\pm$  s.d. of replicate experiments ( $n = 3$  for strain Regular;  $n = 3$  for strain Goofy). Error bars of the phycosphere experiment represent the variance of the ratio of normalized cleavage and demethylation fluorescence signals (Supplementary Note 1). Error bars may be smaller than markers. **b** Inset represents the same data as **a**, plotted on a linear scale on the x-axis to show the saturating relationship between DMSP concentration and cleavage-to-demethylation ratio.

only), our observations are consistent with the hypothesis that cells favor the cleavage pathway when they no longer require additional sulfur but continue to harvest carbon from DMSP.

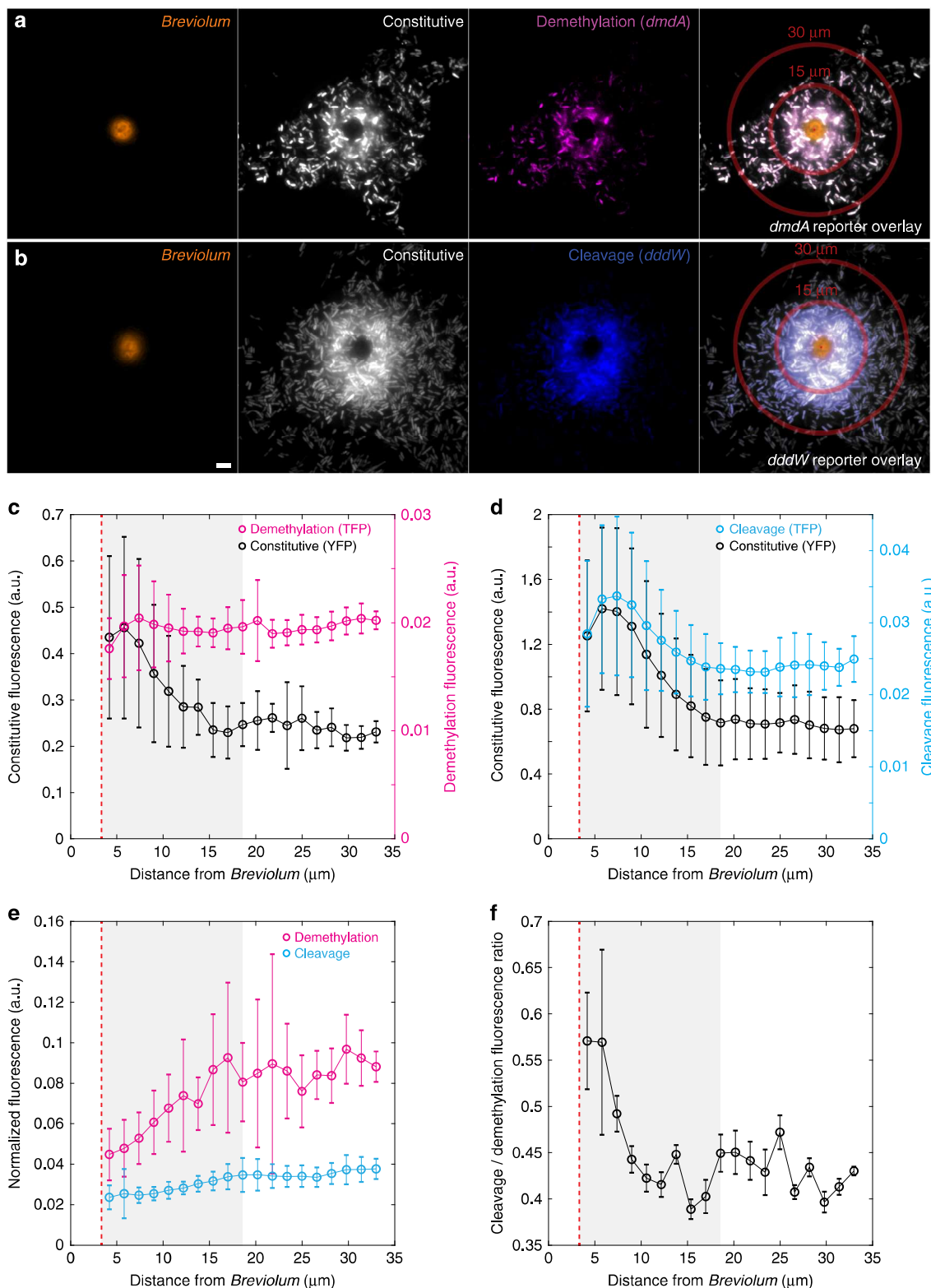
#### Co-incubation of phytoplankton and engineered bacteria.

While uptake of DMSP was detected at all concentrations tested (Supplementary Fig. 10), upregulation of DMSP degradation genes was observed only in relatively high concentrations ( $\geq 1 \mu\text{M}$  in microfluidic chip experiments; Fig. 2). DMSP is not homogeneously distributed in the water column, but often occurs as point sources of high concentration surrounding DMSP-producing organisms<sup>24</sup>. Bacterial exploitation of these enriched microenvironments<sup>25</sup> can influence DMSP transformation rates

and microbial pathway choice in the ocean. To determine DMSP degradation gene expression in the context of microscale hot-spots, we exposed the *R. pomeroyi* fluorescent reporter strains to an ecologically relevant point source of DMSP: a unicellular phytoplankton. Concentration gradients of nutrients, often including DMSP, are present in the microenvironment directly surrounding phytoplankton cells (the phycosphere<sup>24</sup>). We co-incubated the reporter strains with the unicellular dinoflagellate *Breviolum* CCMP2459, which belongs to a family containing some of the most prolific producers of DMSP (Symbiodiniaceae; with intracellular DMSP concentrations of 36–7590 mM)<sup>10</sup>. Co-incubations were performed on agarose pads, which immobilized both phytoplankton and bacterial cells for ease of observation. After 24 h of co-incubation in the dark, high-magnification (100 $\times$  objective) epifluorescence microscopy images of the phycosphere surrounding individual *Breviolum* cells were acquired (Fig. 4a, b and Supplementary Fig. 12). To avoid alterations to the phycosphere due to microscopy light-induced cellular stress, images were acquired at a single time point (24 h). Only teal fluorescence was quantified to represent bacterial pathway expression (due to spectral leakage in the red fluorescence channel by photosynthetic pigments, e.g., chlorophyll and carotenoids), with strain Regular reporting demethylation (*dmdA*;  $n = 15$  *Breviolum* cells) and strain Goofy reporting cleavage (*dddW*;  $n = 18$  *Breviolum* cells) (Fig. 4). Fluorescence intensities of bacteria were averaged across *Breviolum* cells as a function of distance from the phytoplankton cell (Supplementary Note 3).

*R. pomeroyi* gene expression patterns reflected the spatial locations of the bacteria within the phycosphere of *Breviolum* cells. According to modeled DMSP diffusion assuming a leakage rate of 11% of intracellular DMSP per day (Supplementary Note 4), the steady-state concentration at the surface of a *Breviolum* cell (radius =  $3.3 \pm 0.9 \mu\text{m}$ , mean  $\pm$  s.d.) was 197 nM and decayed exponentially with distance,  $r$ , from the center of the phytoplankton cell (Supplementary Fig. 13). In line with the predicted DMSP concentration profile within the phycosphere, bacteria that were nearest to the surface of *Breviolum* cells, but far enough not to be affected by spectral interference from photosynthetic pigments ( $r = 7.4 \mu\text{m}$ ), were the most metabolically active, exhibiting YFP fluorescence intensities that were on average double ( $1.4 \pm 0.5$  a.u., Goofy;  $0.4 \pm 0.2$  a.u., Regular) those exhibited by bacteria located at  $r = 18.6 \mu\text{m}$  ( $0.7 \pm 0.3$  a.u., Goofy;  $0.2 \pm 0.05$  a.u., Regular), beyond which YFP intensities did not change with distance (Fig. 4c, d).

The expression of the cleavage pathway (*dddW*) also increased with decreasing distance from a *Breviolum* cell. The *dddW* expression levels ( $3.4 \pm 1.1 \times 10^{-2}$  a.u., raw TFP signal) were highest near the surface of *Breviolum* ( $r = 7.4 \mu\text{m}$ ; modeled DMSP concentration = 89 nM) (Fig. 4d) and decreased to baseline levels ( $2.4 \pm 0.4 \times 10^{-2}$  a.u., raw TFP signal) at  $r \geq 18.6 \mu\text{m}$  (modeled DMSP concentration = 35 nM). These results differ from our previous microfluidic experiments where exposure to pure DMSP at  $< 1 \mu\text{M}$  did not lead to *dddW* fluorescence upregulation (Supplementary Fig. 7). This discrepancy may be due to the presence of compounds in algal exudates that positively influence the regulation of *dddW* expression, or by the greater sensitivity of the camera setup used in the *Breviolum* experiment. In contrast, the demethylation pathway (*dmdA*) was not expressed above baseline levels at any distance from the *Breviolum* cells (Fig. 4c), but its expression, normalized by the average baseline YFP intensity (proxy for metabolic activity), was still higher than that of the cleavage pathway throughout the phycosphere (Fig. 4e). As a result, relative pathway expression was skewed towards demethylation at all distances from a *Breviolum* cell (Fig. 4f), but with decreasing distance, and thus increasing DMSP concentration, the cleavage-to-demethylation



pathway ratio increased in a pattern consistent with the microfluidic observations (Fig. 3a).

These results suggest that within the phycosphere of a small phytoplankton cell slowly exuding DMSP, elevated production of DMS due to cleavage by marine bacteria occurs close to the surface of the phytoplankton cell, but most of the DMSP within the phycosphere is degraded through the demethylation pathway. However, in the scenario of a lysing phytoplankton cell that

releases its intracellular DMSP at once, for example at the demise of a phytoplankton bloom, DMSP within the phycosphere can reach micro- or millimolar concentration for seconds to minutes<sup>26</sup>. Matching these time scales, bacterial gene expression (transcription and translation) can theoretically be upregulated within a few minutes<sup>27</sup>, although limitations in fluorescence signal detection prevented the observation of such early responses in the present study. Furthermore, oligotrophic DMSP degraders



**Fig. 4 Gene expression patterns in a natural DMSP hotspot.** **a, b** Representative images of co-incubation between DMSP-producing microalgae, *Breviolum* CCM2459 (photosynthetic pigment, orange), and engineered bacteria, *R. pomeroyi*, constitutively expressing YFP (white) and fluorescently reporting *dmdA* (**a** demethylation, strain Regular-TFP, magenta) or *dddW* (**b** cleavage, strain Goofy-TFP, blue) expression. Fluorescence signals are false-colored. Representative concentric rings (widths, 20 pixels = 1.6  $\mu\text{m}$ ) that bin distances from the center (red dots) of *Breviolum* cells for fluorescence quantification are shown at 15 and 30  $\mu\text{m}$ . Scale bar, 5  $\mu\text{m}$ . **c, d** Quantification of YFP (constitutive) and TFP (*dmdA* (**c**), or *dddW* (**d**)) fluorescence at each distance ( $r$ ) from the center of *Breviolum* cells (mean radius = 3.3  $\mu\text{m}$ , red dotted line;  $n = 33$ ). Fluorescence upregulation of YFP (**c, d**) and TFP (*dddW*; **d**) were detectable up to  $r = 18.6 \mu\text{m}$  (gray shading), at which modeled DMSP concentration was 35 nM (Supplementary Fig. 13). YFP of the cleavage pathway reporter (**b, d**) was brighter than that of the demethylation pathway reporter (**a, c**), probably due to differences in metabolic activity levels in each bacterial culture. Bacteria nearest to the surface of the phytoplankton ( $r = 4.2 \mu\text{m}$ , the first concentric ring) appeared dimmer than expected, possibly due to spectral interference from photosynthetic pigments. Data points and error bars represent mean  $\pm$  s.d. of images ( $n = 15$  *Breviolum* cells for *dmdA* (**c**);  $n = 18$  for *dddW* (**d**)), calculated at each concentric ring (image analysis methods in Supplementary Note 3). **e** TFP fluorescence of each cell-containing pixel normalized by the average YFP fluorescence of cell-containing pixels within the corresponding concentric circle to remove the effect of metabolic activity differences on fluorescence intensities. Direct comparisons between demethylation and cleavage after normalization revealed that demethylation expression was higher than cleavage expression at all distances from the phytoplankton. Data points and error bars represent mean  $\pm$  s.d. of normalized fluorescence of images, calculated at each concentric ring. **f** Average normalized TFP intensity (**e**) of strain Goofy (*dddW*,  $n = 18$ ) divided by that of strain Regular (*dmdA*,  $n = 15$ ) at each distance from the phytoplankton. Error bars represent the variance of the ratio of normalized cleavage and demethylation fluorescence signals (Supplementary Note 3).

such as SAR11<sup>28,29</sup> likely employ regulatory mechanisms that differ from copiotrophic bacteria such as *R. pomeroyi*. In general, the results from our microfluidic experiments suggest that in the vicinity of lysing phytoplankton cells (>10  $\mu\text{M}$ ) or in other microenvironments with similarly high DMSP levels<sup>30</sup>, both DMSP degradation genes increase expression, with cleavage more so than demethylation. These microscale dynamics are consistent with macroscale patterns of elevated DMS production that are observed during the decline of phytoplankton blooms<sup>31</sup> and following high rates of viral-induced phytoplankton lysis<sup>32</sup>.

Taken together, our observations reveal that the metabolic machinery of DMSP-degrading copiotrophic bacteria may be adapted for encounters with DMSP hotspots. Baseline expression of both pathways was detected even in the absence of DMSP (Supplementary Fig. 5), possibly owing to promoter leakage of *dmdA* and *dddW*, which likely allows bacteria to be poised for the next encounter with DMSP. Upregulation of DMSP degradation genes, beyond baseline levels, was only observed at high DMSP concentrations that are characteristic of hotspots: above 1  $\mu\text{M}$  for *dmdA* (Fig. 2a and Supplementary Fig. 6) and above 35 nM for *dddW* (Fig. 4b, d and Supplementary Fig. 13). Furthermore,  $K_m$  values of DMSP degradation enzymes (5.4 mM for DmdA<sup>33</sup> and 4.50–8.68 mM for DddW<sup>34</sup>) are orders of magnitude above the mean seawater concentrations of DMSP (16.91  $\pm$  22.17 nM<sup>8</sup>), further supporting the notion that bacteria are adapted to exploit sporadic encounters with DMSP hotspots<sup>35</sup> as we observed by single-cell imaging.

Identifying the environmental determinants of microbial DMSP cycling is key in understanding their effects on global climate and biogeochemical cycles. Two interconnected concepts, the DMSP Availability Hypothesis<sup>6</sup> and the Bacterial Switch<sup>7</sup>, were proposed nearly two decades ago to explain the interplay between the two DMSP degradation pathways and the factors leading to the production of DMS, but have remained largely hypothetical. The present study offers the first direct evidence that the ambient concentration of DMSP regulates the relative (i.e., cleavage-to-demethylation ratios; Figs. 3, 4), rather than mutually exclusive, expression of demethylation and cleavage pathways. We observed that elevated concentrations of DMSP (>10  $\mu\text{M}$ ), which are typically found in microscale hotspots, shift bacterial DMSP degradation toward cleavage and are ultimately expected to increase the bacterial production and release of DMS. Thus, we propose that the concentrations of DMSP that are most relevant for the bacterial production of DMS, and ultimately for global sulfur cycling and for the production of DMS-derived

cloud condensing nuclei, may not be the levels present in bulk seawater, but instead those existing in microscale hotspots. This points to the importance of understanding the relative contribution of DMSP catabolism rates in hotspots compared to the bulk seawater, and the need to develop more realistic microscale methods to quantify the utilization and fate of this ubiquitous and important marine compound.

## Methods

**Construction of tricolor fluorescent reporter strains.** Tricolor fluorescent reporters were constructed in the marine model organism *R. pomeroyi* DSS-3 (wild-type strain, a gift from Prof. M. A. Moran, University of Georgia) to visually report expression of DMSP degradation genes (*dddW* and *dmdA*). *DddW* was chosen due to its strong upregulation response to DMSP reported in previous transcriptomic studies<sup>11,17</sup>, which suggests that *DddW* is the primary DMSP lyase in *R. pomeroyi* DSS-3. Three fluorescent proteins were chosen for brightness, monomeric structures, and spectral separation: mTFP1 (teal)<sup>36</sup>; mVenus-Q69M (yellow)<sup>37</sup>, which is the mVenus YFP<sup>38</sup> modified with a Q69M mutation to reduce environmental sensitivity; and mKate2 (far-red)<sup>39</sup>. To control for bias caused by the choice of color of fluorescent protein (RFP or TFP) fused to each promoter region, we constructed two *R. pomeroyi* reporter strains (Goofy and Regular) in which we interchanged the fluorescent proteins fused to *dmdA* and *dddW* promoter regions (Fig. 1a, b).

Three promoter fusion cassettes were inserted into a single vector backbone (pBBR1MCS-2, a 5.144 kb, broad-host-range, medium copy number plasmid with a kanamycin resistance cassette and origin of replication pBBR1, originally isolated from *Bordetella bronchiseptica*)<sup>40,41</sup> to enable gene expression readouts from individual cells (Supplementary Fig. 14): a *dmdA* promoter reporter cassette; a *dddW* promoter reporter cassette; and a constitutively expressed *yfp* cassette (Fig. 1a, b). The 500 bp sequence upstream of the *dddW* gene and 222 bp upstream of the *dmdA* gene in the *R. pomeroyi* DSS-3 genome were determined as putative promoter regions and used to construct promoter reporter cassettes. A strong, constitutive synthetic promoter  $P_{A1/04/03}$  (an *E. coli lac* promoter derivative)<sup>42,43</sup> controlled the expression of YFP, whose intensity was utilized as a proxy for cell viability, plasmid copy number, and metabolic activity (Supplementary Fig. 15). Transcriptional terminators (RNAI, TSAL, TR2-17, TL17, BS7, and T7TE+) and spacer regions between promoter fusion cassettes were cloned from plasmid pZS2-123<sup>44</sup>. As an intermediate step in the construction of the tricolor reporter strains, a derivative of pZS2-123 (with its original promoters replaced with 500 bp sequence upstream of *dmdA* or *dddW* genes), pZS2-200, was built using restriction enzymes: AvrII, XmaI, XhoI, BamHI, XmnI, and SalI (New England Biolabs).

**Construction of control reporter strains.** Truncated versions of the tricolor reporters (Supplementary Fig. 1), each of which contained one of the promoter fusion cassettes, were built to test the effect of including three promoter fusion cassettes within one DNA construct (Supplementary Fig. 2). We also constructed constitutively fluorescent, single-color *R. pomeroyi* strains (Supplementary Fig. 1) to quantify spectral leakage amongst fluorescent protein colors, and to calculate the spectral leakage correction matrix, *B* (Supplementary Note 1 and Supplementary Fig. 16).

**DNA assembly.** All *R. pomeroyi* strains and plasmids engineered in this study are listed in Supplementary Table 1 and Supplementary Fig. 1. For assembly of the promoter fusion cassettes into the pBBR1MCS-2 vector, DNA fragments containing overlapping regions (~30 bp) were amplified with 25 cycles of polymerase chain reaction (PCR) using KAPA HiFi HotStart ReadyMix (Kapa Biosystems) with primers listed in Supplementary Table 2. Putative promoter regions of *dmaA* and *dddW* were amplified from *R. pomeroyi* DSS-3 genomic DNA isolated with DNeasy Blood & Tissue Kits (Qiagen). Plasmids that were used as PCR templates (Supplementary Table 3) were isolated using the QIAprep Spin Miniprep Kit (Qiagen). Primers for vector backbone amplification were designed to eliminate the multiple cloning site (MCS) within the *lacZα* gene in the pBBR1MCS-2 vector to prevent fusion with the β-galactosidase α-peptide. Two extra stop codons (TAA-TAA) were added to each fluorescent protein gene sequence through primer design.

DNA fragments were assembled using NEBuilder HiFi DNA Assembly Master Mix (New England Biolabs). Assembled plasmids were transformed into electrocompetent *E. coli* (NEB 10-beta; New England Biolabs) through electroporation (Gene Pulser Xcell, Bio-Rad), positive colonies were picked on X-Gal/IPGTG Luria Broth (LB) plates, and correct assembly of DNA fragments was confirmed through sequencing of purified plasmids using diagnostic primers listed in Supplementary Table 2.

**Transformation of *R. pomeroyi* through conjugation.** Reporter plasmids were transformed into *R. pomeroyi* DSS-3 through a triparental conjugation method, which was found to be ideal due to the large sizes of our reporter plasmids (up to 7.974 kb). Overnight liquid culture of wild-type *R. pomeroyi* was prepared in half-strength YTSS (1/2 YTSS) containing (500 ml<sup>-1</sup>) 2 g yeast extract (BD Biosciences), 1.25 g tryptone (BD Biosciences), 10 g sea salts (Sigma-Aldrich). In addition, overnight liquid cultures of helper *E. coli* containing the pRK600 plasmid<sup>45</sup> (15 μg ml<sup>-1</sup> chloramphenicol) and donor *E. coli* containing a constructed reporter plasmid (50 μg ml<sup>-1</sup> kanamycin) were prepared in LB. *E. coli* cultures were washed twice in 1/2 YTSS medium to eliminate antibiotics. The following mixture was concentrated and resuspended in a final volume of 100 μl 1/2 YTSS medium: 2 ml overnight culture of *R. pomeroyi*, 200 μl of washed overnight culture of helper *E. coli*, and 200 μl of washed overnight culture of donor *E. coli*. 50 μl of this bacterial mixture was spotted on a 1/2 YTSS plate, and incubated overnight at 30 °C to allow mating to occur. Selection for plasmid-containing *R. pomeroyi* was achieved by re-streaking onto a 1/2 YTSS plate amended with kanamycin (50 μg ml<sup>-1</sup>) and potassium tellurite (50 μg ml<sup>-1</sup>; Fluorochem). Like many marine microorganisms<sup>46,47</sup>, *R. pomeroyi* was found in this study to be resistant to potassium tellurite, while *E. coli* is known to be sensitive to the oxidant mineral. Successfully transformed *R. pomeroyi* were confirmed through colony PCR and sequencing.

**Bacterial culture preparation for experiments.** A frozen glycerol stock of each *R. pomeroyi* reporter strain was streaked onto a half-strength YTSS (1/2 YTSS) culture plate containing (500 ml<sup>-1</sup>) 7.5 g agar (Bacto Agar, BD Biosciences), amended with 50 μg ml<sup>-1</sup> kanamycin sulfate (Sigma-Aldrich), and incubated at 30 °C for 48–72 h. A single colony was picked from the plate to inoculate 1 ml of 1/2 YTSS liquid medium amended with 25 μg ml<sup>-1</sup> kanamycin for overnight culture (~19 h) in the dark at 30 °C on an orbital shaker (200 rpm). When overnight cultures reached visible turbidity, subcultures were prepared by washing (6300 × g, 3 min) and diluting (1/75 vol/vol) overnight culture cells to a final volume of 1.5 ml in marine basal medium (MBM) consisting of 0.07 M Tris HCl (pH 7.5), 0.24 mM K<sub>2</sub>HPO<sub>4</sub>, 13.4 mM NH<sub>4</sub>Cl, 0.073 mM FeEDTA, 2% (wt/vol) sea salts, and 0.1% (vol/vol) vitamin solution<sup>48</sup>. D-glucose (10 mM) was provided as a sole amended carbon source in MBM, and kanamycin (25 μg ml<sup>-1</sup>) was added for plasmid retention. Initial OD<sub>700</sub> of 10 mM glucose MBM subcultures ranged from 0.04 to 0.05. After a 4-h incubation in similar conditions as overnight cultures, OD<sub>700</sub> decreased to 0.03 to 0.04, probably due to a decrease in cell size as cells transitioned from rich medium (elongated cells) to MBM (shortened cells).

To prepare for the low DMSP concentration (≤1 μM) experiment (Supplementary Fig. 7), several colonies of strain Regular cells on an agar plate were resuspended directly into MBM amended with 1 mM succinate and 50 μg ml<sup>-1</sup> kanamycin, and grown overnight at 30 °C in the light. The overnight culture was diluted (1/50 vol/vol) into fresh 1 mM succinate MBM with kanamycin (50 μg ml<sup>-1</sup>) and incubated for an additional 4 h. Similar to other time-lapse experiments, OD<sub>700</sub> was 0.3 before initiation of incubation with DMSP.

**Carbon sources test.** To assess the validity of engineered reporter strains, as well as to identify an appropriate negative control carbon source, *R. pomeroyi* reporter strains Regular and Goofy were incubated with a range of carbon sources, and their fluorescence response and growth were measured (Supplementary Fig. 3). Carbon sources chosen for this experiment were utilized in previous studies to cultivate *R. pomeroyi*. MBM solutions amended with 10 mM of the following carbon sources were prepared: DMSP (Tokyo Chemical Industry), sodium succinate dibasic hexahydrate (Sigma-Aldrich), sodium propionate (Sigma-Aldrich), sodium acetate (Sigma-Aldrich), sodium acrylate (Sigma-Aldrich), or D-glucose (Sigma-Aldrich). MBM solutions were filter sterilized (0.2 μm) after dissolution of carbon sources.

The 5% 1/2 YTSS was prepared with a dilution (1/20 vol/vol) of the rich medium in non-carbon amended MBM.

Several colonies of *R. pomeroyi* reporter strains on agar plates were washed and resuspended in non-carbon amended MBM. Resuspended cells (2 μl) were seeded into 0.75 ml of each carbon source MBM solution amended with 25 μg ml<sup>-1</sup> kanamycin. Incubations were performed in 2-ml microcentrifuge tubes (Eppendorf) in the dark at 30 °C with 200 rpm orbital shaking for 18.5 h before microscopy imaging.

Glucose was chosen as the most suitable negative control for the following reasons: it elicited no non-specific DMSP gene transcription response (Supplementary Fig. 3); its molecular weight is similar to DMSP; and the metabolic pathways of glucose and organosulfur compounds are distinct. The low DMSP concentration (≤1 μM) experiment (Supplementary Fig. 7) was the only instance in which succinate was used as the negative control, as it had been utilized in previous studies<sup>21,49</sup>. While succinate was also suitable as negative control (Supplementary Fig. 3), it produced slightly higher non-specific fluorescence response than glucose; thus, glucose, unless otherwise noted, was utilized as the negative control for all other experiments.

**Growth curves.** Growth curves of *R. pomeroyi* strains Regular and Goofy in different carbon sources (Supplementary Fig. 3) were measured in a flat-bottom 96-well plate (Thermo Fisher Scientific), containing 200 μl of carbon source-amended MBM per well in the absence of antibiotics. Each carbon source was prepared in triplicates, with corresponding blank wells in duplicates. Each well was inoculated with 2 μl of bacteria, grown overnight in 1/2 YTSS amended with 25 μg ml<sup>-1</sup> kanamycin, and washed and resuspended without dilution in non-carbon amended MBM. Optical density was measured at 700 nm (OD<sub>700</sub>) to avoid spectral interference from fluorescence. The plate was incubated at 25 °C, and OD<sub>700</sub> was measured every 1 h (3 min of fast orbital shaking before each time point) for 56 h using a Synergy HTX Multi-Mode Microplate Reader (BioTek Instruments).

**Microfluidic device fabrication.** The microfluidic device containing nine parallel observation chambers (Fig. 1c) was fabricated using soft lithography<sup>50</sup>. A mold for the observational chamber geometry was fabricated with SU8 on a silicon wafer. The microfluidic device was then created by casting polydimethylsiloxane (PDMS) (SYLGARD 184 Silicone Elastomer Kit; Dow Corning) onto the mold. The cured PDMS was then removed from the mold, perforated with inlet and outlet holes with a biopsy punch (1.5 mm diameter), and permanently fixed to a glass coverslip (60 mm × 24 mm; 0.17 ± 0.005 mm precision thickness; Carl Roth) by plasma bonding. Depth of each observation chamber was ~60 μm.

**Microscopy.** All experiments were performed using an inverted epifluorescence TE2000 microscope (Nikon) controlled through Nikon Elements software (unless otherwise specified). A Spectra X LED light source (Lumencore) provided single wavelength excitation illumination for fluorescence imaging (100% LED power unless otherwise indicated). The Perfect Focus System (Nikon) was engaged to maintain focus in time-lapse experiments. Three filter cubes (Chroma) were used for fluorescence imaging: a custom filter cube optimized for mKate2 RFP (ET580/25x excitation filter, T600lpxr band-pass filter, and ET645/75m emission filter), Chroma 49003 for YFP, and Chroma 49013 for TFP. Unless otherwise indicated, the excitation filter of each cube was removed for imaging to maximize fluorescence signal captured. At each field of view, phase contrast and fluorescence images were captured sequentially in the following order: phase contrast, red fluorescence channel (575 nm excitation), yellow fluorescence channel (508 nm excitation), and teal fluorescence channel (440 nm excitation). Bacteria were introduced into microfluidic devices, allowed to settle for 20–30 min, and imaged at the plane of the glass coverslip surface.

Images were acquired with an electron multiplying CCD (EMCCD) camera (iXon<sub>3</sub> 885; Andor Technology) (1004 × 1002 pixels; 8 μm pixel size) for the following experiments: time-lapse DMSP experiments in microfluidic chips; large-volume DMSP concentration measurement experiment (Supplementary Fig. 10); carbon sources test (Supplementary Fig. 3); DMSP uptake experiment (Supplementary Fig. 11); and phytoplankton co-incubation (Fig. 4 and Supplementary Fig. 12). For time-lapse DMSP experiments in microfluidic chips and the large-volume DMSP concentration measurement experiment, a 40× objective (CFI S Plan Fluor ELWD ADM 40×, correction collar adjusted to 0.17; Nikon) was used with electron multiplier gain at 3×, and the following exposure times: phase contrast (20 ms, 5% white LED power), red (100 ms), yellow (100 ms), and teal (200 ms). Imaging conditions for the carbon sources test were identical, except exposure time for teal fluorescence imaging was 100 ms. Time-lapse imaging for the DMSP uptake experiment was done in parallel with, but on a different microscope from, Raman microspectroscopy measurements (see below). Only phase contrast and teal fluorescence were acquired, with microscopy setup as described above. For phytoplankton co-incubation imaging, an oil-immersion 100× objective (CFI Plan Apo Lambda DM 100× Oil; Nikon) was used, without electron multiplier gain, with the following exposure times (total 240 ms per image) and LED powers: phase contrast, 60 ms, 10%; red, 100 ms, 100%; yellow, 40 ms, 50%; and teal, 40 ms, 100%.

Finally, images for the low DMSP concentration ( $\leq 1 \mu\text{M}$ ) experiment (Supplementary Fig. 7) were acquired with an sCMOS camera (Zyla 4.2; Andor Technology) (2048  $\times$  2048 pixels; 6.5  $\mu\text{m}$  pixel size). A 40 $\times$  objective (described above) was used, with the following camera exposure times: phase contrast, 9.8 ms, 10% white LED power; and all fluorescence channels, 200 ms.

**Image analysis.** Analysis of fluorescence images was performed in MATLAB (MathWorks) using an automated image segmentation and fluorescence quantification software developed in-house. Detailed descriptions of image processing and analysis methodologies for microfluidic and agarose pad co-incubation experiments are provided in Supplementary Notes 1 and 3, respectively. Briefly, cells were segmented by pixel intensity thresholding in phase contrast images. Background subtraction and spectral leakage correction were performed to enable accurate quantification of cellular fluorescence. Thresholding on YFP fluorescence intensity (proxy for metabolic activity) was applied to only include viable cells for further analyses. Finally, fluorescence signals in red and teal channels of each cell were normalized by the mean YFP signal at each time point of each experimental condition.

**DMSP pathway expression time-lapse experiment.** Each replicate experiment represents a biological replicate performed on a single microfluidic device containing nine observation chambers (Fig. 1c). For each replicate experiment, one of the two *R. pomeroyi* reporter strains (Regular or Goofy) was prepared for experimentation as described above. At the end of subculture incubation, cells were washed and concentrated by 4.5 $\times$  in non-carbon amended MBM amended with kanamycin (10  $\mu\text{g ml}^{-1}$ ), and distributed into nine separate microcentrifuge tubes (Eppendorf) representing each treatment condition. For each tested concentration of glucose or DMSP, a 10 $\times$  concentrated stock solution was prepared in non-carbon amended MBM amended with kanamycin (10  $\mu\text{g ml}^{-1}$ ). To initiate incubation, 10 $\times$  stock solutions were diluted to 1 $\times$  final concentration in the cell-containing MBM, resulting in a 4.05 $\times$  cumulative concentration of subcultured cells. Each observation chamber was populated with 12.5  $\mu\text{l}$  of treated cells. Inlet and outlet holes of observation chambers were sealed with clear tape to minimize evaporation. Since PDMS is a gas-permeable material, oxygen is not expected to be limited in our experimental setup. Cells in observation chambers were allowed to settle onto the glass coverslip surface with gravity for 20–30 min before initiation of image capture. Phase contrast and fluorescence images were captured at seven positions, determined manually before start of imaging, per observation chamber every 45 min for ~24 h. Replicate experiment 3 of strain Regular (Supplementary Figs. 4, 6, 15) contained 6 imaging positions (instead of 7) per observation chamber. All fluorescence kinetic experiments, except the low DMSP concentration ( $\leq 1 \mu\text{M}$ ) experiment, were conducted at room temperature (21  $^{\circ}\text{C}$ ) and in the dark. In the low DMSP concentration ( $\leq 1 \mu\text{M}$ ) experiment only (Supplementary Fig. 7), 1 mM succinate was used as negative control, all experimental conditions contained 50  $\mu\text{g ml}^{-1}$  kanamycin, and fluorescence was monitored by microscopy with image acquisition every 30 min for 7.4 h with a cage incubator set to 30  $^{\circ}\text{C}$ .

**Cultivation of phytoplankton.** The dinoflagellate *Breviolum* (strain CCMP2459, formally within genus *Symbiodinium*<sup>51</sup>) was chosen for its prolific production of DMSP. *Breviolum* cells were grown in sterile plastic culture flasks (Nunclon EasyFlasks, 25  $\text{cm}^3$  volume; Thermo Fisher Scientific) under a diel light cycle (14 h light:10 h dark, (100  $\mu\text{mol m}^{-2} \text{s}^{-1}$ )) in 30 ml *f/2* medium at 22  $^{\circ}\text{C}$ . Cells at 22 days post-inoculation (a 1:100 dilution into fresh medium) were harvested for experimentation at 14:00 in the afternoon. Cellular concentration was determined by counting in a microfluidic observation chamber (21 cells  $\mu\text{l}^{-1}$ ).

**Phytoplankton-bacteria co-incubation experiment.** Co-incubations between *Breviolum* cells and *R. pomeroyi* reporter strains Regular or Goofy were performed on agarose pads, which immobilized the algal cells and allowed them to establish their phycospheres (i.e., the immediate regions surrounding unicellular algae cells) through steady exudation. For agarose pad preparation, low melting temperature agarose (Promega) was combined with 1/2 YTSS medium at 15  $\text{mg ml}^{-1}$ , and gently dissolved in a microwave. After partial cooling, kanamycin was added at 25  $\mu\text{g ml}^{-1}$  final concentration. Rubber gaskets (0.5 mm thickness) were manually cut into square frames (~2  $\text{cm} \times 2 \text{ cm}$  inner square area) and placed on glass coverslips (22 mm  $\times$  50 mm; VWR). The inner square areas of rubber gaskets were filled with ~500  $\mu\text{l}$  melted agarose-kanamycin mixture. Agarose pads were allowed to cool and solidify for 1.5 h before seeding with *R. pomeroyi* strains.

Bacteria were first seeded onto agarose pads and allowed to grow for 24 h without phytoplankton. Overnight cultures of *R. pomeroyi* strains grown in 1/2 YTSS were washed and concentrated threefold in non-carbon amended MBM amended with 10  $\mu\text{g ml}^{-1}$  kanamycin. Ten microlitre of this concentrated cell mixture was spotted onto the center of each agarose pad, and loosely covered with a plastic lid (without contacting the agarose) to minimize evaporation. *R. pomeroyi* strains were allowed to grow in patches of monolayer cells on the agarose pads for 24 h at 30  $^{\circ}\text{C}$  in the light before *Breviolum* cells were added to initiate co-incubation.

In preparation for co-incubation with bacteria, *Breviolum* cells were washed and concentrated 20-fold in fresh *f/2* medium amended with 10  $\mu\text{g ml}^{-1}$  kanamycin.

Prepared *Breviolum* cells (10  $\mu\text{l}$ ) were spotted onto the middle of each agarose pad containing monolayer growth of *R. pomeroyi*. Co-incubation agarose pads were incubated at room temperature (21  $^{\circ}\text{C}$ ) in the dark, loosely covered with a plastic lid without contacting the agarose, for 24 h before imaging. Prior to imaging, a glass coverslip (60 mm  $\times$  24 mm; 0.17  $\pm$  0.005 mm precision thickness; Carl Roth) was placed onto the agarose pads carefully to avoid agitation of established phycospheres, and flipped onto the oil immersion objective for imaging. Only one time point (24 h) was taken for microscopy, to avoid microscopy light-induced cell stress that could alter the phycosphere profile.

To calculate the spectral leakage correction matrix ( $B_{\text{agarose}}$ ; Supplementary Note 1), different colors of single-color constitutive control strains of *R. pomeroyi* (Supplementary Fig. 1) were grown on separate agarose pads for 24 h without phytoplankton, and imaged as described above.

**Large-volume DMSP concentration measurement experiment.** To estimate the DMSP concentration evolution in microfluidic observation chambers over time, a large-volume (8 ml) experiment was performed to allow sampling for DMSP concentration measurements (Supplementary Fig. 10). The experiment, while larger in volume by ~800-times compared to microfluidic experiments, preserved cell-to-volume ratio at all steps in the protocol. Three representative initial concentrations of DMSP were chosen, each of which was incubated in triplicates: 1  $\mu\text{M}$ , 75  $\mu\text{M}$ , and 1 mM.

*R. pomeroyi* (strain Regular) was grown and prepared as described above, with modifications as described below. Three biological replicates (i.e., three different colonies as inocula) of overnight cultures were prepared in 2.5 ml of 1/2 YTSS rich medium per replicate. Overnight culture cells were washed and concentrated tenfold in non-carbon amended MBM. For each biological replicate, 153  $\mu\text{l}$  of concentrated overnight culture was used to inoculate subculture flasks containing 115 ml of 10 mM glucose MBM amended with 25  $\mu\text{g ml}^{-1}$  kanamycin. This led to a cumulative dilution factor of 1/75 (vol/vol) of overnight culture for subculture preparation, consistent with microfluidic experiments. Subcultures were incubated in the dark at 30  $^{\circ}\text{C}$  on an orbital shaker (200 rpm) for 4 h, at the end of which OD<sub>700</sub> was measured to be 0.02–0.04. A volume of 110 ml of subcultured cells per biological replicate was washed and concentrated fivefold in non-carbon amended MBM and 7.2 ml of this concentrated cells was allocated into each treatment flask of each biological replicate (150-ml glass Erlenmeyer flasks). The addition of 800  $\mu\text{l}$  concentrated DMSP solution stocks (10 $\times$  concentration, i.e., 10  $\mu\text{M}$ , 750  $\mu\text{M}$ , and 10 mM) and kanamycin (final concentration = 10  $\mu\text{g ml}^{-1}$ ) marked the initiation of incubation, with a starting volume of 8 ml. Final cumulative concentration from subcultured cells was 4.5 $\times$  (nearly consistent with microfluidic experiments). One replicate of blank control flasks (i.e., without cells) representing each DMSP concentration condition was also prepared. All experimental flasks were sealed and incubated in the dark at room temperature (21.4–22.8  $^{\circ}\text{C}$ ) and in the absence of agitation.

At each sampling time point, incubation flasks were swirled to resuspend sunken cells. From each flask, a 1.5-ml sample was taken for DMSP concentration measurement, and an additional 10- $\mu\text{l}$  sample was placed in a microfluidic observation chamber for microscopy observation (imaged as described above). The first time point (0 h) was taken from the blank control flasks, for measurement of initial DMSP concentration. Subsequent time points, at which samples were taken from blank control flasks as well as from all replicate experimental conditions, were approximately 2, 8, and 24 h after the start of incubation with DMSP.

Each sample was immediately centrifuged at 2500  $\times g$  for 3 min to remove cells from solution. One millilitre of the supernatant was placed in an acid-washed 5-ml glass scintillation vial containing 3 ml methanol (>99.9% HPLC gradient grade; VWR International). Sample vials were sealed and stored in the dark at 4  $^{\circ}\text{C}$  until DMSP concentration measurement using ultra-high-pressure liquid chromatography/high-resolution mass spectrometry (UHPLC/HRMS).

**Chromatography/high-resolution mass spectrometry.** To prepare samples for DMSP concentration measurements, 50  $\mu\text{l}$  of each sample (processed and stored as described above) was diluted with 100  $\mu\text{l}$  of a mixture of acetonitrile and water (9:1 v/v), centrifuged (4500  $\times g$ , 5 min), and the supernatant was used for UHPLC/HRMS measurements. All UHPLC/HRMS results were obtained on a Dionex Ultimate 3000 system (Thermo Scientific) coupled to a Q Exactive Plus Orbitrap mass spectrometer (Thermo Scientific).

UHPLC/HRMS quantification followed a previously reported protocol<sup>49</sup>: the eluent consisted of high-purity water with 2% acetonitrile and 0.1% formic acid (solvent A) and 90% acetonitrile with 10% 5 mmol l<sup>-1</sup> aqueous ammonium acetate (solvent B). The flow rate was set to 0.60 ml min<sup>-1</sup>. A linear gradient was used for separation with 100% solvent B (1 min), 20% B (6.5 min), 100% B (7.1 min), and 100% B (10 min). The LC separation column (SeQuant ZIC-HILIC column (5 mm, 2.1  $\times$  150 mm) equipped with a SeQuant ZIC-HILIC guard column (5 mm, 2.1  $\times$  20 mm)) was kept at 25  $^{\circ}\text{C}$ . Electrospray ionization was performed in positive mode ionization, recording the mass range from 75 to 200  $m/z$ , with the following parameters: capillary temperature 380  $^{\circ}\text{C}$ ; spray voltage 3000 V; sheath gas flow 60 arbitrary units; and aux gas flow 20 arbitrary units. The injection volume was 2  $\mu\text{l}$ .

Calibration curves for DMSP were recorded in triplicate using synthetic standards prepared as described in a previous study<sup>49</sup>. Calibration curve for DMSP:

area [DMSP] = 470,540c [DMSP in nM] with  $r = 0.9999$ . Data analyses were performed using the software Thermo Xcalibur version 3.0.63.

**Pre-exposure to sulfur experiment with Raman microspectroscopy.** Raman microspectroscopy was utilized to infer uptake of DMSP at the single-cell level by measuring the deuterium-labeling status of cells incubated with deuterated DMSP ( $^2\text{H}_6$ -DMSP), in which the two  $\text{CH}_3$  groups of the DMSP molecule were labeled with deuterium in a protocol previously reported<sup>52</sup> (Supplementary Fig. 11). Three incubation conditions were tested to probe the effect of sulfur saturation (due to pre-exposure of *R. pomeroyi* to 10 mM methionine) on DMSP uptake and cleavage pathway expression:  $^2\text{H}_6$ -DMSP without pre-exposure to methionine;  $^2\text{H}_6$ -DMSP with pre-exposure to methionine; and non-labeled DMSP without pre-exposure to methionine (negative control for Raman microspectroscopy signal).

The *P<sub>addw::mTFP1</sub>* single-color *R. pomeroyi* reporter strain (cleavage pathway promoter-fusion with TFP) was used to avoid spectral interference with Raman microspectroscopy measurements (see below). An overnight culture in rich medium was prepared as described above. Two subculture conditions, with or without 10 mM L-methionine (Sigma-Aldrich), were prepared in 10 mM glucose MBM amended with 25  $\mu\text{g ml}^{-1}$  kanamycin, and incubated for 4 h as described above. Subcultured cells were washed, concentrated threefold, and resuspended in the appropriate solution for incubation: 1 mM  $^2\text{H}_6$ -DMSP MBM or 1 mM unlabeled DMSP MBM. All incubation conditions contained final concentrations of 1% methanol (solvent in which  $^2\text{H}_6$ -DMSP was dissolved) and 10  $\mu\text{g ml}^{-1}$  kanamycin. Treated cells were incubated at room temperature (22.8 °C) in the dark for 5.5 h before imaging and Raman microspectroscopy measurements.

We utilized a commercial confocal Raman microscope (LabRAM HR Evolution; HORIBA Scientific) based on an inverted microscope (Eclipse Ti; Nikon) with two cameras: an sCMOS camera (ORCA-Flash 4.0; Hamamatsu Photonics; field of view of 221.867  $\mu\text{m} \times 221.867 \mu\text{m}$ ; camera #1) for fluorescence and brightfield measurements with high sensitivity; and a CMOS camera (UI-3580LE; IDS Imaging Development Systems GmbH; camera #2) for positioning the Raman laser (532-nm neodymium-doped yttrium garnet—Nd:YAG) onto each cell. After incubation of cells with deuterated or non-deuterated DMSP as described above, a 4  $\mu\text{l}$ -droplet of cells was placed on a  $\text{CaF}_2$  coverslip (25 mm  $\times$  15 mm  $\times$  0.2 mm; Crystran), which was chosen to avoid background Raman signal noise<sup>53</sup>. A thin liquid column containing cells was achieved by separating the bottom ( $\text{CaF}_2$ ) and top (glass, 18 mm  $\times$  18 mm, no. 1 thickness) coverslips with 0.17 mm-thick glass coverslips placed along two opposing edges of the setup. As the Raman measurements took place at the surface of the  $\text{CaF}_2$  coverslip (i.e., 170  $\mu\text{m}$  away from glass), this arrangement generated sufficient thickness of liquid sample in the z-direction to prevent interference from the glass material of the top coverslip<sup>54</sup>. The coverslip setup was secured onto the microscope stage with the  $\text{CaF}_2$  surface interfacing with the 60 $\times$  water-immersion objective (Plan Apo IR 60XC 1.27 WI; Nikon), and was left undisturbed for 10 min to allow cells to settle to the bottom surface with gravity.

To measure the expression of the cleavage pathway, a fluorescence image in the teal channel (filter cube Chroma 49013 with excitation (445/30 nm) and emission (500/40 nm) filters installed to minimize interference with the Raman measurements performed with the 532 nm laser) was first acquired with camera #1 (50 ms exposure). A matching brightfield image (2 ms exposure, white LED light source) was also captured to visualize all cells. After fluorescence and brightfield image capture, the system was shifted to the Raman configuration (i.e., Raman laser and camera #2).

Single-cell Raman measurements were performed (1.5-s exposure time; 150- $\mu\text{m}$  pinhole size) by manually moving the xy-stage to align the Raman laser (532 nm, 400 mW power), as well as to focus it (confirmed via inspection with camera #2), onto each cell. For each experimental condition sample, Raman measurements of as many cells as possible were taken within 30 min ( $n = 32$ –52 cells per treatment condition). Each cell's Raman measurement and fluorescence signal were retrospectively matched using the brightfield image as the reference.

To determine the presence of DMSP uptake by cells, the DMSP uptake index ( $P_{\text{DMSP}}$ ) was computed for each cell

$$P_{\text{DMSP}} = \frac{I_{2040-2300}}{I_{2400-2450}},$$

where  $I_{2040-2300}$  (numerator) and  $I_{2400-2450}$  (denominator) represent the integrated intensities in the Raman spectrum regions between the wavenumbers 2040 and 2300  $\text{cm}^{-1}$  (the C–D peak whose intensity is affected by deuterium<sup>55</sup>) and between 2400 and 2450  $\text{cm}^{-1}$  (reference region where background intensity was low), respectively.

**Reporting summary.** Further information on research design is available in the Nature Research Reporting Summary linked to this article.

## Data availability

The data that support the findings of this study are available from the corresponding authors on request (total data size approximately 1 TB). The source data underlying Figs. 2, 3, and 4c–f are provided as a Source Data file.

## Code availability

All computer code (in MATLAB) developed for this study is available from the corresponding authors on request.

Received: 24 October 2019; Accepted: 20 March 2020;

Published online: 23 April 2020

## References

- Archer, S. D., Widdicombe, C. E., Tarran, G. A., Rees, A. P. & Burkill, P. H. Production and turnover of particulate dimethylsulphoniopropionate during a coccolithophore bloom in the northern North Sea. *Aquat. Microb. Ecol.* **24**, 225–241 (2001).
- Howard, E. C. et al. Bacterial taxa that limit sulfur flux from the ocean. *Science* **314**, 649–652 (2006).
- Moran, M. A. & Durham, B. P. Sulfur metabolites in the pelagic ocean. *Nat. Rev. Microbiol.* **17**, 665–678 (2019).
- Zubkov, M. V. et al. Linking the composition of bacterioplankton to rapid turnover of dissolved dimethylsulphoniopropionate in an algal bloom in the North Sea. *Environ. Microbiol.* **3**, 304–311 (2001).
- Simó, R., Archer, S. D., Pedrós-Alió, C., Gilpin, L. & Stelfox-Widdicombe, C. E. Coupled dynamics of dimethylsulphoniopropionate and dimethylsulfide cycling and the microbial food web in surface waters of the North Atlantic. *Limnol. Oceanogr.* **47**, 53–61 (2002).
- Kiene, R. P., Linn, L. J. & Bruton, J. A. New and important roles for DMSP in marine microbial communities. *J. Sea Res.* **43**, 209–224 (2000).
- Simó, R. Production of atmospheric sulfur by oceanic plankton: biogeochemical, ecological and evolutionary links. *Trends Ecol. Evol.* **16**, 287–294 (2001).
- Kettle, A. J. et al. A global database of sea surface dimethylsulfide (DMS) measurements and a procedure to predict sea surface DMS as a function of latitude, longitude, and month. *Glob. Biogeochem. Cycles* **13**, 399–444 (1999).
- Malin, G., Turner, S., Liss, P. & Holligan, P. Dimethylsulfide and dimethylsulphoniopropionate in the Northeast Atlantic during the summer coccolithophore bloom. *Deep Sea Res.* **40**, 1487–1508 (1993).
- Caruana, A. M. N. & Malin, G. The variability in DMSP content and DMSP lyase activity in marine dinoflagellates. *Prog. Oceanogr.* **120**, 410–424 (2014).
- Landa, M., Burns, A. S., Roth, S. J. & Moran, M. A. Bacterial transcriptome remodeling during sequential co-culture with a marine dinoflagellate and diatom. *ISME J.* **11**, 2677–2690 (2017).
- Varaljay, V. A. et al. Single-taxon field measurements of bacterial gene regulation controlling DMSP fate. *ISME J.* **9**, 1677–1686 (2015).
- Rinta-Kanto, J. M. et al. Analysis of sulfur-related transcription by *Roseobacter* communities using a taxon-specific functional gene microarray. *Environ. Microbiol.* **13**, 453–467 (2011).
- Moran, M. A., González, J. M. & Kiene, R. P. Linking a bacterial taxon to sulfur cycling in the sea: studies of the marine *Roseobacter* group. *Geomicrobiol. J.* **20**, 375–388 (2003).
- Moran, M. A. et al. Genome sequence of *Silicibacter pomeroyi* reveals adaptations to the marine environment. *Nature* **432**, 910–913 (2004).
- Curson, A. R. J., Todd, J. D., Sullivan, M. J. & Johnston, A. W. B. Catabolism of dimethylsulphoniopropionate: microorganisms, enzymes and genes. *Nat. Rev. Microbiol.* **9**, 849–859 (2011).
- Reisch, C. R. et al. Metabolism of dimethylsulphoniopropionate by *Ruegeria pomeroyi* DSS-3. *Mol. Microbiol.* **89**, 774–791 (2013).
- Young, J. W. et al. Measuring single-cell gene expression dynamics in bacteria using fluorescence time-lapse microscopy. *Nat. Protoc.* **7**, 80–88 (2012).
- Locke, J. C. W. & Elowitz, M. B. Using movies to analyse gene circuit dynamics in single cells. *Nat. Rev. Microbiol.* **7**, 383–392 (2009).
- Kentner, D. & Sourjik, V. Use of fluorescence microscopy to study intracellular signaling in bacteria. *Annu. Rev. Microbiol.* **64**, 373–390 (2010).
- Todd, J. D., Curson, A. R. J., Sullivan, M. J., Kirkwood, M. & Johnston, A. W. B. The *Ruegeria pomeroyi acul* gene has a role in DMSP catabolism and resembles *yhdH* of *E. coli* and other bacteria in conferring resistance to acrylate. *PLoS ONE* **7**, e35947 (2012).
- Kiene, R. P. Production of methanethiol from dimethylsulphoniopropionate in marine surface waters. *Mar. Chem.* **54**, 69–83 (1996).
- Andersen, J. B. et al. New unstable variants of green fluorescent protein for studies of transient gene expression in bacteria. *Appl. Environ. Microbiol.* **64**, 2240–2246 (1998).
- Seymour, J. R., Amin, S. A., Raina, J.-B. & Stocker, R. Zooming in on the phycosphere: the ecological interface for phytoplankton-bacteria relationships. *Nat. Microbiol.* **2**, 17065 (2017).
- Stocker, R. Marine microbes see a sea of gradients. *Science* **338**, 628–633 (2012).

26. Seymour, J. R., Simó, R., Ahmed, T. & Stocker, R. Chemoattraction to dimethylsulfoniopropionate throughout the marine microbial food web. *Science* **329**, 342–345 (2010).
27. Milo, R. & Phillips, R. *Cell Biology By The Numbers*. (Garland Science, 2016).
28. Sun, J. et al. The abundant marine bacterium *Pelagibacter* simultaneously catabolizes dimethylsulfoniopropionate to the gases dimethyl sulfide and methanethiol. *Nat. Microbiol.* **1**, 16065 (2016).
29. Tripp, H. J. et al. SAR11 marine bacteria require exogenous reduced sulphur for growth. *Nature* **452**, 741–744 (2008).
30. Broadbent, A. D. & Jones, G. B. DMS and DMSP in mucus ropes, coral mucus, surface films and sediment pore waters from coral reefs in the Great Barrier Reef. *Mar. Freshw. Res.* **55**, 849–855 (2004).
31. Wilson, W. H., Turner, S. & Mann, N. H. Population dynamics of phytoplankton and viruses in a phosphate-limited mesocosm and their effect on DMSP and DMS production. *Estuar. Coast. Shelf Sci.* **46**, 49–59 (1998).
32. Malin, G., Wilson, W. H., Bratbak, G., Liss, P. S. & Mann, N. H. Elevated production of dimethylsulfide resulting from viral infection of cultures of *Phaeocystis pouchetii*. *Limnol. Oceanogr.* **43**, 1389–1393 (1998).
33. Reisch, C. R., Moran, M. A. & Whitman, W. B. Dimethylsulfoniopropionate-dependent demethylase (DmdA) from *Pelagibacter ubique* and *Silicibacter pomeroyi*. *J. Bacteriol.* **190**, 8018–8024 (2008).
34. Brummett, A. E., Schnicker, N. J., Crider, A., Todd, J. D. & Dey, M. Biochemical, kinetic, and spectroscopic characterization of *Ruegeria pomeroyi* DddW—a mononuclear iron-dependent DMSP lyase. *PLoS ONE* **10**, e0127288 (2015).
35. Azam, F. & Hodson, R. Multiphasic kinetics for D-glucose uptake by assemblages of natural marine bacteria. *Mar. Ecol.* **6**, 213–222 (1981).
36. Ai, H., Henderson, J. N., Remington, S. J. & Campbell, R. E. Directed evolution of a monomeric, bright and photostable version of *Clavularia* cyan fluorescent protein: structural characterization and applications in fluorescence imaging. *Biochem. J.* **400**, 531–540 (2006).
37. Griesbeck, O., Baird, G. S., Campbell, R. E., Zacharias, D. A. & Tsien, R. Y. Reducing the environmental sensitivity of yellow fluorescent protein. *J. Biol. Chem.* **276**, 29188–29194 (2001).
38. Kremers, G.-J., Goedhart, J., van Munster, E. B. & Gadella, T. W. J. Jr. Cyan and yellow super fluorescent proteins with improved brightness, protein folding, and FRET Förster radius. *Biochemistry* **45**, 6570–6580 (2006).
39. Shcherbo, D. et al. Far-red fluorescent tags for protein imaging in living tissues. *Biochem. J.* **418**, 567–574 (2009).
40. Kovach, M. E. et al. Four new derivatives of the broad-host-range cloning vector pBBR1MCS, carrying different antibiotic-resistance cassettes. *Gene* **166**, 175–176 (1995).
41. Antoine, R. & Locht, C. Isolation and molecular characterization of a novel broad-host-range plasmid from *Bordetella bronchiseptica* with sequence similarities to plasmids from Gram-positive organisms. *Mol. Microbiol.* **6**, 1785–1799 (1992).
42. Lanzer, M. & Bujard, H. Promoters largely determine the efficiency of repressor action. *Proc. Natl Acad. Sci. USA* **85**, 8973–8977 (1988).
43. Lamberts, L., Sternberg, C. & Molin, S. Mini-Tn7 transposons for site-specific tagging of bacteria with fluorescent proteins. *Environ. Microbiol.* **6**, 726–732 (2004).
44. Cox, R. S. III, Dunlop, M. J. & Elowitz, M. B. A synthetic three-color scaffold for monitoring genetic regulation and noise. *J. Biol. Eng.* **4**, 10 (2010).
45. Kessler, B., de Lorenzo, V. & Timmis, K. N. A general system to integrate *lacZ* fusions into the chromosomes of Gram-negative eubacteria: regulation of the *Pm* promoter of the *TOL* plasmid studied with all controlling elements in monocopy. *Mol. Genet. Genomics* **233**, 293–301 (1992).
46. Taylor, D. E. Bacterial tellurite resistance. *Trends Microbiol.* **7**, 111–115 (1999).
47. Ollivier, P. R. L. et al. Volatilization and precipitation of tellurium by aerobic, tellurite-resistant marine microbes. *Appl. Environ. Microbiol.* **74**, 7163–7173 (2008).
48. González, J. M., Mayer, F., Moran, M. A., Hodson, R. E. & Whitman, W. B. *Microbulbifer hydrolyticus* gen. nov., sp. nov., and *Marinobacterium georgiense* gen. nov., sp. nov., two marine bacteria from a lignin-rich pulp mill waste enrichment community. *Int. J. Syst. Bacteriol.* **47**, 369–376 (1997).
49. Thume, K. et al. The metabolite dimethylsulfoxonium propionate extends the marine organosulfur cycle. *Nature* **563**, 412–415 (2018).
50. Xia, Y. & Whitesides, G. M. Soft lithography. *Annu. Rev. Mater. Sci.* **28**, 153–184 (1998).
51. LaJeunesse, T. C. et al. Systematic revision of Symbiodiniaceae highlights the antiquity and diversity of coral endosymbionts. *Curr. Biol.* **28**, 2570–2580 (2018).
52. Spielmeier, A. & Pohnert, G. Direct quantification of dimethylsulfoniopropionate (DMSP) with hydrophilic interaction liquid chromatography/mass spectrometry. *J. Chromatogr. B* **878**, 3238–3242 (2010).
53. Chrimes, A. F., Khoshmanesh, K., Stoddart, P. R., Mitchell, A. & Kalantar-zadeh, K. Microfluidics and Raman microscopy: current applications and future challenges. *Chem. Soc. Rev.* **42**, 5880–5906 (2013).
54. Lee, K. S. et al. An automated Raman-based platform for the sorting of live cells by functional properties. *Nat. Microbiol.* **4**, 1035–1048 (2019).
55. Berry, D. et al. Tracking heavy water (D<sub>2</sub>O) incorporation for identifying and sorting active microbial cells. *Proc. Natl Acad. Sci. USA* **112**, E194–E203 (2015).

## Acknowledgements

The authors thank F. Moser and Prof. C.A. Voigt (MIT) for assisting in reporter construction; Prof. C.R. Reisch (University of Florida) for discussions on genetic design of reporters; G. D'Souza (ETH Zurich) for providing fluorescent protein genes; Prof. M.E. Kovach (Baldwin Wallace University) for providing pBBR1MCS cloning vectors; and A.S. Burns (Georgia Tech) for assisting in *R. pomeroyi* transformations. We thank Prof. L. Behrendt (Uppsala University) for *Breviolum* cell culture; Prof. F. Menolascina (University of Edinburgh) for assisting in development of the image analysis software; and F.J. Peudecerf for assisting with microscopy imaging. We also thank Prof. D.A. Lauffenburger, Prof. K. Ribbeck (MIT), C.S. Smillie (Broad Institute), and U. Alcolombri (ETH Zurich) for scientific discussions. This research was funded by a Gordon and Betty Moore Foundation Marine Microbiology Initiative Investigator Award (GBMF3783) to R.S., a grant from the Simons Foundation through the Principles of Microbial Ecosystems (PriME) collaboration (542395) to R.S., and a National Science Foundation Graduate Research Fellowship (Grant no. 1122374) to C.G. J.-B.R. was supported by Australian Research Council fellowship DE160100636. We acknowledge the International Max Planck Research School “The Exploration of Ecological Interactions with Molecular and Chemical Techniques” for a fellowship to S.F., and the German Research Foundation for funding within the framework of the Cluster of Excellence Balance of the Microverse EXC 2051 to G.P.

## Author contributions

J.R.S., J.-B.R., and R.S. designed the study. C.G. constructed the reporter strains and performed the microfluidic and agarose pad experiments. C.G., and K.S.L. performed the Raman microspectroscopy experiments. C.G., S.F., and G.P. performed the large-volume DMSP concentration measurement experiment. C.G., V.I.F., and R.S. created the image analysis software. C.G., V.I.F., J.R.S., J.-B.R., and R.S. wrote the paper. All authors edited the paper before submission.

## Competing interests

The authors declare no competing interests.

## Additional information


Supplementary information is available for this paper at <https://doi.org/10.1038/s41467-020-15693-z>.

Correspondence and requests for materials should be addressed to J.-B.R. or R.S.

Peer review information *Nature Communication* thanks Scott Gifford and other, anonymous, reviewers for their contributions to the peer review of this work.

Reprints and permission information is available at <http://www.nature.com/reprints>

Publisher's note Springer Nature remains neutral with regard to jurisdictional claims in published maps and institutional affiliations.

 **Open Access** This article is licensed under a Creative Commons Attribution 4.0 International License, which permits use, sharing, adaptation, distribution and reproduction in any medium or format, as long as you give appropriate credit to the original author(s) and the source, provide a link to the Creative Commons license, and indicate if changes were made. The images or other third party material in this article are included in the article's Creative Commons license, unless indicated otherwise in a credit line to the material. If material is not included in the article's Creative Commons license and your intended use is not permitted by statutory regulation or exceeds the permitted use, you will need to obtain permission directly from the copyright holder. To view a copy of this license, visit <http://creativecommons.org/licenses/by/4.0/>.

© The Author(s) 2020

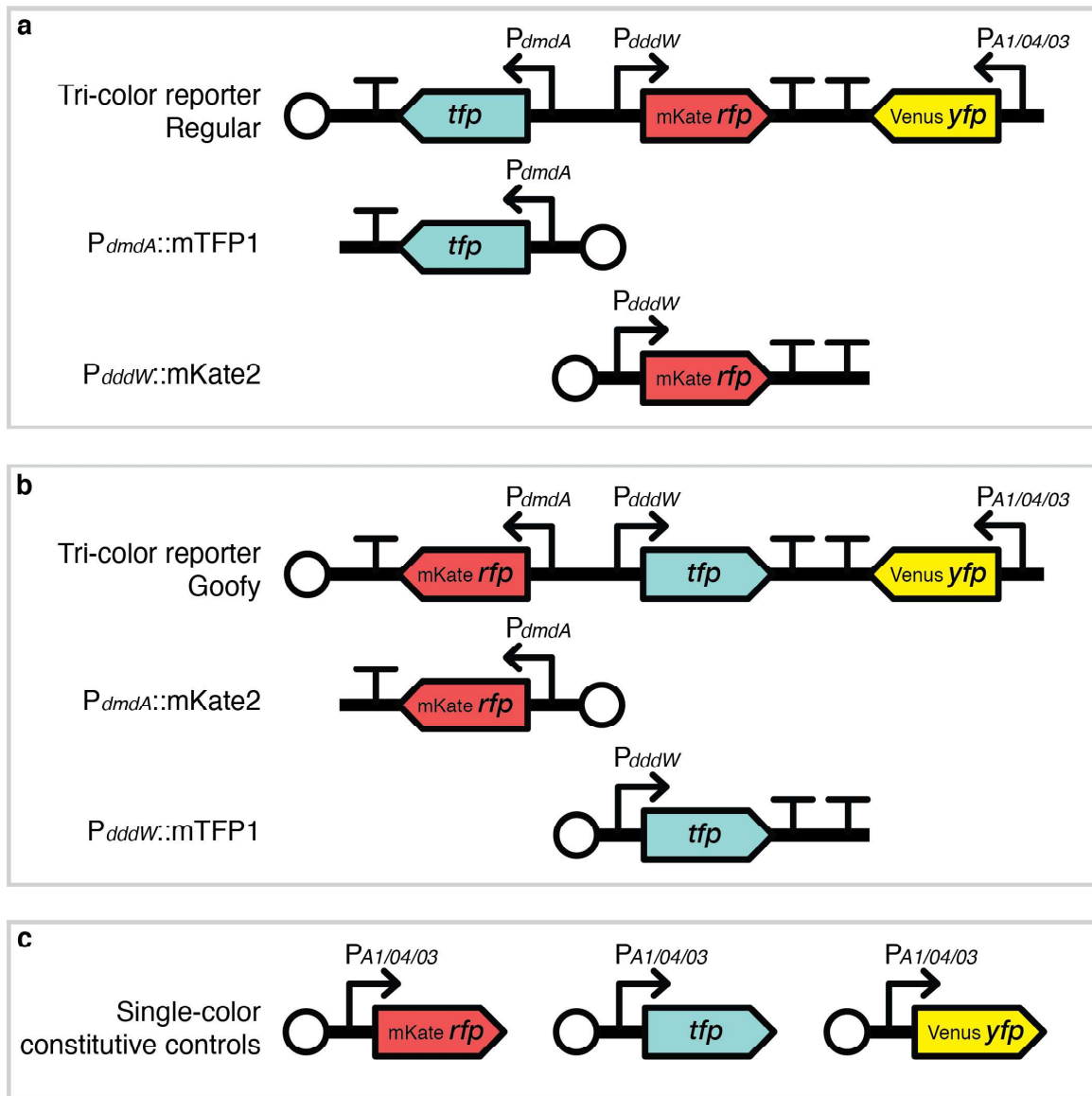
Supplementary Information for

**Single-cell bacterial transcription measurements reveal the importance of  
dimethylsulfoniopropionate (DMSP) hotspots in ocean sulfur cycling**

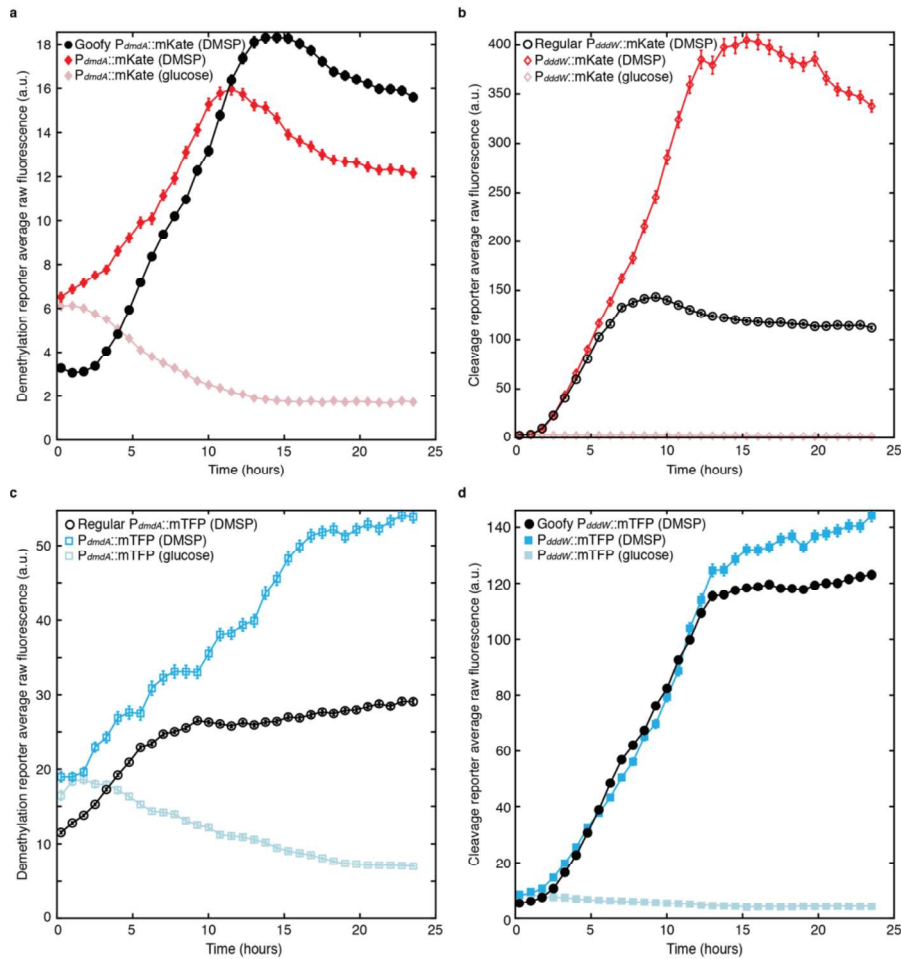
by

*Gao et al.*

## Supplementary Figures

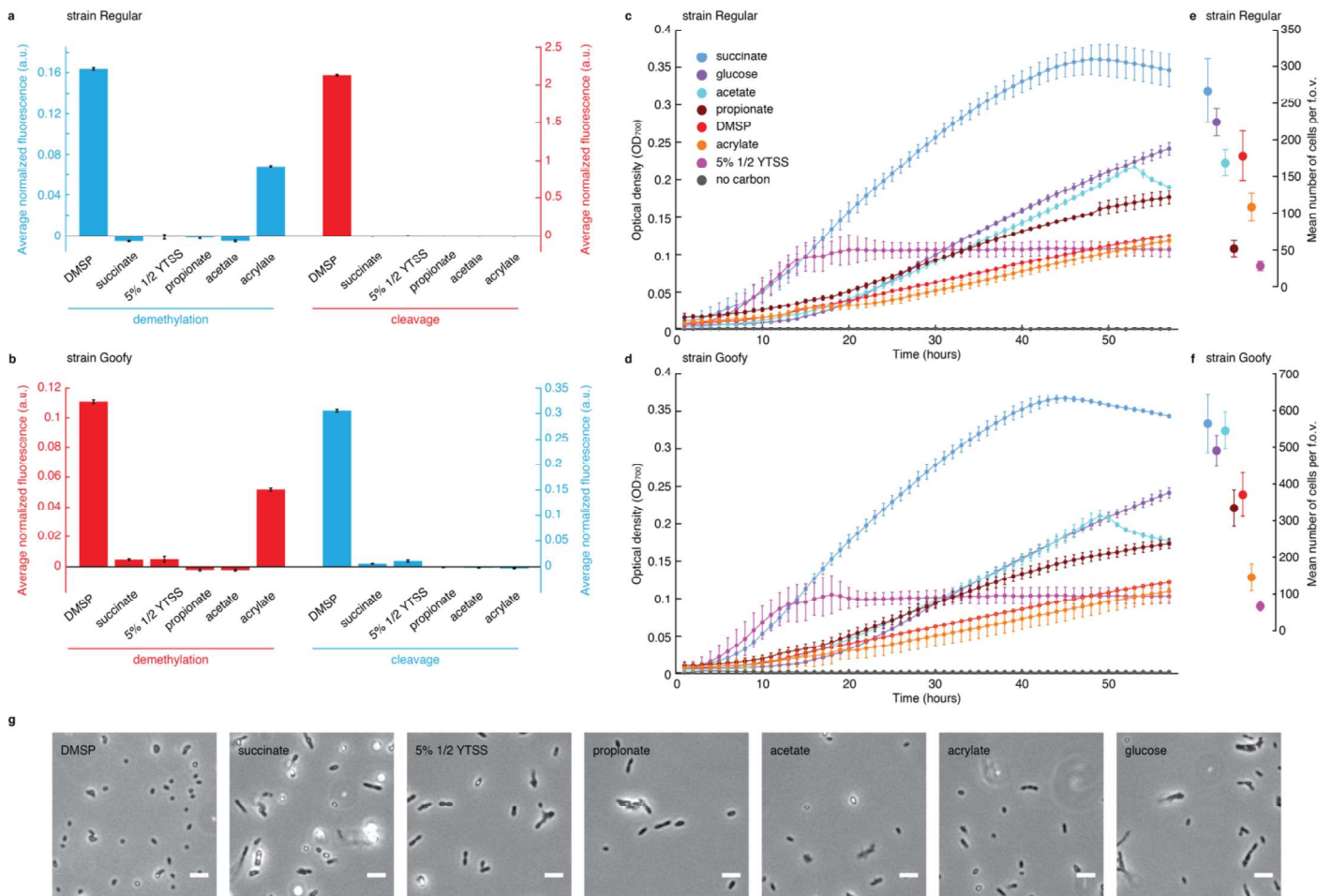


**Supplementary Fig. 1** All engineered fluorescent *R. pomeroyi* DSS-3 strains used in this study. Two tricolor reporter strains, Regular (**a**) and Goofy (**b**), with interchanged colors of fluorescent proteins fused to *dmdA* and *dddW* promoter regions were built to control for spectral bias during fluorescence intensity quantification. Four single-color reporter strains, representing truncated versions Regular and Goofy, were built to verify that incorporating three promoter fusion cassettes within one DNA construct did not affect our conclusions (Supplementary Fig. 2):  $P_{dmdA}::mTFP1$  and  $P_{dddW}::mKate2$  (truncated Regular, **a**) and  $P_{dmdA}::mKate2$  and  $P_{dddW}::mTFP1$  (truncated Goofy, **b**). Finally, a spectral leakage correction matrix,  $B$  (Supplementary Note 1), was calculated using images of constitutively fluorescent single-color control strains (**c**). Vector backbone: pBBR1MCS-2 with origin of replication pBBR1 (open circles).

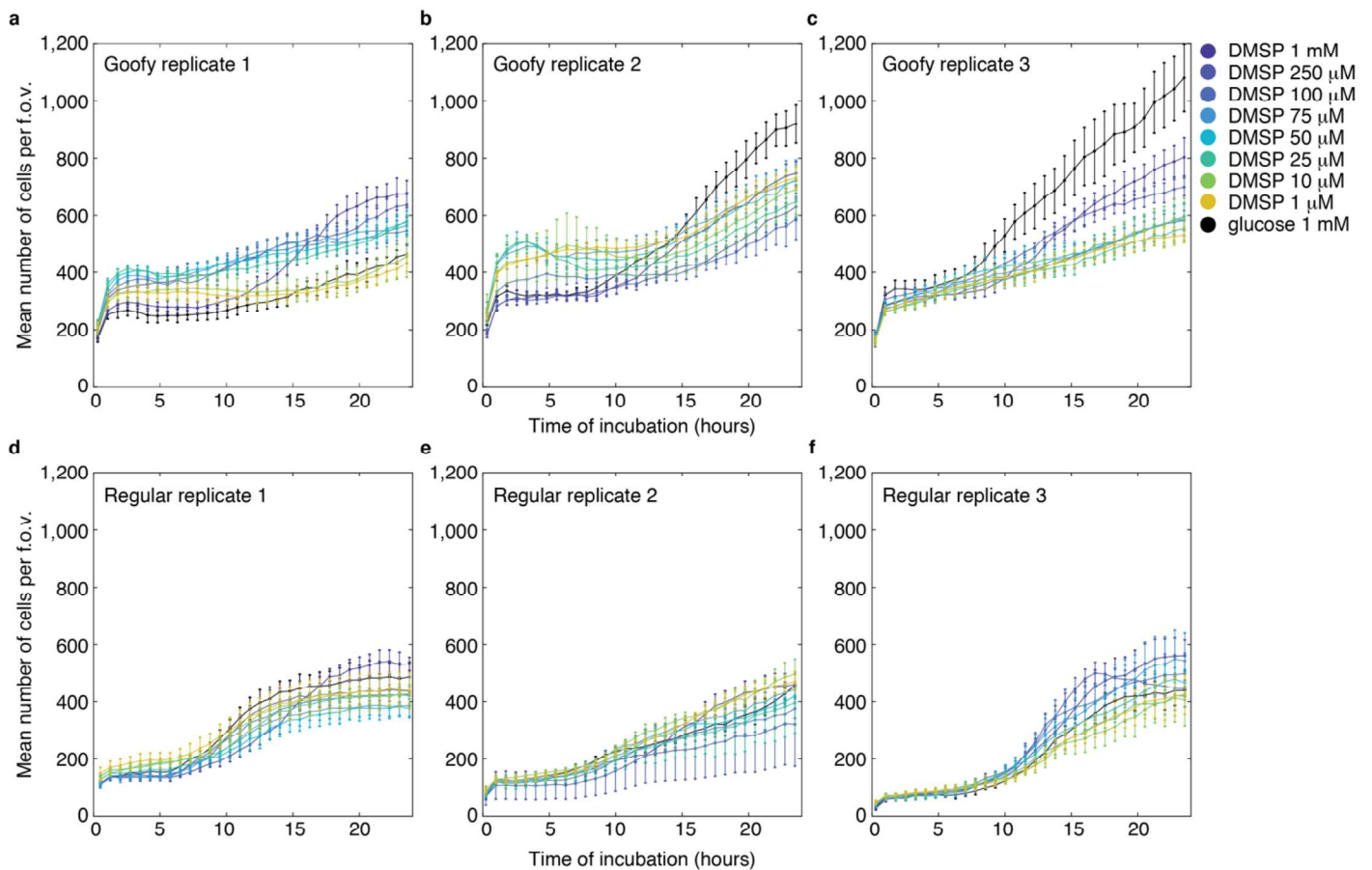


**Supplementary Fig. 2** Tricolor and truncated single-color reporter strains yield similar fluorescence responses in the presence of DMSP. To confirm that the incorporation of three promoter fusion cassettes within one DNA construct (*i.e.*, in tricolor reporter strains Regular and Goofy) did not affect our overall conclusions, four single-color reporter strains, representing truncated versions of tricolor reporter strains Regular and Goofy, were incubated with DMSP or glucose (1 mM), and their fluorescence signals were recorded:  $P_{dmdA}::mKate2$  (a);  $P_{dddW}::mKate2$  (b);  $P_{dmdA}::mTFP1$  (c); and  $P_{dddW}::mTFP1$  (d). Tricolor reporters Goofy (a,d) and Regular (b,c) were also incubated with DMSP in the same experiment for comparison. Image segmentation and background subtraction were performed as described in Methods. For tricolor reporters only, spectral leakage correction and YFP thresholding (at 25 a.u.) were performed, but normalization by constitutive YFP was not (*i.e.*, raw fluorescence). While absolute magnitudes and slopes of fluorescence responses were not identical between tricolor and truncated single-color reporter strains (probably due to slight differences in physiological states in different bacterial cultures), and the choice of fluorescent protein led to slight differences in the temporal evolution of fluorescence signals, the general patterns of fluorescence kinetics were preserved (*i.e.*, initial lag, followed by linear increase that flattens after ~8–17 h; further discussion in Supplementary Note 2). These conserved behaviors validate the tricolor reporters' design and accuracy of their fluorescence signals in reporting *dmdA* and *dddW* expression dynamics and relative expression levels. Data points and error bars represent mean  $\pm$  s.e.m. of raw fluorescence intensities of cells.

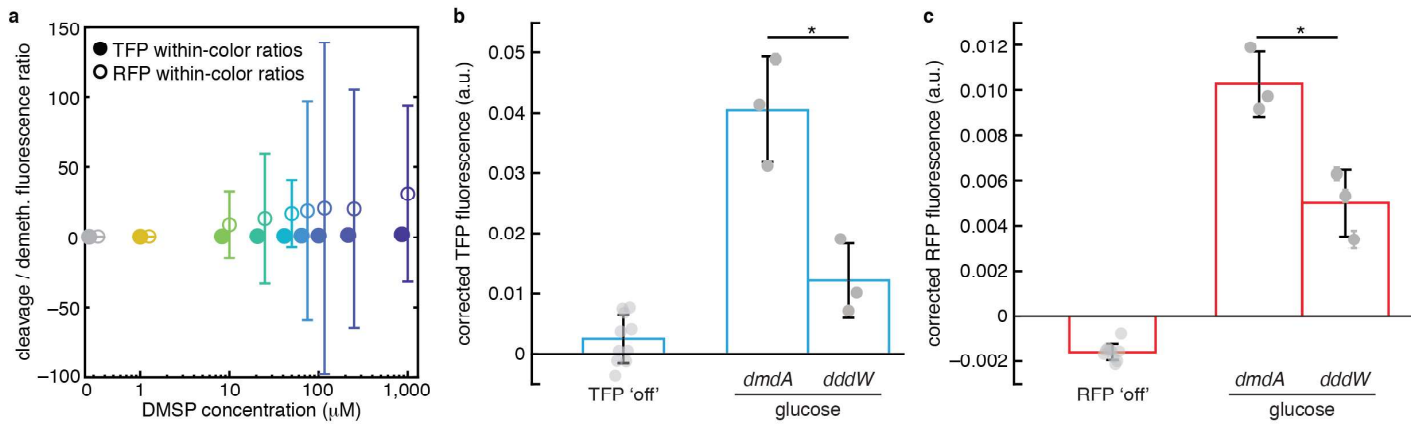




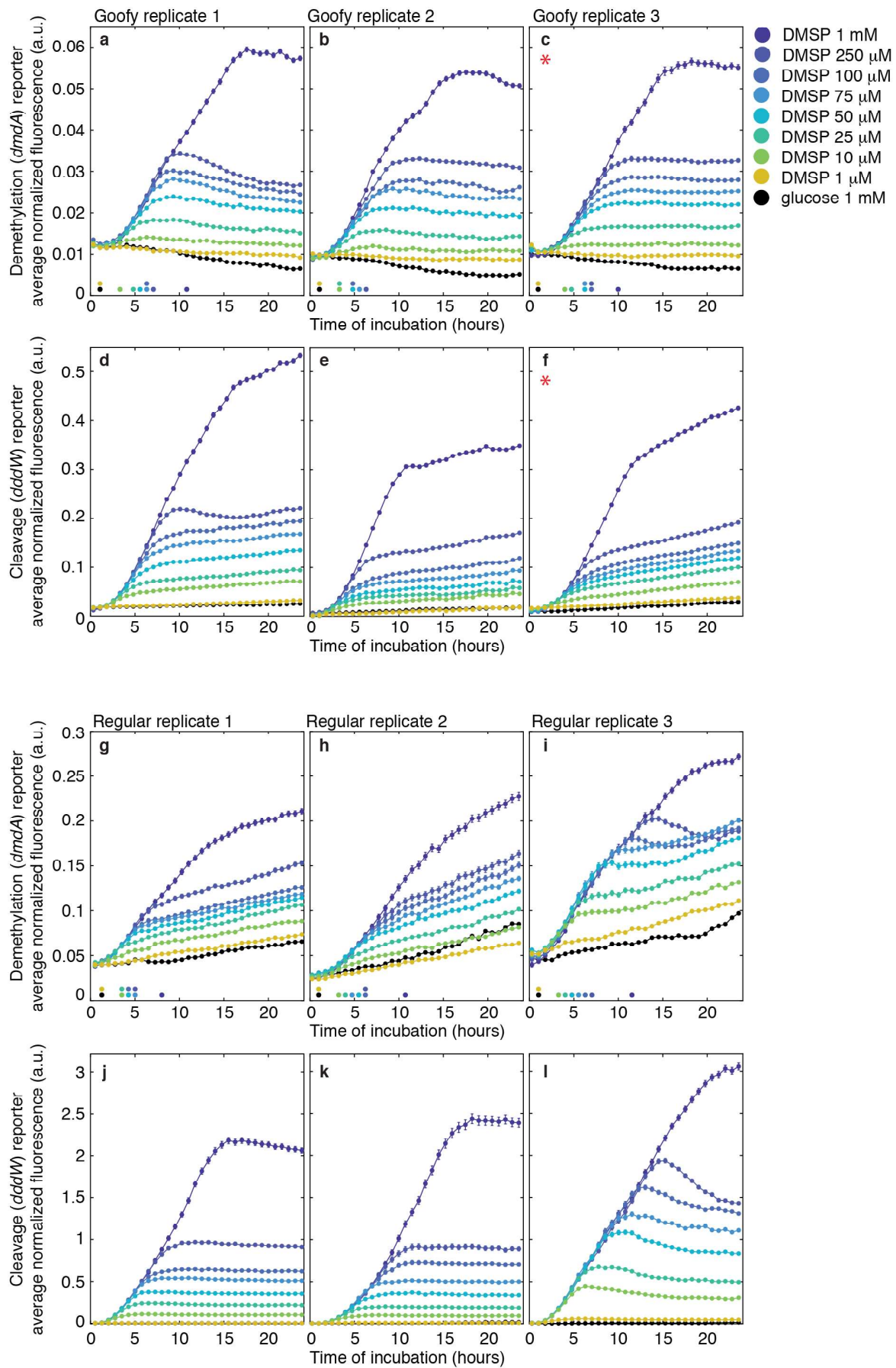
**Supplementary Fig. 3** Fluorescence response and growth of engineered *R. pomeroyi* reporters in diverse carbon sources. **a** and **b** Mean fluorescence intensities of strains Regular (**a**) and Goofy (**b**) after incubation with DMSP; succinate; 5% rich media (1/2 YTSS); propionate; acetate; acrylate; or glucose provided as sole amended carbon sources for 18.5 h in the presence of antibiotic pressure (25  $\mu$ M kanamycin; 30  $^{\circ}$ C; continuously shaken). All carbon sources were provided at 10 mM concentration except rich media (1/2 YTSS). YFP threshold of 10 a.u. was applied, and each cell's teal and red fluorescence were normalized by its own yellow fluorescence. After spectral leakage correction and background fluorescence subtraction, mean fluorescence values of glucose (used as negative controls in experiments) were subtracted from each cell's signals in corresponding color channels before calculation of mean; thus, some mean fluorescence values were negative. Bars and error bars represent mean  $\pm$  s.e.m. of fluorescence signals of cells. **c** and **d** Growth curves of *R. pomeroyi* reporter strains incubated with different organic compounds as sole amended carbon sources in the absence of antibiotic pressure (25  $^{\circ}$ C). Data points and error bars represent mean  $\pm$  s.d. of blank-subtracted triplicate wells. **e** and **f** Average number of YFP-positive cells per field of view (f.o.v.; 200  $\mu$ m  $\times$  200  $\mu$ m) in images acquired for fluorescence quantification (**a,b**). Example phase microscopy images are shown in **g** (strain Regular; scale bars, 5  $\mu$ m). Relative growth yields according to optical density (**c,d**; OD<sub>700</sub>) were consistent with cell counts (**e,f**) except in DMSP, due to their smaller cell size compared to bacteria grown in other carbon sources. Data points and error bars represent mean  $\pm$  s.d. of cell number in a field of view.



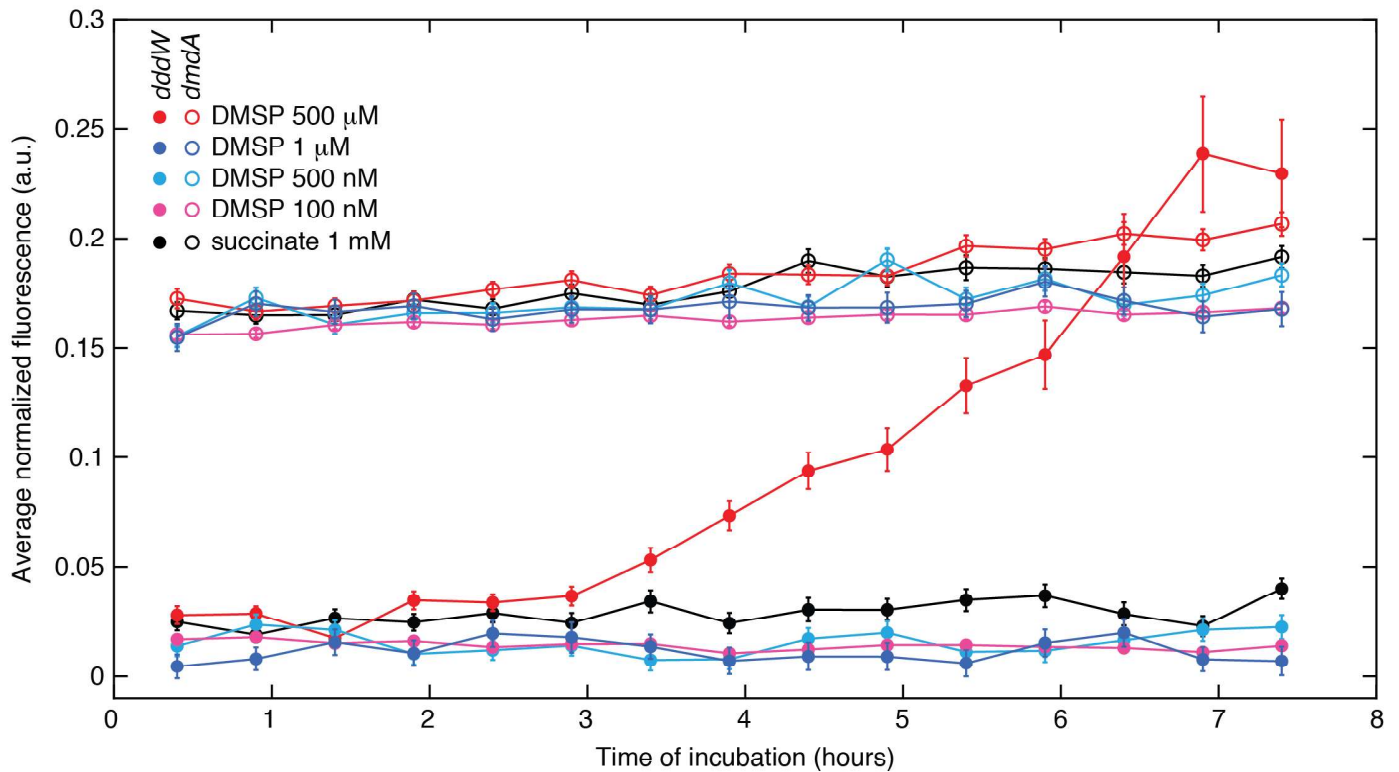
**Supplementary Fig. 4** Number of cells in time-lapse DMSP experiments performed in microfluidic chips (all replicate experiments). Mean number of cells per field of view (f.o.v.; 200 μm × 200 μm) in time-lapse DMSP experiments. Images were acquired at seven different fields of view per observation chamber (Fig. 1c) except strain Regular replicate experiment 3 (f), in which six fields of view were taken. Only cells that passed the YFP intensity threshold were included in the analysis. The large increase in cell number between the first and second time points is likely attributed to cells settling into the field of view due to gravity. On average, the number of cells in a field of view at the second time point was  $218 \pm 120$  (mean  $\pm$  s.d.) across replicate experiments. Replicate experiments correspond to those presented in Supplementary Fig. 6. Data points and error bars represent mean  $\pm$  s.d. across seven (or six for f) fields of view.



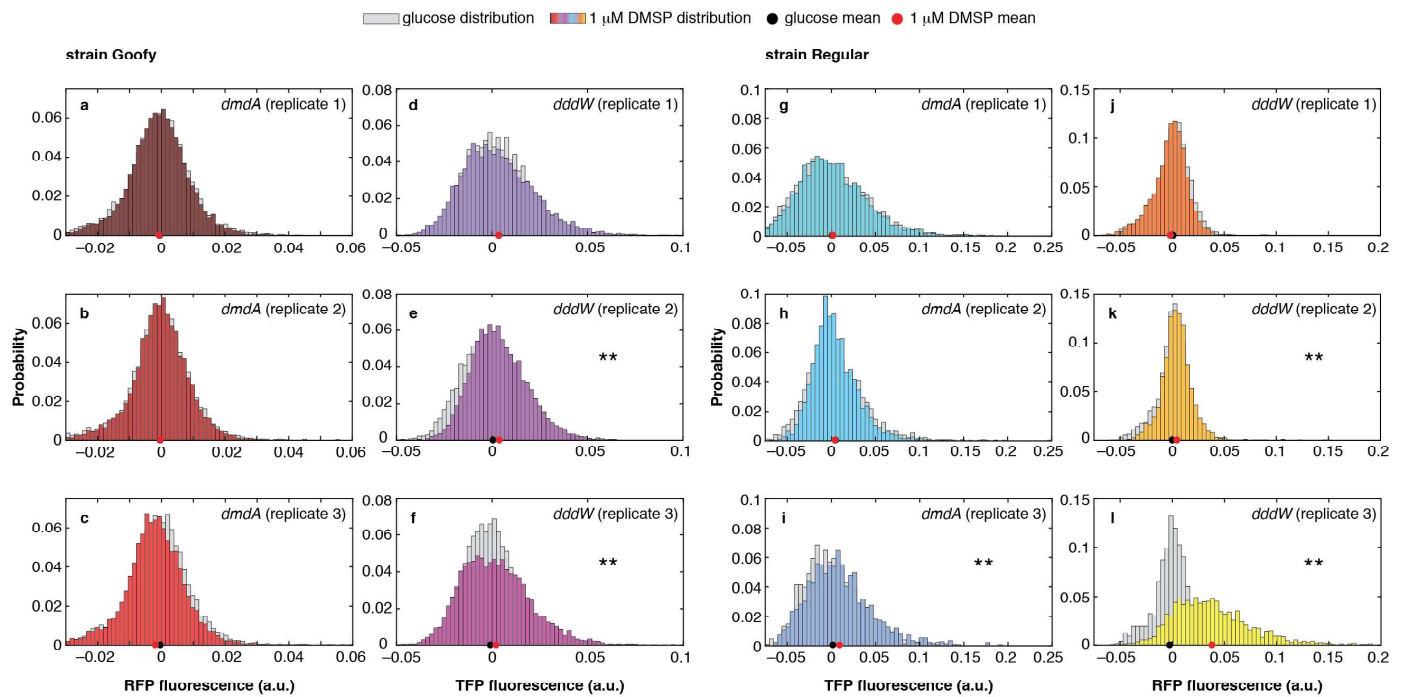
**Supplementary Fig. 5** Within-color comparisons of demethylation (*dmdA*) and cleavage (*dddW*) pathway reporters. **a** Cleavage-to-demethylation fluorescence ratios were calculated within each color (TFP/TFP (●) or RFP/RFP (○)) similarly to Fig. 3. At  $\geq 10 \mu\text{M}$  DMSP, the variability amongst replicate experiments resulted in large variance (error bars) for RFP within-color ratios (though not TFP, probably due to the relatively small signal values of TFP (Supplementary Fig. 6)). This result prevented within-color comparisons of pathway reporters except in glucose (**b,c**) and  $1 \mu\text{M}$  DMSP (similar values). Thus, across-color ratio calculation, which enabled comparisons of pathway expression within the same experiment, was employed in our study for consistency (Fig. 3). Error bars represent the variance of the cleavage-to-demethylation ratio calculated using Eq. S6 (Supplementary Note 3;  $n = 3$  for each reporter). **b** and **c** Average baseline fluorescence of demethylation and cleavage reporters incubated in glucose (cells aggregated over three time points,  $\sim 2.5\text{--}4\text{h}$ ). In glucose, baseline demethylation expression was significantly higher than that of cleavage (two-tailed *t*-tests; \*  $p \leq 0.05$ ; ratios 0.3 in TFP, **b**; 0.5 in RFP, **c**). Importantly, this higher baseline demethylation expression was conserved in both within-color and across-color ratios (0.15–1.0; Fig. 3). Fluorescence signals in glucose were significantly higher than the theoretical ‘off’ intensities of TFP ( $2.5 \pm 4.1 \times 10^{-3}$  a.u.) and RFP ( $-1.6 \pm 0.37 \times 10^{-3}$  a.u.), indicating that *dmdA* and *dddW* are expressed at a baseline level even in the absence of DMSP (two-tailed *t*-tests,  $p \leq 0.01$ ). Some theoretical ‘off’ intensities were slightly overcorrected to below zero due to background subtraction and spectral leakage correction (Supplementary Note 1). Each grey symbol represents a replicate experiment (symbols and error bars = mean  $\pm$  s.e.m. of fluorescence signals of cells), and each bar represents the average of replicate experiments (bars and error bars = mean  $\pm$  s.d. of replicate experiments,  $n = 3$ ).



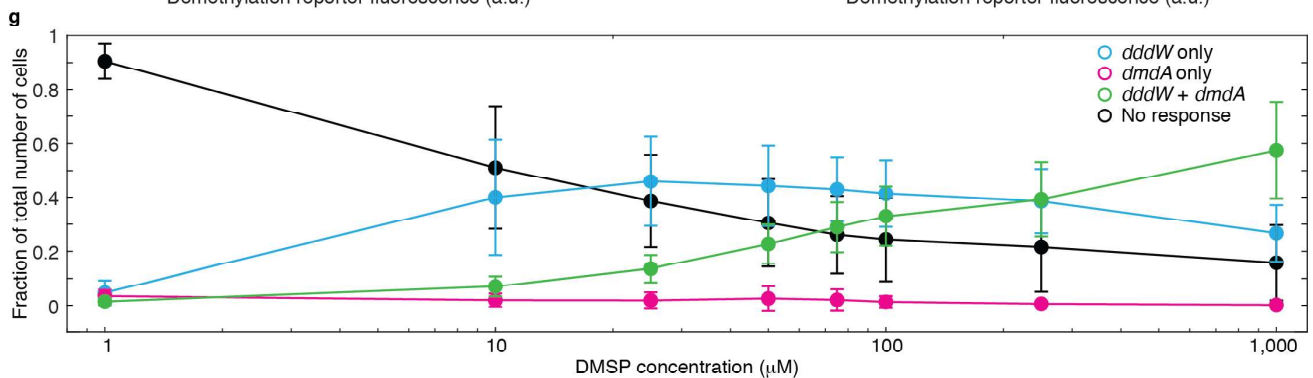
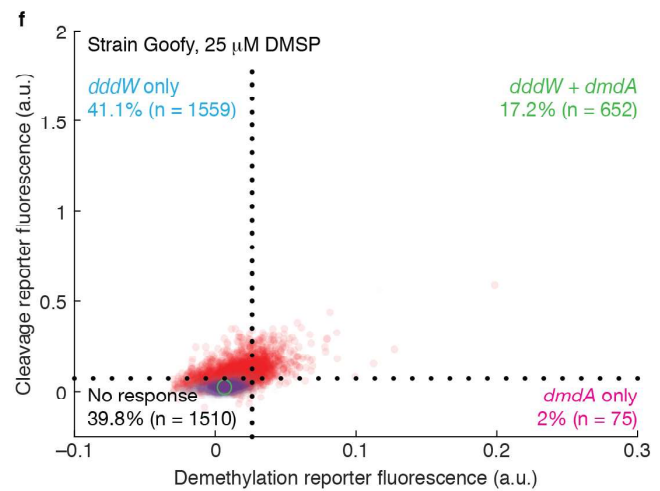
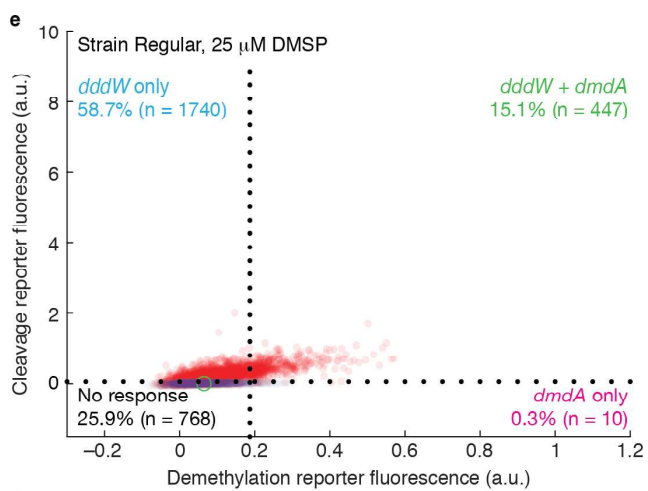
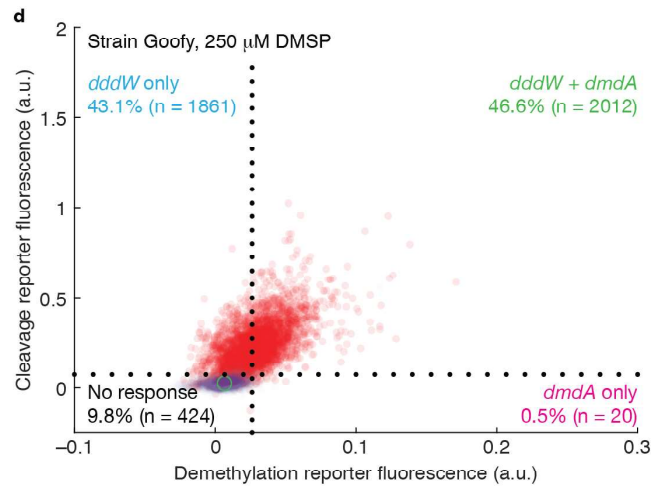
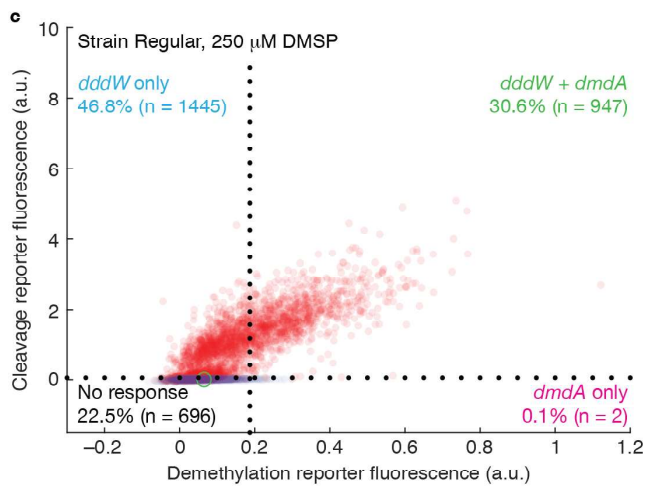
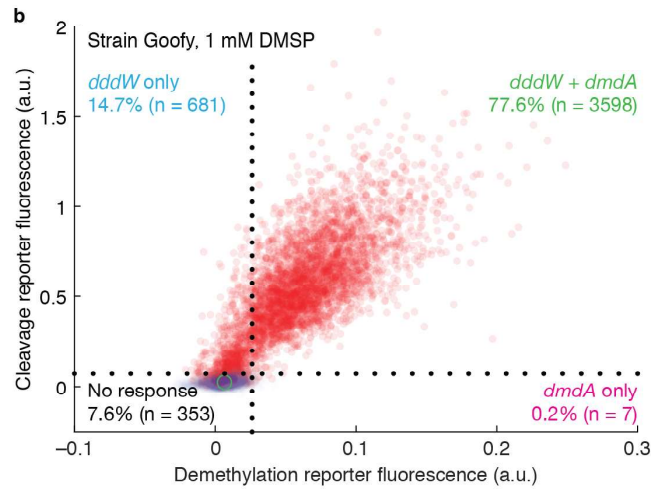
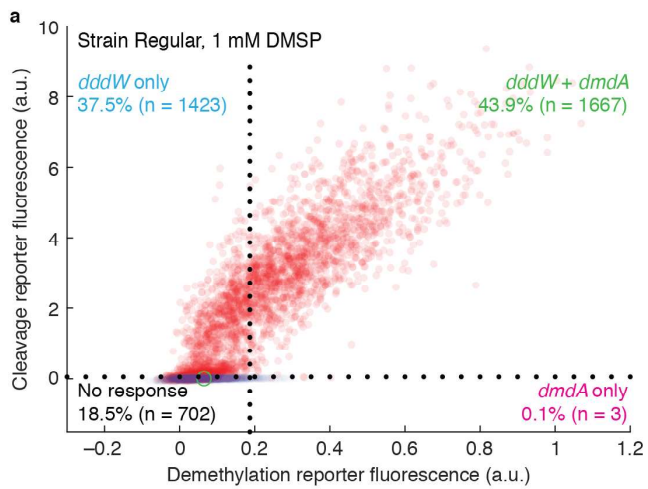
**Supplementary Fig. 6** Demethylation and cleavage pathway expression measurements in time-lapse DMSF experiments performed in microfluidic chips (all replicate experiments). Results from all replicate experiments ( $n = 3$  for strain Goofy (**a–f**);  $n = 3$  for strain Regular (**g–l**)). In strain Goofy, *dmdA* was reported by RFP (**a–c**) and *dddW* by TFP (**d–f**). In strain Regular, *dmdA* was reported by TFP (**g–i**) and *dddW* by RFP (**j–l**). The time points of mid-exponential in *dmdA* expression, used for cleavage-to-demethylation ratio calculation (shown in Fig. 3), are represented as colored dots at the appropriate time points on the x-axis in demethylation pathway plots (**a–c**, **g–i**). Red asterisks (\*) identify the replicate experiment shown in Fig. 2 (**c,f**). While the magnitudes of end-point fluorescence intensities, and the timepoints of mid-exponential and saturation of fluorescence kinetics curves, were not the same across replicate experiments and strains, other aspects (*e.g.*, concentration-dependence of end-point fluorescence intensities, and the preservation of slopes of the fluorescence curves across concentrations) were consistent (further discussion in Supplementary Note 2). Data points and error bars represent mean  $\pm$  s.e.m. of fluorescence signals of cells.



**Supplementary Fig. 7** Fluorescence response to DMSP concentrations below 1  $\mu\text{M}$  was undetectable in the microfluidic chip experimental setup. Lower DMSP concentration experiment ( $\leq 1 \mu\text{M}$ ): *R. pomeroyi* reporter strain Regular was incubated with succinate (negative control) or DMSP (at 100 nM, 500 nM, 1  $\mu\text{M}$ , or 500  $\mu\text{M}$ ) in observation chambers of a microfluidic chip in the presence of 50  $\mu\text{g/ml}$  kanamycin. TFP (*dmdA* reporter; open circles) and RFP (*dddW* reporter; closed circles) fluorescence of each cell were normalized by its own YFP intensity (constitutive expression). Each experimental condition was imaged at 4–10 different positions, with each field of view containing 25–200 cells that passed the constitutive YFP fluorescence intensity threshold. No cell division was observed over the experimental duration. Fluorescence signal upregulation above baseline was either absent, or not detectable, in DMSP concentrations at and below 1  $\mu\text{M}$  compared to succinate (two-tailed *t*-test at 6.4 h,  $p > 0.01$ ). Data points and error bars represent mean  $\pm$  s.e.m. of normalized fluorescence intensities of cells. This represents the only experiment in which succinate was used as negative control. Succinate, which did not elicit a fluorescence reporter response (Supplementary Fig. 3) and possesses a molecular weight that is similar to DMSP, was initially used as negative control in some early experiments. All other experiments presented in this manuscript used glucose as the negative control.

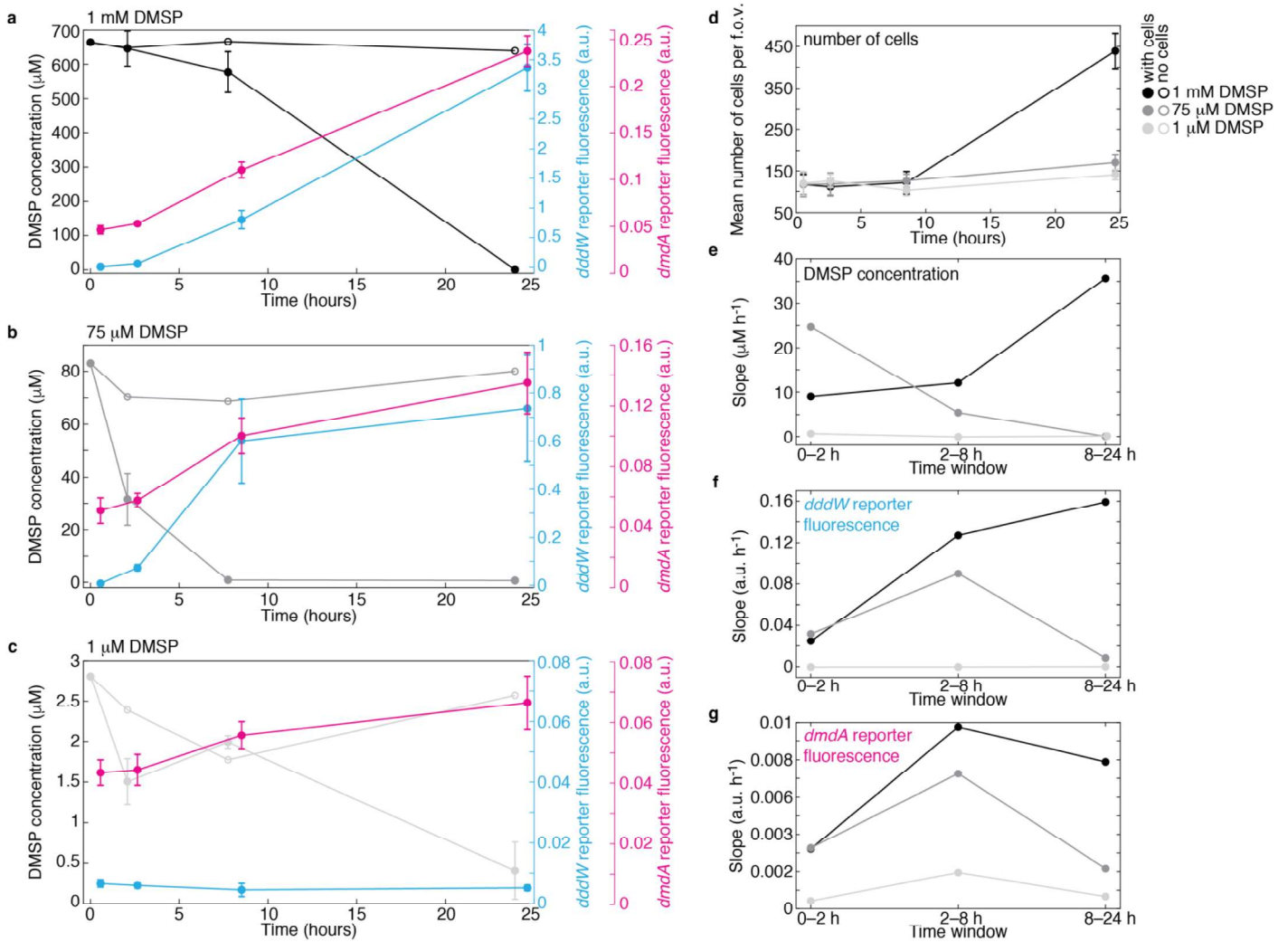


**Supplementary Fig. 8** Onset of *dmdA* and *dddW* upregulation at 1  $\mu\text{M}$  DMSP in microfluidic experiments. Probability distributions of fluorescence signals of *dmdA* (a–c, g–i) or *dddW* (d–f, j–l) reporters (strain Goofy (a–f) or Regular (g–l)) incubated with 1 mM glucose or 1  $\mu\text{M}$  DMSP in microfluidic chip experiments (cells aggregated across three time points,  $\sim 2.5\text{--}4$  h). Mean fluorescence of the first time point was subtracted from the fluorescence of each cell in appropriate color channels. Two-tailed *t*-test was performed on fluorescence data within each replicate experiment to determine statistically significant upregulation of *dmdA* or *dddW* in DMSP compared to glucose (glucose,  $n = 1,284\text{--}7,191$  cells; DMSP,  $n = 1,488\text{--}9,362$  cells; \*\*, significant upregulation with  $p < 0.01$ ). Only one (i) out of six replicate experiments showed significant upregulation of the demethylation pathway (*dmdA*) at 1  $\mu\text{M}$  DMSP compared to glucose, while at higher concentrations ( $\geq 10$   $\mu\text{M}$ ) all experiments exhibited upregulation of *dmdA* (Supplementary Fig. 6). These results suggest that 1  $\mu\text{M}$  approximates the threshold DMSP concentration above which bacteria increase *dmdA* gene expression beyond baseline levels.



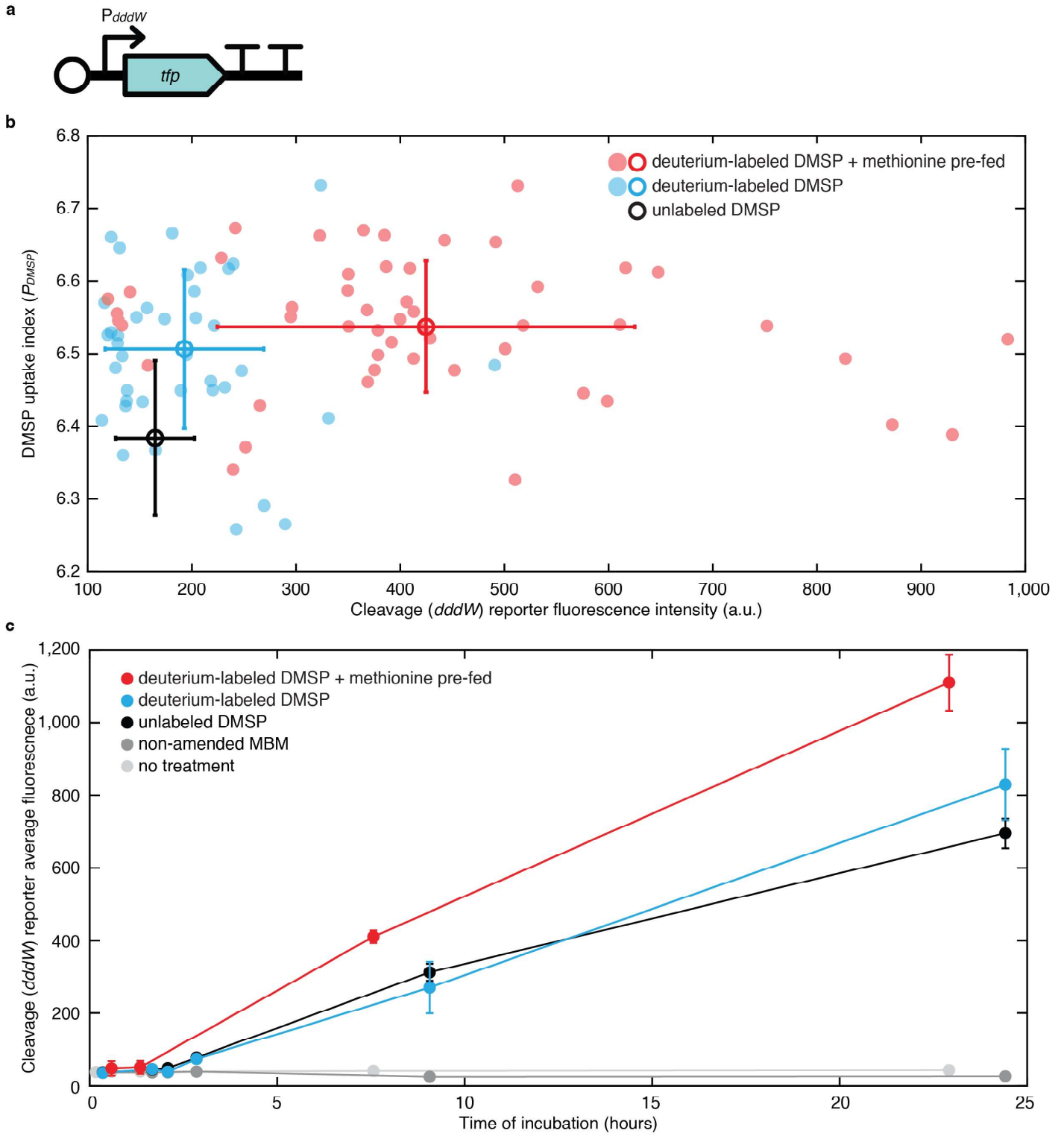


**Supplementary Fig. 9** Upregulation of demethylation (*dmdA*) and cleavage (*dddW*) at the single-cell level. **a–f**, Fluorescence of *dmdA* and *dddW* reporters at ~23 h (time point 30) from representative microfluidic chip experiments are shown (also in Supplementary Fig. 6): replicate experiment 1 of strain Regular (**a,c,e**) and replicate experiment 1 of strain Goofy (**b,d,f**). Each data point represents fluorescence signals of a single cell. Blue dots represent cells that have been incubated with 1 mM glucose, while red dots represent cells that have been incubated with DMSP at 1 mM (**a,b**), 250  $\mu$ M (**c,d**), or 25  $\mu$ M (**e,f**). Dotted lines mark two standard deviations from the mean (green circle) of the glucose population, representing cutoffs for defining the four populations: cells that upregulated (1) *dddW* only (cyan), (2) *dmdA* only (magenta), (3) both pathways (green), and (4) neither pathways (no response, black). **g**, Fractions of total number of cells at ~23 h (time point 30) in each of the four populations, averaged across all replicate experiments of both reporter strains (Goofy and Regular). At DMSP concentrations ranging between 10–100  $\mu$ M, the ‘*dddW* only’ population (cyan) represented the majority of responsive cells. At DMSP concentrations ranging from 250  $\mu$ M–1 mM, cells that upregulate both pathways (green) formed the majority. Data points and error bars represent mean  $\pm$  s.d. of replicate experiments ( $n = 6$ ). Heterogeneity in DMSP degradation gene upregulation is discussed in Supplementary Note 2.

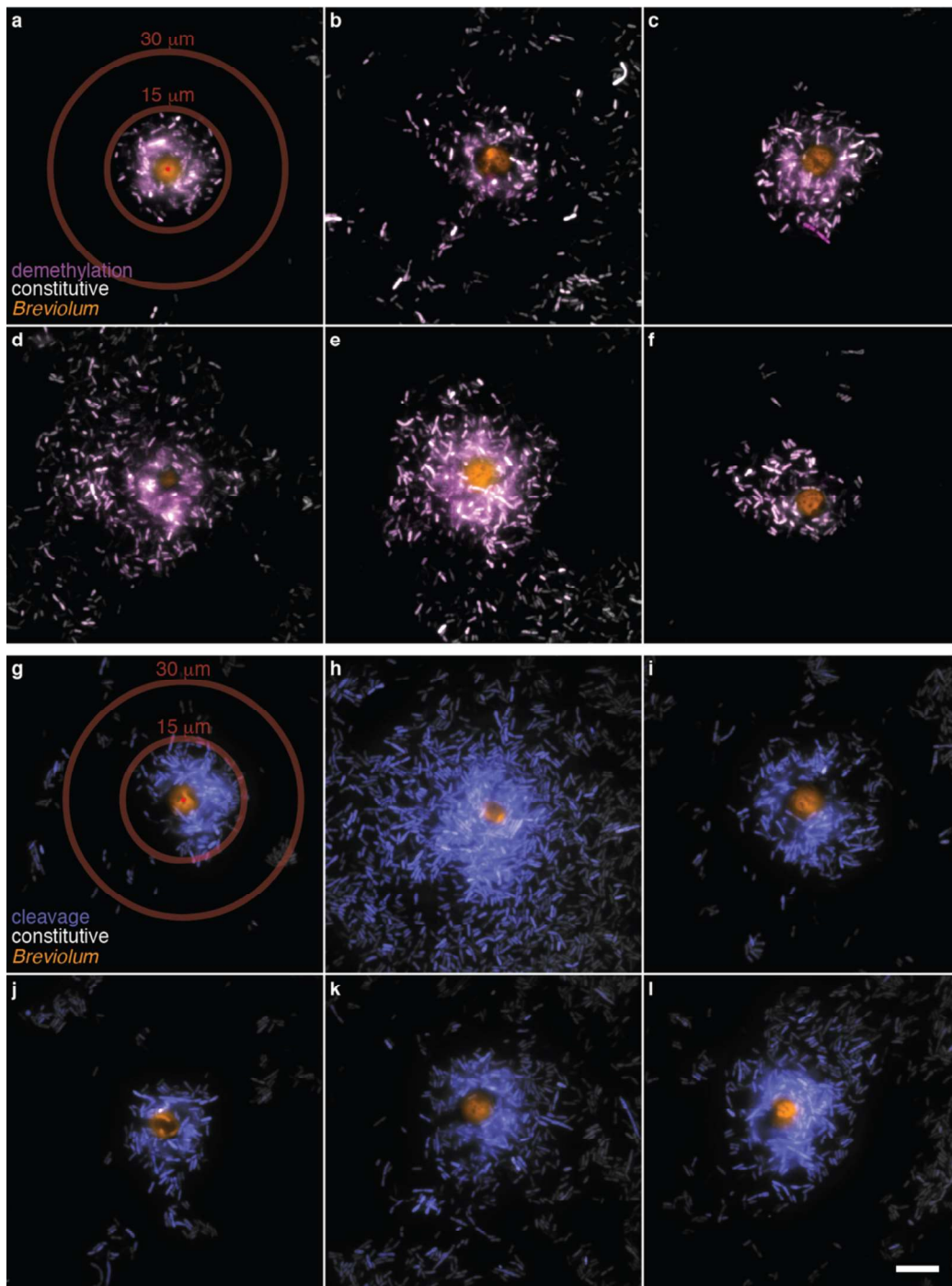


**Supplementary Fig. 10** Concentrations of DMSP in time-lapse experiments decrease over time due to cell uptake. **a–c** DMSP concentration measurements in a large-volume (8 ml) experiment with engineered *R. pomeroyi* (strain Regular) incubated with 1 mM DMSP (**a**), 75  $\mu$ M DMSP (**b**), or 1  $\mu$ M DMSP (**c**). Small differences between measured and expected initial concentrations are attributed to experimental or measurement errors. Samples were taken for DMSP concentration measurements (left y-axis, black) and fluorescence microscopy (right y-axes, cyan and magenta) at approximately 0, 2, 8, and 24 h after the start of incubation. Consistent with our microfluidic chip experiments, both pathways increased expression when bacteria were incubated with 75  $\mu$ M and 1 mM DMSP, but 1  $\mu$ M DMSP led to little or no response in either pathway. Data points and error bars represent mean  $\pm$  s.d. of three biological replicates for DMSP concentration measurements and fluorescence intensities. Specifically, mean fluorescence intensities of cells within a field of view, then across fields of views, were calculated before averaging across the three biological replicates ( $n = 90$ –151 average number of cells per field of view at 0 h; seven fields of views per condition at 0 h; two fields of views per condition at subsequent time points). Each cell's fluorescence signals were normalized by its own constitutive-YFP signal. **d** Mean number of cells per field of view (f.o.v.; 200  $\mu$ m  $\times$  200  $\mu$ m), counted in images taken for fluorescence intensity quantification at each sampling time point. Growth was observed in all DMSP concentrations. At 1 mM DMSP, a burst of growth during the last two time

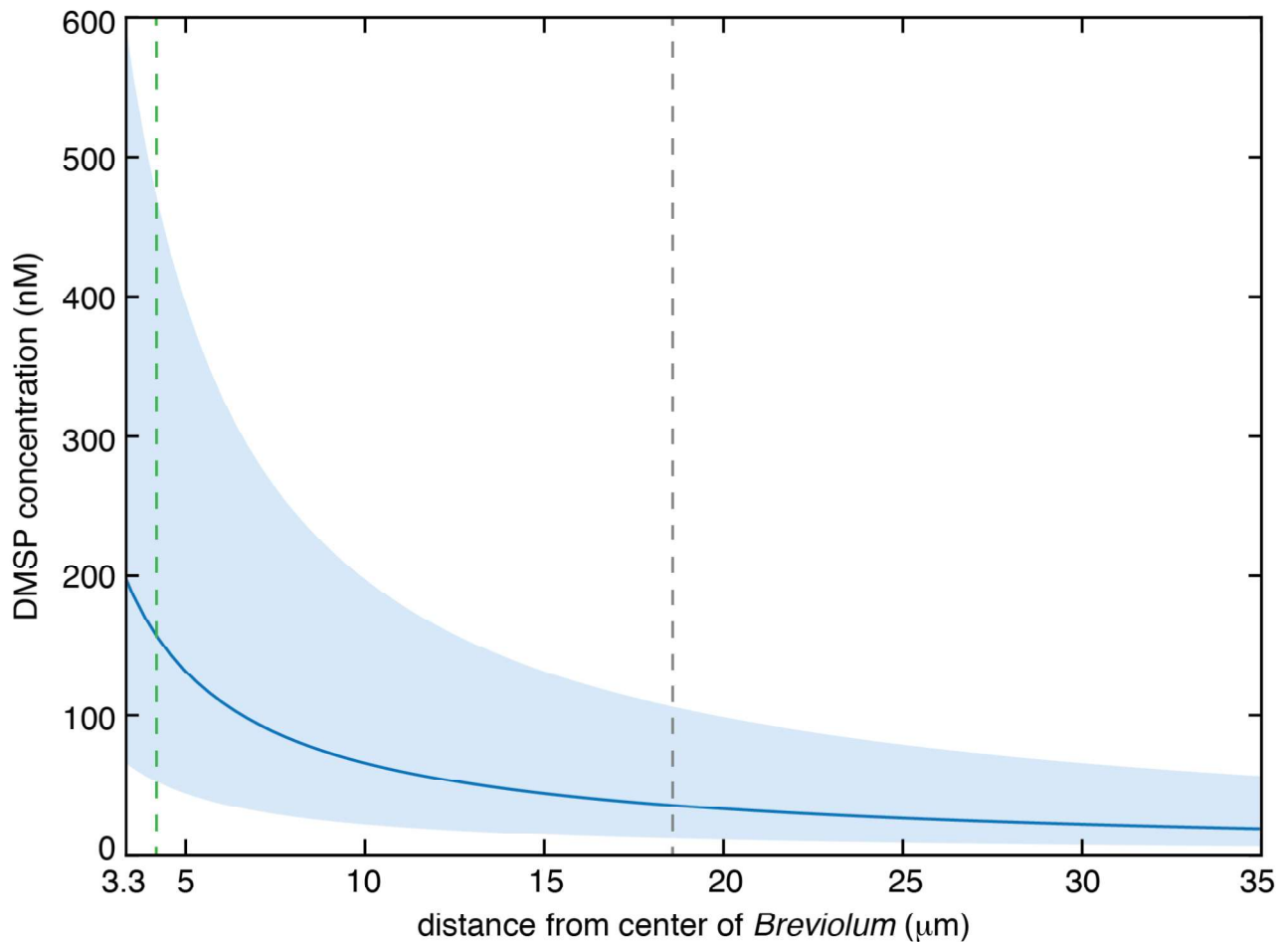
points (between 8 and 24 h after start of incubation), coincided with the largest DMSP concentration decrease (**a**). Data points and error bars represent mean  $\pm$  s.d. across three biological replicates of average number of cells per f.o.v. **e–g** Rates of change in DMSP concentration (**e**), cleavage (*dddW*) reporter fluorescence (**f**), and demethylation (*dmdA*) reporter fluorescence (**g**). Slopes between pairwise time points were calculated for each DMSP concentration condition. The 1 mM condition (black) is marked by an initial period (0–8 h) of slow DMSP concentration decay (**e**) but rapid pathway upregulation (**f,g**). This initial period is followed by fast DMSP uptake (8–24 h; **e**) coinciding with rapid increase in cell number (**d**) and continued increase in pathway expression (**f,g**). In contrast, the 75  $\mu$ M condition (dark grey) is marked by a rapid initial decline in DMSP concentration during the first time points (0–2 h; **e**), followed by a period of fast pathway expression increase (2–8 h; **f,g**), which plateau at the same time as DMSP is depleted (8–24 h; **b**). Differences in rates of DMSP uptake, growth, and pathway expression between 75  $\mu$ M and 1 mM DMSP conditions point to potentially different physiological adaptations corresponding to low and high nutrient conditions.



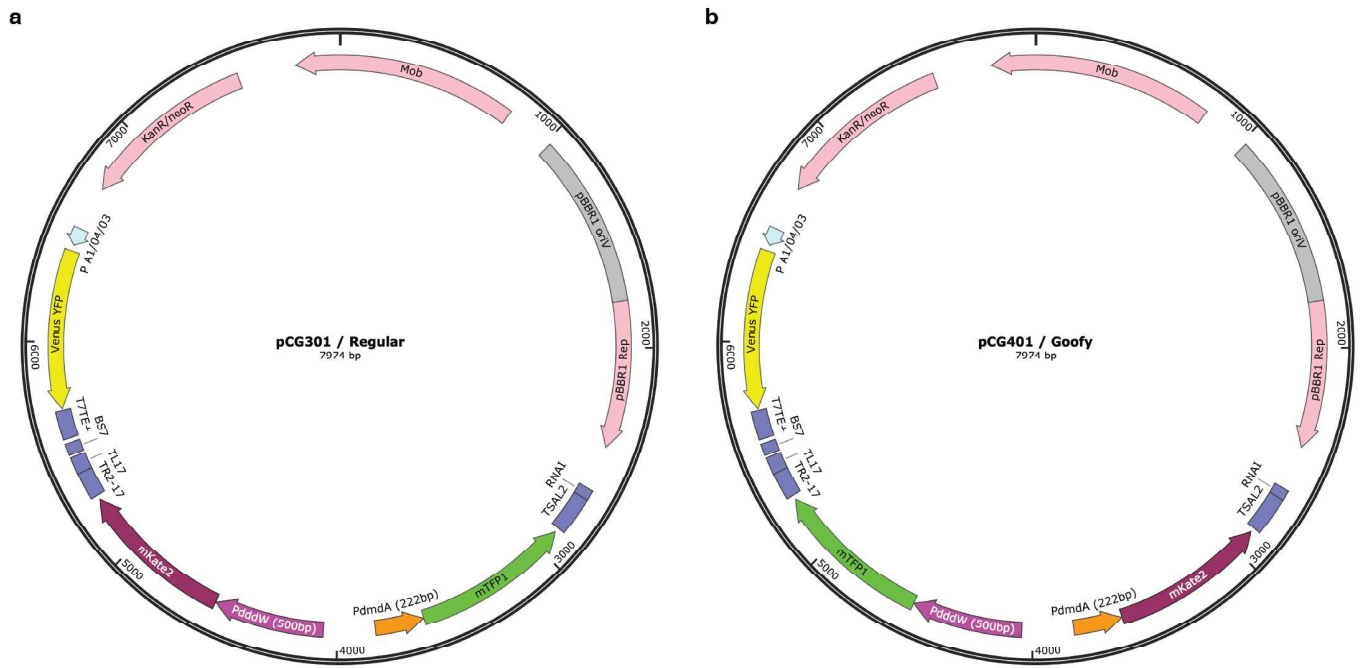
**Supplementary Fig. 11** Cells satiated in sulfur maintain DMSP uptake but increase cleavage pathway expression. **a** The  $P_{dddW}::mTFP1$  single-color *R. pomeroyi* reporter strain (cleavage pathway promoter-fusion with TFP) was used to avoid spectral interference with Raman microspectroscopy measurements. **b** Raman microspectroscopy measurements were performed at 5.5 h after incubation initiation. The reporter strain (**a**) was incubated with 1 mM deuterium-labeled DMSP ( $[^2H_6]$ -DMSP), either with or without prior exposure to 10 mM L-methionine (an alternative sulfur source to DMSP). All DMSP and methionine were dissolved in marine basal medium (MBM). The DMSP uptake index,  $P_{DMSP}$ , was calculated as the ratio of integrated intensities at Raman spectrum regions between the Raman wavenumbers 2040 and 2300  $cm^{-1}$  (C-D peak) and between 2400 and 2450  $cm^{-1}$  (reference region where background intensity was low) (Methods). Each filled-circle data point represents the  $P_{DMSP}$  value and the background-subtracted, raw TFP fluorescence signal of a single cell, measured by the Raman microspectroscopy setup (Methods) ( $n = 43$  cells treated with deuterium-labeled DMSP only (cyan);  $n = 50$  cells pre-fed with methionine and treated with deuterium-labeled DMSP (red)). For clarity of presentation, individual cell data points for unlabeled DMSP condition are not shown. Empty circles and error bars represent mean  $\pm$  s.d. of fluorescence (horizontal) and DMSP uptake index (vertical) of cells in each experimental condition. **c** Fluorescence response of cells incubated with deuterium-labeled DMSP (red and cyan), unlabeled DMSP (black), non-carbon amended MBM (dark grey), or no treatment (light grey) in observation chambers, monitored over time by microscopy (start of incubation at 0h). All conditions except 'no treatment' contained a final concentration of 1% methanol (solvent in which  $[^2H_6]$ -DMSP was dissolved). At each time point, seven images were taken at different positions within each observation chamber ( $n = 330 \pm 325$  (mean  $\pm$  s.d.) cells per image). Following image segmentation and background subtraction (Methods), the mean cellular fluorescence was calculated for each image, then averaged across images. Results confirmed that DMSP, unlabeled (black) or deuterium-labeled (cyan), elicit the same fluorescence response. Pre-feeding with methionine (red) led to faster upregulation and higher fluorescence signals of the cleavage (*dddW*) reporter cells compared to control cells (*i.e.*, not pre-fed with methionine). Data points and error bars represent mean  $\pm$  s.d. of average cellular fluorescence of seven images.



**Supplementary Fig. 12** Images of phytoplankton-bacteria co-incubation experiment. Representative images of the agarose pad co-incubation experiment (also shown in Fig. 4) with DMSP-producing phytoplankton, *Breviolum* CCMP2459, surrounded by *R. pomeroyi* bacteria fluorescently reporting *dmdA* (**a–f**, strain Regular; out of 15 total images) or *dddW* (**g–l**, strain Goofy; out of 18 total images) gene expression. Fluorescence signals are false-colored orange for photosynthetic pigments of phytoplankton, white for YFP (constitutive expression), magenta for *dmdA* reporter (TFP; **a–f**), and blue for *dddW* reporter (TFP; **g–l**). Representative concentric rings (widths of 20 pixels = 1.6  $\mu\text{m}$ ), used to bin distances from the center of *Breviolum* cells (red dots; **a,g**) for quantification of fluorescence signals, are shown for distances 15 and 30  $\mu\text{m}$ . Scale bar, 15  $\mu\text{m}$ .

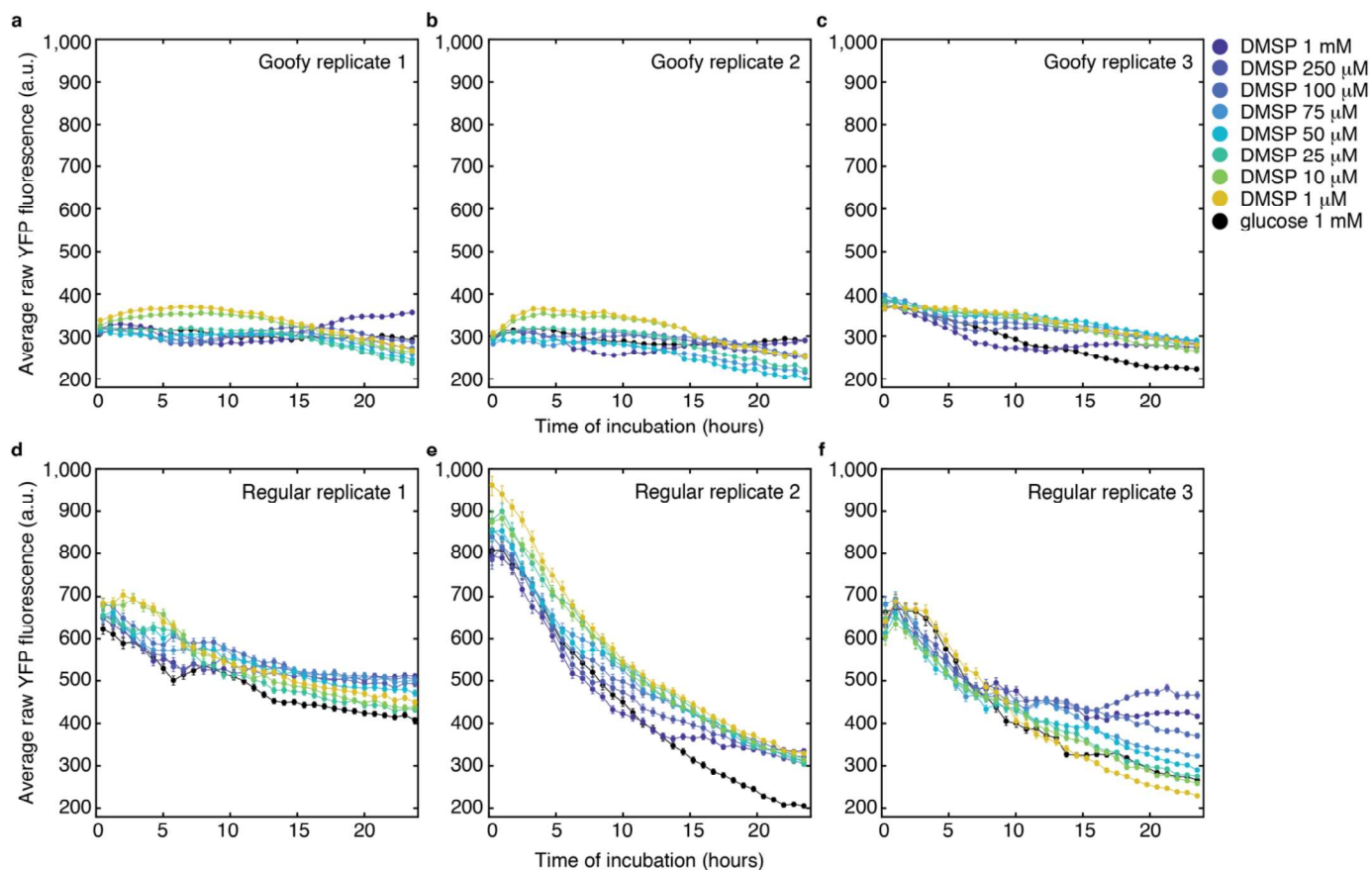


**Supplementary Fig. 13** Model of DMSP concentration in a phycosphere. Concentration profile of DMSP within a phycosphere predicted using Eq. S7 (Supplementary Note 4). The dark blue line shows modeled DMSP concentrations at distances ( $r$ ) from the center of a *Breviolum* cell, with a radius of  $3.3 \mu\text{m}$  (average radius in our co-incubation experiment; lower x-axis limit). Modeled DMSP concentration at the surface of the cell ( $r = 3.3 \mu\text{m}$ ) was  $197 \text{ nM}$ . Green dotted line marks the distance of the first concentric ring at which bacterial fluorescence was quantified ( $r = 4.2 \mu\text{m}$ ; modeled DMSP concentration =  $157 \text{ nM}$ ). Grey dotted line represents the distance within the phycosphere beyond which bacterial fluorescence signals were observed to return to baseline levels ( $r = 18.6 \mu\text{m}$ ; modeled DMSP concentration =  $35 \text{ nM}$ ). Shaded regions show two further cases in which modeled DMSP concentrations are 3-fold greater (upper boundary of the shaded region) or 3-fold smaller (lower boundary) than in the baseline case.

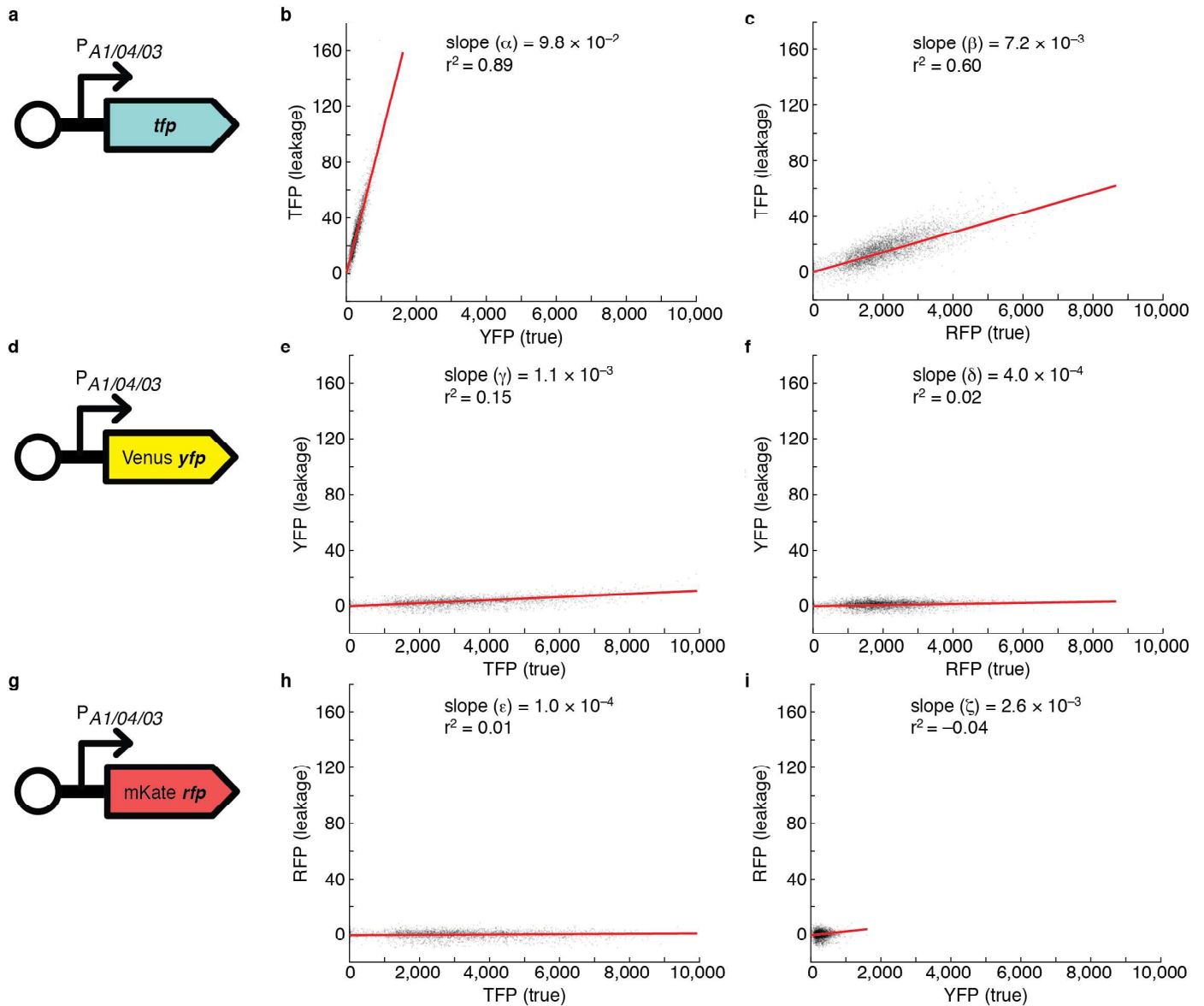


**Supplementary Fig. 14** Plasmid maps of tricolor reporter constructs, pCG301 (a, strain Regular) and pCG401 (b, strain Goofy).





**Supplementary Fig. 15** YFP fluorescence in time-lapse DMSP experiments performed in microfluidic chips (all replicate experiments). Replicate experiments correspond to those presented in Supplementary Fig. 6. Background subtraction, spectral leakage correction, and YFP intensity thresholding (50 a.u.) were performed. YFP signals decreased over the duration of experiments, which may be due to a number of factors including plasmid-loss by bacteria and fluorescence signal dilution due to cell division. Data points and error bars represent mean  $\pm$  s.e.m. of fluorescence signals of cells.



**Supplementary Fig. 16** Calculation of spectral leakage correction matrix,  $B$ , with constitutively fluorescent single-color control strains. Each constitutively fluorescent single-color control strain of *R. pomeroiyi* (**a**,  $P_{A1/04/03}::mTFP1$ ; **d**,  $P_{A1/04/03}::YFP$ ; **g**,  $P_{A1/04/03}::mKate2$ ) was imaged in its appropriate color channel ('true') and the two inappropriate color channels ('leakage') ( $n = 10$  biological replicates per strain; data point = one cell in **b–c**, **e–f**, **h–i**). Non-fluorescent cells were eliminated from analyses by applying minimum intensity thresholds in the true fluorescence channels (Supplementary Note 1). Only 10% of cells, randomly sampled across ten biological replicates, are plotted for clarity. In images of tricolor reporter strains (Regular or Goofy), recorded fluorescence signals are sums of 'true' and 'leakage' signals (Eq. S1–3). Specifically, recorded teal fluorescence ( $\hat{t}$ ) includes leakage from YFP ( $\alpha y$ ; **b**) and RFP ( $\beta r$ ; **c**); recorded yellow fluorescence ( $\hat{y}$ ) includes leakage from TFP ( $\gamma t$ ; **e**) and RFP ( $\delta r$ ; **f**); recorded red fluorescence ( $\hat{r}$ ) includes leakage from TFP ( $\epsilon t$ ; **h**) and YFP ( $\zeta y$ ; **i**). Slopes of linear regressions ( $\alpha, \beta, \gamma, \delta, \epsilon, \zeta$ ) were used to generate the spectral leakage correction matrix,  $B$ , which was used for quantification of true fluorescence signals of tricolor reporter strains (Supplementary Note 1).

## Supplementary Tables

### Supplementary Table 1

Fluorescent strains constructed in *R. pomeroyi* DSS-3 for this study.

Strain / Plasmid	Description	GenBank Accession #
Regular / pCG301	tricolor reporter ( $P_{dmdA}::mTFP1$ , $P_{dddW}::mKate2$ , $P_{A1/04/03}::YFP$ )	MN744962
pCG302	single-color reporter ( $P_{dmdA}::mTFP1$ )	MN744963
pCG303	single-color reporter ( $P_{dddW}::mKate2$ )	MN744964
Goofy / pCG401	tricolor reporter ( $P_{dmdA}::mKate2$ , $P_{dddW}::mTFP1$ , $P_{A1/04/03}::YFP$ )	MN744965
pCG402	single-color reporter ( $P_{dmdA}::mKate2$ )	MN744966
pCG403	single-color reporter ( $P_{dddW}::mTFP1$ )	MN744967
pCG101	single-color constitutive control ( $P_{A1/04/03}::mKate2$ )	MN744959
pCG102	single-color constitutive control ( $P_{A1/04/03}::YFP$ )	MN744960
pCG103	single-color constitutive control ( $P_{A1/04/03}::mTFP1$ )	MN744961
pZS2-200	pZS2-123 with replaced promoters ( $P_{dmdA}$ , $P_{dddW}$ , $P_{lac}$ ) for cloning aid only	MN744968

### Supplementary Table 2

Sequences of all oligonucleotide primers used in this study (in accompanying Excel sheet).

### Supplementary Table 3

Plasmids externally obtained and used in this study.

Plasmid	Description	Source / Reference
pZS2-123	DNA architecture of tricolor reporters; source of Venus YFP and terminators	AddGene #26598 (Reference: 1)
pBBR1MCS-2	vector backbone (Kan <sup>R</sup> )	Provided by Prof. M.E. Kovach (Reference: 2)
pXGFPC-2 P <sub>lac</sub> ::mKate2	source of mKate2 and P <sub>A1/04/03</sub> modified <i>lac</i> promoter	Provided by G. D'Souza (Reference: 3)
pXGFPC-2 P <sub>lac</sub> ::mTFP1	source of mTFP1	Provided by G. D'Souza (Reference: 3)
pRK415	source of <i>lac</i> promoter that is weakly active in DSS-3	Provided by Prof. C.R. Reisch (Reference: 4, 5)
pKR600	helper strain ( <i>E. coli</i> ) for triparental mating (Cam <sup>R</sup> )	Provided by Prof. C.R. Reisch (Reference: 6)

# Supplementary Notes

## Supplementary Note 1: Image analysis for cellular fluorescence quantification

### 1.1. Cell segmentation, thresholding, and generation of 'cell mask' and 'background mask'

Analysis of fluorescence images was performed in MATLAB (MathWorks) using an automated image segmentation and fluorescence quantification software developed in-house. First, cell-containing pixels were recognized by applying a threshold (determined manually for each replicate experiment) on pixel intensity in phase contrast images, in which cells appear as dark (*i.e.*, low intensity) pixels. Subsequently, cells were segmented by grouping cell-containing pixels that were in contact with each other.

Not all recognized cells were suitable for further analyses due to their orientation or size. Cells that were positioned perpendicular to the glass slide, which contained high intensity pixels in phase contrast images, were not suitable for quantification due to the larger integration distance in the z-direction for fluorescence signals. These perpendicular cells were eliminated from further analyses by applying a threshold (determined manually for each replicate experiment) on the upper quartile pixel intensity within each cell in phase contrast images, whereby cells containing many high intensity (*i.e.*, white) pixels were eliminated from further analyses. Furthermore, thresholds on maximum and minimum size (*i.e.*, number of pixels within a segmented cell; pixel size = 0.2  $\mu\text{m}$   $\times$  0.2  $\mu\text{m}$ ) eliminated aggregates of many cells (large size; maximum area threshold = 200 pixels), or other particles (small size; minimum area threshold = 10 pixels). The average size of a cell was  $39.0 \pm 4.02$  pixels (mean  $\pm$  s.d. of cells in replicate experiments). As a result of thresholding,  $\sim 20\%$  of originally recognized cells were eliminated from further analyses. The position of each cell was recorded, and a 'cell mask' was generated from each phase contrast image. Appropriate cell segmentation and thresholding were visually inspected and confirmed for each image. In some images, a small offset (*e.g.*, by 1–5 pixels) between 'cell masks' and fluorescence images were manually corrected.

Background fluorescence was defined as the average intensity of pixels that do not contain cells, within a fluorescence channel image. Cell-containing areas of 'cell masks' were dilated by a radius of 20–30 pixels, and the negatives of these expanded 'cell masks' served as 'background masks'. Representative samples of 'background masks' were visually inspected for appropriate background pixel identification. The background intensity for each fluorescence image was calculated as the average intensity of pixels containing no cells, labeled in 'background masks'.

Cell and background masks were applied to fluorescence images for cellular and background fluorescence intensity quantification. Fluorescence intensity (TFP, YFP, or RFP) of each cell was defined as the mean intensity of pixels contained within a recognized cell. Background fluorescence was subtracted from each cell to account for variation in background signal levels in different images.

## 1.2. Spectral leakage correction in image processing and analyses

Our tricolor reporter strains (Fig. 1a,b) expressed three fluorescent proteins (TFP, YFP, and RFP) which were chosen for maximum spectral separation. However, the wide excitation and emission spectra of fluorescent proteins, combined with the range of wavelengths that pass through emission filters of filter cubes, led to some fluorescence emission signals leaking into inappropriate channels (*e.g.*, fluorescence emission from YFP leaking into the teal channel). Thus, spectral leakage correction was applied during image processing and analyses for accurate quantification of true fluorescence intensities. True fluorescence intensities expressed by the tricolor reporter strains are represented in the following equations:

$$\hat{t} = t + \alpha y + \beta r \quad (\text{Eq. S1})$$

$$\hat{y} = \gamma t + y + \delta r \quad (\text{Eq. S2})$$

$$\hat{r} = \varepsilon t + \zeta y + r \quad (\text{Eq. S3})$$

where  $\hat{t}$ ,  $\hat{y}$ , and  $\hat{r}$  represent the recorded intensities in teal, yellow, and red channels, respectively. The recorded intensity ( $\hat{t}$ ,  $\hat{y}$ , or  $\hat{r}$ ) of each fluorescent protein was expressed as a sum of (i) the *true* intensity ( $t$ ,  $y$ , or  $r$ ) in the color channel that match the fluorescent protein of interest and (ii) *leakage* intensities from the other two fluorescent proteins, which were represented as fractions ( $\alpha$ ,  $\beta$ ,  $\gamma$ ,  $\delta$ ,  $\varepsilon$ , and  $\zeta$ ) of the true intensities of the two auxiliary fluorescent proteins. Equations S1–S3 can also be represented in aggregate:

$$\begin{bmatrix} \hat{t} \\ \hat{y} \\ \hat{r} \end{bmatrix} = B \times \begin{bmatrix} t \\ y \\ r \end{bmatrix} \quad (\text{Eq. S4})$$

where

$$B = \begin{bmatrix} 1 & \alpha & \beta \\ \gamma & 1 & \delta \\ \varepsilon & \zeta & 1 \end{bmatrix} \quad (\text{Eq. S5})$$

Thus,  $B$  is the spectral leakage correction matrix that enabled us to solve for the true intensities ( $t$ ,  $y$ , and  $r$ ) from recorded intensities ( $\hat{t}$ ,  $\hat{y}$ , and  $\hat{r}$ ).

## 1.3. Calculation of spectral leakage correction matrix, $B$

To calculate the spectral leakage correction matrix,  $B$ , the intensities of signals that leaked into inappropriate channels were quantified for each fluorescent protein (Supplementary Fig. 16). Constitutively fluorescent single-color control strains (TFP-, YFP-, or RFP-expressing strains) were grown as described in Methods. These control strains were placed in separate observation chambers of a microfluidic device, allowed to settle for ~30 minutes, and imaged in every fluorescence color channel with microscopy specifications as described in Methods. Images were obtained from ten

biological replicates (*i.e.*, from overnight cultures prepared on 10 different days) of each single-color control strain.

Cells in images were segmented by thresholding on pixel intensity in phase contrast images, followed by background fluorescence subtraction. Only cells with fluorescence intensity values above 0 a.u. in the true fluorescent color channel were included for calculation of  $B$  (mean  $\pm$  s.d. number of cells included for analysis in a biological replicate were  $n = 4,765 \pm 1,955$ ;  $n = 3,246 \pm 1,938$ ;  $n = 3,367 \pm 1,952$  for RFP, YFP, and TFP single-color strains, respectively). All cells across all biological replicates ( $n = 10$ ) were pooled, and the signals of each cell measured in all three fluorescence channels were plotted on pairs of axes each representing a color channel ( $n = 47,648$ ;  $n = 32,458$ ;  $n = 33,672$  cells after pooling, for RFP, YFP, and TFP single-color strains, respectively) (Supplementary Fig. 16). Linear least squares regression, assuming an intercept at  $x = 0$  and  $y = 0$ , was performed on the pooled fluorescence signal data for the calculation of  $B$  (Supplementary Fig. 16):

$$B = \begin{bmatrix} 1 & 9.8 \times 10^{-2} & 7.2 \times 10^{-3} \\ 1.1 \times 10^{-3} & 1 & 4.0 \times 10^{-4} \\ 1.0 \times 10^{-4} & 2.6 \times 10^{-3} & 1 \end{bmatrix}$$

The spectral leakage correction matrix,  $B$ , was used to solve for the true fluorescence intensities ( $t$ ,  $y$ , or  $r$ ) of each cell in microfluidic experiments using Equation S4.

A similar method, with images of single-color strains grown on agarose pads, was used to calculate a different spectral leakage correction matrix,  $B_{\text{agarose}}$ , for the phytoplankton-bacteria co-incubation experiment:

$$B_{\text{agarose}} = \begin{bmatrix} 1 & 8.9 \times 10^{-2} & 1.9 \times 10^{-3} \\ 6.0 \times 10^{-4} & 1 & 1.0 \times 10^{-4} \\ -2.0 \times 10^{-4} & 1.1 \times 10^{-2} & 1 \end{bmatrix}$$

#### 1.4. Spectral leakage correction, and thresholding and normalization by constitutive YFP

True fluorescence intensities of each cell were solved for by using the spectral leakage correction matrix,  $B$ . The largest correction occurred with teal fluorescence signals, into which YFP leaked significantly (Supplementary Fig. 16). After spectral leakage correction, dim or non-fluorescent (*i.e.*, low metabolic activity or dead) cells were eliminated from further analyses by applying a threshold (50 a.u.) on constitutive YFP fluorescence. The distribution of cellular YFP signals revealed a bimodal distribution: one population with a sharp peak near 0 a.u. containing non-fluorescent or dim cells, and a second, larger population consisting of bright cells. A cutoff YFP intensity of 50 a.u. was applied to all replicate experiments of time-lapse DMSP experiments in microfluidic chips (Supplementary Fig. 6) to eliminate non-fluorescent or dim cells. As a result of thresholding on YFP intensity, 6–33% of recognized cells were eliminated from further analyses.

Finally, RFP and TFP signals of each cell were normalized by YFP fluorescence, which served as a proxy for metabolic activity level and plasmid number. Fluorescence signals in red and teal channels

of each cell were normalized by the mean YFP signal at the corresponding time point and experimental condition (Supplementary Fig. 15).

### **1.5. Calculation of theoretical ‘off’ fluorescence intensity**

Due to detector noise, a non-zero signal was detected even in the absence of fluorescence expression by cells. Thus, the theoretical ‘off’ intensity value of cells had to be determined to differentiate absence of fluorescence (*e.g.*, promoters that are turned off) from weak signal intensities (*e.g.*, leaky promoters).

The theoretical ‘off’ fluorescence intensities were defined as the values of signal leakage detected in the red and teal fluorescence channels while imaging the single-color YFP control strain, after background subtraction, and spectral-leakage correction using *B*. Only YFP cells whose true fluorescence intensities in the yellow channel were above 30 a.u. were included in the analysis.

To calculate the average theoretical ‘off’ fluorescence intensities, signals in red and teal channels were first averaged across cells in each image, then subsequently averaged across images within a replicate, and normalized by the average YFP intensity of the corresponding replicate. Finally, normalized leakage intensities were averaged across all replicate experiments ( $n = 10$ ). The values (mean  $\pm$  s.d.) of the theoretical ‘off’ fluorescence were  $-1.6 \pm 0.37 \times 10^{-3}$  a.u. (red channel) and  $2.5 \pm 4.1 \times 10^{-3}$  a.u. (teal channel) (Supplementary Fig. 5).



## Supplementary Note 2: Interpretation of fluorescence results

### 2.1. Time-lapse DMSP experiments in microfluidic chips

Results from all replicates of time-lapse DMSP experiments are presented in Supplementary Fig. 6. While the magnitudes of end-point fluorescence intensities (*i.e.*, average fluorescence signals over the final five (~20.4–24 h) time points), and the timepoints of mid-exponential and saturation of fluorescence kinetics curves, were not the same across replicates and strains, other aspects (concentration-dependence of fluorescence intensities and the preservation of slopes of the kinetics curves across concentration) were consistent. The decline in RFP signal after signal saturation may be due to bleaching, plasmid loss, or fluorescent protein degradation. The slight increase in TFP signal in glucose negative control and after signal saturation may be due to a delay in protein folding, or clumping of cells as they reach overgrowth in the experimental chamber, leading to a perceived increase in brightness of cell-containing pixels over time. Due to spectral (*i.e.*, bleaching and effect of cell clumping on signal) and biological (*i.e.*, rate of protein folding and degradation, and effect of plasmid loss) differences between the fluorescent proteins, these phenomena are expected to affect signals detected in red and teal fluorescence channels in different ways. However, these small artefacts did not affect our overall conclusions outlined in the main text.

Temporal evolution of constitutively-expressed YFP fluorescence in all time-lapse DMSP experiments are presented in Supplementary Fig. 15. All experiments were performed with antibiotics (kanamycin) to slow plasmid-loss during experiments, but at a low concentration (10 µg/ml) to minimize interference with biological processes. We observed a  $13.4 \pm 17.0\%$  (mean  $\pm$  s.d. of replicate experiments) decay in YFP signals in glucose between 1 h and 10 h of the microfluidic experiments (Supplementary Fig. 15), which may be a predictor of the rate of plasmid-loss in our experiments. Loss of plasmid over the experimental duration may contribute to an underestimation of fluorescence signals reporting *dmdA* and *dddW* expression. However, the relatively small variability in the level of YFP signal decay across replicate experiments suggests that the rate of plasmid-loss is comparable amongst cells on average. Thus, we conclude that comparisons of cell fluorescence relative to each other (e.g., between different concentrations of DMSP, or between *dddW* and *dmdA*) is valid.

### 2.2. Heterogeneity in DMSP degradation gene expression

Our single-cell approach revealed the emergence of heterogeneity in the DMSP degradation pathway response within a single bacterial strain (*R. pomeroyi* DSS-3). Underlying the population averages were concentration-dependent shifts in the proportions of cells classified in four discrete categories: (1) *dddW* response only, (2) *dmdA* response only, (3) *dddW* + *dmdA* response, and (4) no response (Supplementary Fig. 9).

End-point expression levels were defined as the average fluorescence signals over the last five time points (*i.e.*, ~20.4–24 h) of a time-lapse DMSP experiment performed in observation chambers, and were used as proxies for maximum gene expression levels that *dddW* and *dmdA* reached as a result of exposure to a DMSP concentration (Fig. 2c,d). For DMSP concentrations ranging between 10–50 µM, the mean end-point cleavage (*dddW*) pathway expression level (shown in Fig. 2d) was driven by a population of cells that solely upregulated the *dddW* gene (the ‘*dddW* response only’ population),

which made up nearly half ( $40.0 \pm 21.4\%$  to  $44.3 \pm 14.9\%$ ) of total cells at 10–50  $\mu\text{M}$  (Supplementary Fig. 9g); while the other half of the population maintained baseline expression of the DMSP pathways (the ‘no response’ population). In contrast, the average end-point demethylation (*dmdA*) pathway expression level (Fig. 2c) was driven by a subpopulation of cells that upregulated both *dmdA* and *dddW* genes (the ‘both pathways on’ population; Supplementary Fig. 9g). This population grew exponentially between DMSP concentrations of 10  $\mu\text{M}$  ( $7.0 \pm 3.7\%$  of total cells) and 75  $\mu\text{M}$  ( $28.9 \pm 9.3\%$  of total cells), and surpassed all other subpopulations at 250  $\mu\text{M}$  (Supplementary Fig. 9), at which the increase in the maximum gene expression levels with DMSP concentration also dampened (Fig. 2c,d).

Taken together, these results suggest that specific cell subpopulations drove the average increases in *dmdA* and *dddW* gene expression in different DMSP concentration regimes. At the highest DMSP concentrations tested ( $>100 \mu\text{M}$ ), the majority of cells shifted their metabolic strategy towards upregulating both pathways (*dddW* + *dmdA*), probably in order to capitalize on the abundance of DMSP. However, upregulation of both pathways came at the expense of the ability to respond sensitively to DMSP concentration, as the positive relationship between end-point gene expression levels and concentration dampened above 100  $\mu\text{M}$  (Fig. 2c,d). Finally, we speculate that the shift in the relative expression towards cleavage pathway with increasing DMSP concentration (Fig. 3) is controlled at two distinct levels: (i) at the single cell level (*i.e.*, individual cells increase *dddW* expression levels), as well as (ii) at the population level (*i.e.*, increasing fractions of ‘*dddW* only’ or ‘*dddW* + *dmdA*’ subpopulations with concentration).

## Supplementary Note 3: Image analysis for phytoplankton-bacteria co-incubation experiment

### 3.1. Segmentation of *Breviolum* cells and identification of concentric rings

Phycosphere images were analyzed using a similar MATLAB software as that described for the analysis of observation chamber experiments (Supplementary Note 2). Additional steps and differences in image processing of phycosphere images are described below.

Due to spectral leakage in the red channel by photosynthetic pigments (which masked any RFP signals from bacteria), only signals in the teal (reporting *dmdA* in strain Regular and *dddW* in strain Goofy) and yellow (constitutive YFP expression) channels were quantified, while the red channel was used only to assess the fluorescence signal of *Breviolum* photosynthetic pigments. Images were selected for analysis by screening for bright photosynthetic pigment fluorescence in the red channel (*Breviolum* cells with diffuse, low-intensity pigment fluorescence were excluded from analysis). Furthermore, images with only one phytoplankton cell per field of view (80  $\mu\text{m}$   $\times$  80  $\mu\text{m}$ ) were selected. These selection criteria yielded 15 images for strain Regular (reporting *dmdA* with TFP) and 18 images for strain Goofy (reporting *dddW* with TFP), with a combined total of 33 phycosphere images for further analyses.

Segmentation of *Breviolum* cells was achieved through pixel intensity thresholding on photosynthetic pigment signal in the red channel, and approximating *Breviolum* cells as circles. Concentric rings with 20 pixels width (1.6  $\mu\text{m}$ ), emanating from the surface of circularly approximated *Breviolum* cells, were used to bin distances within phycospheres. Since the radii of *Breviolum* cells slightly differed across 33 cells ( $3.3 \pm 0.9$   $\mu\text{m}$ ; mean radius  $\pm$  s.d.), the distance of concentric rings from the center of *Breviolum* cells varied slightly from image to image. The largest concentric ring (*i.e.*, the farthest distance within the phycosphere) was determined to be the ring before the one that contacted any edge of the image.

### 3.2. Uneven illumination correction, background fluorescence subtraction, and spectral leakage correction with *B<sub>agarose</sub>*

Uneven illumination across the field of view was observed at high magnification (100 $\times$ ), probably due to factors related to the light path between the camera and the microscope. To quantitatively correct for uneven illumination, images of agarose pads in the absence of cells were taken in each channel at different stage positions ( $n = 4$ ). At each pixel position, intensities were averaged across the 4 images to create a master 'uneven illumination correction' image. Phycosphere images in teal and yellow channels were corrected by division, at each pixel position, by the master 'uneven illumination correction' image at the corresponding pixel position in corresponding channels. The effect of uneven illumination was small: as an estimate of the magnitude of the maximum correction, the ratio of minimum and maximum intensities in the 'uneven illumination correction' images were 0.81 in teal and 0.87 in yellow.

Background fluorescence intensity was calculated by first roughly identifying *Breviolum*- and bacteria-containing regions by thresholding on pixel intensity in the phase contrast channel (to identify dark/low- and bright/high-intensity pixels), then expanding the region by a distance of 35 pixels. The

negative of this expanded area generated the 'background masks'. Average intensities of background pixels were calculated in teal and yellow fluorescence channels for each phycosphere image, and were subtracted from each non-background pixel.

Phycosphere experiment-specific spectral leakage correction matrix,  $B_{agarose}$ , was generated by analyzing images of constitutively fluorescent single-color control strains (RFP, YFP, or TFP) grown on agarose pads in the absence of phytoplankton. Single-color bacteria-containing pixels were identified by thresholding on fluorescence intensity, and linear regression on pixel intensities were performed to calculate the spectral leakage correction matrix,  $B_{agarose}$ . The spectral leakage correction matrix was applied to each pixel of co-incubation images to solve for the true fluorescence intensities in teal and yellow channels.

### 3.3. Quantification of bacterial *dmdA* and *dddW* gene expression in phycospheres

After background subtraction and spectral leakage correction, pixels containing *R. pomeroyi* cells were identified by thresholding for high YFP fluorescence (proxy for metabolic activity), and for positive teal fluorescence values. Due to differences in magnification and experimental setups, different fluorescence intensity thresholds were chosen for the phycosphere experiments than those applied in the time-lapse DMSP experiments performed in observation chambers. Constitutive YFP was brighter in strain Goofy than in strain Regular, reporting *dddW* and *dmdA* in TFP, respectively, probably due to slight differences in growth phase in each bacterial culture. As such, different thresholds of YFP intensity ( $>0.08$  a.u. for *dmdA* and  $>0.23$  a.u. for *dddW* reporters) were chosen through visual inspection of resulting images, whereby appropriate YFP intensity thresholds accepted cell-containing pixels but excluded background pixels. The YFP intensity threshold values were roughly in the same place in the distribution of pixel intensities for the two reporter strains. Finally, pixels that passed the YFP intensity threshold had to also have positive teal fluorescence values ( $>0$  a.u.) for inclusion in further analyses. Appropriate cell-associated pixel identification and thresholding were visually inspected and confirmed for each image.

Rather than segmenting each bacterial cell, each bacteria-containing pixel was independently quantified. In each phycosphere, only distances at which the area of 20-pixel-width concentric rings contained at least 500 bacteria-associated pixels (equivalent area of a  $6.3 \mu\text{m} \times 6.3 \mu\text{m}$  square, or approximately 3 cells) were included for further analyses. Despite this 500-pixel threshold, at least 10 images (out of 15, for *dmdA*) and 14 images (out of 18, for *dddW*) were included for analyses at any given concentric ring distance within the phycosphere. Fluorescence intensity values at each concentric ring were aggregated across images to calculate the average values presented in Fig. 4c,d.

### 3.4. Calculation of relative expression of *dmdA* and *dddW* in phycospheres

To compare *dmdA* and *dddW* expression levels, TFP intensity (reporting *dmdA* or *dddW*) of each pixel was normalized by its own YFP intensity (Fig. 4e). Cleavage-to-demethylation ratio ( $dddW / dmdA$ ) was calculated as the product of the mean normalized TFP intensity of strain Goofy (*dddW*,  $n = 18$ ) and the mean of the inverse of normalized TFP intensity of strain Regular (*dmdA*,  $n = 15$ ) at each distance within the phycosphere (Fig. 4f). Error bars represent the variance of the cleavage-to-

demethylation ratio, or the product of cleavage and inverse of demethylation gene expression ( $\mu_W \cdot \mu_{\frac{1}{A}}$ ), and was calculated with the following equation at each distance within the phycosphere:

$$\text{Var}\left(\mu_W \cdot \mu_{\frac{1}{A}}\right) = \sigma^2_W \cdot \sigma^2_{\frac{1}{A}} + \sigma^2_W \cdot \mu^2_{\frac{1}{A}} + \sigma^2_{\frac{1}{A}} \cdot \mu^2_W \quad (\text{Eq. S6})$$

where  $\mu_W$  and  $\sigma_W$  represent the mean and standard deviation of *dddW* expression level at a concentric ring; and  $\mu_{\frac{1}{A}}$  and  $\sigma_{\frac{1}{A}}$  are the mean and standard deviation of the inverse of *dmdA* expression levels at a concentric ring.

#### Supplementary Note 4: Model of DMSP concentrations in the phycosphere

The microenvironment surrounding a unicellular phytoplankton, the ‘phycosphere’, is often characterized by a concentration gradient of exudates and dissolved organic matter (DOM)<sup>7</sup>. Exudates include DMSP, which comprises up to 10% of fixed carbon in some phytoplankton species<sup>8</sup>. Here, we predict the concentration of exuded DMSP in the phycosphere as a function of the leakage rate,  $L$ , and its molecular diffusivity,  $D$  (Supplementary Fig. 13).

Experimentally, we simulated a phycosphere by seeding *R. pomeroyi* fluorescent reporter bacteria with *Breviolum* phytoplankton cells on agarose pads, which preserved the spatial arrangement of co-incubated organisms (Methods). We assumed a 30% reduction in diffusivity of DMSP in agarose ( $D_{\text{agarose}}$ ) compared to solution ( $D_{\text{solution}} = 0.5 \times 10^{-5} \text{ cm}^2 \text{ s}^{-1}$ )<sup>9</sup>. A similar percentage of diffusivity reduction was observed for sucrose in agarose in a previous study<sup>10</sup>. The thickness of agarose (~0.5 mm) was much larger (150×) than the average radius of *Breviolum* cells (3.3  $\mu\text{m}$ ); thus, a 3D diffusion model was used to describe the concentration of DMSP in agarose. However, since the phytoplankton cell was immobilized with agarose on one side, diffusion may be more accurately approximated on a half-volume around the cell, instead of its entire volume. Thus, the effective leakage rate would be double of that expected ( $2L$ ). Taken together, the concentration of DMSP in agarose at distance  $r$  from the center of a phytoplankton cell is modeled as:

$$C_r = \frac{2L}{4\pi D_{\text{agarose}} r} \quad (\text{Eq. S7})$$

with  $L$ , the constant exudation rate (mol/s) of DMSP, defined as:

$$L = \mu\theta f \quad (\text{Eq. S8})$$

where  $\mu$  is the doubling rate of the *Breviolum* cell,  $\theta$  is the amount of intracellular DMSP if there were no leakage ( $\mu\theta$  is thus the rate of production of DMSP by the cell), and  $f$  is the fraction of the production rate that is leaked.

The actual, stable quantity of intracellular DMSP that is maintained by the cell,  $\phi$ , is defined with the following relationship with  $\theta$  and  $f$ :

$$\phi = \theta(1 - f) \quad (\text{Eq. S9})$$

Thus,  $L$ , the constant exudation rate (mol/s) of DMSP, is described as:

$$L = \frac{\mu\phi f}{1-f} \quad (\text{Eq. S10})$$

*Breviolum* cells in our experiment were most likely under physiological stress, or undergoing senescence, due to immobilization on an agarose pad, proximity to high numbers of bacteria, and

exposure to vigorous shaking of cell cultures prior to co-incubation; stress and shaking have been shown to increase intracellular DMSP and exudation rate<sup>11,12</sup>. However, all *Breviolum* cells included in our image analyses maintained high fluorescence signal from photosynthetic pigments to ensure viable phycospheres at the time of imaging. We considered the leakage fraction ( $f$ ) to be constant and not dependent on cell size; however, in reality, leakage fraction may be expected to decrease with increasing cell size, though little information is available on this issue.

Up to 50% of all organic materials produced can be released by phytoplankton<sup>13,14</sup>, and a survey of intracellular DMSP measurements of 55 samples of Symbiodiniaceae found a range of 0.021–3.831 pmol DMSP per cell<sup>15</sup>. In this model, we assumed a doubling rate ( $\mu$ ) of 1 day<sup>-1</sup> or 86,400 s<sup>-1</sup>, a leakage fraction ( $f$ ) of 1/9 (~11%), and an intracellular content ( $\phi$ ) of 1 pmol per cell for a small, spherical phytoplankton (mean radius of *Breviolum* cells in our experiment was 3.3  $\mu$ m), in the absence of fluid flow.

Two further cases, in which  $\mu$ ,  $\phi$ ,  $\frac{f}{1-f}$ , or  $1/D_{\text{agarose}}$  by themselves, or the product of these four terms overall, is 3-fold greater or 3-fold smaller, are calculated and shown as upper and lower boundaries compared to the baseline case scenario (the edges of the shaded region in Supplementary Fig. 13). The former case (*i.e.*, upper boundary) represents the scenario in which parameters are as in the baseline case, but leakage or intracellular DMSP content is high (as is the case for stressed cells<sup>11</sup>; in our model,  $f = 0.25$  or  $\phi = 3$  pmol per cell) or diffusivity is low (*e.g.*, agarose reduces diffusivity by more than 30% of  $D_{\text{solution}}$ ; in our model,  $D_{\text{agarose}} = 0.12 \times 10^{-5}$  cm<sup>2</sup> s<sup>-1</sup>). The same reasoning applies to the lower boundary. Parameters for the baseline case were chosen to represent realistic values, and the two further curves thus provide a measure of possible DMSP concentration ranges in a phycosphere under different conditions.

## Supplementary References

1. Cox III, R. S., Dunlop, M. J. & Elowitz, M. B. A synthetic three-color scaffold for monitoring genetic regulation and noise. *J. Biol. Eng.* **4**, 10 (2010).
2. Kovach, M. E. *et al.* Four new derivatives of the broad-host-range cloning vector pBBR1MCS, carrying different antibiotic-resistance cassettes. *Gene* **166**, 175–176 (1995).
3. Persat, A., Stone, H. A. & Gitai, Z. The curved shape of *Caulobacter crescentus* enhances surface colonization in flow. *Nat. Commun.* **5**, 3824 (2014).
4. Keen, N. T., Tamaki, S., Kobayashi, D. & Trollinger, D. Improved broad-host-range plasmids for DNA cloning in Gram-negative bacteria. *Gene* **70**, 191–197 (1988).
5. Reisch, C. R. *et al.* Novel pathway for assimilation of dimethylsulphonioacetate widespread in marine bacteria. *Nature* **473**, 208–211 (2011).
6. Kessler, B., de Lorenzo, V. & Timmis, K. N. A general system to integrate *lacZ* fusions into the chromosomes of Gram-negative eubacteria: regulation of the *Pm* promoter of the *TOL* plasmid studied with all controlling elements in monocopy. *Mol. Genet. Genomics* **233**, 293–301 (1992).
7. Mitchell, J. G., Okubo, A. & Fuhrman, J. A. Microzones surrounding phytoplankton form the basis for a stratified marine microbial ecosystem. *Nature* **316**, 58–59 (1985).
8. Matrai, P. A. & Keller, M. D. Total organic sulfur and dimethylsulfonylacetate in marine phytoplankton: intracellular variations. *Mar. Biol.* **119**, 61–68 (1994).
9. Spiess, C. E. Determination of the diffusion constants of dimethylsulfide and dimethylsulfonylacetate by diffusion-ordered nuclear magnetic resonance spectroscopy. *Mar. Chem.* **207**, 77–83 (2018).
10. Lundberg, P. & Kuchel, P. W. Diffusion of solutes in agarose and alginate gels:  $^1\text{H}$  and  $^{23}\text{Na}$  PFGSE and  $^{23}\text{Na}$  TQF NMR studies. *Magn. Reson. Med.* **37**, 44–52 (1997).
11. Stefels, J. Physiological aspects of the production and conversion of DMSP in marine algae and higher plants. in *Journal of Sea Research* **43**, 183–197 (2000).
12. Berdalet, E., Llaveria, G. & Simó, R. Modulation of dimethylsulfonylacetate (DMSP) concentration in an *Alexandrium minutum* (Dinophyceae) culture by small-scale turbulence: a link to toxin production? *Harmful Algae* **11**, 88–95 (2011).
13. Thornton, D. C. O. Dissolved organic matter (DOM) release by phytoplankton in the contemporary and future ocean. *Eur. J. Phycol.* **49**, 20–46 (2014).
14. Seymour, J. R., Amin, S. A., Raina, J.-B. & Stocker, R. Zooming in on the phycosphere: the ecological interface for phytoplankton-bacteria relationships. *Nat. Microbiol.* **2**, 17065 (2017).
15. Caruana, A. M. N. & Malin, G. The variability in DMSP content and DMSP lyase activity in marine dinoflagellates. *Prog. Oceanogr.* **120**, 410–424 (2014).



Supplementary Information: Single-cell measurements of marine bacterial transcription reveal the importance of dimethylsulfoniopropionate (DMS) hotspots in ocean sulfur cycling.

Supplementary Table 2: Sequences of all oligonucleotide primers used in this study.

Overlapping regions (~30 bp) for DNA assembly are underlined.

Two extra STOP codons inserted in fluorescent protein sequence are indicated in **red**.

For restriction enzyme cloning (pZS2-200), underlined region contains random sequence (~5 bp) and restriction sites; restriction sites are indicated in **bold**.

Constructed Plasmid	Primer Name	Sequence (5' to 3')	Equivalent Primer	Description of PCR Product or Primer	Template
pCG302	ATFP-frag1-F	<u>CGCTACCAACGGTGGTTTTTTGGCCGGATCGCCCTTCGGTATAATATTT</u>		vector backbone	pBBR1MCS-2
pCG302	ATFP-frag1-R	<u>CCGGTGGGACCCGGGGTCCAGGACCAAGCCATCATTTATCTGCCTCCCA</u>			
pCG302	ATFP-frag2-F	<u>TATCAGGCTCTGGGAGGCGAATAAATGATGGCTGTGGCTCTGACGCC</u>	<i>dmdA</i> promoter (222 bp)		DSS-3 genomic DNA
pCG302	ATFP-frag2-R	<u>CATTGTGGTCTCCTGCCCTTGGTCCACCATGATCGGATCCGACGAGC</u>			
pCG302	ATFP-frag3-F	<u>ATACCAAAACGCTCGTCTGGAGATCGGATCGATGGTGAACAGGGCGAG</u>			pXGFP-2 <i>P<sub>1003</sub></i> :mTFP1
pCG302	ATFP-frag3-R	<u>GCACGATCAAGCTCTCGGATGATATATTAATCTGTACAGCTGGTCCA</u>	mTFP1		
pCG302	ATFP-frag4-F	<u>ACCSAGGCGATGGAGGAGCTGTACAGTAATAATAATCATCGGAGACT</u>			pZS2-123
pCG302	ATFP-frag4-R	<u>CCCATGGGCAATATATACGCAAGGGGATCGCGCAAAACACCAC</u>	15-bp spacer region + RN <sup>II</sup> and TSAL terminators		
pCG303	Wmk4-frag1-F	<u>AGTGAAGCTTTCGTTTTATTTGATGCTGGTGGCTTCGCTATGATATATTT</u>		vector backbone	pBBR1MCS-2
pCG303	Wmk4-frag1-R	<u>GTTCATTGATTCCTATTATTTTGTGACATCATTATCTGCCTCCCA</u>			
pCG303	Wmk4-frag2-F	<u>TATCAGGCTCTGGGAGGCGAATAAATGATGTCGACAAAATAATGAGAATCA</u>	231-bp inter-promoter spacer region + <i>dddW</i> promoter (500 bp)		pZS2-200
pCG303	Wmk4-frag2-R	<u>GATGTTCTCCTTAATGAGTCCCTCAGCATGATGGCCCTCTTGTGGTTG</u>			
pCG303	Wmk4-frag3-F	<u>TAAGTACCCCAAGCAAGGAGCCCATCATGGTGAAGGAGCTGATTA</u>			pXGFP-2 <i>P<sub>1003</sub></i> :mKate2
pCG303	Wmk4-frag3-R	<u>CTTCTGATCCGAGCAGCCTGCATATATTAATCTGTGCCCAAGTTTCG</u>	mKate2		
pCG303	Wmk4-frag4-F	<u>CCTAGCAACTGGGGCAAGATAATAATAAGTGGAGCTGTCTCGAT</u>	TR2-17, TL17, BS7, T7E1 terminators		pZS2-123
pCG303	Wmk4-frag4-R	<u>CCCATGGGCAATATATACGCAAGGGGACCCAGGCATCAATAAACA</u>			
pCG301	reguln-frag1-F	<u>CGCTACCAAGTCAACACTCTTTTGTGATAAATCGCCTTCGGTATAATTT</u>		vector backbone	pBBR1MCS-2
pCG301	reguln-frag1-R	<u>CGCTACCAACGGTGGTTTTTTGGCCGGATCATCATTTATCTGCCTCCCA</u>			
pCG301	reguln-frag2-F	<u>TATCAGGCTCTGGGAGGCGAATAAATGATGTCGCGCAAGCAAGCACC</u>	<i>P<sub>1003</sub></i> :mTFP1 + terminators		pCG302
pCG301	reguln-frag2-R	<u>GTTCATTGATTCCTATTATTTTGTGACGGCTGTGGCTCGACGC</u>			
pCG301	reguln-frag3-F	<u>CCGGTGGGACCCGGGCTCAGGACCAAGCCGTCGACAAAATAATGAGAATC</u>	<i>P<sub>1003</sub></i> :mKate2 + terminators		pCG303
pCG301	reguln-frag3-R	<u>GGTATGAGCAAGCTGATAAATAATAATAAAGCCAGGCATCAATAAACA</u>			
pCG301	reguln-frag4-F	<u>CGTTTGGTTTTTATGATGCTGGTTATATATTTATACAGTTCGTCACCC</u>	Venus YFP		pZS2-123
pCG301	reguln-frag4-R	<u>CATCTAGATAAAGAGGAGAAATTAAGCATGAGCAAGGTGAAGAATC</u>			
pCG301	reguln-frag5-F	<u>CCCGGTGACAGTCTTGCACCTTTCGCTGCTTAACTCTCTTTAATCTAG</u>	<i>P<sub>1003</sub></i> promoter (107 bp)		pXGFP-2 <i>P<sub>1003</sub></i> :mTFP1
pCG301	reguln-frag5-R	<u>CGCCATGGGCAATATATACGCAAGGGGATTTATCAAAAAGAGTGGACTTG</u>			
pCG401	goofy-frag1-F	<u>ACCGAGCGCATGGAGGAGCTGTACAGTAATAATAATGCAGGTGCTCG</u>	(WTFP-frag1-F)	vector backbone + <i>P<sub>1003</sub></i> promoter + Venus YFP	pCG301
pCG401	goofy-frag1-R	<u>GACCTCCGCAAGTGGGGGACAGATAATAATCATCGCGAAGCTTGATC</u>			
pCG401	goofy-frag2-F	<u>GCACCCTCAAGTCTTCGGGATGATATATATATCTGTCCCCAGTTTC</u>	(AmK-frag2-R)	mKate2	pXGFP-2 <i>P<sub>1003</sub></i> :mKate2
pCG401	goofy-frag2-R	<u>ATACCAATACCGCTCGTGGAGATCCGATGATGGTGAAGGAGCTGATTA</u>	(AmK-frag2-F)		
pCG401	goofy-frag3-F	<u>CATGTTCTCCTTAATGAGCTGGCTCACCATGATGGGATCTCCAGAGGAGC</u>	<i>dmdA</i> promoter (222 bp) + inter-promoter spacer region (231 bp) + <i>dddW</i> promoter (500 bp)		pCG301
pCG401	goofy-frag3-R	<u>CATTGTGGTCTCCTGCCCTTGGTCCACCATGATGGGATCCGACGAGC</u>	(WTFP-frag1-R)		
pCG401	goofy-frag4-F	<u>TAAGTACCCCAAGCAAGGAGCCCATCATGGTGAAGGAGGCGA</u>	(WTFP-frag2-F)		pXGFP-2 <i>P<sub>1003</sub></i> :mTFP1
pCG401	goofy-frag4-R	<u>CTTCTGATCCGAGGAGCCTGCATATATTAATCTGTACAGCTGTCCATGC</u>	(WTFP-frag2-R)		
pCG402	AmK-frag1-F	<u>CGCTACCAACGGTGGTTTTTTGGCCGGATCGCCCTTCGGTATAATTTGCC</u>		vector backbone + <i>dmdA</i> promoter (222 bp)	pCG302
pCG402	AmK-frag1-R	<u>CATGTTCTCCTTAATGAGCTGGCTCACCATGATGGGATCTCCAGAGGAGC</u>	(goofy-frag3-F)		
pCG402	AmK-frag2-F	<u>ATACCAATACCGCTCGTGGAGATCCGATCATGGTGAAGGAGCTGATTA</u>	(goofy-frag2-F)	mKate2	pXGFP-2 <i>P<sub>1003</sub></i> :mKate2
pCG402	AmK-frag2-R	<u>GCACCCTCAAGTCTTCGGGATGATATATATATCTGTCCCCAGTTTC</u>	(goofy-frag2-R)		
pCG403	WTFP-frag1-F	<u>ACCGAGCGCATGGAGGAGCTGTACAGTAATAATAATGCAGGTGCTCG</u>	(goofy-frag1-F)	vector backbone + <i>dddW</i> promoter (500 bp)	pCG303
pCG403	WTFP-frag1-R	<u>CATTGTGGTCTCCTGCCCTTGGTCCACCATGATGGGATCCGACGAGC</u>	(goofy-frag3-R)		
pCG403	WTFP-frag2-F	<u>TAAGTACCCCAAGCAAGGAGCCCATCATGGTGAAGGAGGCGA</u>	(goofy-frag4-F)	mTFP1	pXGFP-2 <i>P<sub>1003</sub></i> :mTFP1
pCG403	WTFP-frag2-R	<u>CTTCTGATCCGAGGAGCCTGCATATATTAATCTGTACAGCTGTCCATGC</u>	(goofy-frag4-R)		
pCG101	PAmkKate-frag2-F	<u>TATCAGGCTCTGGGAGGCGAATAAATGATTTTATCAAAAAGAGTGGACTTG</u>	(PATFP-frag2-F)	<i>P<sub>1003</sub></i> promoter + mKate2	pXGFP-2 <i>P<sub>1003</sub></i> :mKate2
pCG101	PAmkKate-frag2-R	<u>GGGCAATATATACGCAAGGGGATATATATATCTGTGCCCCAGTTTC</u>			
pCG102	PAVenus-frag2-F	<u>TATCAGGCTCTGGGAGGCGAATAAATGATTTTATCAAAAAGAGTGGACTTG</u>	<i>P<sub>1003</sub></i> promoter (107 bp)		pXGFP-2 <i>P<sub>1003</sub></i> :mTFP1
pCG102	PAVenus-frag2-R	<u>CCCGGTGACAGTCTTGCACCTTTCGCTGCTTAACTCTCTTTAATCTAG</u>			
pCG102	PAVenus-frag3-F	<u>ACATCTAGATAAAGAGGAGAAATTAAGCATGAGCAAGGTGAAGAATC</u>	Venus YFP		pZS2-123
pCG102	PAVenus-frag3-R	<u>GGGCAATATATACGCAAGGGGATATATATTTATACAGTTCGTCACCC</u>			
pCG103	PATFP-frag2-F	<u>TATCAGGCTCTGGGAGGCGAATAAATGATTTTATCAAAAAGAGTGGACTTG</u>	(PAmkKate-frag2-F)	<i>P<sub>1003</sub></i> promoter + mTFP1	pXGFP-2 <i>P<sub>1003</sub></i> :mTFP1
pCG103	PATFP-frag2-R	<u>GGGCAATATATACGCAAGGGGATATATATTTACTGTGACAGCTGTCCA</u>			
pZS2-200	PdmdA-F	<u>CTGATACCTAGGATCGGATCTCCAGACGAGC</u>		AvrII restriction site + <i>dmdA</i> promoter (500 bp)	DSS-3 genomic DNA
pZS2-200	PdmdA-R	<u>ATATCCGGGAGATCGAGGTGGTACTGCTG</u>		XmaI restriction site + <i>dmdA</i> promoter (500 bp)	DSS-3 genomic DNA
pZS2-200	PdddW-F	<u>ATTTCTGAGCGGGGCTCGCCTCACCATCTCC</u>		XhoI restriction site + <i>dddW</i> promoter (500 bp)	DSS-3 genomic DNA
pZS2-200	PdddW-R	<u>ACTGGATCCGATGGCTCTTTGTGCTTG</u>		BamHI restriction site + <i>dddW</i> promoter (500 bp)	DSS-3 genomic DNA
pZS2-200	Pfbc-F	<u>CGCCGAAAGATCTTCAGCTGTTCCCTGTGAAAT</u>		XmI restriction site + <i>lac</i> promoter weakly active in DSS-3	pRR415
pZS2-200	Pfbc-R	<u>AACCTCGACATGTGAGTTAGTCACTCA</u>		Sall restriction site + <i>lac</i> promoter weakly active in DSS-3	pRR415
-	R-dlag-PdmdA	GGAAGTCGAGGTGGTACT		primer for diagnostic sequencing of pZS2-200	
-	F-dlag-PdddW	CAGGAGTATGGTAGGCCACC		primer for diagnostic sequencing of pZS2-200	
-	R-dlag-PdddW	CCATCCGGATCCCGGTGACAGAAA		primer for diagnostic sequencing of pZS2-200	
-	pBBR <sub>1</sub> -F	CTTGGGCTGTATGGCCTTC		primer for diagnostic sequencing of all pBBR1MCS-2 vector backbone plasmids	
-	pBBR <sub>1</sub> -R	TGAAGCCCTTCTGGAC		primer for diagnostic sequencing of all pBBR1MCS-2 vector backbone plasmids	
-	pBBR <sub>1</sub> -diag <sub>1</sub> -F	GCACCTGCTACGGATTCA		primer for diagnostic sequencing of all pBBR1MCS-2 vector backbone plasmids; binding site 37 bp upstream of cloning site	
-	pBBR <sub>1</sub> -diag <sub>1</sub> -R	CCCTATACCTTGTCTGC		primer for diagnostic sequencing of all pBBR1MCS-2 vector backbone plasmids; binding site 118 bp upstream of cloning site	
-	pBBR <sub>1</sub> -diag <sub>2</sub> -F	GGGATCTCATCTGGAATT		primer for diagnostic sequencing of all pBBR1MCS-2 vector backbone plasmids; binding site 40 bp downstream of cloning site	
-	3cv <sub>3</sub> -diag <sub>1</sub> -F	AAGGTGGTACCCGTAC		primer for diagnostic sequencing; binding site in the middle of <i>dddW</i> promoter sequence	
-	3cv <sub>3</sub> -diag <sub>1</sub> -R	AAACGCCCTTCCGCAAG		primer for diagnostic sequencing; binding site in the middle of terminator sequence	
-	midmKate <sub>2</sub> -diag <sub>1</sub> -R	CGGCATCTTGAGTTC		primer for diagnostic sequencing; binding site in the middle of mKate2 sequence	

## Reporting Summary

Nature Research wishes to improve the reproducibility of the work that we publish. This form provides structure for consistency and transparency in reporting. For further information on Nature Research policies, see [Authors & Referees](#) and the [Editorial Policy Checklist](#).

### Statistics

For all statistical analyses, confirm that the following items are present in the figure legend, table legend, main text, or Methods section.

n/a Confirmed

- The exact sample size ( $n$ ) for each experimental group/condition, given as a discrete number and unit of measurement
- A statement on whether measurements were taken from distinct samples or whether the same sample was measured repeatedly
- The statistical test(s) used AND whether they are one- or two-sided  
*Only common tests should be described solely by name; describe more complex techniques in the Methods section.*
- A description of all covariates tested
- A description of any assumptions or corrections, such as tests of normality and adjustment for multiple comparisons
- A full description of the statistical parameters including central tendency (e.g. means) or other basic estimates (e.g. regression coefficient) AND variation (e.g. standard deviation) or associated estimates of uncertainty (e.g. confidence intervals)
- For null hypothesis testing, the test statistic (e.g.  $F$ ,  $t$ ,  $r$ ) with confidence intervals, effect sizes, degrees of freedom and  $P$  value noted  
*Give  $P$  values as exact values whenever suitable.*
- For Bayesian analysis, information on the choice of priors and Markov chain Monte Carlo settings
- For hierarchical and complex designs, identification of the appropriate level for tests and full reporting of outcomes
- Estimates of effect sizes (e.g. Cohen's  $d$ , Pearson's  $r$ ), indicating how they were calculated

*Our web collection on [statistics for biologists](#) contains articles on many of the points above.*

### Software and code

Policy information about [availability of computer code](#)

Data collection

Data analysis

For manuscripts utilizing custom algorithms or software that are central to the research but not yet described in published literature, software must be made available to editors/reviewers. We strongly encourage code deposition in a community repository (e.g. GitHub). See the Nature Research [guidelines for submitting code & software](#) for further information.

### Data

Policy information about [availability of data](#)

All manuscripts must include a [data availability statement](#). This statement should provide the following information, where applicable:

- Accession codes, unique identifiers, or web links for publicly available datasets
- A list of figures that have associated raw data
- A description of any restrictions on data availability

### Field-specific reporting

Please select the one below that is the best fit for your research. If you are not sure, read the appropriate sections before making your selection.

- Life sciences       Behavioural & social sciences       Ecological, evolutionary & environmental sciences

For a reference copy of the document with all sections, see [nature.com/documents/nr-reporting-summary-flat.pdf](https://www.nature.com/documents/nr-reporting-summary-flat.pdf)

## Ecological, evolutionary & environmental sciences study design

All studies must disclose on these points even when the disclosure is negative.

Study description	In this study, a model marine microorganism ( <i>Ruegeria pomeroyi</i> DSS-3) was genetically engineered to visually report the expression of dimethylsulfoniopropionate (DMSP) degradation genes. Unless otherwise noted, three replicate experiments, each with hundreds to thousands of cells, were performed.
Research sample	<i>Ruegeria pomeroyi</i> DSS-3 strains transformed with engineered plasmids containing 1–3 promoter-fluorescent protein fusions.
Sampling strategy	For each experiment, a single colony was picked from a culture plate to inoculate overnight liquid cultures (unless otherwise noted). Cells were prepared for experimentation at the same growth phase (OD) for each experiment. In each observation chamber of a microfluidic chip, microscopy fields of views were manually selected with roughly equal spacing for time-lapse observation.
Data collection	We used phase contrast and fluorescence microscopy to capture time-resolved images.
Timing and spatial scale	Images were captured every 45 minutes for 24 hours. Images were acquired with an electron multiplying CCD (EMCCD) camera (iXon3 885; Andor Technology) (1004 × 1002 pixels at 8 μm/pixel), unless otherwise indicated.
Data exclusions	N/A
Reproducibility	Unless otherwise indicated, three replicates were generated and confirmed to generate consistent results.
Randomization	N/A
Blinding	N/A
Did the study involve field work?	<input type="checkbox"/> Yes <input checked="" type="checkbox"/> No

## Reporting for specific materials, systems and methods

We require information from authors about some types of materials, experimental systems and methods used in many studies. Here, indicate whether each material, system or method listed is relevant to your study. If you are not sure if a list item applies to your research, read the appropriate section before selecting a response.

### Materials & experimental systems

- | n/a                                 | Involved in the study                                |
|-------------------------------------|--|
| <input checked="" type="checkbox"/> | <input type="checkbox"/> Antibodies                  |
| <input checked="" type="checkbox"/> | <input type="checkbox"/> Eukaryotic cell lines       |
| <input checked="" type="checkbox"/> | <input type="checkbox"/> Palaeontology               |
| <input checked="" type="checkbox"/> | <input type="checkbox"/> Animals and other organisms |
| <input checked="" type="checkbox"/> | <input type="checkbox"/> Human research participants |
| <input checked="" type="checkbox"/> | <input type="checkbox"/> Clinical data               |

### Methods

- | n/a                                 | Involved in the study                           |
|-------------------------------------|---|
| <input checked="" type="checkbox"/> | <input type="checkbox"/> ChIP-seq               |
| <input checked="" type="checkbox"/> | <input type="checkbox"/> Flow cytometry         |
| <input checked="" type="checkbox"/> | <input type="checkbox"/> MRI-based neuroimaging |

## 2.2 Publication 2

“A new glance at the chemosphere of macroalgal–bacterial interactions: In situ profiling of metabolites in symbiosis by mass spectrometry.”

Marine Vallet, Filip Kaftan, Veit Grabe, Fatemeh Ghaderiardakani, Simona Fenizia, Aleš Svatoš, Georg Pohnert, Thomas Wichard

*Beilstein Journal of Organic Chemistry*, Vol. 17, 1313–1322, 2021  
DOI: 10.3762/bjoc.17.91

Open Access This article is licensed under a Creative Commons Attribution 4.0 International License

Vallet M.<sup>1</sup>, Kaftan F.<sup>2</sup>, Veit G.<sup>3</sup>, Ghaderiardakani F.<sup>4</sup>, Fenizia S.<sup>5</sup>, Svatoš A.<sup>6</sup>, Pohnert G.<sup>7</sup>, Wichard T.<sup>8</sup> A new glance at the chemosphere of macroalgal–bacterial interactions: In situ profiling of metabolites in symbiosis by mass spectrometry. *Beilstein Journal of Organic Chemistry*, 2021 17, 1313–1322. 10.3762/bjoc.17.91

Author	1	2	3	4	5	6	7	8
Development of concept	x							x
Planning of research	x							x
Data collection	x	x	x					x
Data analysis	x	x	x	x	x			
Preparation of the manuscript	x	x	x	x	x	x	x	x
Correction of the manuscript	x	x	x	x	x	x	x	x
Proposed publication equivalent					0.5			

### Authors contribution:

Marine Vallet	Conceptualization, research planning, data analysis, writing-original draft, writing-review, editing
Filip Kaftan	Experiment preparation and implementation, data analysis, writing-original draft, writing-review, editing
Veit Grabe	Experiment preparation and implementation, data analysis, writing-original draft, writing-review, editing
Fatemeh Ghaderiardakani	Experiment preparation and implementation, data analysis, writing-original draft, writing-review, editing
Simona Fenizia	Data analysis, writing-original draft, writing-review, editing
Aleš Svatoš	Supervision, writing-review, editing
Georg Pohnert	Supervision, writing-review, editing
Thomas Wichard	Conceptualization, research planning, experiment preparation and implementation, writing-review, editing





# A new glance at the chemosphere of macroalgal–bacterial interactions: In situ profiling of metabolites in symbiosis by mass spectrometry

Marine Vallet<sup>\*1</sup>, Filip Kaftan<sup>2</sup>, Veit Grabe<sup>3</sup>, Fatemeh Ghaderiardakani<sup>4</sup>,  
Simona Fenizia<sup>4,5</sup>, Aleš Svatoš<sup>2</sup>, Georg Pohnert<sup>1,4,6</sup> and Thomas Wichard<sup>\*4</sup>

## Full Research Paper

Open Access

### Address:

<sup>1</sup>Research Group Phytoplankton Community Interactions, Max Planck Institute for Chemical Ecology, Jena, Germany, <sup>2</sup>Research Group Mass Spectrometry/Proteomics, Max Planck Institute for Chemical Ecology, Jena, Germany, <sup>3</sup>Research Group Olfactory Coding, Department of Evolutionary Neuroethology, Max Planck Institute for Chemical Ecology, Jena, Germany, <sup>4</sup>Institute for Inorganic and Analytical Chemistry, Friedrich Schiller University Jena, Germany, <sup>5</sup>Max Planck Institute for Chemical Ecology, Jena, Germany and <sup>6</sup>Microverse Cluster, Friedrich Schiller University Jena, Germany

### Email:

Marine Vallet<sup>\*</sup> - [mvallet@ice.mpg.de](mailto:mvallet@ice.mpg.de); Thomas Wichard<sup>\*</sup> - [Thomas.Wichard@uni-jena.de](mailto:Thomas.Wichard@uni-jena.de)

\* Corresponding author

### Keywords:

algae; AP-SMALDI; ectoine; holobiont; high-resolution mass spectrometry; mass spectrometry imaging; marine bacteria; Ulva

*Beilstein J. Org. Chem.* **2021**, *17*, 1313–1322.

<https://doi.org/10.3762/bjoc.17.91>

Received: 31 December 2020

Accepted: 28 April 2021

Published: 19 May 2021

This article is part of the thematic issue "Chemical ecology".

Guest Editor: C. Beemelmanns

© 2021 Vallet et al.; licensee Beilstein-Institut.

License and terms: see end of document.

## Abstract

Symbiosis is a dominant form of life that has been observed numerous times in marine ecosystems. For example, macroalgae coexist with bacteria that produce factors that promote algal growth and morphogenesis. The green macroalga *Ulva mutabilis* (Chlorophyta) develops into a callus-like phenotype in the absence of its essential bacterial symbionts *Roseovarius* sp. MS2 and *Maribacter* sp. MS6. Spatially resolved studies are required to understand symbiont interactions at the microscale level. Therefore, we used mass spectrometry profiling and imaging techniques with high spatial resolution and sensitivity to gain a new perspective on the mutualistic interactions between bacteria and macroalgae. Using atmospheric pressure scanning microprobe matrix-assisted laser desorption/ionisation high-resolution mass spectrometry (AP-SMALDI-HRMS), low-molecular-weight polar compounds were identified by comparative metabolomics in the chemosphere of *Ulva*. Choline (2-hydroxy-*N,N,N*-trimethylethan-1-aminium) was only determined in the alga grown under axenic conditions, whereas ectoine (1,4,5,6-tetrahydro-2-methyl-4-pyrimidinecarboxylic acid) was found in bacterial presence. Ectoine was used as a metabolic marker for localisation studies of *Roseovarius* sp. within the tripartite community because it was produced exclusively by these bacteria. By combining confocal laser scanning microscopy (cLSM) and AP-SMALDI-HRMS, we proved that *Roseovarius* sp. MS2 settled mainly in the rhizoidal zone (holdfast) of *U. mutabilis*. Our findings provide the fundament to decipher bacterial symbioses with multicellular hosts in aquatic ecosystems

in an ecologically relevant context. As a versatile tool for microbiome research, the combined AP-SMALDI and cLSM imaging analysis with a resolution to level of a single bacterial cell can be easily applied to other microbial consortia and their hosts. The novelty of this contribution is the use of an in situ setup designed to avoid all types of external contamination and interferences while resolving spatial distributions of metabolites and identifying specific symbiotic bacteria.

## Introduction

In intertidal zones with high temporal and spatial ecosystem variations, bacteria and macroalgae establish close mutualistic relationships, in which both gain reciprocal benefits forming an ecological unit (holobiont) [1–3]. Chemical exchange and physical proximity are the basis of this algae–bacterial mutualism [4], but little is known about the spatial distribution of the bacteria on the algal host and the locally released and exchanged compounds within the algal chemosphere [3]. Bacterial biofilms on macroalgae can be crucial for developing algae and their interactions with other marine organisms. The exchange of resources in this spatially limited region is of high interest for understanding the macroalgal–bacterial interactions. The chemosphere was proposed as a region that supports chemical mediator-based cross-kingdom interactions [3]. High-throughput sequencing analysis provides the abundance and composition of the bacterial community on macroalgal surfaces [5,6]. It does not reveal any information on the metabolically active bacteria and the spatial distribution of substances exchanged. While the study of bacterial symbiosis is often limited to either chemistry or microscopy work, recent functional and metabolomics methods are available to enable chemical imaging of specialised metabolites involved in host–bacteria interactions.

In our study, comparative metabolomics using atmospheric pressure scanning microprobe matrix-assisted laser desorption/ionisation high-resolution mass spectrometry (AP-SMALDI-HRMS) enables the identification of specialised metabolites of the marine macroalga *Ulva mutabilis* (Chlorophyta) and its associated essential bacteria, a model system for cross-kingdom interactions [7]. The method provides a tool to formulate hypotheses about metabolic processes in the phycosphere while preserving spatial structure. This novel depth of insight into a multicellular host and bacteria interactions can characterise natural products in symbiotic interactions.

Algal growth and morphogenesis-promoting factors (AGMPFs) are required for the development of the model organism *U. mutabilis* [7]. They are provided by a combination of two essential bacteria, *Maribacter* sp. MS6 and *Roseovarius* sp. MS2 forming a tripartite community [3,7,8] (see also Figure 1a and the Graphical Abstract). In turn, *Roseovarius* sp. benefits from the released photosynthate glycerol as a carbon source [9]. Axenic *Ulva* germ cells (i.e. gametes) develop into a callus-like phenotype composed of undifferentiated cells with malformed

cell walls [8,10]. Up to now, the bacterial sesquiterpenoid thalusin, released by *Maribacter* spp. [11,12], is the only known AGMPF that induces morphogenesis such as rhizoid and cell-wall formation in *Ulva* spp. [11,12] or thallus development in *Monostroma* spp. [13]. The *Roseovarius*-factor that promotes cell division is still unknown [3,8]. Algal substances are released into the surrounding environment to attract epiphytic bacteria and initiate the cross-kingdom interaction [14,15]. *Ulva* attracts *Roseovarius* sp. MS2 through the sulphur-containing zwitterion dimethylsulphoniopropionate (DMSP), resulting in biofilm formation on the algal surrounding [9]. The bacterium subsequently uses the provided glycerol for growth and transforms DMSP into methanethiol and dimethyl sulphide [9].

The metabolic activities of marine bacteria and algae can be surveyed using mass spectrometry-based methods. For example, stable sulphur isotope ( $^{34}\text{S}$ ) labelled DMSP was used to track DMSP uptake and degradation by marine bacteria, and secondary ion mass spectrometry was applied to visualise it at the single-cell level [16]. The interaction between epibiotic bacteria on algal surfaces and their metabolic activities can be monitored in situ or using an imprinting method by desorption electrospray ionisation mass spectrometry [17,18]. In *U. mutabilis* gametophytes, matrix-assisted laser desorption ionisation mass spectrometry imaging (MALDI-MSI) was used to identify cell differentiation markers [19]. However, there has yet to be a thorough investigation of associated-mutualistic bacteria. MALDI-MSI has been shown to have high sensitivity and spatial resolution at the microscale in plant tissues, plankton, and other microbes [20,21].

The application of a MALDI matrix to a sample is an important part of the MALDI-MSI experiment. MALDI-MS can be used to identify proteins and metabolic signatures [22–24] from bacteria and microalgae, as well as biofilms [25]. The primary function of the applied matrix is to improve the quality of the MS spectra, particularly the signal intensities of the compounds of interest. In some cases, the matrix might also work in opposition to this premise, suppressing desired ions. Then, matrix-free approaches such as LDI-HRMS can overcome this limiting phenomenon and have been applied for species-level microalgal identification based on metabolic profile fingerprint matching [26–28].

Our research combines cutting-edge laser scanning microscopy and high-resolution mass spectrometry to uncover *Ulva*/bacteria interactions and specialised metabolites at the microscale level. In this study, we demonstrate that the chemosphere of *U. mutabilis* changes depending on the presence or absence of the bacterial symbionts (*Roseovarius* sp. MS2 and *Maribacter* sp. MS6). As a result, specific metabolic markers can be used to identify bacteria in the vicinity of *U. mutabilis*. We used an untargeted comparative metabolomics approach that also provides micrometre-resolved MS imaging data through AP-SMALDI-HRMS. Two sample preparations, matrix-free LDI and MALDI, were performed to increase the range of metabolites recovered with this type of ionisation. We identified significant metabolites that define the host–bacteria interactions based on spectral similarity with standards. Using combined imaging mass spectrometry and confocal laser scanning microscopy, we then linked the chemical and microscopic observations that characterise the symbiotic association (cLSM).

## Results and Discussion

### Comparative metabolomics using AP-SMALDI-HRMS identifies metabolites in axenic algae and those present during macroalgal–bacterial symbiosis

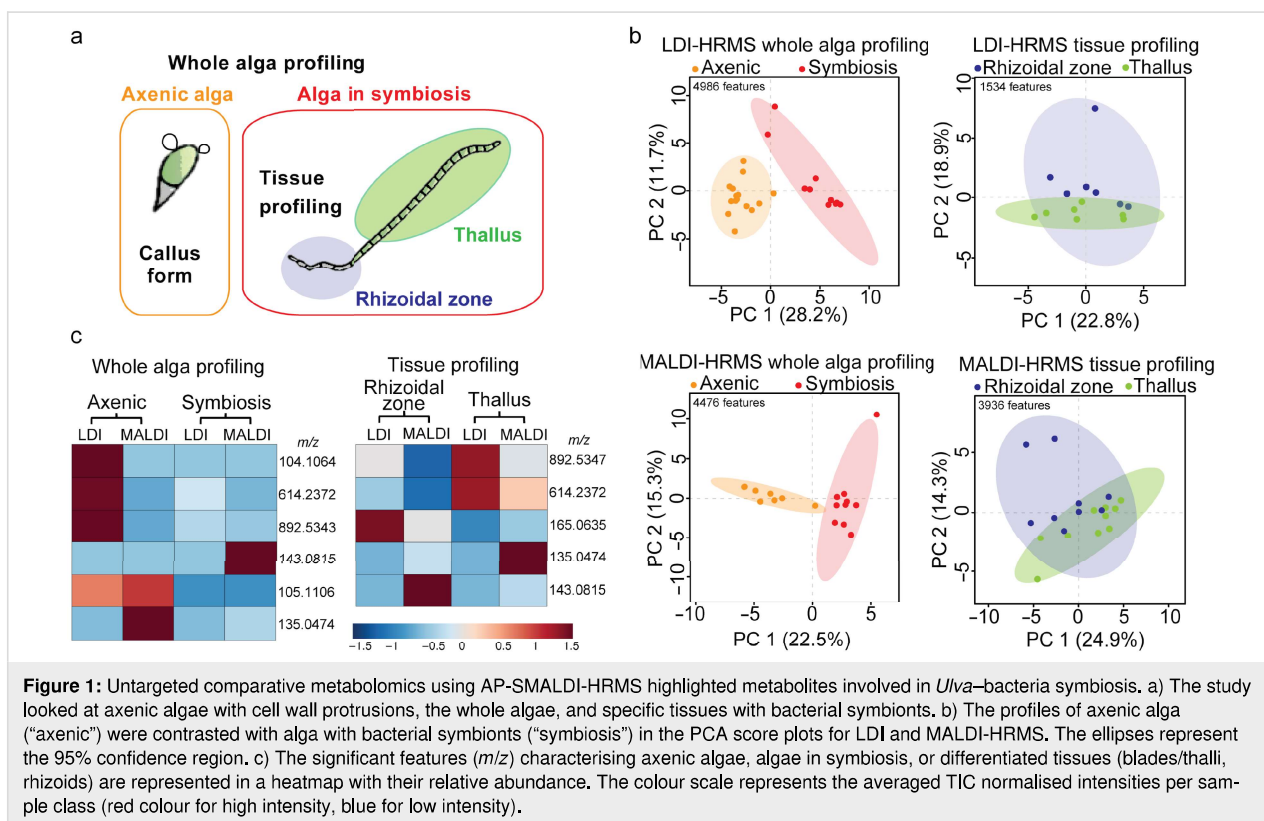
Axenic gametes of *U. mutabilis* (phenotype slender) were allowed to settle onto glass plates in Petri dishes filled with growth medium. In the absence of the symbionts, the axenic gametes developed into undifferentiated cells known as the callus-like form [8,29]. In the second set of samples, algae were inoculated with the two marine bacteria, *Roseovarius* sp. MS2 and *Maribacter* sp. MS6, developing into a phenotype composed of bilayer cells and organised tissues, as previously reported [8]. The algal germlings incubated with the marine bacteria showed a rhizoidal zone that serves for substrate attachment and a thallus zone. From apex to rhizoid, *Ulva* germlings had an average length of 50 to 150  $\mu\text{m}$  after three weeks of growth. The samples were recovered, dried on tissue, and for MALDI, immediately covered with 2,5-dihydroxybenzoic acid (DHB) applied by spraying. We targeted either specialised tissues (rhizoidal zone versus thallus) or the whole alga germlings (axenic callus versus alga in symbiosis) using a mounted AP-SMALDI camera (Figure 1a). The metabolic profiles of tissue and whole alga were obtained from callus or alga in symbiosis using AP-SMALDI-HRMS with the two sample preparations, either with matrix deposition (MALDI-HRMS) or matrix-free analysis (LDI-HRMS) (Figure 1a and b). The data matrix was generated by processing the raw spectra, and the data tables produced were from 1534 to 4986 features ( $m/z$ ) (Figure 1b and Table S1 in Supporting Information

File 1). The principal component analysis (PCA) visualised differences between metabolic profiles of axenic algae, algae in symbiosis, and specialised tissues (thallus, rhizoidal zone), analysed either with LDI or MALDI-HRMS. The metabolic profiles of axenic algae and algae in symbiosis were significantly different, while tissue-specialised metabolomes were less differentiated in the PCA score plots (Figure 1b). Significant features in the loading plots were listed in a heatmap to compare their relative abundance of intensities averaged per sample class (Figure 1c). Among the statistically significant features in all datasets (Table S1, Supporting Information File 1), six metabolites were identified, which were annotated using spectral similarity with analytical standards. For example, the features  $m/z$  104.1064 and  $m/z$  143.0815 were selected among the significant markers of the MALDI-HRMS profiling of axenic algae and the rhizoid tissue (whole alga profiling) of *U. mutabilis* grown with the marine symbiotic bacteria, respectively (Figure 1c). The heatmap shows the complementarities of both methods, LDI or MALDI-HRMS, as the significant features  $m/z$  104.1064 and  $m/z$  143.0815 have only been detected by one of the two methods.

### Identification of metabolites in *Ulva*–bacteria symbiosis

To identify the selected markers found by the comparative metabolomics study, we searched several mass spectra libraries, including METLIN, and determined the chemical formula based on exact mass. We also used spectral similarity matching of data acquired from analytical standards. Choline was identified from the molecular peak  $m/z$  104.1064 for  $[\text{M}]^+$  (calculated  $m/z$  as  $104.1069 \pm 4.8$  ppm for  $\text{C}_5\text{H}_{14}\text{NO}$ ) in the profiles of axenic *U. mutabilis* (Figure 2a). This small polar metabolite was linked to the metabolic homeostasis of *Ulva lactuca* during tidal cycles [30]. Choline is the precursor of the membrane constituent phosphatidylcholine [31]. We inferred that the accumulation of choline in axenic *U. mutabilis* germlings might correlate with the absence of the key bacterial morphogen thalassin, which induces cell wall and rhizoid formation. The accompanying formation of cell wall protrusions might disrupt the cell membrane arrangement indicated by choline accumulation. Screening the tripartite community *Ulva*–*Roseovarius*–*Maribacter* identified ectoine as a metabolic marker of the rhizoidal zone (Figure 2b). The molecular formula  $\text{C}_6\text{H}_{10}\text{N}_2\text{O}_2$  was deduced from the molecular peak at  $m/z$  143.0817 for  $[\text{M} + \text{H}]^+$  ( $\pm 1.4$  ppm) and  $m/z$  165.0636 for  $[\text{M} + \text{Na}]^+$  ( $\pm 1.2$  ppm) detected in the AP-SMALDI-HRMS profiles of the standard and rhizoid tissue of *U. mutabilis* in symbiosis with the marine bacteria. To separate algal and bacterial metabolism, single colonies of *Roseovarius* sp. MS2 and *Maribacter* sp. MS6 were deposited onto glass slides and analysed with AP-SMALDI-HRMS/MS. Using spectral similarity matching based on the fragmentation pattern





obtained from AP-SMALDI-HRMS/MS experiments, we proved that the bacterial symbiont *Roseovarius* sp. MS2 produces ectoine (Figure 2c). This observation supports earlier assumptions that the rhizoidal zone is mainly colonised by *Roseovarius* sp. MS2 [8,29].

Ectoine is a known osmoprotectant produced by marine bacteria and phytoplankton with high concentrations during saline stress conditions [32]. It has not yet been described in the *Ulva*–bacteria symbiosis. Not all essential genes for ectoine biosynthesis reported by [33] were found in the *U. mutabilis* genome [34], providing further support for the bacterial origin of ectoine. Homologs of EctA (UM017\_0070.1, E value 0.34), EctB (UM084\_0040.1, E value < 0.0001) that provide the central intermediate *N*-acetyl-2,4-diaminobutyrate and EctD (UM025\_0127.1, E value 0.094) an ectoine hydroxylase could be identified. However, a homolog gene for EctC (ectoine synthase) is missing in the *U. mutabilis* genome. In addition, despite the low E value of EctB, the reciprocal NCBI-blast search against the anoxygenic photosynthetic halophile and ectoine-producing bacterium *Halorhodospira halochloris* [35] did not confirm the presence of the sequence in the algal genome. Therefore, it is unlikely that the alga produces ectoine. In summary, ectoine is indicative of *Roseovarius* sp. MS2 in the tripartite community and can serve for localisation studies.

### Localisation of bacterial symbionts of *Ulva mutabilis* using fluorescence microscopy and imaging mass spectrometry

Based on the above results, we combined LDI-MS imaging mass spectrometry and cLSM using a non-specific fluorescence labelling probe to visualise the bacterial cells living in symbiosis with *U. mutabilis*. Following a one-month incubation in clean cuvette slides placed in Petri dishes filled with medium, axenic and bacteria-inoculated *U. mutabilis* germlings were stained with SYBR Gold, a sensitive probe forming a complex with DNA with high fluorescence quantum yield [36]. In the axenic callus-like form, the nuclei of algal cells and the bacterial cells accumulated around the rhizoidal tissue and exhibited the specific fluorescence after SYBR Gold staining (Figure 3a) as previously described [8,37]. These findings indicated that bacteria are associated with their algal host during symbiosis.

In parallel, we visualised the metabolites produced by the biofilm formed around *U. mutabilis* by imaging analysis with AP-SMALDI-HRMS. Three replicates each of the axenic algae, algae in symbiosis, germlings, and bacterial cells in monocultures were imaged after matrix deposition by AP-SMALDI-HRMS over a centimetre-scaled area (Figure 3b). The algal pigment chlorophyll was localised with the algal tissues (Figure 3b and Figure S1 in Supporting Information File 1). Even though

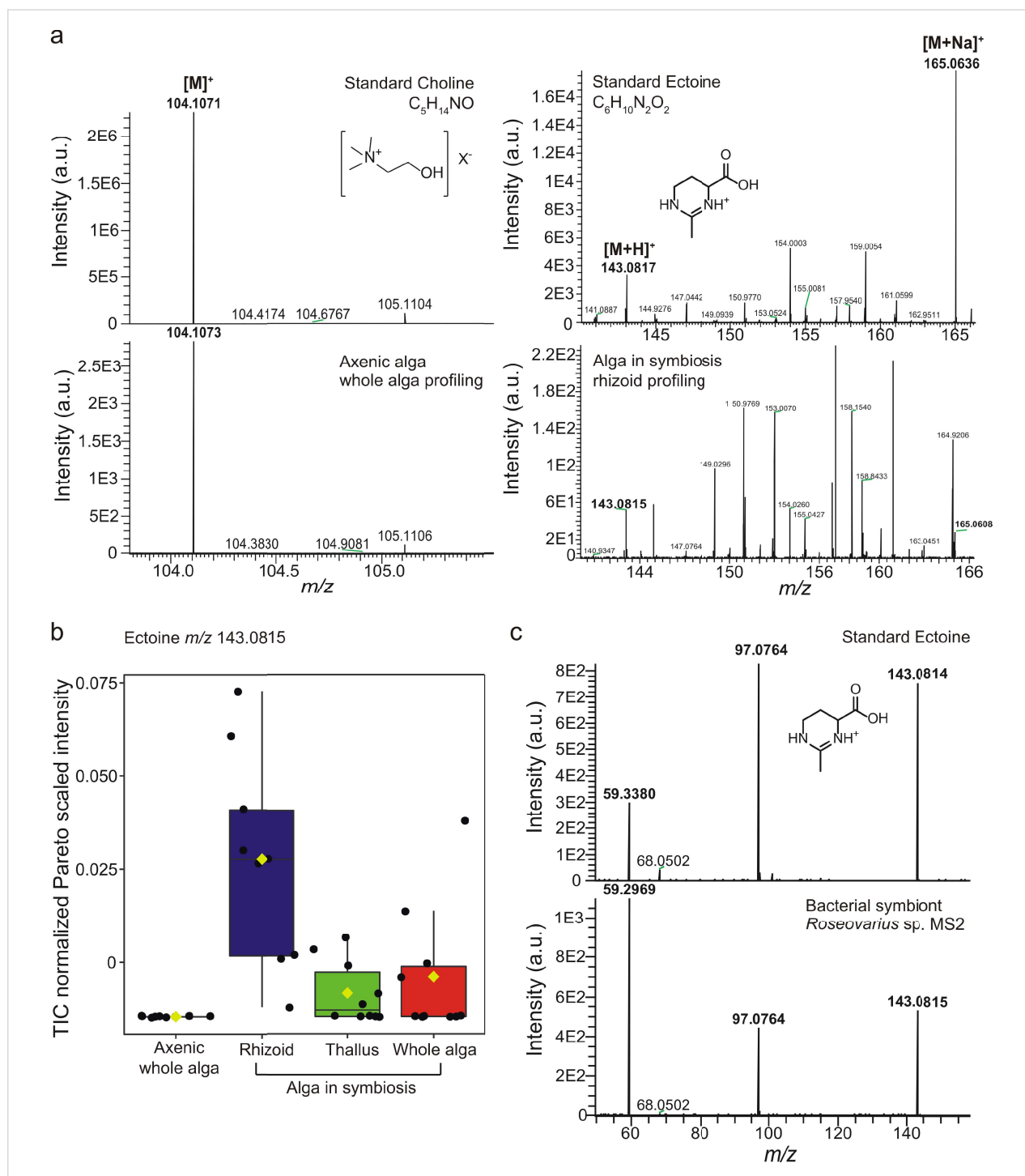
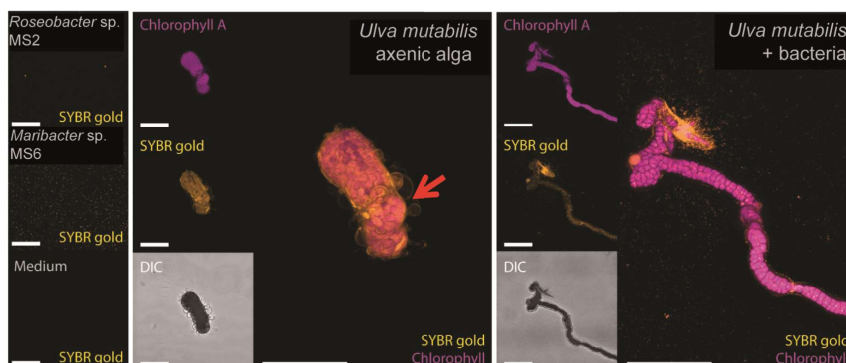


**Figure 2:** Identification of significant features associated with axenic or bacterial symbiont-associated alga *Ulva mutabilis* (phenotype slender). a) The structural determination was achieved by spectral matching with the analytical standards using AP-SMALDI-HRMS. b) Relative amounts of ectoine (*m/z* 143.0815 for [M + H]<sup>+</sup>) were determined by AP-SMALDI-HRMS measurements to compare different tissues: axenic and algae in symbiosis. One-way ANOVA with a Fisher HSD post hoc test found choline to be significant in profiles of axenic algae ( $F = 42$ ,  $P$ -value < 0,0001) and ectoine in profiles of rhizoidal zones of algae in symbiosis ( $F = 4$ ,  $P$ -value < 0,005) (colour code with reference to Figure 1a). c) Ectoine (*m/z* 143.0815 for [M + H]<sup>+</sup>, precursor ion) was identified in a single colony of the bacterial symbiont *Roseovarius* sp. MS2 using AP-SMALDI-HRMS/MS analysis.

most of the seawater media was removed from the *Ulva* samples during sample preparation, crystallisation of seawater salts on the sample surface occurred. The size of the crystals and

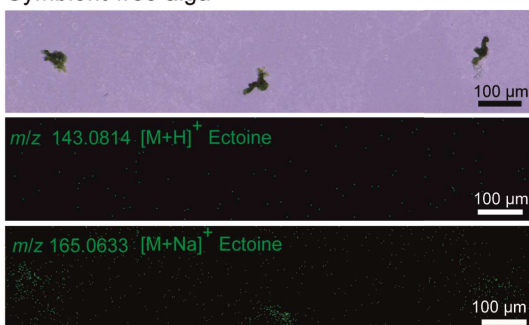
their distribution within an imaged area were examined using a digital microscope and found to be homogeneous and consistent across the samples and experiments. As a result, the ion

## a Cytochemical staining with confocal laser scanning microscopy



## b AP-SMALDI-HRMS

## Symbiont-free alga



## Roseovarius sp. MS2

## Alga in symbiosis with bacteria

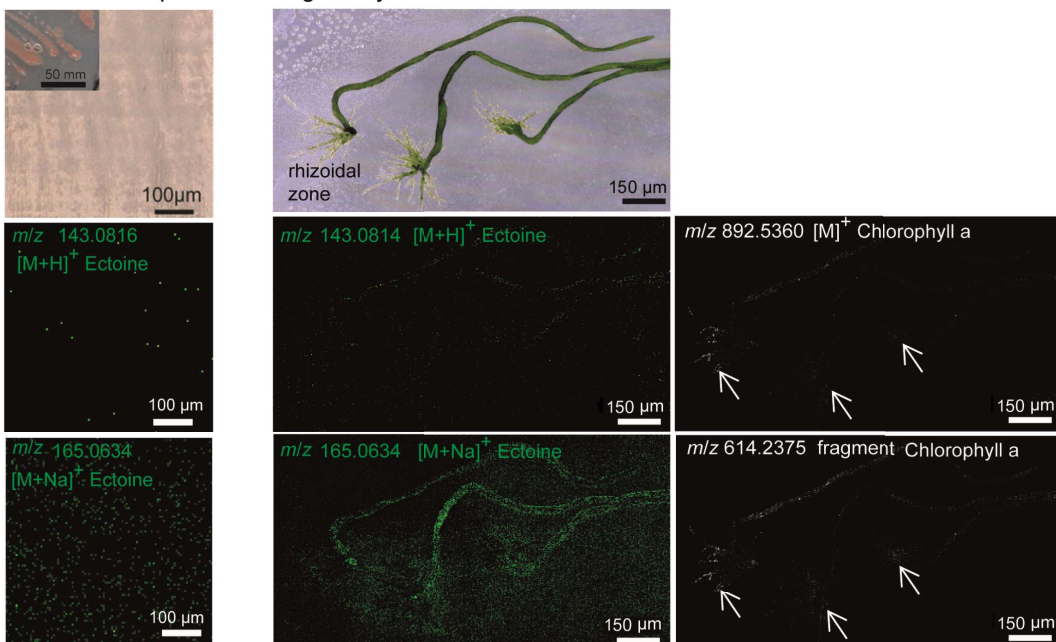


**Figure 3:** Visualisation of algae *Ulva mutabilis* grown under axenic conditions or with bacterial symbionts *Roseovarius* sp. MS2 and *Maribacter* sp. MS6. a) Images acquired after nucleic acid staining with SYBR gold and with confocal laser scanning microscopy. The protrusion of alga grown without bacterial symbiont is highlighted (red arrow). DIC: differential interference microscopy. b) The images show ectoine spatial localisation and thus the presence of *Roseovarius* sp. ( $m/z$  143.0814 for  $[M + H]^+$ ,  $m/z$  165.0633 for  $[M + Na]^+$ , shown in green) as well as chlorophyll ( $m/z$  892.5360 for  $[M + H]^+$ ,  $m/z$  614.2375 fragment shown in white). These metabolite traces are visible in axenic algae, symbiotic algae, and cell cultures of bacteria *Roseovarius* sp. MS2. White arrows indicate the rhizoidal zones.

suppression effect caused by the presence of seawater crystals on the *Ulva* samples and surroundings was consistent across all measurements (Supporting Information File 1, Figures S1 and S2).

Ectoine was detected in both profiling and imaging MS spectra as the  $[M + Na]^+$  adduct at  $m/z$  165.0633. Ectoine was mainly found around the rhizoid in elevated amounts. Thus, *Roseovarius* sp. MS2 became visible in the rhizoidal zone and on the thallus due to the exclusive production of ectoine within the tripartite community (Figure 3b). AP-SMALDI-HRMS studies extended to the entire clade of motile Rhodobacteraceae will reveal other characteristic metabolites of the *Ulva*–bacteria interactions. Those species attracted by *U. mutabilis* (e.g., through DMSP) that use the provided photosynthates [9], will preferentially succeed the previously described competitive colonisations of *Ulva* spp. [38,39]. Also, related species of *Roseovarius* sp. MS2 can often release unknown AGMPFs [29,40], which further foster the bacterial–algal interactions. As more species-specific metabolic markers become available, AP-SMALDI imaging will be a powerful tool to track these dynamic microbial colonisation processes using the *U. mutabilis* model system with a designed microbiome.

## Conclusion

Metabolic profiling of whole alga and specialised tissues conducted with AP-SMALDI-HRMS enabled identifying specific metabolites in host–bacteria symbiosis. We report the first identification of choline and ectoine as markers of symbiont-free *U. mutabilis* and rhizoid tissue of algae in symbiosis with bacteria. We visualised the rhizoidal zone formed by the bacterial symbionts using chemical staining, confocal laser scanning microscopy, and imaging mass spectrometry. Notably, ectoine was used as a metabolic marker to identify bacteria in the biofilm associated with *U. mutabilis* and the algal surface. Visualising the spatial distribution of epiphytic bacteria in the phycosphere will contribute to the general understanding of the chemically mediated cross-kingdom interactions. The combined AP-SMALDI and cLSM imaging with resolution down to the level of a single bacterial cell introduced here can be applied to other microbial consortia and their hosts and will be instrumental for microbiome research.

## Experimental

### Biological experiments and imaging microscopy

The laboratory strains of *U. mutabilis* (sl-G[mt+]) are direct descendants of the original isolates collected by B. Føyn in Portugal (Ria Formosa) in 1958 [8]. This strain is used as a model organism in cross-kingdom interactions [7,34,37] and

cultivated under standardised conditions [41,42]. *Ulva* strains are available from the corresponding author (Thomas Wichard, Friedrich-Schiller-Universität Jena, Germany).

Gametogenesis of *U. mutabilis* was induced by chopping harvested algal tissue, and released gametes were purified from accompanying bacteria according to the protocol of Wichard and Oertel (2010) [41]. The strains *Roseovarius* sp. MS2 (Genbank EU359909) and *Maribacter* sp. MS6 (Genbank EU359911) were originally isolated from *U. mutabilis* [8] and were cultivated in Marine Broth medium (Roth, Germany) at 20 °C. *Ulva* gametes were either grown axenically or inoculated with the bacteria (final optical density  $OD_{620} = 0.001$ ). All algae were cultivated in *Ulva* culture medium (UCM) [43] at 18 °C with the illumination of about 60  $\mu\text{mol photons m}^{-2} \text{s}^{-1}$  under a 17:7 light/dark regime. Axenic *Ulva* gametes deposited on cleaned glass slides and inoculated with bacteria MS2/MS6 were prepared following the procedure for in situ MS imaging described by Kessler et al. [19]. Briefly, algal gametes were inoculated to 10 mL medium in 9 cm diameter sterile Petri dishes with a clean and autoclaved glass slide (25 mm  $\times$  75 mm) with cavities (Paul Marienfeld, Germany) on the bottom; samples were incubated for one month at 18 °C in static conditions. An inverted microscope was used to monitor the algal growth. Transmitted light microscopy pictures were obtained using a Keyence BHX-500 digital microscope. Samples were recovered with pliers and fixed with glutaraldehyde 1% (Merck), stained with SYBR Gold (1% in DMSO, Invitrogen, Thermo Fisher); a cover slide was added, followed by incubation in the dark at 15 °C for 15 min. Cavity slides were spotted with 100  $\mu\text{L}$  of SYBR Gold or unstained bacterial monoculture (*Roseovarius* sp MS2 or *Maribacter* sp. MS6) to use them as controls. Fluorescence images (1024  $\times$  1024) were acquired using a Zeiss cLSM 880 (Carl Zeiss AG, Oberkochen, Germany) with a Plan-Apochromat 20  $\times$  0.8 and 488 nm Argon-laser excitation (5% transmission). Emission wavelengths for SYBR Gold (490–650 nm) and chlorophyll A (653–735 nm) were separated via the spectral detection unit. Transmitted light was detected by the transmitted light-PMT. The effect of an additional quick washing step was tested by gently adding 100  $\mu\text{L}$  of sterile MQ water for two seconds. The controls consisted of bacteria grown for one week in monoculture in 40 mL of marine broth medium and the axenic medium with fixative and stain. All the experiments with glass slides were performed in biological triplicates.

### Genome analysis

To identify the putative biosynthetic gene cluster (*ect* gene cluster) in *U. mutabilis* [34], the algal genome was searched for the gene ectoine hydroxylase (*ectD*) and also for a specialised aspartokinase (*ask\_ect*). Aspartokinase (Ask), along with

L-aspartate- $\beta$ -semialdehyde-dehydrogenase (Asd), provides the precursor L-ASA for ectoine biosynthesis [33,44,45]. Homologs of the enzymes of the ectoine pathway from *Halorhodospira halochloris* were identified by BLAST searches of the *U. mutabilis* genome at ORCAE using default parameters (<https://bioinformatics.psb.ugent.be/orcae/overview/Ulvmu>).

## AP-SMALDI-HRMS metabolic profiling and imaging

All standards and *Ulva* samples were analysed via AP-SMALDI (AP-SMALDI10, TransMit, Germany) ion source equipped with a UV (337 nm) nitrogen laser (LTB MNL-106, LTB, Germany) coupled to a high-resolution mass spectrometer Q-Exactive Plus (Thermo Fisher Scientific, Bremen, Germany). Glass slides with one month-grown algal gametophytes were gently recovered from a Petri dish filled with UCM using a sterile tweezer and dipped for one second in sterile ultrapure water to remove the excess salts before metabolic profiling. When algae were investigated directly on a glass slide before in situ MS imaging, blotting paper was used to remove sea water (see also Supporting Information File 1). The desired area of a glass slide covered with algal individuals was first marked, photographed, and finally fixed on the AP-SMALDI metal target.

AP-SMALDI profiling and imaging experiments unless otherwise stated were enhanced by a 2,5-dihydroxybenzoic acid (DHB) MALDI matrix. A methanolic solution of the DHB matrix at a concentration of 4 mg mL<sup>-1</sup> was applied onto a sample via SunChrom MALDI spotter (SunChrom GmbH, Germany). The spraying method was optimised using the following parameters: line distance 2 mm, spraying speed 800 mm min<sup>-1</sup> with 5 seconds drying time, and matrix solution flow rate in 4 cycles from 10  $\mu$ L up to 30  $\mu$ L min<sup>-1</sup>. Solvents used in this study were all LCMS analytical grade. 2,5-Dihydroxybenzoic acid with a purity of above 98% and high purity MS-grade methanol were purchased from Sigma-Aldrich (Germany).

All *Ulva* samples were imaged in the positive ion mode using a step size of 5  $\mu$ m and with the number of laser shots per spot set to 30 (approximately 1.2  $\mu$ J shot<sup>-1</sup>) within the laser frequency of 60 Hz. MS spectra were acquired in a mass range from  $m/z$  100 to  $m/z$  1000 with a resolving power of 280000. Pseudo ion intensity maps of selected  $m/z$  values were generated using the Mirion V3 software package with an  $m/z$  width of 0.01 u.

In the profiling mode, the single *Ulva* individuals were targeted visually and ablated with a laser spot size of approximately 10  $\mu$ m in positive and negative polarity in a mass range from  $m/z$  100 to  $m/z$  1000. The other parameters stayed like for the

MSI mode. In profiling, the same area of the rhizoid and the tip of the thallus of different individuals were analysed by laser ablation over one-minute time acquisition. Axenic and alga in symbiosis germlings were profiled with a UV laser along a longitudinal axis to investigate the effect of bacteria on metabolism changes in *U. mutabilis*.

The size of the sample groups analysed by AP-SMALDI-HRMS in profiling mode was  $n = 10$  for thallus tissue,  $n = 9$  for rhizoid tissue,  $n = 8$  for axenic callus, and  $n = 10$  for alga in symbiosis. Matrix-free experiments (LDI-HRMS) were performed in profiling mode under the same experimental conditions as the AP-SMALDI-HRMS. The size of the sample groups was defined as follows:  $n = 6$  for rhizoid,  $n = 7$  for thallus and whole alga profiling,  $n = 10$  for alga in symbiosis, and  $n = 15$  for axenic alga.

The metabolic profiles of nutrient media were obtained by analysing 30  $\mu$ L deposited onto cleaned glass slides and following the same protocol used for the *Ulva* samples. In the late exponential stage, bacterial monoculture was recovered from agar plates with a 10  $\mu$ L loop and diluted in 100  $\mu$ L of sterile water. Five microliters of the solution were spotted onto a glass slide and analysed in AP-SMALDI-HRMS mode in positive and negative polarity.

The data acquired in MSI mode were collected with Xcalibur software version 2.8 SP1 Build 2806 (Thermo Fisher Scientific, Germany) while the acquisition of spatial scans, pre-defined in the  $x$ - and  $y$ -direction as rectangular sample regions, was controlled by the MCP (Master Control Program, TransMIT GmbH, Giessen, Germany). The raw data acquired in profiling mode were visualised in Thermo Xcalibur™ version 3.0.63 (Thermo Fisher Scientific, Germany) and then converted to netCDF format using the Thermo File Converter tool. Data pre-processing was performed to extract the intensities in each profile, excluding the features of the nutrient medium using a script adapted from the MALDIquand package [46]. Spectra were de-noised with a signal-to-noise ratio of 5. Normalisation was done based on total ion current (TIC) recommended for MALDI-MS analysis [47]. All spectra, images, R data, scripts, and results from the statistical analysis were uploaded and are freely accessible in the Max Planck repository Edmond (<https://dx.doi.org/10.17617/3.4v>).

## Significant features analysis and metabolite identification

Data analysis was conducted in MetaboAnalyst 4.0 [48] to perform univariate and multivariate statistical tests and find significant differences in intensities and the presence or absence of metabolites in the samples. Pareto scaling and cube root trans-

formation were conducted to normalise the datasets before the multivariate statistics. PCA highlighted the metabolic differences between axenic and alga in symbiosis and between thallus and rhizoid tissues. Significant features were searched in the PCA loading plots and also in the pattern hunter plots obtained from a correlation analysis based on the Pearson correlation coefficient  $R$ . A one-way ANOVA with Fisher's LSD post hoc test ( $P$ -value < 0.05) was performed, and the relative amounts of the significant features were displayed as a boxplot. The selected significant features were further searched in the raw HRMS profiles to identify those with the reliable isotopic pattern assigned to a metabolite. The  $m/z$  values were searched in the METLIN database, using a mass deviation equal to or lower than five ppm, which suggested several known natural products such as ectoine [49].

To confirm the identity of the significant features, mass spectral information was compared with analytical standards analysed with the AP-SMALDI-HRMS (DMSP, chlorophyll-*a*, ectoine, choline). MS/MS experiments were performed with AP-SMALDI-HRMS to match the fragmentation pattern between the standard ectoine and bacteria monoculture profile. Fragmentation spectra of ectoine were acquired from the bacterial isolate *Roseovarius* sp. MS2 and an ectoine standard. To perform a measurement, 4  $\mu$ L of ectoine at concentration 50  $\mu$ M was pipetted onto a clean glass slide (washed with  $\text{dH}_2\text{O}$ , acetone) and overlaid with 2  $\mu$ L of a methanolic solution of the DHB matrix at a concentration of 4 mg  $\text{mL}^{-1}$ . For a bacterial isolate, the sample was prepared from one colony smeared onto a glass slide and covered with the DHB matrix, following the standard ectoine procedure. Samples were analysed in positive ion mode, with the number of laser shots per spot set to 30 (approximately 1.2  $\mu\text{J shot}^{-1}$ ). All-ion fragmentation (AIF) mode was set as follows: molecular ion of ectoine at  $m/z$  143.1; isolation window  $m/z \pm 0.2$ ; 45 NCE. The peak resolution was set at 280000, and the mass range was set from  $m/z$  50 to  $m/z$  300.

## Supporting Information

### Supporting Information File 1

Details on sample preparation and additional figures.

[<https://www.beilstein-journals.org/bjoc/content/supplementary/1860-5397-17-91-S1.pdf>]

## Funding

SF was funded by the International Max Planck Research School Exploration of Ecological Interactions with Molecular Techniques. This work was supported by an MPG Fellowship

awarded to GP and by the Deutsche Forschungsgemeinschaft through Grant No. SFB 1127/2 ChemBioSys–239748522 (GP, TW) and within the framework of the priority program (SPP 1158) "Antarctic Research with comparative investigations in Arctic ice areas" under the project number #424256657 (FG, TW).

## ORCID® iDs

Marine Vallet - <https://orcid.org/0000-0002-6878-0459>

Filip Kaftan - <https://orcid.org/0000-0002-5851-945X>

Veit Grabe - <https://orcid.org/0000-0002-0736-2771>

Fatemeh Ghaderiardakani - <https://orcid.org/0000-0003-3497-8421>

Simona Fenizia - <https://orcid.org/0000-0002-3592-9368>

Aleš Svatoš - <https://orcid.org/0000-0003-1032-7288>

Georg Pohnert - <https://orcid.org/0000-0003-2351-6336>

Thomas Wichard - <https://orcid.org/0000-0003-0061-4160>

## References

- Ramanan, R.; Kim, B.-H.; Cho, D.-H.; Oh, H.-M.; Kim, H.-S. *Biotechnol. Adv.* **2016**, *34*, 14–29. doi:10.1016/j.biotechadv.2015.12.003
- Singh, R. P.; Reddy, C. R. K. *FEMS Microbiol. Ecol.* **2014**, *88*, 213–230. doi:10.1111/1574-6941.12297
- Wichard, T.; Beemelmanns, C. J. *Chem. Ecol.* **2018**, *44*, 1008–1021. doi:10.1007/s10886-018-1004-7
- Croft, M. T.; Lawrence, A. D.; Raux-Deery, E.; Warren, M. J.; Smith, A. G. *Nature* **2005**, *438*, 90–93. doi:10.1038/nature04056
- Selvarajan, R.; Sibanda, T.; Venkatachalam, S.; Ogola, H. J. O.; Christopher Obieze, C.; Msagati, T. A. *Sci. Rep.* **2019**, *9*, 19835. doi:10.1038/s41598-019-56269-2
- Burke, C.; Thomas, T.; Lewis, M.; Steinberg, P.; Kjelleberg, S. *ISME J.* **2011**, *5*, 590–600. doi:10.1038/ismej.2010.164
- Wichard, T.; Charrier, B.; Mineur, F.; Bothwell, J. H.; Clerck, O. D.; Coates, J. C. *Front. Plant Sci.* **2015**, *6*, 72. doi:10.3389/fpls.2015.00072
- Spoerner, M.; Wichard, T.; Bachhuber, T.; Stratmann, J.; Oertel, W. *J. Phycol.* **2012**, *48*, 1433–1447. doi:10.1111/j.1529-8817.2012.01231.x
- Kessler, R. W.; Weiss, A.; Kuegler, S.; Hermes, C.; Wichard, T. *Mol. Ecol.* **2018**, *27*, 1808–1819. doi:10.1111/mec.14472
- Alsufyani, T.; Weiss, A.; Wichard, T. *Mar. Drugs* **2017**, *15*, 14. doi:10.3390/md15010014
- Alsufyani, T.; Califano, G.; Deicke, M.; Grueneberg, J.; Weiss, A.; Engelen, A. H.; Kwantes, M.; Mohr, J. F.; Ulrich, J. F.; Wichard, T. *J. Exp. Bot.* **2020**, *71*, 3340–3349. doi:10.1093/jxb/eraa066
- Weiss, A.; Costa, R.; Wichard, T. *Bot. Mar.* **2017**, *60*, 197–206. doi:10.1515/bot-2016-0083
- Matsuo, Y.; Imagawa, H.; Nishizawa, M.; Shizuri, Y. *Science* **2005**, *307*, 1598. doi:10.1126/science.1105486
- Bell, W.; Mitchell, R. *Biol. Bull. (Woods Hole, MA, U. S.)* **1972**, *143*, 265–277. doi:10.2307/1540052
- Joint, I.; Tait, K.; Callow, M. E.; Callow, J. A.; Milton, D.; Williams, P.; Cámara, M. *Science* **2002**, *298*, 1207. doi:10.1126/science.1077075
- Raina, J.-B.; Clode, P. L.; Cheong, S.; Bougoure, J.; Kilburn, M. R.; Reeder, A.; Forêt, S.; Stat, M.; Beltran, V.; Thomas-Hall, P.; Tapiolas, D.; Motti, C. M.; Gong, B.; Pernice, M.; Marjo, C. E.; Seymour, J. R.; Willis, B. L.; Bourne, D. G. *eLife* **2017**, *6*, e23008.

17. Lane, A. L.; Nyadong, L.; Galhena, A. S.; Shearer, T. L.; Stout, E. P.; Parry, R. M.; Kwasnik, M.; Wang, M. D.; Hay, M. E.; Fernandez, F. M.; Kubanek, J. *Proc. Natl. Acad. Sci. U. S. A.* **2009**, *106*, 7314–7319. doi:10.1073/pnas.0812020106
18. Parrot, D.; Blümel, M.; Utermann, C.; Chianese, G.; Krause, S.; Kovalev, A.; Gorb, S. N.; Tasdemir, D. *Sci. Rep.* **2019**, *9*, 1061. doi:10.1038/s41598-018-37914-8
19. Kessler, R. W.; Crecelius, A. C.; Schubert, U. S.; Wichard, T. *Anal. Bioanal. Chem.* **2017**, *409*, 4893–4903. doi:10.1007/s00216-017-0430-7
20. Mandal, A.; Singha, M.; Addy, P. S.; Basak, A. *Mass Spectrom. Rev.* **2019**, *38*, 3–21. doi:10.1002/mas.21545
21. Hansen, R. L.; Lee, Y. J. *Chem. Rec.* **2018**, *18*, 65–77. doi:10.1002/tcr.201700027
22. Yang, Y.; Lin, Y.; Qiao, L. *Anal. Chem. (Washington, DC, U. S.)* **2018**, *90*, 10400–10408. doi:10.1021/acs.analchem.8b02258
23. Barbano, D.; Diaz, R.; Zhang, L.; Sandrin, T.; Gerken, H.; Dempster, T. *PLoS One* **2015**, *10*, e0135337. doi:10.1371/journal.pone.0135337
24. Sandrin, T. R.; Goldstein, J. E.; Schumaker, S. *Mass Spectrom. Rev.* **2013**, *32*, 188–217. doi:10.1002/mas.21359
25. Dunham, S. J. B.; Ellis, J. F.; Li, B.; Sweedler, J. V. *Acc. Chem. Res.* **2017**, *50*, 96–104. doi:10.1021/acs.accounts.6b00503
26. Peterson, D. S. *Mass Spectrom. Rev.* **2007**, *26*, 19–34. doi:10.1002/mas.20104
27. Baumeister, T. U. H.; Vallet, M.; Kaftan, F.; Guillou, L.; Svatoš, A.; Pohnert, G. *Metabolomics* **2020**, *16*, 28. doi:10.1007/s11306-020-1646-7
28. Baumeister, T. U. H.; Vallet, M.; Kaftan, F.; Svatoš, A.; Pohnert, G. *Front. Plant Sci.* **2019**, *10*, 172. doi:10.3389/fpls.2019.00172
29. Ghaderiardakani, F.; Coates, J. C.; Wichard, T. *FEMS Microbiol. Ecol.* **2017**, *93*, fix094. doi:10.1093/femsec/fix094
30. Gupta, V.; Kushwaha, H. R. *Sci. Rep.* **2017**, *7*, 16430. doi:10.1038/s41598-017-15994-2
31. Zeisel, S. H. Phosphatidylcholine: endogenous precursor of choline. In *Lecithin: Technological, Biological, and Therapeutic Aspects*; Hanin, I.; Ansell, G. B., Eds.; Advances in Behavioral Biology, Vol. 33; Springer US: Boston, MA, USA, 1987; pp 107–120. doi:10.1007/978-1-4757-1933-8\_11
32. Fenizia, S.; Thume, K.; Wirgenings, M.; Pohnert, G. *Mar. Drugs* **2020**, *18*, 42. doi:10.3390/md18010042
33. Richter, A. A.; Mais, C.-N.; Czech, L.; Geyer, K.; Hoepfner, A.; Smits, S. H. J.; Erb, T. J.; Bange, G.; Bremer, E. *Front. Microbiol.* **2019**, *10*, 2811. doi:10.3389/fmicb.2019.02811
34. De Clerck, O.; Kao, S.-M.; Bogaert, K. A.; Blomme, J.; Fofflonker, F.; Kwantes, M.; Vancaester, E.; Vanderstraeten, L.; Aydogdu, E.; Boesger, J.; Califano, G.; Charrier, B.; Clewes, R.; Del Cortona, A.; D'Hondt, S.; Fernandez-Pozo, N.; Gachon, C. M.; Hanikenne, M.; Lattermann, L.; Leliaert, F.; Liu, X.; Maggs, C. A.; Popper, Z. A.; Raven, J. A.; Van Bel, M.; Wilhelmsson, P. K. I.; Bhattacharya, D.; Coates, J. C.; Rensing, S. A.; Van Der Straeten, D.; Vardi, A.; Sterck, L.; Vandepoele, K.; Van de Peer, Y.; Wichard, T.; Bothwell, J. H. *Curr. Biol.* **2018**, *28*, 2921–2933.e5. doi:10.1016/j.cub.2018.08.015
35. Schuh, W.; Puff, H.; Galinski, E. A.; Trüper, H. G. *Z. Naturforsch., C: J. Biosci.* **1985**, *40*, 780–784. doi:10.1515/znc-1985-11-1206
36. Tuma, R. S.; Beaudet, M. P.; Jin, X.; Jones, L. J.; Cheung, C.-Y.; Yue, S.; Singer, V. L. *Anal. Biochem.* **1999**, *268*, 278–288. doi:10.1006/abio.1998.3067
37. Wichard, T. *Front. Plant Sci.* **2015**, *6*, 86. doi:10.3389/fpls.2015.00086
38. Frank, O.; Michael, V.; Päuker, O.; Boedeker, C.; Jogler, C.; Rohde, M.; Petersen, J. *Syst. Appl. Microbiol.* **2015**, *38*, 120–127. doi:10.1016/j.syapm.2014.12.001
39. Rao, D.; Webb, J. S.; Kjelleberg, S. *Appl. Environ. Microbiol.* **2006**, *72*, 5547–5555. doi:10.1128/aem.00449-06
40. Grueneberg, J.; Engelen, A. H.; Costa, R.; Wichard, T. *PLoS One* **2016**, *11*, e0146307. doi:10.1371/journal.pone.0146307
41. Wichard, T.; Oertel, W. J. *Phycol.* **2010**, *46*, 248–259. doi:10.1111/j.1529-8817.2010.00816.x
42. Nahor, O.; Morales-Reyes, C. F.; Califano, G.; Wichard, T.; Golberg, A.; Israel, Á. *Bot. Mar.* **2021**, *64*, 83–92. doi:10.1515/bot-2020-0050
43. Stratmann, J.; Papatoglu, G.; Oertel, W. J. *Phycol.* **1996**, *32*, 1009–1021. doi:10.1111/j.0022-3646.1996.01009.x
44. Peters, P.; Galinski, E. A.; Trüper, H. G. *FEMS Microbiol. Lett.* **1990**, *71*, 157–162. doi:10.1111/j.1574-6968.1990.tb03815.x
45. Reshetnikov, A. S.; Khmelenina, V. N.; Trotsenko, Y. A. *Arch. Microbiol.* **2006**, *184*, 286–297. doi:10.1007/s00203-005-0042-z
46. Gibb, S.; Strimmer, K. Mass spectrometry analysis using MALDIquant. In *Statistical Analysis of Proteomics, Metabolomics, and Lipidomics Data Using Mass Spectrometry*; Datta, S.; Mertens, B. J. A., Eds.; Springer International Publishing: Cham, Switzerland, 2017; pp 101–124. doi:10.1007/978-3-319-45809-0\_6
47. Emara, S.; Amer, S.; Ali, A.; Abouleila, Y.; Oga, A.; Masujima, T. Single-Cell Metabolomics. In *Metabolomics: From Fundamentals to Clinical Applications*; Sussulini, A., Ed.; Advances in Experimental Medicine and Biology, Vol. 965; Springer International Publishing: Cham, Switzerland, 2017; pp 323–343. doi:10.1007/978-3-319-47656-8\_13
48. Chong, J.; Soufan, O.; Li, C.; Caraus, I.; Li, S.; Bourque, G.; Wishart, D. S.; Xia, J. *Nucleic Acids Res.* **2018**, *46*, W486–W494. doi:10.1093/nar/gky310
49. Guijas, C.; Montenegro-Burke, J. R.; Domingo-Almenara, X.; Palermo, A.; Warth, B.; Hermann, G.; Koellensperger, G.; Huan, T.; Uritboonthai, W.; Aisporna, A. E.; Wolan, D. W.; Spilker, M. E.; Benton, H. P.; Siuzdak, G. *Anal. Chem. (Washington, DC, U. S.)* **2018**, *90*, 3156–3164. doi:10.1021/acs.analchem.7b04424

## License and Terms

This is an Open Access article under the terms of the Creative Commons Attribution License (<https://creativecommons.org/licenses/by/4.0>). Please note that the reuse, redistribution and reproduction in particular requires that the author(s) and source are credited and that individual graphics may be subject to special legal provisions.

The license is subject to the *Beilstein Journal of Organic Chemistry* terms and conditions: (<https://www.beilstein-journals.org/bjoc/terms>)

The definitive version of this article is the electronic one which can be found at: <https://doi.org/10.3762/bjoc.17.91>



## Supporting Information

for

### **A new glance at the chemosphere of macroalgal–bacterial interactions: In situ profiling of metabolites in symbiosis by mass spectrometry**

Marine Vallet, Filip Kaftan, Veit Grabe, Fatemeh Ghaderiardakani, Simona Fenizia, Aleš Svatoš, Georg Pohnert and Thomas Wichard

*Beilstein J. Org. Chem.* **2021**, *17*, 1313–1322. [doi:10.3762/bjoc.17.91](https://doi.org/10.3762/bjoc.17.91)

### **Details on sample preparation and additional figures**



## Content

Table S1 Descriptive information and significant features found .....	S2
Notes on sample preparation methodology .....	S3
Figure S1: The effect of seawater salt crystallisation .....	S4
Figure S2: AP-SMALDI HR MSI on a map of sodium adducts .....	S5

**Table S1:** Descriptive information and significant features found by the Student's test in the LDI and MALDI-HRMS datasets for tissue profiling and whole alga profiling (compare with Figure 1b). The results of the Student's tests can be found on the Edmond – the Open Research Data Repository of the Max Planck Society. (Title: “High-resolution mass spectrometry-guided identification of metabolites in *Ulva*-bacteria symbiosis”; Max Planck Society, submitted by Marine Vallet, 2020; <https://dx.doi.org/10.17617/3.4v>)

Dataset	Samples number	Total number of features analyzed	Number of significant features found by Student's test (p-value < 0.05)	Number of significant features found by Student's test (p-value < 0.01)
LDI-HRMS tissue profiling: (rhizoidal zone <i>versus</i> thallus)	14	1534	653	66
LDI-HRMS whole alga profiling: (axenic culture <i>versus</i> symbiosis)	25	4986	1399	970
MALDI-HRMS tissue profiling: (rhizoidal zone <i>versus</i> thallus)	19	3936	290	86
MALDI-HRMS whole alga profiling: (axenic culture <i>versus</i> symbiosis)	18	4476	676	327

**Notes on the sample preparation methodology:** Excess seawater salts were removed from the glass slide substrate's surface with a fine blotting paper placed on the side of the glass slide while the medium was absorbed. This simple method was successful in removing most of the diluted salts without disrupting the actual sample. This sample preparation step ensured that the seawater crystals were distributed almost uniformly across the imaged area.

Ion maps of potassium ( $[M + K]^+$ ) and sodium adduct ( $[M + Na]^+$ ) of the compound(s) with the molecular formula  $C_{10}H_{16}O_3$  were generated to show the presence of seawater salts and their distribution across the *Ulva* sample attached to a glass slide (Figure S1).

Ion maps confirmed that both cations were distributed uniformly throughout the imaged area, albeit at slightly different concentrations. A region covered with slightly larger crystals served better as a source of potassium cations, according to optical images taken with a digital microscope before and after UV laser ablation. Fine crystal-covered regions, on the other hand, appear to facilitate the formation of sodium adducts.

Based on the exact mass (error 0.5 ppm) and calculated best matching chemical formula and isotope simulation generated by Qual Browser/Xcalibur software 3.0.63, ions at  $m/z$  207.0991 ( $[M + Na]^+$ ) and  $m/z$  223.0731 ( $[M + K]^+$ ) were assigned to  $C_{10}H_{16}O_3$ .

The 2D ion map of the sodium adduct of ectoine at  $m/z$  165.0634 ( $[M + Na]^+$ ) is completely consistent with the interpretation of sodium cation distribution within an imaged area (Figure S2).

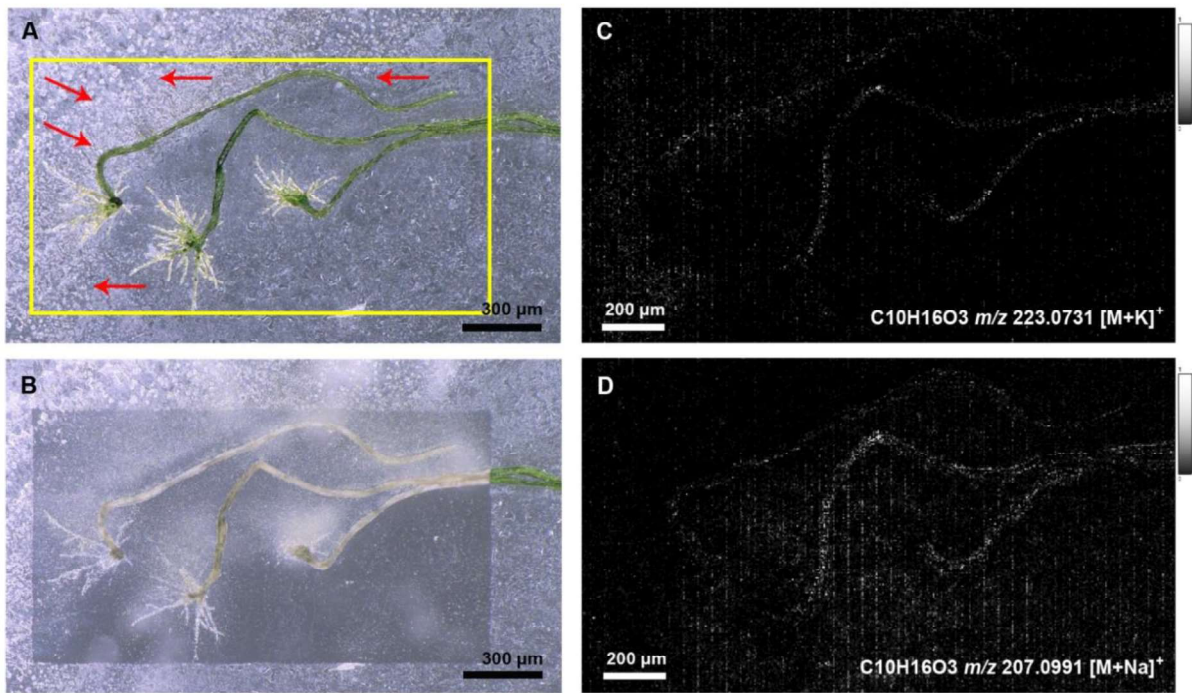


**Figure S1:** The effect of seawater salt crystallisation on the distribution of sodium and potassium cations on a glass substrate. Panel (A) optical image of a dry *Ulva* germling sample attached to a glass slide prior to the AP-SMALDI-HR MSI experiment, with arrows pointing to regions with thicker salt coating; (B) *Ulva* germling samples after the AP-SMALDI-HR MSI experiment; (C) ion map representing a potassium adduct of  $C_{10}H_{16}O_3$  at  $m/z$  223.0731 acquired during the AP-SMALDI-HR MSI experiment; (D) ion map representing a sodium adduct of  $C_{10}H_{16}O_3$  at  $m/z$  207.0991 acquired during AP-SMALDI-HR MSI experiment.

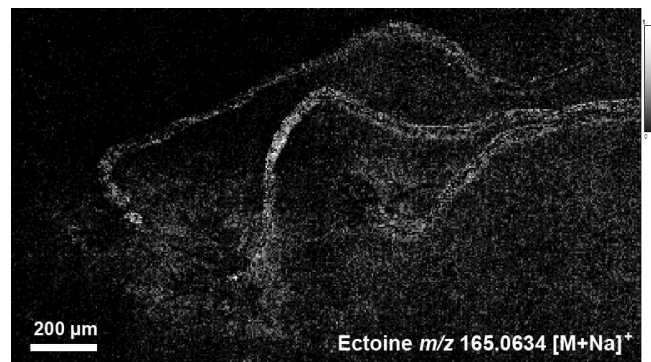


**Figure S2:** AP-SMALDI-HRMS on a ion map of sodium adduct of ectoine at  $m/z$  165.0634, indicating *Roseovarius* sp. in the biofilm and on the *Ulva* algal surface of the germling.

### 2.3 Publication 3

“Ectoine from bacterial and algal origin is a compatible solute in microalgae.”

Simona Fenizia, Kathleen Thume, Marino Wirgenings, Georg Pohnert

*Marine Drugs*, Vol. 18(1), 42, 2020

DOI: 10.3390/md18010042

Open Access This article is licensed under a Creative Commons Attribution 4.0 International License

Fenizia S.<sup>1</sup>, Thume K.<sup>2</sup>, Wirgenings M.<sup>3</sup>, Pohnert G.<sup>4</sup> Ectoine from bacterial and algal origin is a compatible solute in microalgae. *Marine Drugs* 2020 18, 1. 10.3390/md18010042

Author	1	2	3	4
Development of concept	x			x
Planning of research	x			x
Data collection	x	x	x	
Data analysis	x	x		
Preparation of the manuscript	x			x
Correction of the manuscript	x	x	x	x
Proposed publication equivalent	1.0			

#### Authors contribution:

Simona Fenizia	Conceptualization, research planning, experiment preparation and implementation, data analysis, writing-original draft, writing-review, editing
Kathleen Thume	Experiment preparation, data analysis, writing-review, editing
Marino Wirgenings	Chemical synthesis, writing-review, editing
Georg Pohnert	Conceptualization, research planning, writing-review, editing, supervision



Article

# Ectoine from Bacterial and Algal Origin Is a Compatible Solute in Microalgae

Simona Fenizia <sup>1,2</sup>, Kathleen Thume <sup>1</sup>, Marino Wirgenings <sup>1</sup> and Georg Pohnert <sup>1,2,\*</sup> 

<sup>1</sup> Institute for Inorganic and Analytical Chemistry, Bioorganic Analytics, Friedrich Schiller University, Lessingstrasse 8, D-07743 Jena, Germany; simona.fenizia@uni-jena.de (S.F.); Kathleen.thume@uni-jena.de (K.T.); Marino.wirgenings@uni-jena.de (M.W.)

<sup>2</sup> Max Planck Institute for Chemical Ecology, Hans-Knöll-Straße 8, D-07745 Jena, Germany

\* Correspondence: Georg.Pohnert@uni-jena.de

Received: 17 November 2019; Accepted: 23 December 2019; Published: 6 January 2020



**Abstract:** Osmoregulation in phytoplankton is attributed to several highly polar low-molecular-weight metabolites. A widely accepted model considers dimethylsulfoniopropionate (DMSP) as the most important and abundant osmotically active metabolite. Using an optimized procedure for the extraction and detection of highly polar metabolites, we expand the group of phytoplankton osmolytes by identifying ectoine in several microalgae. Ectoine is known as a bacterial compatible solute, but, to the best of our knowledge, was never considered as a phytoplankton-derived product. Given the ability of microalgae to take up zwitterions, such as DMSP, we tested the hypothesis that the algal ectoine is derived from associated bacteria. We therefore analyzed methanol extracts of xenic and axenic cultures of two different species of microalgae and could detect elevated concentrations of ectoine in those that harbor associated bacteria. However, also microalgae without an associated microbiome contain ectoine in smaller amounts, pointing towards a dual origin of this metabolite in the algae from their own biosynthesis as well as from uptake. We also tested the role of ectoine in the osmoadaptation of microalgae. In the model diatoms *Thalassiosira weissflogii* and *Phaeodactylum tricornutum*, elevated amounts of ectoine were found when cultivated in seawater with salinities of 50 PSU compared to the standard culture conditions of 35 PSU. Therefore, we add ectoine to the family of osmoadaptive metabolites in phytoplankton and prove a new, potentially synergistic metabolic interplay of bacteria and algae.

**Keywords:** ectoine; osmoadaptation; compatible solutes; phytoplankton; LC/MS analysis; osmoregulation; diatoms; DMSP

## 1. Introduction

Diatoms are photosynthetic unicellular algae, responsible for 20% of global carbon fixation and 40% of marine primary production. They are important producers of zwitterionic metabolites, a class of small organic compounds that has central osmoregulatory, antioxidant, and cryoprotectant functions [1,2]. Dimethylsulfoniopropionate (DMSP) is the main representative of this class of molecules: it is a sulfur-containing metabolite reaching high cellular concentrations in marine algae [1,3]. Marine bacteria and algae metabolize DMSP into the correspondent volatile compound dimethylsulfide (DMS), contributing to the flux of sulfur from the hydrosphere to the atmosphere [3]. Other sulfur-containing metabolites, like dimethylsulfonioacetate (DMSA), gonyol, and the most recently identified dimethylsulfoxonium propionate (DMSOP); as well as nitrogen-containing metabolites, like glycine betaine (GBT), homarine, and trigonelline, have been discovered and studied in phytoplankton as well [2,4]. These metabolites are classified as “compatible solutes”, organic water-soluble compounds accumulated by micro-organisms either by de novo synthesis or by uptake



from the surrounding environment. They protect the cells from stress factors, such as environmental changes in temperature, pH, and salinity [5].

Salinity is an environmental master factor for marine organisms, affecting their distribution, reproduction, and behavior [6]. To cope with changing salinity in the oceans, marine algae synthesize, take up, and accumulate compatible solutes to keep physiological levels of cellular hydration and turgor [7,8]. The synthesis of these compounds is energetically costly, requiring assimilation and reduction of sulfate or nitrate [1]. Since nitrogen sources are often limiting in marine habitats, sulfur-containing osmolytes are more abundant compared to N-containing counterparts. It can thus be argued that the high production of DMS can be linked to the preference of N-limited phytoplankton communities that use DMSP instead of, for example, glycine betaine [9].

In the last years, many organic osmolytes produced by microalgae were identified and their contribution to the osmoadaptation and osmoregulation of marine ecosystems pointed out [2]. A complex picture emerges, showing that the common DMSP/DMS concept represents a massive oversimplification. Osmoadaptation seems to depend on a plethora of metabolites of which only few have been structurally elucidated [2]. Major progress in the field is enabled by the development of direct analytical methods of zwitterions. Spielmeier and Pohnert [10,11] introduced an ultra performance liquid chromatography (UPLC) method for separation and direct determination of DMSP, GBT, and other zwitterionic metabolites produced by marine phytoplankton. A further liquid chromatography/mass spectrometry (LC/MS) survey of microalgal extracts revealed that the structure and function of several highly polar, most likely zwitterionic small metabolites are still uncharacterized [4]. This study aims to identify such uncharacterized metabolites and to investigate their regulation under osmotic stress. We took advantage of a refined analytical method using high-resolution mass spectrometry (based on [7] and [10]) to analyze, qualitatively and quantitatively, unknown components in the “zwittermetabolome” of the diatoms *Thalassiosira weissflogii* and *Phaeodactylum tricorutum*. These two diatoms were selected because they are well-established model organisms for phytoplankton studies. *P. tricorutum* is the first pennate diatom for which the complete genome is known [12]. *T. weissflogii* is one of the few diatoms identified that does not produce quantifiable amounts of DMSP [7]. The alga has previously been used to study acclimation to hyposalinity with a reported detailed transcriptomic and physiologic survey of the response to this stress factor [13]. We observed that osmoadaptation is achieved in both algae by adjustment of intracellular concentrations of different zwitterionic compounds, including the novel algal mediator, ectoine. This metabolite can thus be counted among the phytoplankton-compatible solutes. Moreover, direct uptake of bacteria-derived ectoine by the diatom *T. weissflogii* was detected in a mechanism that represents an economic strategy to acquire essential metabolites instead of their de novo production.

## 2. Results and Discussion

To identify novel zwitterionic metabolites involved in the osmoadaptation of marine organisms, we analyzed the endometabolome of the diatoms *Thalassiosira weissflogii* and *Phaeodactylum tricorutum* using ultra-high-pressure liquid chromatography high-resolution mass spectrometry (UHPLC–HRMS). Algae were grown at standard culture conditions of 35 Practical Salinity Units (PSU, g NaCl kg<sup>-1</sup> sea water) and under increased salinity of 50 PSU, where the growth of *T. weissflogii* still follows a standard growth curve with slightly reduced cell counts [14]. The selected salinities span the range of saline water and allow the linking of our results to previous studies on osmoregulation of algae [14–16]. We detected the production of several known, but also of structurally unassigned, highly polar low-molecular-weight metabolites under the different salinity concentrations.

### 2.1. *Thalassiosira weissflogii*

Figure 1 shows UHPLC–HRMS chromatographic profiles obtained from extracts of xenic and axenic *T. weissflogii* (respective strains used were RCC76 and CCMP1336). This diatom does not produce any quantifiable amount of DMSP [7], the main zwitterionic metabolite produced by many

other planktonic algae [4]. In the xenic algal culture, we detected three major zwitterionic metabolites, glycine betaine and homarine, previously identified in diatoms, as well as an unknown metabolite [9].

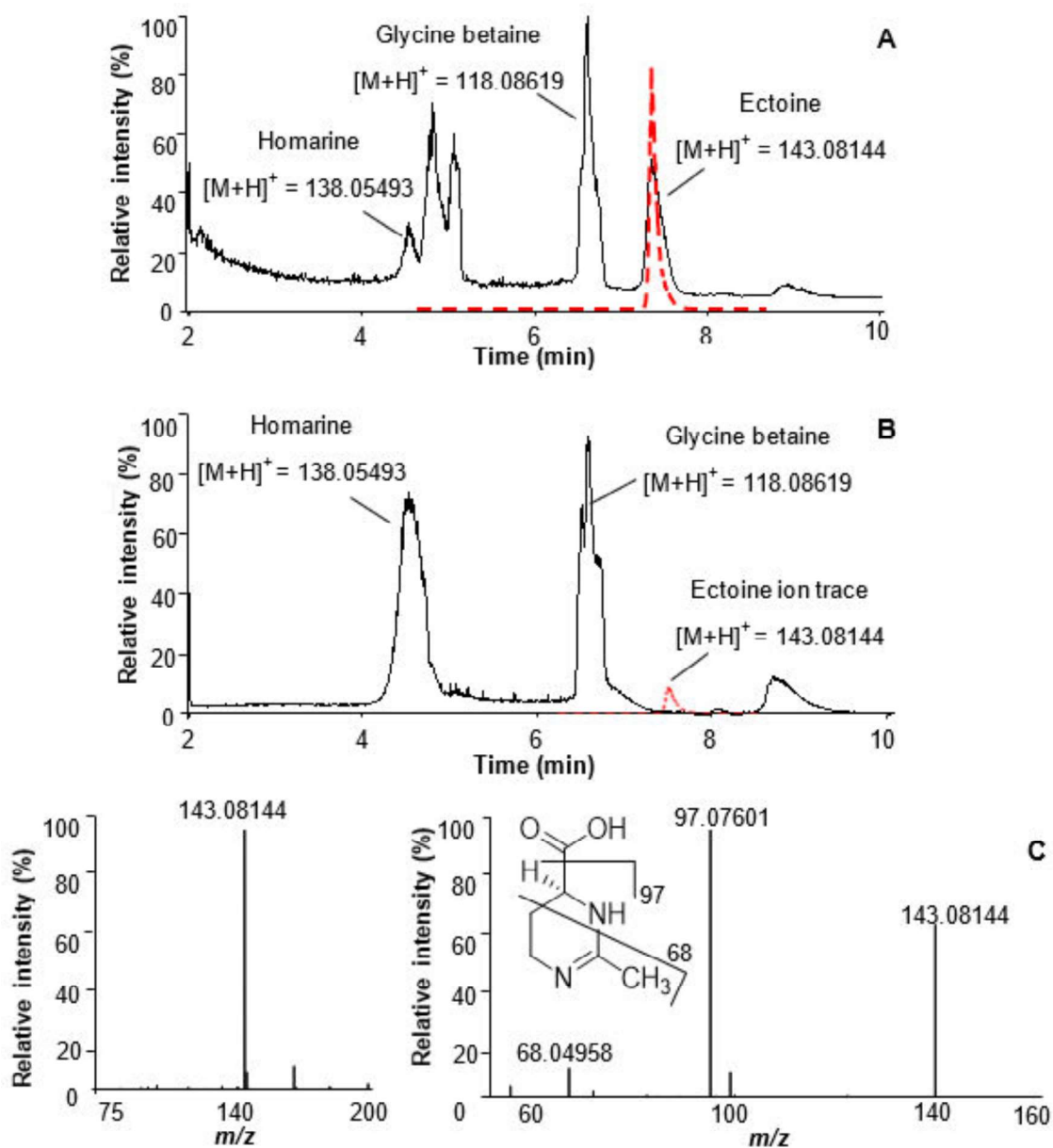


**Figure 1.** Chromatographic separation of zwitterionic metabolites in *Thalassiosira weissflogii* RCC76 (35 PSU xenic, (A)) and CCMP1336 (35 PSU axenic, (B)) using UHPLC–HRMS. The red line in (A) represents the UHPLC–HRMS monitoring of the ion trace  $m/z = 143.08144 \pm 0.0005$  after addition of a synthetic ectoine standard, peaks at 5 and 5.2 min are contaminants. The dashed red line in (B) depicts the ion trace of  $m/z = 143.08144 \pm 0.0005$ . (C), electrospray ionization (ESI) MS and tandem mass spectrometry (MS/MS) of ectoine with characteristic fragments depicted. The identity of the metabolites glycine betaine and homarine were assigned using synthetic standards according to previous studies [2].

The identity of glycine betaine was verified by co-injection with a commercially available standard. This metabolite is the nitrogen-containing analog of DMSP and is produced by marine phytoplankton dependent on nitrogen availability [17]. Homarine was synthesized in our laboratory according to a published procedure [2,4], and co-injection with the algal extract confirmed its identity (see experimental section for details). Homarine is a nitrogen-containing zwitterion, but, to the best of our knowledge, it was described only as a minor component in the microalgae *Emiliania huxleyi* and *Platymonas subcordiformis* [2,4,18]. Our data shows that it is a major zwitterionic metabolite in *T. weissflogii*.

In addition to the signals of these two metabolites known from microalgae, the chromatogram and the HRMS spectrum in positive ionization mode shows a peak with  $m/z$  of the  $[M + H]^+ = 143.08144$ , corresponding to the molecular formula  $C_6H_{11}O_2N_2$  (Figure 1). A fragment ion  $m/z$  97.07601 was detected by tandem mass spectrometry (MS/MS) and was attributed to the loss of a carboxylic group. An ion at  $m/z$  68.04958 indicated a loss of  $C_3H_4O_2N$  (Figure 1C). Based on the mass spectrometric data, by comparison with databases (METLIN, MassBank of North America, MetaboLights), and by using bioinformatics tools (Sirius v4.0.1, CSI:FingerID), the signal was tentatively assigned to ectoine. The identity was verified by co-injection of the algal extract with a commercially available standard. Coelution and matching MS/MS data of the analyte and the standard proves the identity of this metabolite as ectoine (Figure 1).

Ectoine, 2-methyl-1,4,5,6-tetrahydropyrimidine-4-carboxylic acid, was initially isolated and identified from the halophilic phototrophic sulfur bacterium *Halorhodospira halochloris*. This metabolite has protective and osmoregulatory functions during adaptation to salinity changes and is therefore classified as bacterial compatible solute [19,20]. Thanks to its hydrophilicity, ectoine has additional protective properties, stabilizing bacterial cells against different kinds of stress like UV radiation and cytotoxins [21]. Besides in bacteria [21,22], ectoine is also found in halophilic ciliates including *Schmidingerothrix salinarum* [23,24], and the halophilic bacterivorous nanoflagellate *Halocafeteria seosinensis* [25]. Some members of Archaea acquired ectoine genes through horizontal gene transfer to cope with a high-salinity environment [26]. Based on gene expression patterns of bacteria in coculture with the diatom *T. pseudonana*, Landa et al. postulated that the alga might provide ectoine to the bacterium *Rugeria pomeroyi* [27]. However, to the best of our knowledge, the production of this metabolite by diatoms has never been reported.

The fact that axenic diatoms produce low, but significant amounts of ectoine (Figure 2) prompted us to mine the genome of the fully sequenced diatom *Phaeodactylum tricorutum* for genes involved in ectoine biosynthesis. In bacteria, ectoine is synthesized by three proteins: EctA, EctB, and EctC. We found homologues of EctA (XP\_002181681.1, E value 0.15) and EctB (XP\_002185537.1, E value  $6 \times 10^{-50}$ ) that provide the central intermediate N $\gamma$ -acetyl-2,4-diaminobutyrate but not for EctC. If the last step, namely, the condensation to ectoine is catalyzed by an EctC protein with low homology or if another condensating enzyme activity is involved remains still open.

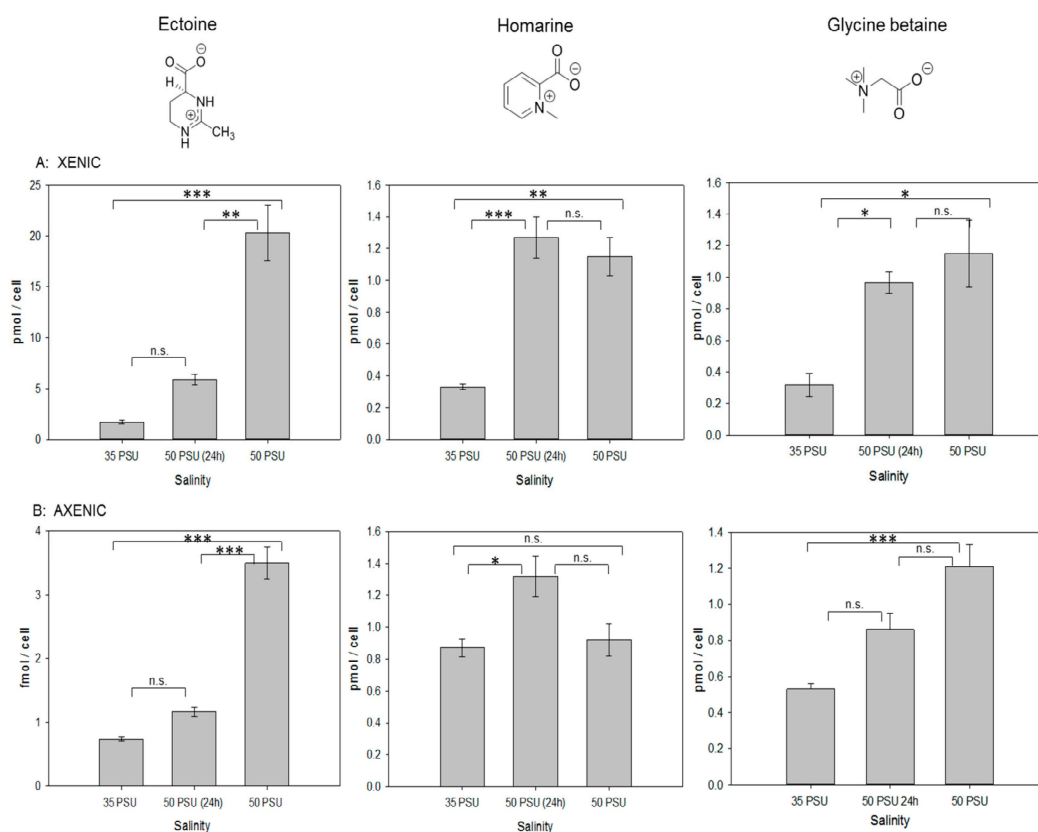


**Figure 2.** Comparison of intracellular amounts of ectoine and homarine in xenic (A) and axenic (B) cultures of *T. weissflogii*. The value of 35 PSU indicates that cultures were maintained constantly at this salinity, 50 PSU (24 h) indicates that cultures grown at 35 PSU were transferred into medium of 50 PSU and analyzed 24 h after transfer, and 50 PSU indicates cultures that were grown for two generations at this elevated salinity. Concentrations are normalized per cell, error bars represent standard deviation (biological replicates,  $N = 4$ ). Statistical analysis is based on One-Way ANOVA with a Tukey Test for multiple comparison procedures. \*  $P \leq 0.05$ , \*\*  $P \leq 0.01$ , \*\*\*  $P \leq 0.001$ .

## 2.2. Response to Osmotic Stress of *T. weissflogii*

To verify osmoregulatory functions of ectoine in the diatom, cells were grown at low (35 PSU) and high (50 PSU) salinity. The higher salinity resulted in reduced cell counts, indicating salinity stress as already observed previously [15]. For short-term salinity stress experiments, cells were grown at 35 PSU to the late exponential phase and transferred to 50 PSU. Analysis of these cells was done 24 h after transfer. Tests were performed on both xenic and axenic cultures of *T. weissflogii* (Figure 2). Xenic cultures were harvested by filtration on GF/C filters, which removes the most part of the bacteria. We verified the removal of bacteria by flow cytometry of the filtrate and found no significant difference between filtrate and culture (filtrate,  $17.550 \pm 19$  cells  $\mu\text{L}^{-1}$ ; xenic culture,  $17.5120 \pm 31$  cells  $\mu\text{L}^{-1}$ ). We also observed remaining bacteria caught in the filter that might contribute to the detected osmolytes. This fraction can, however, be only minor given the high filtration success.

Quantification of ectoine revealed that the cellular content in *T. weissflogii* increases during osmotic stress conditions, in particular in xenic cultures, where this molecule is the dominant detected osmolyte (Figure 2). When a short-term stress was introduced, ectoine concentration increased by 3.5-fold compared to the concentration under 35 PSU conditions. Long-term salinity stress led to an over 11-fold increase of ectoine. In axenic cultures, the intracellular concentration of ectoine was more than three orders of magnitude lower compared to xenic ones. In the cultures lacking the associated bacteria, the ectoine content increased 1.6-fold during the short-term salinity stress and 4.8-fold during the long-term stress (Figure 2B). Cell size and volume determined by light microscopy did not

change in *T. weissflogii* under osmotic stress conditions (Table 1). Therefore, changes in intracellular amounts of the osmoprotectants also reflect changes of intracellular concentration. The observed plasticity of ectoine content indicates that the associated microbial community contributes substantially to the intracellular ectoine pool and that ectoine content in the xenic cultures can compensate for salinity changes. In contrast, the minor amounts of ectoine in the axenic cultures will not contribute substantially when compared to the other osmolytes present in the cells.

**Table 1.** Cell size and volume of *T. weissflogii* and *P. tricorutum* under the different salinity conditions.

	Length (µm)	Width (µm)	Cell Volume (µm <sup>3</sup> )	Standard Deviation	Difference (Δ%)	One Way ANOVA
<i>T. weissflogii</i>						
35 PSU	188	95.1	$1.32 \times 10^6$	$\pm 2.59 \times 10^5$		
50 PSU (24 h)	227	85.7	$1.23 \times 10^6$	$\pm 1.74 \times 10^5$	−6.82%	n.s.
50 PSU	207	88.9	$1.29 \times 10^6$	$\pm 3.12 \times 10^5$	−2.27%	n.s.
<i>P. tricorutum</i>						
35 PSU	21.6	11.8	131	±39.1		
50 PSU (24 h)	20.7	10.4	113	±29	−13.70%	n.s.
50 PSU	22.4	13.6	159	±33.8	21.40%	p < 0.01

In axenic conditions, homarine together with glycine betaine are the dominant, compatible solutes (Figure 1). Glycine betaine increased under salinity stress (0.5-fold in short term, more than 2-fold in long-term treatments, Figure 2). However, in contrast to ectoine, no influence of the microbial community on the content of this osmolyte was observed. Glycine betaine has been earlier observed as a metabolite compensating for salinity changes in phytoplankton including *T. weissflogii* [2,17]. The independence of the associated microbial community on glycine betaine levels indicates that its regulation in algae is independent of biotic interactions with the associated microbiome, but rather depends on the external salinity.

The third dominant osmolyte is homarine (Figure 1). Homarine has not been described as osmolyte in diatoms before, but in the prasinophyte *Platymonas subordiformis*, as well as in the coccolithophore *E. huxleyi* [2,28]. In xenic cultures, homarine concentrations were substantially lower compared to ectoine concentrations but both were in the pmol cell<sup>−1</sup> range at 35 PSU salinity (Figure 2). At 35 PSU, homarine production under axenic conditions nearly doubled compared to xenic cultures, indicating a predominant or exclusive algal origin of this metabolite. The elevated amount in axenic cultures is potentially compensating for their overall lower ectoine content. Homarine in xenic cultures increases 3.9-fold after short-term and 3.5-fold after long-term salinity stress. In axenic conditions, a 1.5-fold increase due to short-term salinity stress was observed, while long-term stress had no significant impact on the concentration of this metabolite (Figure 2). In contrast to the ectoine concentration that is substantially dependent on bacterial presence at both salinities, intracellular concentrations of homarine at high salinity are similar in xenic and axenic cultures. Under both axenic and xenic conditions, the response to homarine is already at its maximum after short-term stress and seems to be a fast response in comparison to ectoine and glycine betaine that are both building up during prolonged culturing under high salinity.

### 2.3. Ectoine Uptake by *T. weissflogii*

Due to the difference of intracellular compatible solute concentration between xenic and axenic cultures, we investigated whether microalgae can take up extracellular ectoine that might be provided by associated bacteria. Therefore, we incubated axenic cultures of *T. weissflogii* cultivated in artificial seawater of different salinities, supplied with 1 µM of stable isotope (deuterium) labeled D<sub>3</sub>-ectoine. We determined the relative amount of the labeled metabolite in relation to the cellular ectoine by integrating the respective ions of the labeled and unlabeled form (Figure 3). Under all salinity

conditions, labeled ectoine exceeded that of the unlabeled form, indicating a substantial uptake of the externally supplied substrate. The relative amount of labeled ectoine in comparison to the unlabeled metabolite was maximal at 35 PSU, the salinity at which the lowest cellular content was observed in Figure 2B. With increasing salinity, the proportion of ectoine taken up in its labeled form decreased, which is mainly due to the increased content of the unlabeled metabolite (Figures 2 and 3). According to these results, the higher content of ectoine in xenic cultures of *T. weissflogii* compared to the axenic ones can be explained by uptake of the compound supplied by bacteria. Microalgae can thus act as a sink of this metabolite, which becomes particularly available when environmental changes in salinity occur.

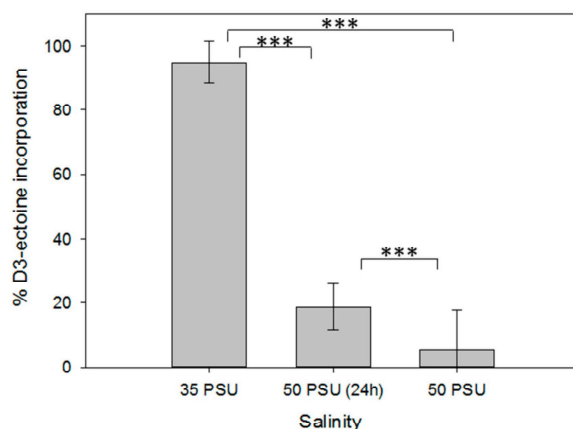


**Figure 3.** Uptake of stable isotope labeled D<sub>3</sub>-ectoine in axenic cultures of *Thalassiosira weissflogii* CCMP1336 under different salinity conditions (see legend of Figure 2 for explanation of the respective treatments). Error bars represent standard deviation (biological replicates,  $N = 4$ ). Statistical analysis is based on One-Way ANOVA with a Tukey Test for multiple comparison procedures. \*\*\*  $P \leq 0.001$ .

Several studies reported uptake mechanisms for zwitterionic osmolytes in marine algae [8,29]. *T. weissflogii*, a diatom that is not producing DMSP, relies entirely on the uptake of DMSP to fulfill cellular functions [7]. Our results demonstrate that this diatom also takes up ectoine very efficiently. This suggests that *T. weissflogii* generally uses external zwitterionic metabolites to counteract osmotic stress. Two transport systems for compatible solutes (ATP-Binding Cassette Transporters (ABC Transporters) and Betaine-Choline-Carnitine Transporters (BCCT)) have been reported in marine micro-organisms. They recognize DMSP and structurally related compounds like glycine betaine and transport them into the cells [7,8,29–31]. Likewise, in Gram-positive and Gram-negative bacteria, transport systems for compatible solutes are part of the strategy used by microbial cells to overcome stress. Often there are several systems involved in the uptake of these osmolytes in order to provide a robust strategy to counter the adverse condition [32]. Several ectoine transport systems involved in adaptation to osmotic stress, temperature, and nutrient stress conditions were characterized in bacteria and assigned to four different transport families: (i) binding protein-dependent ABC transporters, (ii) major facilitator family (MFS), (iii) BCCT, and (iv) periplasmic binding protein-dependent tripartite ATP independent periplasmic transporter family (TRAP-T) [33,34]. Generally, transport systems have a broad specificity, being able to transport other compatible solutes; but there are also cases, like the TeaABC transporter system in *Halomonas elongata* [35] and the EctT transporter in *Virgibacillus pantothenticus* [36], where the system is specific for ectoine. However, no detailed information on related systems is available for diatoms.

#### 2.4. Ectoine in *Phaeodactylum tricornutum*

We also detected ectoine in the model diatom *Phaeodactylum tricornutum*. In contrast to *T. weissflogii* and most other diatoms, *P. tricornutum* is capable of adjusting its cell size according to

the physicochemical conditions in the environment. We were thus interested in the question to which degree the diatom adapts to changes in salinity through adjustment of the cellular ectoine content and its cell size.

As in *T. weissflogii*, in xenic cultures of *P. tricornutum*, increased salinity resulted in significantly elevated cellular ectoine concentrations (Figure 4). Counterintuitively, the cell size increased with increasing salinity by 20.6 % in the long-term salinity stress treatment, compared to the control ( $P < 0.01$ , Table 1). Thus, there is no adaptation by decreased cell volume and consequently, higher concentrations of cellular metabolites, as it is observed in plant cells. Compensation with acquired ectoine is thus a means of adaptation in this diatom as well.

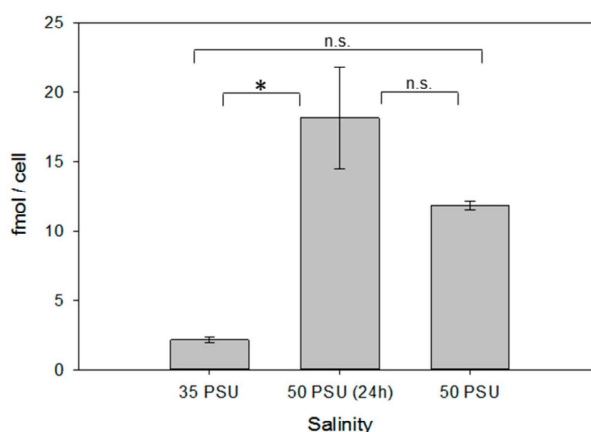


**Figure 4.** Ectoine content in xenic cultures of *P. tricornutum* under different salinity conditions (see legend of Figure 2 for explanation of the respective treatments). Error bars represent standard deviation (biological replicates,  $N = 4$ ). Statistical analysis is based on One-Way ANOVA with a Tukey Test for multiple comparison procedures. \*  $P < 0.05$ .

### 2.5. Ectoine in Other Microalgae

Data of a survey of zwitterionic osmolytes [4] could be used to re-evaluate the distribution of ectoine. Integration of the ectoine signals in the chromatograms revealed that ectoine was always detected in LC-MS in amounts similar to those of DMSP (Table 2). This substantial amount of a novel compatible solute, in diatoms (*T. weissflogii*, *Skeletonema costatum*, and *Phaeodactylum tricornutum*), a dinoflagellate (*Prorocentrum minimum*), two haptophytes (*Prymnesium parvum* and *Isochrysis galbana*), and a coccolithophore (*Emiliana huxleyi*), suggests a massive contribution to overall carbon fluxes in the oceans. Given the turnover of DMSP of ca.  $10^9$  tons annually [37,38] and the similar ectoine content, we suggest a massive contribution of this metabolite to nitrogen shuttling within the plankton. Together with DMSP, glycine betaine, and homarine, it clearly belongs to the class of major osmolytes according to the classification in Gebser et al. [2].

**Table 2.** Quantitative survey of ectoine production by xenic marine microalgae compared to other zwitterionic metabolites. Chromatograms for ectoine evaluation and values of dimethylsulfoniopropionate (DMSP) and dimethylsulfoxonium propionate (DMSOP) are obtained from Thume et al. 2018 [4]. Replicates:  $N = 3$ , error bars are based on standard deviation.

Species	GBT	DMSA	Gonyol	<i>n</i> DMSP (fmol per cell)	<i>n</i> DMSOP (fmol per cell)	<i>n</i> Ectoine (fmol per cell)
<i>P. minimum</i>	+	+	+	304.5 ± 61.2	3.66 ± 1.23	141.67 ± 13.43
<i>P. parvum</i>	+	-	+	16.2 ± 4.4	0.029 ± 0.005	7.85 ± 1.61
<i>S. costatum</i>	+	-	-	6.56 ± 2.06	0.029 ± 0.005	5.42 ± 1.89
<i>E. huxleyi</i>	+	-	+	4.83 ± 0.57	0.029 ± 0.013	2.26 ± 0.45
<i>I. galbana</i>	+	-	+	4.69 ± 0.27	0.017 ± 0.003	2.62 ± 0.53

### 3. Materials and Methods

#### 3.1. Cultivation of Microalgae

Xenic and axenic cultures of *Thalassiosira weissflogii* (RCC76, Roscoff Culture Collection, Roscoff, France; CCMP 1336, Provasoli-Guillard National Center for Marine Algae and Microbiota, East Boothbay, ME, USA) as well as a culture of *Phaeodactylum tricorutum* (SCCAP K-1280, <http://www.sccap.dk>) were cultivated in artificial seawater medium according to Maier and Calenberg [39]. Standing cultures in 50 mL polystyrene cell culture bottles with membrane filter screw caps for gas exchange were maintained at a temperature of  $14\text{ }^{\circ}\text{C} \pm 2\text{ }^{\circ}\text{C}$ . A 14:10 light–dark cycle with light was provided by Osram biolux lamps ( $40\text{ }\mu\text{mol photons m}^{-2}\text{s}^{-1}$  between 400 and 700 nm). Cultures were grown to the exponential phase (determined in independent preliminary experiments recording cell counts), diluted 20-fold with fresh medium, and cultivated again to the exponential phase before the analysis. Their axenity was checked during the growth and before the extraction by microscopy and by plating aliquots of each culture on marine broth-agar plates.

#### 3.2. Salinity Treatment

For long-term salinity stress tests, cultures of *T. weissflogii* and *P. tricorutum* were grown in artificial seawater with a standard salinity of 35 Practical Salinity Units (PSU), as well as in artificial sea water where the salinity was adjusted, by addition of NaCl, to reach a final concentration of 50 PSU. For short-term salinity stress test, cultures of diatoms were grown in 35 PSU artificial seawater to the exponential phase and 24 h before the extraction, 5 mL of a 2.65 M solution of NaCl was added after sterile filtration to 35 mL cultures, in order to reach a final salinity of 50 PSU. All media were autoclaved before use. For each salinity, microalgae were cultivated in triplicates.

#### 3.3. Cell Counting and Size Measurement

To determine the final cell densities, 50  $\mu\text{L}$  of diatoms cultures were analyzed using a BD Accuri™ C6 flow cytometer, with standard filters. The discriminator was set to forward light scatter and samples were analyzed with a flow rate of 35  $\mu\text{L}/\text{min}$ . Prior to data collection, the instrument was validated using diluted beads solutions with a known concentration. Pictures for cell size determination were taken with a Leica DFC280 microscope using a Nikon DS-U3 camera. Pictures of 50 randomly selected cells for every salinity were evaluated. Measurements were performed with NIS-Elements Viewer Ver4.50.00. Calculations of the average cell volumes were based on a rectangular shape for *T. weissflogii* and on an ellipsoid shape for *P. tricorutum* [40]. To determine the efficiency of the GF/C filtration to remove bacteria from algal cells (see Section 3.4), 30 mL of a xenic culture of *T. weissflogii* was split. One 15 mL aliquot was diluted with 45 mL of sterile artificial seawater, while the other 15 mL were filtered on Whatman GF/C filters as described below. Filters were washed three times with 15 mL of sterile artificial seawater and the filtered medium was collected. Samples of the filtered medium (250  $\mu\text{L}$ ) and of the diluted culture (250  $\mu\text{L}$ ) were fixed with glutaraldehyde (1% final concentration) for 15 min and stained with SYBR GOLD® (SYBR™ Gold Nucleic Acid Gel Stain (10,000× Concentrate in DMSO), Thermo Scientific, 10,000-fold diluted from stock solution) for 15 min in the dark. Then, the samples were measured with a BD Accuri™ C6 flow cytometer with the following settings: 25  $\mu\text{L}$  per sample, 4  $\mu\text{L}/\text{min}$ , 3 washing steps between each sample with milliQ water.

#### 3.4. Sample Preparation

Diatom cells were extracted at the late exponential phase of growth, by filtration of 30 mL of each culture under reduced pressure (Whatman GF/C grade microfiber filters) of 500 mbar, followed by vacuum filtration of 90 mL of sea water. In xenic cultures, this procedure allowed to remove most bacteria as verified by flow cytometry. Filters were immediately transferred into 4 mL glass vials containing 500  $\mu\text{L}$  of methanol, while another 500  $\mu\text{L}$  of methanol was added directly on the filter. After 30 min at room temperature, samples were stored at  $-20\text{ }^{\circ}\text{C}$ . For ultra-high-pressure liquid



chromatography high-resolution mass spectrometry (UHPLC-HRMS) analysis, 50  $\mu\text{L}$  of each extract were diluted with 100  $\mu\text{L}$  of a mixture of acetonitrile and water (9:1 *v/v*). After centrifugation (5 min,  $4.500\times g$ ), the supernatant was submitted to UHPLC-HRMS analysis.

### 3.5. Equipment

Analytical separation and quantification were performed on a Dionex Ultimate 3000 system (Thermo Scientific) coupled to a Q-Exactive Plus Orbitrap mass spectrometer (Thermo Scientific). Electrospray ionization was performed in positive mode ionization, with the following parameters: capillary temperature, 380  $^{\circ}\text{C}$ ; spray voltage, 3.000 V; sheath gas flow, 60 arbitrary units; and aux gas flow, 20 arbitrary units. The LC separation column was a SeQuant ZIC-HILIC column (5  $\mu\text{m}$ ,  $2.1 \times 150$  mm, SeQuant), equipped with a SeQuant ZIC-HILIC guard column (5  $\mu\text{m}$ ,  $2.1 \times 20$  mm). NMR spectra were recorded on a Bruker Avance 400 MHz instrument.

### 3.6. Osmolyte Analysis

For separation of osmolytes, the eluent consisted of high-purity water with 2% acetonitrile and 0.1% formic acid (solvent A) and 90% acetonitrile with 10% water and 5  $\text{mmol L}^{-1}$  ammonium acetate (solvent B) [11]. The flow rate was set to 0.6  $\text{mL min}^{-1}$  and a linear gradient was used for separation with 100% solvent B (2 min), 60% B (11 min), 20% B (11.8 min), 20% B (14.9 min), 100% B (15 min), 100% B (18 min). The column was kept at 25  $^{\circ}\text{C}$ ; the injection volume was 2  $\mu\text{L}$ . Identification of ectoine was carried out by addition of ectoine (Sigma-Aldrich) as internal standard; for a proper quantification, a calibration curve of the standard followed by comparisons of the peak area of the analytes with the peak area of the internal standard was performed. The calibration curve ( $n = 3$ ) for the area of the molecular ion was  $y = 7.58 \times 10^7 x$  with  $r = 0.9964$ , limit of detection (LOD) = 0.90 nM, limit of quantification (LOQ) = 2.7 nM. For homarine, the calibration curve ( $n = 3$ ) for the areas of the molecular ion was  $y = 1.29 \times 10^8 x$  with  $r = 0.9915$ , limit of detection (LOD) = 4.96 nM, limit of quantification (LOQ) = 15.03 nM; for glycine betaine,  $y = 1.54 \times 10^8 x$  with  $r = 0.9495$ , limit of detection (LOD) = 0.28  $\mu\text{M}$ , limit of quantification (LOQ) = 0.85  $\mu\text{M}$ .

### 3.7. Uptake of Labeled Ectoine by Marine Diatoms

For determination of ectoine uptake, 40-mL cultures of *T. weissflogii* supplied with 1  $\mu\text{M}$  of  $\text{D}_3$ -ectoine were prepared, four replicates per each salinity treatment. Cultures were gravity-filtered on Whatman GF/C during the late exponential phase of growth, and cells on the filter were washed three times with 20 mL of the respective medium. Filters were immediately transferred into 1 mL of methanol. Samples were frozen and further analyzed as described above. During separation, H/D isotope exchange was observed and mass spectrometric data were corrected for the scrambling using data from a run of the pure labeled compound.

### 3.8. Homology Search

Homologues of the enzymes of the ectoine pathway from *Halorhodospira halochloris* were identified by BLAST searches of the *P. tricornutum* genome at NCBI (<http://www.ncbi.nlm.nih.gov/sites/genome>) using default parameters.

### 3.9. Synthesis of $\text{D}_3$ -ectoine

All reactions were performed under an argon atmosphere. All solvents and chemicals were used without further purification. Dry solvents were obtained from VWR (ethanol, electronic grade) and Acros (diethylether ( $\text{Et}_2\text{O}$ ), extra dry, over molecular sieve, AcroSeal<sup>®</sup>).  $\text{D,L}$ -diaminobutyric acid was bought from Sigma-Aldrich, (Germany) and  $\text{D}_3$ -labeled acetonitrile from Euriso-Top (Cambridge Isotope Laboratories).

**Synthesis of D<sub>3</sub>-ethyl acetimidate** [41,42]: Dry HCl gas was bubbled through 5 mL (85.6 mmol) of dry ethanol over a period of 3 h at room temperature. The HCl gas was generated in an argon-purged round-bottom flask by slow dropwise addition of concentrated H<sub>2</sub>SO<sub>4</sub> onto solid NaCl. The gas outlet of the flask was connected to a drying line filled with CaSO<sub>4</sub> and introduced to the reaction flask through a syringe needle. Under positive argon pressure, the reaction flask was placed in a dry ice/acetone bath and 5.0 mL (95.7 mmol) of D<sub>3</sub>-labeled acetonitrile was added dropwise. The reaction was brought to 0 °C and stirred overnight. A white solid precipitate formed and dry Et<sub>2</sub>O (12.5 mL) was added. The resulting slurry was stirred for 15–30 min; after this time, the solvent was removed with a syringe and the product was dried under argon flow to give (1) (3.48 g, 27.6 mmol, 43%) as a white solid. <sup>1</sup>H NMR (400 MHz, CDCl<sub>3</sub>) δ ppm: 1.44 (s, 3H, CH<sub>3</sub>), 4.56 (s, -OCH<sub>2</sub>-), 11.19–12.08 (br d, 2H, NH<sub>2</sub>); <sup>13</sup>C NMR (100 MHz, CDCl<sub>3</sub>) δ ppm: 13.63 (CH<sub>3</sub>), 70.69 (-OCH<sub>2</sub>-), 176.77 (-C=NH<sub>2</sub>).

**Synthesis of D<sub>3</sub>-ectoine:** In a flask, 3.4 g of D<sub>3</sub>-ethyl acetimidate was dissolved in ethanol (30 mL). Under a stream of argon, 6.0 g (30 mmol) of D,L-diaminobutyric acid was added and the reaction was stirred overnight at room temperature. Then, the mixture was heated to reflux for two hours and cooled to 0 °C. After centrifugation, Et<sub>2</sub>O (10 mL) was added to the supernatant and the product precipitated. The solvent was decanted and the precipitate redissolved in ethanol (500 μL). Precipitation with Et<sub>2</sub>O was repeated four times to yield 2 (148 mg, 1.01 mmol, 2%) as a white solid. <sup>1</sup>H NMR (400 MHz, CDCl<sub>3</sub>): δ 2.24 (m, 2H, C5 CH<sub>2</sub>), 3.45 (m, 2H, C6 CH<sub>2</sub>), 4.36 (t, 1H, C4 CH); <sup>13</sup>C NMR (100 MHz, CDCl<sub>3</sub>): δ 16.7 (m, CD<sub>3</sub>), 20.51 (C5), 36.73 (C6), 50.66 (C4), 161.09 (C2), 170.87 (C7). ESI-MS (positive) *m/z* 146.100 [M + H]<sup>+</sup>.

#### 4. Conclusions

We describe here the prevalence of a novel phytoplankton osmolyte, ectoine, that is found in all investigated marine microalgae. Cellular ectoine content in *T. weissflogii* and *P. tricornutum* is substantially elevated in the presence of bacteria. The axenic algae also produce minor amounts of the compounds, indicating both algae and bacteria as producers. Externally applied ectoine is readily taken up by the algae in amounts sufficient to compensate for osmotic stress.

**Author Contributions:** Conceptualization, S.F. and G.P.; Sample Preparation, S.F. and K.T.; Synthesis, S.F. and M.W.; Analysis, S.F.; Writing-Original Draft Preparation, S.F.; Writing-Review & Editing, S.F., K.T., M.W. and G.P.; Supervision, G.P. All authors have read and agreed to the published version of the manuscript.

**Funding:** This research was funded by the International Max Planck Research School Exploration of Ecological Interactions with Molecular Techniques.

**Conflicts of Interest:** The authors declare no conflict of interest.

#### References

1. Moran, M.A.; Durham, B.P. Sulfur metabolites in the pelagic ocean. *Nat. Rev. Microbiol.* **2019**, *17*, 665–678. [[CrossRef](#)] [[PubMed](#)]
2. Gebser, B.; Pohnert, G. Synchronized regulation of different zwitterionic metabolites in the osmoadaptation of phytoplankton. *Mar. Drugs* **2013**, *11*, 2168–2182. [[CrossRef](#)] [[PubMed](#)]
3. Yoch, D.C. Dimethylsulfoniopropionate: Its sources, role in the marine food web, and biological degradation to dimethylsulfide. *Appl. Environ. Microbiol.* **2002**, *68*, 5804–5815. [[CrossRef](#)] [[PubMed](#)]
4. Thume, K.; Gebser, B.; Chen, L.; Meyer, N.; Kieber, D.J.; Pohnert, G. The metabolite dimethylsulfoxonium propionate extends the marine organosulfur cycle. *Nature* **2018**, *563*, 412–415. [[CrossRef](#)]
5. Curson, A.R.J.; Todd, J.D.; Sullivan, M.J.; Johnston, A.W.B. Catabolism of dimethylsulphoniopropionate: Microorganisms, enzymes and genes. *Nat. Rev. Microbiol.* **2011**, *9*, 849–859. [[CrossRef](#)]
6. Smyth, K.; Elliott, M. Effects of changing salinity on the ecology of the marine environment. In *Stressors in the Marine Environment*; Solan, M., Whiteley, N., Eds.; Oxford University Press: Oxford, UK, 2016; pp. 161–174. [[CrossRef](#)]
7. Spielmeyer, A.; Gebser, B.; Pohnert, G. Investigations of the uptake of dimethylsulfoniopropionate by phytoplankton. *ChemBioChem* **2011**, *12*, 2276–2279. [[CrossRef](#)]

8. Dickschat, J.S.; Rabe, P.; Citron, C.A. The chemical biology of dimethylsulfiopropionate. *Org. Biomol. Chem.* **2015**, *13*, 1954–1968. [[CrossRef](#)]
9. Keller, M.D.; Kiene, R.P.; Matrai, P.A.; Bellows, W.K. Production of glycine betaine and dimethylsulphoniopropionate in marine phytoplankton. II. N-limited chemostat cultures. *Mar. Biol.* **1999**, *135*, 249–257. [[CrossRef](#)]
10. Spielmeier, A.; Pohnert, G. Direct quantification of dimethylsulfiopropionate (DMSP) with hydrophilic interaction liquid chromatography/mass spectrometry. *J. Chromatogr. B* **2010**, *878*, 3238–3242. [[CrossRef](#)]
11. Spielmeier, A.; Gebser, B.; Pohnert, G. Dimethylsulfide sources from microalgae: Improvement and application of a derivatization-based method for the determination of dimethylsulfiopropionate and other zwitterionic osmolytes in phytoplankton. *Mar. Chem.* **2011**, *124*, 48–56. [[CrossRef](#)]
12. Zhao, P.P.; Gu, W.; Wu, S.; Huang, A.; He, L.; Xie, X.; Gao, S.; Zhang, B.; Niu, J.; Lin, A.P.; et al. Silicon enhances the growth of *Phaeodactylum tricorutum* Bohlin under green light and low temperature. *Sci. Rep.* **2014**, *4*, 3958. [[CrossRef](#)] [[PubMed](#)]
13. Bussard, A.; Corre, E.; Hubas, C.; Duvernois-Berthet, E.; Le Corguille, G.; Jourden, L.; Coulpier, F.; Claquin, P.; Lopez, P.J. Physiological adjustments and transcriptome reprogramming are involved in the acclimation to salinity gradients in diatoms. *Environ. Microbiol.* **2017**, *19*, 909–925. [[CrossRef](#)] [[PubMed](#)]
14. Garcia, N.; Lopez-Elias, J.A.; Miranda, A.; Martinez-Porchas, M.; Huerta, N.; Garcia, A. Effect of salinity on growth and chemical composition of the diatom *Thalassiosira weissflogii* at three culture phases. *Lat. Am. J. Aquat. Res.* **2012**, *40*, 435–440. [[CrossRef](#)]
15. Ito, T.; Asano, Y.; Tanaka, Y.; Takabe, T. Regulation of biosynthesis of dimethylsulfiopropionate and its uptake in sterile mutant of *Ulva pertusa* (Chlorophyta). *J. Phycol.* **2011**, *47*, 517–523. [[CrossRef](#)]
16. Takagi, M.; Karseno; Yoshida, T. Effect of salt concentration on intracellular accumulation of lipids and triacylglyceride in marine microalgae *Dunaliella cells*. *J. Biosci. Bioeng.* **2006**, *101*, 223–226. [[CrossRef](#)]
17. Keller, M.D.; Kiene, R.P.; Matrai, P.A.; Bellows, W.K. Production of glycine betaine and dimethylsulphoniopropionate in marine phytoplankton. I. Batch cultures. *Mar. Biol.* **1999**, *135*, 237–248. [[CrossRef](#)]
18. Dickson, D.M.J.; Kirst, G.O. The role of b-dimethylsulphoniopropionate, glycine betaine and homarine in the osmoacclimation of *Platymonas subcordiformis*. *Planta* **1986**, *167*, 536–543. [[CrossRef](#)]
19. Galinski, E.A.; Pfeiffer, H.-P.; Trüper, H.G. 1,4,5,6-Tetrahydro-2-methyl-4-pyrimidinecarboxylic acid. A novel cyclic amino acid from halophilic phototrophic bacteria of the genus *Ectothiorhodospira*. *Eur. J. Biochem.* **1985**, *149*, 135–139. [[CrossRef](#)]
20. Kolp, S.; Pietsch, M.; Galinski, E.A.; Gutschow, M. Compatible solutes as protectants for zymogens against proteolysis. *Biochim. Biophys. Acta* **2006**, *1764*, 1234–1242. [[CrossRef](#)]
21. Kunte, H.J.; Lentzen, G.; Galinski, E.A. Industrial production of the cell protectant ectoine: Protection mechanisms, processes and products. *Curr. Biotechnol.* **2014**, *3*, 10–25. [[CrossRef](#)]
22. Waditee-Sirisattha, R.; Kageyama, H.; Takabe, T. Halophilic microorganism resources and their applications in industrial and environmental biotechnology. *AIMS Microbiol.* **2016**, *2*, 42–54. [[CrossRef](#)]
23. Weinisch, L.; Kuhner, S.; Roth, R.; Grimm, M.; Roth, T.; Netz, D.J.A.; Pierik, A.J.; Filker, S. Identification of osmoadaptive strategies in the halophile, heterotrophic ciliate *Schmidingerothrix salinarum*. *PLoS Biol.* **2018**, *16*, e2003892. [[CrossRef](#)] [[PubMed](#)]
24. Weinisch, L.; Kirchner, I.; Grimm, M.; Kuhner, S.; Pierik, J.J.; Rossello-Mora, R.; Filker, S. Glycine betaine and ectoine are the major compatible solutes used by four different halophilic heterotrophic ciliates. *Microb. Ecol.* **2019**, *77*, 317–331. [[CrossRef](#)]
25. Harding, T.; Roger, A.J.; Simpson, A.G.B. Adaptations to high salt in a halophilic protist: Differential expression and gene acquisitions through duplications and gene transfers. *Front. Microbiol.* **2017**, *8*, 944. [[CrossRef](#)] [[PubMed](#)]
26. Widderich, N.; Czech, L.; Elling, F.J.; Könneke, M.; Stöveken, N.; Pittelkow, M.; Riclea, R.; Dickschat, J.S.; Heider, J.; Bremer, E. Strangers in the archaeal world: Osmostress-responsive biosynthesis of ectoine and hydroxyectoine by the marine thaumarchaeon *Nitrosopumilus maritimus*. *Environ. Microbiol.* **2016**, *18*, 1227–1248. [[CrossRef](#)] [[PubMed](#)]
27. Landa, M.; Burns, A.S.; Roth, S.J.; Moran, M.A. Bacterial transcriptome remodeling during sequential co-culture with a marine dinoflagellate and diatom. *ISME J.* **2017**, *11*, 2677–2690. [[CrossRef](#)]
28. Dickson, D.M.J.; Kirst, G.O. Osmotic adjustment in marine eukaryotic algae—The role of inorganic-ions, quaternary ammonium, tertiary sulfonium and carbohydrate solutes. I. Diatoms and a Rhodophyte. *New Phytol.* **1987**, *106*, 645–655. [[CrossRef](#)]

29. Kiene, R.P.; Williams, L.P.H.; Walker, J.E. Seawater microorganisms have a high affinity glycine betaine uptake system which also recognizes dimethylsulfoniopropionate. *Aquat. Microb. Ecol.* **1998**, *15*, 39–51. [[CrossRef](#)]
30. Van Bergeijk, S.A.; Van der Zee, C.; Stal, L.J. Uptake and excretion of dimethylsulphoniopropionate is driven by salinity changes in the marine benthic diatom *Cylindrotheca closterium*. *Eur. J. Phycol.* **2003**, *38*, 341–349. [[CrossRef](#)]
31. Torstensson, A.; Young, J.N.; Carlson, L.T.; Ingalls, A.E.; Deming, J.W. Use of exogenous glycine betaine and its precursor choline as osmoprotectants in Antarctic sea-ice diatoms. *J. Phycol.* **2019**, *55*, 663–675. [[CrossRef](#)]
32. Czech, L.; Bremer, E. With a pinch of extra salt—Did predatory protists steal genes from their food? *PLoS Biol.* **2018**, *16*, e2005163. [[CrossRef](#)] [[PubMed](#)]
33. Onraedt, A.; De Mey, M.; Walcarius, B.; Soetaert, W.; Vandamme, E.J. Transport kinetics of ectoine, an osmolyte produced by *Brevibacterium epidermis*. *Biotechnol. Lett.* **2006**, *28*, 1741–1747. [[CrossRef](#)] [[PubMed](#)]
34. Czech, L.; Hermann, L.; Stoveken, N.; Richter, A.A.; Hoppner, A.; Smits, S.H.J.; Heider, J.; Bremer, E. Role of the extremolytes ectoine and hydroxyectoine as stress protectants and nutrients: Genetics, phylogenomics, biochemistry, and structural analysis. *Genes* **2018**, *9*, 177. [[CrossRef](#)] [[PubMed](#)]
35. Grammann, K.; Volke, A.; Kunte, H.J. New type of osmoregulated solute transporter identified in halophilic members of the *Bacteria* domain: TRAP transporter TeaABC mediates uptake of ectoine and hydroxyectoine in *Halomonas elongata* DSM 2581T. *J. Bacteriol.* **2002**, *184*, 3078–3085. [[CrossRef](#)]
36. Kuhlmann, A.U.; Hoffmann, T.; Bursy, J.; Jebbar, M.; Bremer, E. Ectoine and hydroxyectoine as protectants against osmotic and cold stress: Uptake through the SigB-controlled betaine-choline- carnitine transporter-type carrier EctT from *Virgibacillus pantothenticus*. *J. Bacteriol.* **2011**, *193*, 4699–4708. [[CrossRef](#)]
37. Kiene, R.P.; Linn, L.J.; Bruton, J.A. New and important roles for DMSP in marine microbial communities. *J. Sea Res.* **2000**, *43*, 209–224. [[CrossRef](#)]
38. Simó, R. Production of atmospheric sulfur by oceanic plankton: Biogeochemical, ecological and evolutionary links. *Trends Ecol. Evolut.* **2001**, *16*, 287–294. [[CrossRef](#)]
39. Maier, I.; Calenberg, M. Effect of extracellular Ca<sup>2+</sup> and Ca<sup>2+</sup>-antagonists on the movement and chemoorientation of male gametes of *Ectocarpus siliculosus* (Phaeophyceae). *Bot. Acta* **1994**, *107*, 451–458. [[CrossRef](#)]
40. Hillebrand, H.; Durselen, C.D.; Kirschtel, D.; Pollinger, U.; Zohary, T. Biovolume calculation for pelagic and benthic microalgae. *J. Phycol.* **1999**, *35*, 403–424. [[CrossRef](#)]
41. Himdi-Kabbab, S.; Lavrador, K.; Bazureau, J.P.; Hamelin, J. Synthesis of 1,4,5,6-Tetrahydro 2-Methyl 4-Pyrimidine Carboxylic Acid: Osmoprotector Amino Acid. *Synth. Commun.* **1995**, *25*, 2223–2227. [[CrossRef](#)]
42. Shortreed, M.R.; Lamos, S.M.; Frey, B.L.; Phillips, M.F.; Patel, M.; Belshaw, P.J.; Smith, L.M. Ionizable isotopic labeling reagent for relative quantification of amine metabolites by mass spectrometry. *Anal. Chem.* **2006**, *78*, 6398–6403. [[CrossRef](#)] [[PubMed](#)]





## 2.4 Publication 4

“Cysteinolic acid is a widely distributed compatible solute of marine microalgae.”

Simona Fenizia, Jerrit Weissflog, Georg Pohnert

*Marine Drugs*, Vol. 19(12):683, 2021

DOI: 10.3390/md19120683

Open Access This article is licensed under a Creative Commons Attribution 4.0 International License

Fenizia S.<sup>1</sup>, Weissflog J.<sup>2</sup>, Pohnert G.<sup>3</sup> Cysteinolic acid is a widely distributed compatible solute in marine microalgae. *Marine Drugs* **2021** 19, 12. 10.3390/md19120683.

Author	1	2	3
Development of concept	x		x
Planning of research	x		x
Data collection	x		
Chemical synthesis		x	
Data analysis	x		
Preparation of the manuscript	x	x	x
Correction of the manuscript	x	x	x
Proposed publication equivalent	1.0		

### Authors contribution:

Simona Fenizia	Conceptualization, research planning, experiment preparation and implementation, data analysis, writing-original draft, writing-review, editing
Jerrit Weissflog	Chemical synthesis, writing-review, editing
Georg Pohnert	Conceptualization, research planning, writing-review, editing, supervision



## Article

# Cysteinolic Acid Is a Widely Distributed Compatible Solute of Marine Microalgae

Simona Fenizia <sup>1,2</sup>, Jerrit Weissflog <sup>2</sup> and Georg Pohnert <sup>1,2,\*</sup>

<sup>1</sup> Bioorganic Analytics, Institute for Inorganic and Analytical Chemistry, Friedrich Schiller University Jena, Lessingstrasse 8, D-07743 Jena, Germany; simona.fenizia@uni-jena.de

<sup>2</sup> MPG Fellow Group, Max Planck Institute for Chemical Ecology, Hans-Knöll-Straße 8, D-07745 Jena, Germany; jweissflog@ice.mpg.de

\* Correspondence: georg.pohnert@uni-jena.de

**Abstract:** Phytoplankton rely on bioactive zwitterionic and highly polar small metabolites with osmoregulatory properties to compensate changes in the salinity of the surrounding seawater. Dimethylsulfoniopropionate (DMSP) is a main representative of this class of metabolites. Salinity-dependent DMSP biosynthesis and turnover contribute significantly to the global sulfur cycle. Using advanced chromatographic and mass spectrometric techniques that enable the detection of highly polar metabolites, we identified cysteinolic acid as an additional widely distributed polar metabolite in phytoplankton. Cysteinolic acid belongs to the class of marine sulfonates, metabolites that are commonly produced by algae and consumed by bacteria. It was detected in all dinoflagellates, haptophytes, diatoms and prymnesiophytes that were surveyed. We quantified the metabolite in different phytoplankton taxa and revealed that the cellular content can reach even higher concentrations than the ubiquitous DMSP. The cysteinolic acid concentration in the cells of the diatom *Thalassiosira weissflogii* increases significantly when grown in a medium with elevated salinity. In contrast to the compatible solute ectoine, cysteinolic acid is also found in high concentrations in axenic algae, indicating biosynthesis by the algae and not the associated bacteria. Therefore, we add this metabolite to the family of highly polar metabolites with osmoregulatory characteristics produced by phytoplankton.

**Keywords:** cysteinolic acid; osmoadaptation; osmoregulation; ectoine; DMSP; diatoms; phytoplankton; salinity; LC/MS analysis



**Citation:** Fenizia, S.; Weissflog, J.; Pohnert, G. Cysteinolic Acid Is a Widely Distributed Compatible Solute of Marine Microalgae. *Mar. Drugs* **2021**, *19*, 683. <https://doi.org/10.3390/md19120683>

Academic Editor: Hitoshi Sashiwa

Received: 5 November 2021

Accepted: 26 November 2021

Published: 30 November 2021

**Publisher's Note:** MDPI stays neutral with regard to jurisdictional claims in published maps and institutional affiliations.



**Copyright:** © 2021 by the authors. Licensee MDPI, Basel, Switzerland. This article is an open access article distributed under the terms and conditions of the Creative Commons Attribution (CC BY) license (<https://creativecommons.org/licenses/by/4.0/>).

## 1. Introduction

Free-floating phytoplankton in the open ocean contribute substantially to primary production. Phytoplankton can be exposed to changing salinity levels due to vertical migration or transport within ocean currents [1]. Adaptation to the changing environment is thus a pre-requisite for the survival of the cells [1,2]. Changes in salinity that occur, for example, in coastal waters or sea ice represent an environmental stress factor that must be compensated by the unicellular algae of the phytoplankton [3]. Cells respond by production/uptake or degradation/exudation of compatible solutes. These polar organic compounds adjust the osmolality of the cells to that of the environment [4–7]. Dimethylsulfoniopropionate (DMSP) is a major compatible solute in many phytoplankton species. The amount of this sulfur-containing zwitterionic metabolite produced globally by marine organisms is estimated to be around two petagrams per year [8,9]. The enzymatic cleavage of this osmolyte results in the release of the volatile dimethylsulfide (DMS). This metabolite contributes significantly (30 teragram per year) to the global sulfur flux from the hydrosphere to the atmosphere [10–13]. Besides DMSP, many other highly polar metabolites that can serve as compatible solutes have been discovered in phytoplankton. Analysis of these metabolites has proven problematic because it is difficult to extract and enrich the small, polar metabolites. The introduction of a ZIC-HILIC separation protocol combined with highly



sensitive MS analysis has enabled the systematic investigation of zwitterionic metabolites and other polar metabolites in marine microalgae and seawater [14–17]. The identification of dimethylsulfoxoniumpropionate (DMSOP) produced and released by phytoplankton is a remarkable demonstration of the validity of this analytical approach. DMSOP is produced by phytoplankton and is readily taken up by marine bacteria, confirming that this class of molecules supports bacterial heterotrophy in the ocean [11,18,19].

Besides sulfur-containing zwitterionic metabolites, marine organisms also produce nitrogen-containing compounds, such as glycine betaine (GBT) and homarine, with osmoregulatory and osmoadaptive properties [4]. The bacterial zwitterionic metabolite ectoine, for example, is also a common metabolite produced by marine phytoplankton and bacteria [7]. It can be taken up from bacteria by diatoms to fulfill physiological requirements and to compensate for osmotic stress [7].

Despite the considerable advances in the characterization of the phytoplankton metabolome, organic polar compounds are still not comprehensively analyzed [4,7,11]. A detailed analysis of sulfonates from cultured eukaryotic phytoplankton showed up to millimolar cellular concentrations. The analysis of the production and catabolism of this compound class revealed a tightly coupled microbial network based on sulfonates. Sources and sinks were deduced from genomic data, expression analysis and mass spectrometric evidence [20].

Our study aims to expand our knowledge of the metabolome of marine algae, focusing on the production and regulation of polar compounds produced under osmotic stress conditions. For this purpose, we selected the diatom *Thalassiosira weissflogii* as a study organism. It is a centric marine diatom, ubiquitously distributed in the oceans [21]. *T. weissflogii* has been utilized previously for several studies on the osmoadaptation of marine phytoplankton [22,23]. It was also used as a model organism for the investigation of diatom responses to different types of environmental stress, such as seawater acidification [24], temperature and light changes [25] and anoxia [21]. Interestingly, *T. weissflogii* does not produce the ubiquitous osmolyte DMSP but compensates this lack by uptake of the metabolite from the surrounding water [23]. We detected and quantified cysteinolic acid under osmotic stress conditions in this alga and undertook a survey of its prevalence in other members of the phytoplankton. We observed a significant contribution of this metabolite to the osmoadaptation of microalgae during short- and long-term environmental salinity changes. Therefore, cysteinolic acid can be included among the phytoplankton-derived “compatible solute”.

## 2. Results and Discussion

Xenic and axenic cultures of the diatom *Thalassiosira weissflogii* were grown under standard culture conditions of 35 Practical Salinity Units (PSU, g NaCl kg<sup>-1</sup> seawater) and under increased salinity of 50 PSU to cover the effect of a substantial salinity increase according to previous studies [7,26,27]. Using ultra-high-pressure liquid chromatography and high-resolution mass spectrometry (UHPLC-MS) [4], we mined for uncharacterized highly polar metabolites potentially involved in osmoregulation. Up-regulation under increased salinity was selected as a criterion in a metabolic profiling approach. Among the up-regulated masses that could not be assigned to common and fully structurally proven metabolites, we detected  $[M + H]^+ = 156$  with a characteristic sulfur isotope signature. It was characterized as cysteinolic acid, a compound with osmoregulatory properties.

### 2.1. Identification of Cysteinolic Acid in the Diatom *Thalassiosira weissflogii*

Figure 1 shows the UHPLC-HRMS chromatographic profile obtained from methanolic extracts of xenic and axenic cultures of *T. weissflogii* (the respective strains used were RCC76 and CCMP1336). This diatom does not produce quantifiable amounts of DMSP, but other major zwitterionic metabolites, such as homarine, glycine betaine and ectoine, are detectable [7,23]. The identities of these osmolytes were verified by co-injection either with

commercially available standards (glycine betaine and ectoine) or with the corresponding standard synthesized in our laboratory (homarine) according to a published procedure [4].

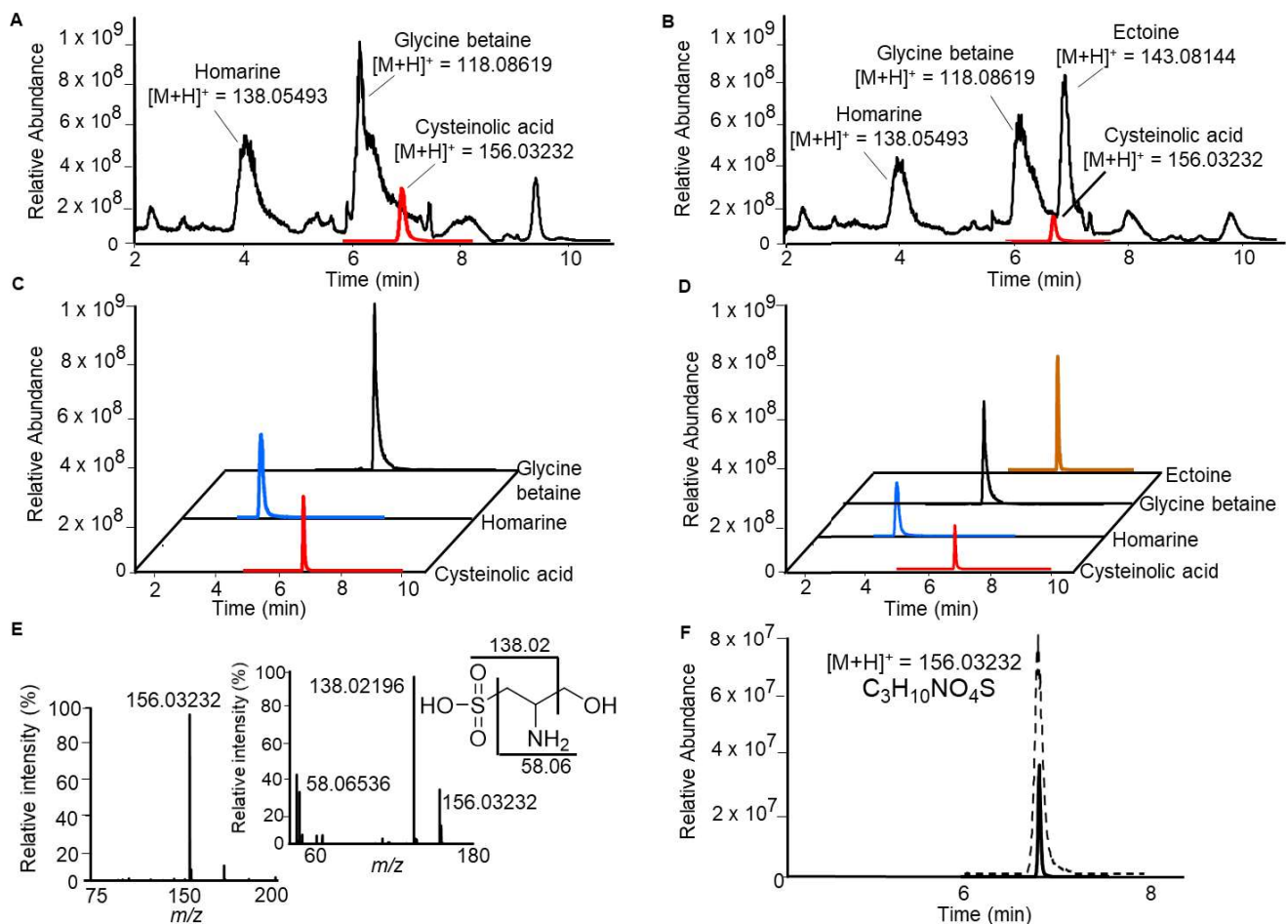


**Figure 1.** Chromatographic separation of highly polar and zwitterionic metabolites in the diatom *Thalassiosira weissflogii* CCMP1336 (axenic cultures, **A**), RCC76 (xenic cultures, **B**), using ultra-high-pressure liquid chromatography (UHPLC) with detection by electrospray ionization mass spectrometry. The total ion current is shown in black. The identity of the metabolites glycine betaine, homarine and ectoine was assigned according to previous studies. The ion trace of cysteinolic acid (solid red line) is shown at a fivefold magnification in (**A**) and at a tenfold magnification in (**B**). The extracted ion chromatograms for the selected zwitterions are shown in (**C**, axenic culture) and in (**D**, xenic culture). The MS and MS/MS spectra of cysteinolic acid are shown in (**E**), and fragmentation is indicated in the inserted structure. In (**F**), the solid black line is the UHPLC profile monitoring the ion trace of  $m/z = 156.03232 \pm 0.0005\%$  of the methanol extract of cultures of *T. weissflogii*; the dashed black line is the same extract treated with synthetic cysteinolic acid in roughly equal amounts to confirm structural identity by co-elution.

Analysis of the chromatogram and the HRMS spectra in positive mode revealed a peak with  $m/z$  of the  $[M + H]^+ = 156.03232$ , corresponding to the molecular formula  $C_3H_{10}NO_4S$  (calculated:  $[M + H]^+ = 156.03251$ ). This initially caught our attention due to the isotope pattern with a  $M + 1.9958$  signal, characteristic for sulfur-containing metabolites. The incorporation of  $^{13}C$  from  $^{13}CO_2$  confirmed its biosynthetic origin. The fragmentation pattern of this peak, analyzed by tandem mass spectrometry (MS/MS), showed a fragment ion  $m/z$  138.02196, attributed to the loss of  $H_2O$ , and a second one with  $m/z$  56.04979 attributed to the loss of water and the sulfonic group (Figure 1). By comparison with the online database METLIN and using the tools Sirius v4.0.1, and CSI:FingerID [28,29], the signal was initially attributed to cysteinolic acid, whose identity was proven by co-injection of the algal extract with synthetic cysteinolic acid. Both exact mass and retention time matched the standard and co-injection confirmed the identity of the metabolite (Figure 1F).

Cysteinolic acid (2-amino-3-hydroxy-1-propanesulfonic acid) belongs to the class of sulfonates common in aquatic systems. Unlike the zwitterions, such as homarine, DMSP, glycine betaine, DMSOP and gonyol, cysteinolic acid can be present in a neutral form as depicted in Figure 2.

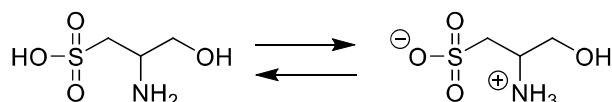


Figure 2. All neutral (left) and zwitterionic (right) forms of cysteinolic acid.

In 1957, Wickberg et al. reported the isolation and identification of this C3-sulfonate in the red alga *Polysiphonia fastigiata* and thereby expanded the knowledge about sulfonates in algae that was limited to taurine and taurine derivatives [30]. Other studies reported cysteinolic acid in brown algae [31] and in the freshwater diatom *Navicula pelliculosa* where it occurs together with the structurally related 2,3-dihydroxypropane-1-sulfonate (DHPS). In this alga, it is one of the major sulfonic acids and plays a role as sulfur reservoir during sulfur starvation [32,33]. Based on the incorporation of radioactive sulfate, it was concluded that cysteinolic acid accounts for ca. 11% of the total soluble  $^{35}\text{S}$ . Besides these early reports on freshwater diatoms, little is known about the distribution, abundance and role of cysteinolic acid in marine microalgae. Recent studies have focused on DHPS and have pointed out the presence of sulfonate transport and catabolism genes in terrestrial and marine bacteria and microalgae [20,34]. In an untargeted metabolomics approach, evidence for the production of cysteinolic acid in marine diatoms and a haptophyte was given based on MS/MS data similar to those reported above, but the final structural confirmation, as well as information about its concentration and physiological role, remained open [20]. It was speculated that such a highly polar metabolite could contribute to osmoadaptation and that this compound class could also be involved in the balance of redox reactions [20].

DHPS and other osmolytes, particularly DMSP, betaine and proline, increase with salinity in the diatom *T. pseudonana*. The high cellular concentration (mM) of sulfonates produced by marine phytoplankton supports the notion that this class of metabolites plays an important role in the environment and makes a substantial contribution to global sulfur and carbon cycles likely [20,34,35].

## 2.2. Salinity-Dependent Changes in Cysteinolic Acid Concentration in *T. weissflogii*

To verify if cysteinolic acid contributes to the intracellular osmotic balance in marine diatoms, *T. weissflogii* was grown at low (35 PSU) and high (50 PSU) salinity, according to protocols of previous studies [7,26]. For short-term salinity stress experiments, cells were grown at 35 PSU to the late exponential phase, transferred to 50 PSU, and analyzed 24 h after this transfer. Long-term salinity stress was achieved by growing cells at 50 PSU over two generations. Tests were performed on both axenic and xenic cultures. *T. weissflogii* cells were harvested by filtration on GF/C filters, which also removes most of the bacteria present in xenic cultures [7].

Quantification of cysteinolic acid revealed that it is also a substantial osmolyte in this diatom with intracellular concentrations reaching the 100 fmol/cell level (Figure 3). This is lower compared to ectoine, homarine and glycine betaine that reach pmol/cell concentrations [7].

After short-term salinity stress in xenic cultures, the concentration of cysteinolic acid increased by ca. 2-fold compared to the concentration under 35 PSU conditions. A 2.4-fold increase was observed after long-term stress (Figure 3). In axenic cultures, compared to the xenic, the intracellular content of cysteinolic acid was 1.5-fold higher at 35 PSU, and it did not increase significantly during the short-term salinity stress, but increased by 2.6-fold during the long-term stress (Figure 3). In axenic cultures, the higher amount of cysteinolic acid might compensate for the lower amount of ectoine (observed in a previous study [7]). Ectoine is predominantly supplied by bacteria and taken up by the algae, and thus reaches

lower concentrations in axenic cultures [7]. This is not the case for cysteinolic acid, which is higher in axenic studies. It is thus produced by the algae and might be consumed or converted by associated bacteria in xenic cultures. These regulations support a contribution of the microbial community to the physiology of an algal cell and the existence of a coupled microbial metabolic network between eukaryotic phytoplankton (sulfonate producers) and heterotrophic bacteria (sulfonate consumers, ectoine producers) [20,35–37].

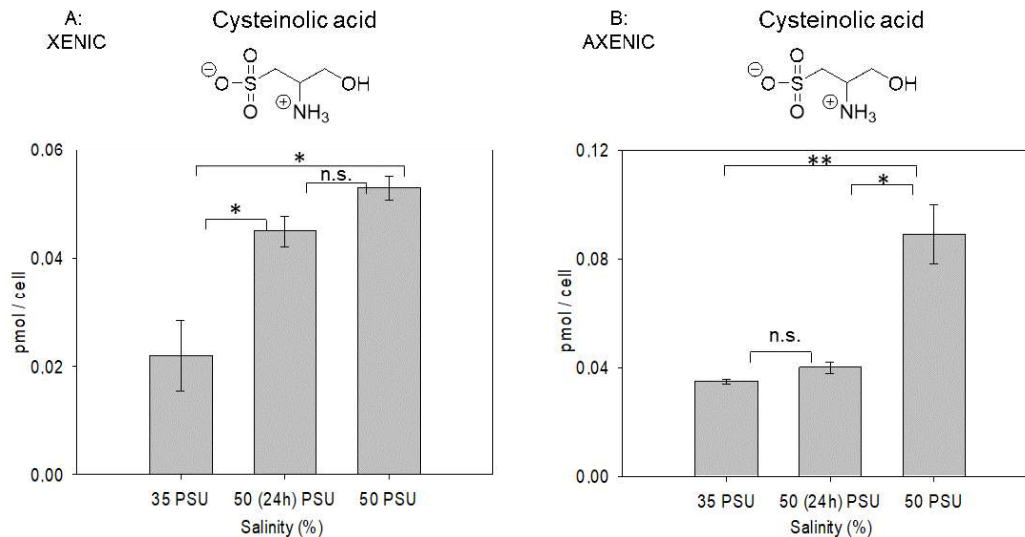


**Figure 3.** Intracellular amounts of cysteinolic acid in xenic (A) and axenic (B) cultures of *T. weissflogii* grown under different salinity regimes. The label 35 PSU indicates that cultures were maintained constantly at this salinity; 50 PSU (24 h) indicates that cultures grown at 35 PSU were transferred into a medium of 50 PSU and analyzed 24 h after the transfer; 50 PSU indicates cultures grown for two generations at this elevated salinity. Concentrations are normalized per cell; error bars represent standard deviation (biological replicates,  $N = 3$ ). Statistical analysis is based on one-way ANOVA with a Tukey test for multiple comparison procedures. \*  $p \leq 0.05$ , \*\*  $p \leq 0.01$ , n.s. not significant). Note the different scales of the  $y$ -axes.

### 2.3. Cysteinolic Acid in Other Microalgae

With the purpose of investigating the distribution of cysteinolic acid in phytoplankton, the metabolome of several species of microalgae was screened and the intracellular amounts of cysteinolic acid were compared to those of other zwitterionic osmolytes [7,11]. The amount of cysteinolic acid in all the investigated species was obtained by integration of the correspondent signal in each chromatogram and an external calibration curve prepared with three repeated measurements before each batch analysis. The concentration was then normalized to cell counts and cellular volume. The concentrations of cysteinolic acid can reach levels in the same range of those of DMSP, which is a dominant zwitterionic osmolyte in many species (Table 1) [11,38]. It is even the most abundant osmolyte quantified in this study in the dinoflagellate *Amphidinium carterae*. The intracellular concentrations of cysteinolic acid are in the same range as those of DHPS, a major cytosolic diatom component that supports bacterial growth [20].

The abundance and the regulation under different salinity regimes suggest a contribution of this zwitterionic metabolite to the osmoregulation of different plankton phyla. It adds to the family of zwitterionic metabolites as a major component in the algal cells that support osmoadaptation. The abundance of cysteinolic acid also supports the notion of sulfonates as a valuable target for tracking microbial interactions in the sea. As revealed by Durham et al. [20], sulfonate metabolism in the marine biosphere is widely distributed and highly complex. Our result adds a new algal metabolite to this family by providing full structural proof and confirms eukaryotic phytoplankton as major sulfonate producers [18]. We also show its contribution to salinity adaptation. Since cellular content will eventually also contribute to the dissolved organic carbon and dissolved organic sulfur in the ocean that can be used by other microorganisms of the plankton, the consequence

of this additional metabolite on the microbiome functioning should be investigated. In agreement, genes connected to the uptake and metabolism of dissolved organic sulfur are also abundant.

**Table 1.** Quantitative survey of cysteinolic acid and other osmolytes in xenic marine microalgae at 35 PSU. Replicates:  $N = 3$ , error based on standard deviations. A plus (+) indicates the presence of a signal below the limit of quantification, a minus (−) indicates the absence of the correspondent signal. Cell volumes of *T. weissflogii* for determination of intracellular cysteinolic acid concentration were obtained from Fenizia et al. 2020 [7]; cell volumes of the other species were based microscopy measurement and calculation according to their geometric shape [39]. Data for DMSOP from Thume et al. 2018 [11].

Species	DMSA	Gonyol	GBT (Fmol Cell <sup>-1</sup> )	Homarine (Fmol Cell <sup>-1</sup> )	DMSP (Fmol Cell <sup>-1</sup> )	DMSOP (Fmol Cell <sup>-1</sup> )	Ectoine (Fmol Cell <sup>-1</sup> )	Cysteinolic Acid (Fmol Cell <sup>-1</sup> )	Cysteinolic Acid (mM)
<i>Prorocentrum minimum</i>	+	+	37.9 ± 4.8	0.27 ± 0.06	463.4 ± 52.6	3.66 ± 1.23	42.0 ± 6.1	50.6 ± 8.1	71.1 ± 11.4
<i>Prymnesium parvum</i>	−	+	1.5 ± 0.7	0.04 ± 0.02	47.4 ± 5.3	0.029 ± 0.005	4.8 ± 1.2	1.9 ± 0.8	17.9 ± 7.3
<i>Amphidinium carterae</i>	+	+	+	0.09 ± 0.04	+	−	9.1 ± 1.5	17.2 ± 2.8	18.5 ± 3.0
<i>Thalassiosira pseudonana</i>	+	−	7.7 ± 0.9	2.0 ± 0.2	4.8 ± 0.6	−	1.9 ± 0.2	2.8 ± 0.3	17.5 ± 2.0
<i>Skeletonema costatum</i>	−	−	+	0.06 ± 0.01	28.5 ± 4.1	0.029 ± 0.005	10.0 ± 1.5	10.9 ± 0.5	42.2 ± 2.1
<i>Emiliana huxleyi</i>	−	+	0.73 ± 0.04	0.41 ± 0.03	7.3 ± 0.7	0.029 ± 0.013	0.54 ± 0.06	1.0 ± 0.1	11.9 ± 0.7
<i>Isochrysis galbana</i>	−	+	4.8 ± 0.2	1.3 ± 0.1	13.8 ± 0.6	0.017 ± 0.003	1.6 ± 0.1	1.0 ± 0.03	10.8 ± 0.4
<i>Thalassiosira weissflogii</i>	−	−	234.7 ± 35.7	35.4 ± 2.5	−	−	85.2 ± 13.1	22.3 ± 11.3	8.0 ± 4.0

### 3. Materials and Methods

The results in this work arise from an in-depth analysis of an experiment reported by Fenizia et al. [7]. There, the full experimental details are given. Here we only outline the methods for cultivation and extraction briefly. The full methods for structure elucidation and quantification are given here.

#### 3.1. Cultivation of Microalgae

Xenic and axenic cultures of *Thalassiosira weissflogii* (RCC76, Roscoff Culture Collection, Roscoff, France; CCMP 1336; Provasoli-Guillard National Center for Marine Algae and Microbiota, East Boothbay, ME, USA) were cultivated as standing cultures in artificial seawater medium according to Maier and Calenberg [40] at 14 °C ± 2 °C. A 14:10 light–dark cycle with 40 μmol photons m<sup>-2</sup>s<sup>-1</sup> between 400 and 700 nm light was used. Cultures were grown to the exponential phase; 2 mL was diluted 20-fold with fresh medium and cultivated again to the exponential phase before the start of the experiments. Axenicity was checked by microscopy and by plating aliquots of each culture on marine broth agar plates.

#### 3.2. Salinity Treatment

For long-term salinity stress treatments, cultures of *T. weissflogii* were grown in artificial seawater with a normal salinity of 35 Practical Salinity Units (PSU), and in artificial sea water where the salinity was adjusted to 50 PSU [7]. For a short-term salinity stress test, cultures of the diatom were grown in 35 PSU artificial seawater to the exponential phase and, 24 h before the extraction, 5 mL of a sterile filtered 2.65 M solution of NaCl was added to 35 mL cultures in order to reach a final salinity of 50 PSU.

#### 3.3. Cell Counting and Size Measurement

To determine cell densities, 50 μL of culture was analyzed using a BD Accuri™ C6 flow cytometer (BD Biosciences, East Rutherford, NJ, USA) as described in [7]. Pictures for cell size measurements were taken with a Leica DFC280 microscope (Leica, Wetzlar, Germany) using a Nikon DS-U3 camera (Nikon, Tokyo, Japan). Pictures of 50 randomly selected cells for every salinity were evaluated. Calculations of the average cell volumes were based on a corresponding geometric shape, as reported by Hillebrand et al. [7,39].

### 3.4. Sample Preparation

Diatom cells were harvested in the late exponential growth phase by filtration of 30 mL culture under a reduced pressure of 500 mbar using GF/C-grade microfiber filters (Sigma-Aldrich, Deisenhofen, Germany), followed by washing through a vacuum filtration of 90 mL of artificial sea water [7]. Filters were immediately transferred into 4 mL screw cap glass vials containing 500  $\mu$ L of methanol, while another portion of 500  $\mu$ L of methanol was added directly on the filter. Samples were manually shaken three times and, after 30 min at room temperature, stored at  $-20$  °C. For ultra-high-pressure liquid chromatography high-resolution mass spectrometry (UHPLC-HRMS) analysis, 50  $\mu$ L of each extract was diluted with 100  $\mu$ L of acetonitrile and water (9:1 *v/v*). After centrifugation (5 min,  $4.500\times g$ ) the supernatant was submitted to UHPLC-HRMS analysis.

### 3.5. UHPLC/HRMS-Equipment and Settings

Analytical separation and quantification were performed on a Dionex™ UltiMate™ 3000 system (Thermo Fisher Scientific, Dreieich, Germany) equipped with a SeQuant ZIC-HILIC column (5  $\mu$ m,  $2.1 \times 150$  mm, SeQuant with guard column, Merck, Darmstadt, Germany). Mass spectra were recorded on a Q-Exactive™ Plus Orbitrap mass spectrometer (Thermo Fisher Scientific, Dreieich, Germany). The electrospray ionization conditions are given in [7]. The column temperature was set to 25 °C. Mass measurements were performed in the HESI-positive mode, full scan mode from 75 to 200 *m/z*, at a resolution of 70,000. For qualitative MS/MS analysis, the collision energy was set to 35 V and data were collected in DIA (Data Independent Acquisition) mode.

### 3.6. Osmolyte Analysis

The eluent consisted of high-purity water with 2% acetonitrile and 0.1% formic acid (solvent A) and 90% acetonitrile with 10% water and 5 mmol L<sup>-1</sup> ammonium acetate (solvent B) [15]. The flow rate was set to 0.6 mL min<sup>-1</sup>, and a linear gradient was used for separation with 100% solvent B (2 min), 60% B (11 min), 20% B (11.8 min), 20% B (14.9 min), 100% B (15 min) and 100% B (18 min) at 25 °C. Identification by co-injection of cysteinolic acid was carried out after addition of synthetic cysteinolic acid to the sample. For quantification, a calibration curve of the synthetic standard was recorded in the seawater medium also used for algal culturing. The purity and concentration of the synthetic standard were verified by <sup>1</sup>H-NMR. The calibration curve ( $n = 3$ ) for the area of the molecular ion of cysteinolic acid was  $y = 1.27 \times 10^7 x$  with  $r = 0.9734$ , limit of detection (LOD) = 2.17  $\mu$ M in the medium and limit of quantification (LOQ) = 7.15  $\mu$ M in the medium. Related to ectoine, the calibration curve ( $n = 3$ ) for the area of the molecular ion was  $y = 2.96 \times 10^8 x$  with  $r = 0.9970$ , limit of detection (LOD) = 0.33  $\mu$ M and limit of quantification (LOQ) = 1.08  $\mu$ M; for homarine, the calibration curve ( $n = 3$ ) for the area of the molecular ion was  $y = 5.26 \times 10^8 x$  with  $r = 0.9931$ , limit of detection (LOD) = 0.04  $\mu$ M, limit of quantification (LOQ) = 0.12  $\mu$ M; for glycine betaine,  $y = 1.59 \times 10^8 x$  with  $r = 0.9364$ , limit of detection (LOD) = 0.18  $\mu$ M and limit of quantification (LOQ) = 0.58  $\mu$ M. The calibration curve ( $n = 3$ ) for the area of the molecular ion of DMSP was  $y = 8.28 \times 10^7 x$  with  $r = 0.9878$ , limit of detection (LOD) = 0.07  $\mu$ M and limit of quantification (LOQ) = 0.23  $\mu$ M. MS and MS/MS data are deposited in [https://edmond.mpdl.mpg.de/imeji/collection/wP7a\\_7LNwS3DMf](https://edmond.mpdl.mpg.de/imeji/collection/wP7a_7LNwS3DMf) (accessed on 25 November 2021).

### 3.7. Synthesis of Cysteinolic Acid

The synthesis was carried out using a slightly modified protocol of that of Xu et al. [41]. If not otherwise indicated, all solvents and chemicals were obtained from Sigma (Sigma, Deisenhofen, Germany) and used without further purification. In a 100 mL round-bottom flask, 200 mg (1.98 mmol) of methyl aziridine-2-carboxylate (TCI Co. Ltd., Tokyo, Japan) was dissolved in 20 mL of deionized water, and sodium borohydride (150 mg, 3.96 mmol) and lithium chloride (168 mg, 3.96 mmol) were added to the solution. After the mixture was stirred overnight at room temperature, sodium bisulfite (412 mg, 3.96 mmol) was

added portion-wise under stirring. The resulting solution was stirred for another 24 h at room temperature. After this time, the complete reaction mixture was passed through a column of Amberlite IR-120 (H<sup>+</sup> form) and then of Amberlyst A21 (free base form) using deionized water to rinse the columns. The pooled eluate fractions were concentrated under reduced pressure back to a volume of ~20 mL before being passed through a column of Dowex 1 × 8 (acetate form, prepared from chloride form). The eluate was evaporated to dryness under reduced pressure, and the residue was recrystallized from EtOH/H<sub>2</sub>O (3:1, v/v) three times to give (1) (80 mg, 0.51 mmol, 26%) as a white solid, which was dried in vacuum. <sup>1</sup>H-NMR (400 MHz, 0.2M NaOD in D<sub>2</sub>O) δppm: 3.64 + 3.55 (2 × dd, 2H, -CH<sub>2</sub>OH), 3.40 (m, 1H -CHNH<sub>3</sub><sup>+</sup>), 3.10 + 2.90 (2 × dd, 2H, -CH<sub>2</sub>SO<sub>3</sub><sup>-</sup>), <sup>13</sup>C-NMR (400 MHz, 0.2M NaOD in D<sub>2</sub>O) δppm: 64.0 (-CH<sub>2</sub>OH), 53.0 (CH<sub>2</sub>SO<sub>3</sub><sup>-</sup>), 49.2 (-CHNH<sub>3</sub><sup>+</sup>) (ESI-MS (positive) m/z 156.03232 [M + H]<sup>+</sup>).

#### 4. Conclusions

In this work, we describe the identification and quantification of cysteinolic acid, which underline its importance as an algal osmolyte. Cysteinolic acid is widespread among different phyla of phytoplankton and is an abundant highly polar compatible solute.

**Author Contributions:** Conceptualization, S.F. and G.P.; sample Preparation, analysis, writing—original draft preparation, S.F.; synthesis, J.W.; writing—review and editing, S.F., J.W. and G.P.; supervision, G.P. All authors have read and agreed to the published version of the manuscript.

**Funding:** This research was funded by the International Max Planck Research School Exploration of Ecological Interactions with Molecular Techniques and by the Deutsche Forschungsgemeinschaft (DFG, German Research Foundation) under Germany's Excellence Strategy—EXC 2051—Project-ID 390713860.

**Informed Consent Statement:** Informed consent was obtained from all subjects involved in the study.

**Data Availability Statement:** The underlying data are deposited in the zenodo repository under the following link: <https://doi.org/10.5281/zenodo.5697964> (accessed on 25 November 2021).

**Conflicts of Interest:** The authors declare no conflict of interest.

#### References

1. Erga, S.R.; Lie, G.C.; Aarø, L.H.; Frette, Ø.; Hamre, B. Migratory behaviour of *Skeletonema grethae* (Bacillariophyceae) in stratified waters. *Diatom Res.* **2014**, *30*, 13–25. [[CrossRef](#)]
2. Mousing, E.A.; Richardson, K.; Bendtsen, J.; Cetinić, I.; Perry, M.J.; Cornell, W. Evidence of small-scale spatial structuring of phytoplankton alpha- and beta-diversity in the open ocean. *J. Ecol.* **2016**, *104*, 1682–1695. [[CrossRef](#)]
3. Smyth, K.; Elliott, M. Effects of changing salinity on the ecology of the marine environment. In *Stressors in the Marine Environment*; Solan, M., Whiteley, N., Eds.; Oxford University Press: Oxford, UK, 2016; pp. 161–174. [[CrossRef](#)]
4. Gebser, B.; Pohnert, G. Synchronized regulation of different zwitterionic metabolites in the osmoadaptation of phytoplankton. *Mar. Drugs* **2013**, *11*, 2168–2182. [[CrossRef](#)]
5. Welsh, D.T. Ecological significance of compatible solute accumulation by micro-organisms: From single cells to global climate. *FEMS Microbio. Rev.* **2000**, *24*, 263–290. [[CrossRef](#)]
6. Yancey, P.H. Organic osmolytes as compatible, metabolic and counteracting cytoprotectants in high osmolarity and other stresses. *J. Exp. Biol.* **2005**, *208*, 2819–2830. [[CrossRef](#)]
7. Fenizia, S.; Thume, K.; Wirgenings, M.; Pohnert, G. Ectoine from bacterial and algal origin is a compatible solute in microalgae. *Mar. Drugs* **2020**, *18*, 42. [[CrossRef](#)]
8. Ksionzek, K.B.; Lechtenfeld, O.J.; McCallister, S.L.; Schmitt-Kopplin, P.; Geuer, J.K.; Geibert, W.; Koch, B.P. Dissolved organic sulfur in the ocean: Biogeochemistry of a petagram inventory. *Science* **2016**, *354*, 456–459. [[CrossRef](#)]
9. Curson, A.R.; Liu, J.; Bermejo-Martinez, A.; Green, R.T.; Chan, Y.; Carrion, O.; Williams, B.T.; Zhang, S.H.; Yang, G.P.; Bulman-Page, P.C.; et al. Dimethylsulfoniopropionate biosynthesis in marine bacteria and identification of the key gene in this process. *Nat. Microbiol.* **2017**, *2*, 17009. [[CrossRef](#)]
10. Lana, A.; Bell, T.G.; Simó, R.; Vallina, S.M.; Ballabrera-Poy, J.; Kettle, A.J.; Dachs, J.; Bopp, L.; Saltzman, E.S.; Stefels, J.; et al. An updated climatology of surface dimethylsulfide concentrations and emission fluxes in the global ocean. *Global Biogeochem. Cycles* **2011**, *25*. [[CrossRef](#)]

11. Thume, K.; Gebser, B.; Chen, L.; Meyer, N.; Kieber, D.J.; Pohnert, G. The metabolite dimethylsulfoxonium propionate extends the marine organosulfur cycle. *Nature* **2018**, *563*, 412–415. [[CrossRef](#)] [[PubMed](#)]
12. Charlson, R.J.; Lovelock, J.E.; Andreae, M.O.; Warren, S.G. Oceanic phytoplankton, atmospheric sulphur, cloud albedo and climate. *Nature* **1987**, *326*, 655–661. [[CrossRef](#)]
13. Andreae, M.O.; Crutzen, P.J. Atmospheric aerosols: Biogeochemical sources and role in atmospheric chemistry. *Science* **1997**, *276*, 1052–1058. [[CrossRef](#)]
14. Spielmeyer, A.; Pohnert, G. Direct quantification of dimethylsulfoniopropionate (DMSP) with hydrophilic interaction liquid chromatography/mass spectrometry. *J. Chromatogr. B* **2010**, *878*, 3238–3242. [[CrossRef](#)]
15. Spielmeyer, A.; Gebser, B.; Pohnert, G. Dimethylsulfide sources from microalgae: Improvement and application of a derivatization-based method for the determination of dimethylsulfoniopropionate and other zwitterionic osmolytes in phytoplankton. *Mar. Chem.* **2011**, *124*, 48–56. [[CrossRef](#)]
16. Boysen, A.K.; Heal, K.R.; Carlson, L.T.; Ingalls, A.E. Best-matched internal standard normalization in liquid chromatography-mass spectrometry metabolomics applied to environmental samples. *Anal. Chem.* **2018**, *90*, 1363–1369. [[CrossRef](#)]
17. Heal, K.R.; Kellogg, N.A.; Carlson, L.T.; Lionheart, R.M.; Ingalls, A.E. Metabolic consequences of cobalamin scarcity in the diatom *Thalassiosira pseudonana* as revealed through metabolomics. *Protist* **2019**, *170*, 328–348. [[CrossRef](#)]
18. Wang, R.; Gallant, E.; Seyedsayamdost, M.R. Investigation of the genetics and biochemistry of Roseobactioid production in the Roseobacter clade bacterium *Phaeobacter inhibens*. *MBio* **2016**, *7*, e02118-15. [[CrossRef](#)] [[PubMed](#)]
19. Landa, M.; Burns, A.S.; Durham, B.P.; Esson, K.; Nowinski, B.; Sharma, S.; Vorobev, A.; Nielsen, T.; Kiene, R.P.; Moran, M.A. Sulfur metabolites that facilitate oceanic phytoplankton-bacteria carbon flux. *ISME J.* **2019**, *13*, 2536–2550. [[CrossRef](#)]
20. Durham, B.P.; Boysen, A.K.; Carlson, L.T.; Groussman, R.D.; Heal, K.R.; Cain, K.R.; Morales, R.L.; Coesel, S.N.; Morris, R.M.; Ingalls, A.E.; et al. Sulfonate-based networks between eukaryotic phytoplankton and heterotrophic bacteria in the surface ocean. *Nat. Microbiol.* **2019**, *4*, 1706–1715. [[CrossRef](#)] [[PubMed](#)]
21. Kamp, A.; Stief, P.; Knappe, J.; de Beer, D. Response of the ubiquitous pelagic diatom *Thalassiosira weissflogii* to darkness and anoxia. *PLoS ONE* **2013**, *8*, e82605. [[CrossRef](#)]
22. Bussard, A.; Corre, E.; Hubas, C.; Duvernois-Berthet, E.; Le Corquille, G.; Jourden, L.; Couplier, F.; Claquin, P.; Lopez, P.J. Physiological adjustments and transcriptome reprogramming are involved in the acclimation to salinity gradients in diatoms. *Environ. Microbiol.* **2017**, *19*, 909–925. [[CrossRef](#)]
23. Spielmeyer, A.; Gebser, B.; Pohnert, G. Investigations of the uptake of dimethylsulfoniopropionate by phytoplankton. *Chem-BioChem Comb. Chem. Biol.* **2011**, *12*, 2276–2279. [[CrossRef](#)] [[PubMed](#)]
24. Li, W.; Yang, Y.; Li, Z.; Xu, J.; Gao, K. Effects of seawater acidification on the growth rates of the diatom *Thalassiosira (Conticribra) weissflogii* under different nutrient, light, and UV radiation regimes. *J. Appl. Phycol.* **2016**, *29*, 133–142. [[CrossRef](#)]
25. Walter, B.; Peters, J.; van Beusekom, J.E.E.; St. John, M.A. Interactive effects of temperature and light during deep convection: A case study on growth and condition of the diatom *Thalassiosira weissflogii*. *ICES J. Mar. Sci.* **2015**, *72*, 2061–2071. [[CrossRef](#)]
26. Garcia, N.; Lopez-Elias, J.A.; Miranda, A.; Martinez-Porchas, M.; Huerta, N.; Garcia, A. Effect of salinity on growth and chemical composition of the diatom *Thalassiosira weissflogii* at three culture phases. *Lat. Am. J. Aquat. Res.* **2012**, *40*, 435–440. [[CrossRef](#)]
27. Takagi, M.; Yoshida, T. Effect of salt concentration on intracellular accumulation of lipids and triacylglyceride in marine microalgae *Dunaliella* cells. *J. Biosci. Bioeng.* **2006**, *101*, 223–226. [[CrossRef](#)]
28. Duhrkop, K.; Fleischauer, M.; Ludwig, M.; Aksenov, A.A.; Melnik, A.V.; Meusel, M.; Dorrestein, P.C.; Rousu, J.; Bocker, S. SIRIUS 4: A rapid tool for turning tandem mass spectra into metabolite structure information. *Nat. Methods* **2019**, *16*, 299–302. [[CrossRef](#)]
29. Duhrkop, K.; Shen, H.; Meusel, M.; Rousu, J.; Böcker, S. Searching molecular structure databases with tandem mass spectra using CSI: Finger ID. *Proc. Natl. Acad. Sci. USA* **2015**, *112*, 12580–12585. [[CrossRef](#)]
30. Wickberg, B. Isolation of 2-L-amino-3-hydroxy-1-propane sulfonic acid from *Polysiphonia fastigiata*. *Acta Chem. Scand.* **1957**, *11*, 506–511. [[CrossRef](#)]
31. Ito, K. Distribution of D-cysteinolic acid in marine algae. *Bull. Japan. Soc. Sci. Fish* **1963**, *29*, 771–775. [[CrossRef](#)]
32. Busby, W.F. Sulfopropanedial and cysteinolic acid in the diatom. *Biochim. Biophys. Acta* **1966**, *121*, 160–161. [[CrossRef](#)]
33. Busby, W.F.; Benson, A.A. Sulfonic acid metabolism in the diatom *Navicula pelliculosa*. *Plant Cell Physiol.* **1973**, *14*, 1123–1132. [[CrossRef](#)]
34. Gotz, F.; Longnecker, K.; Kido Soule, M.C.; Becker, K.W.; McNichol, J.; Kujawinski, E.B.; Sievert, S.M. Targeted metabolomics reveals proline as a major osmolyte in the chemolithoautotroph *Sulfurimonas denitrificans*. *MicrobiologyOpen* **2018**, *7*, e00580. [[CrossRef](#)] [[PubMed](#)]
35. Durham, B.P.; Sharma, S.; Luo, H.; Smith, C.B.; Amin, S.A.; Bender, S.J.; Dearth, S.P.; Van Mooy, B.A.; Campagna, S.R.; Kujawinski, E.B.; et al. Cryptic carbon and sulfur cycling between surface ocean plankton. *Proc. Natl. Acad. Sci. USA* **2015**, *112*, 453–457. [[CrossRef](#)] [[PubMed](#)]
36. Williams, B.T.; Todd, J.D. A day in the life of marine sulfonates. *Nat. Microbiol.* **2019**, *4*, 1610–1611. [[CrossRef](#)]
37. Azam, F.; Malfatti, F. Microbial structuring of marine ecosystems. *Nat. Rev. Microbiol.* **2007**, *5*, 782–791. [[CrossRef](#)]
38. McParland, E.L.; Levine, N.M. The role of differential DMSP production and community composition in predicting variability of global surface DMSP concentrations. *Limnol. Oceanogr.* **2018**, *64*, 757–773. [[CrossRef](#)]
39. Hillebrand, H.; Dürselen, C.D.; Kirschtel, D.; Utsa Pollinger, U.; Zohary, T. Biovolume calculation for pelagic and benthic microalgae. *J. Phycol.* **1999**, *35*, 403–424. [[CrossRef](#)]



- 
40. Maier, I.; Calenberg, M. Effect of extracellular  $\text{Ca}^{2+}$  and  $\text{Ca}^{2+}$ -antagonists on the movement and chemoorientation of male gametes of *Ectocarpus siliculosus* (Phaeophyceae). *Bot. Acta* **1994**, *107*, 451–458. [[CrossRef](#)]
  41. Xu, J. A new and expeditious asymmetric synthesis of (*R*)- and (*S*)-2-aminoalkanesulfonic acids from chiral amino alcohols. *Tetrahedron Asymmetry* **2002**, *13*, 1129–1134. [[CrossRef](#)]

## 2.5 Publication 5

“Metabolite profiling reveals insights into the species-dependent cold stress response of the green seaweed holobiont *Ulva* (Chlorophyta).”

Fatemeh Ghaderiardakani, Linda Langhans, Valentin B. Kurbel,  
Simona Fenizia, Thomas Wichard

*Environmental and Experimental Botany*, Vol. 200(104913), 2022  
DOI: 10.1016/j.envexpbot.2022.104913

Open Access This article is licensed under a Creative Commons Attribution 4.0 International License

Ghaderiardakani F.<sup>1</sup>, Langhans L.<sup>2</sup>, Kurbel V.B.<sup>3</sup>, Fenizia S.<sup>4</sup>, Wichard T.<sup>5</sup> Metabolite profiling reveals insights into the species-dependent cold stress response of the green seaweed holobiont *Ulva* (Chlorophyta). *Environmental and Experimental Botany*, 2022 200, 104913. 10.1016/j.envexpbot.2022.104913

Author	1	2	3	4	5
Development of concept					x
Planning of research	x				x
Data collection	x	x	x	x	
Data analysis	x	x	x	x	x
Preparation of the manuscript	x				x
Correction of the manuscript	x				x
Proposed publication equivalent				0.5	

### Authors contribution:

Fatemeh Ghaderiardakani Research planning, experiment preparation and implementation, data analysis, writing-original draft, editing

Linda Langhans Experiment preparation, data analysis

Valentin B. Kurbel Experiment preparation, data analysis

Simona Fenizia Experiment implementation, data analysis

Thomas Wichard Conceptualization, research planning, data analysis, writing-review, editing, supervision





## Metabolite profiling reveals insights into the species-dependent cold stress response of the green seaweed holobiont *Ulva* (Chlorophyta)

Fatemeh Ghaderiardakani<sup>a</sup>, Linda Langhans<sup>a</sup>, Valentin B. Kurbel<sup>a</sup>, Simona Fenizia<sup>a,b</sup>, Thomas Wichard<sup>a,\*</sup>

<sup>a</sup> Institute for Inorganic and Analytical Chemistry, Friedrich Schiller University Jena, Lessingstraße 8, 07743 Jena, Germany

<sup>b</sup> Max Planck Institute for Chemical Ecology, Hans-Knoll-Strasse 8, 07745 Jena, Germany

### ARTICLE INFO

#### Keywords:

Antarctica  
Cold adaptation  
Cold stress adaptation factors  
Cross-kingdom interactions  
Cryoprotective  
DMSP  
Ectoine  
Seaweed  
Taurine  
*Ulva* microbiome

### ABSTRACT

The green seaweed *Ulva* (Chlorophyta) and its associated epibacterial microbiome form a functional holobiont that adapts to stress as a whole. As the macroalga provides carbon sources for bacteria and relies on algal growth and morphogenesis-promoting factors (AGMPF) released by bacteria, those cross-kingdom interactions are especially fascinating. We hypothesized that the *Ulva* holobionts from the warm-temperate Mediterranean-Atlantic and cold Antarctic habitats respond to cold stress differently depending on the production of highly polar low molecular weight compounds (LMWCs) with stress-regulating activity. We compared the microbiome of and metabolic changes in *U. compressa* (cultivar *U. mutabilis*), initially collected in Ria Formosa (Portugal), with that of *U. bulbosa* (strain AWI #1002) collected in Antarctica by performing a warm-cold temperature shift experiment. Microbiome analysis indicated significant differences between the two species and that the number of operational taxonomic units (OTUs) was lower in cultivated *U. bulbosa* than in freshly isolated *Ulva*; despite this, AGMPF-producing bacteria were detected in both holobionts. Significant differences in metabolite profiles were observed between both species using hydrophilic interaction liquid chromatography coupled with electrospray ionization mass spectrometry (HILIC-ESI-MS). Biomarkers such as dimethylsulfoniopropionate (DMSP) and taurine were identified following a temperature shift from 18 °C to 5 °C in the warm-temperate *U. mutabilis* and the cold-adapted *U. bulbosa*, respectively. Our findings show that metabolic changes in the holobiont in response to cold are species-dependent.

To evaluate the contribution of the metabolic changes of bacteria and algae to the stress response, the reductionistic model system of the tripartite community formed by *U. mutabilis* and its two essential bacteria, *Roseovarius* sp. strain MS2 and *Maribacter* sp. strain MS6, which release all essential AGMPFs, was investigated. We examined the production of polar LMWCs in the presence and absence of bacteria following a shift to cold temperatures. Among the metabolites studied, ectoine ((4S)-2-methyl-3,4,5,6-tetrahydropyrimidine-4-carboxylic acid) was only detected in the presence of bacteria, highlighting the role of bacteria in releasing compounds that mitigate environmental stresses through cold stress adaptation factors (CSAF). Our findings suggest that microbiome engineering will allow us to improve macroalgae adaptability to stressful situations, which can be further applied to the sustainable management of (land-based) aquaculture systems.

### 1. Introduction

The settlement of the earliest plants in terrestrial habitats was accompanied by exposure to a completely different habitat. To deal with changing climatic circumstances and abiotic stresses such as ultraviolet radiation, temperature change, and dehydration, extensive adaptation at the morphological, physiological, and molecular levels was required

(Becker and Marin, 2009; Rensing, 2018). The evolution of heteromorphic life and the establishment of symbiotic interactions (Delaux et al., 2013; Field et al., 2015; Ghaderiardakani et al., 2020) were essential innovations in the plant terrestrialization process (Becker and Marin, 2009). Heat stress has recently attracted the attention of plant biologists not only because it may hold answers to fundamental questions about plant evolution and the transition from algae to embryophytes, but also

\* Corresponding author.

E-mail address: [thomas.wichard@uni-jena.de](mailto:thomas.wichard@uni-jena.de) (T. Wichard).

<https://doi.org/10.1016/j.envexpbot.2022.104913>

Received 27 January 2022; Received in revised form 23 April 2022; Accepted 10 May 2022

Available online 13 May 2022

0098-8472/© 2022 The Author(s). Published by Elsevier B.V. This is an open access article under the CC BY license (<http://creativecommons.org/licenses/by/4.0/>).

because it has implications for crop yields and the associated threats to food security under global warming and the projected impacts of climate change (Fürst-Jansen et al., 2020; Ohama et al., 2017). In contrast, a significant proportion of the Earth's biosphere is permanently exposed to temperatures  $\leq 5\text{ }^{\circ}\text{C}$  (Rodrigues and Tiedje, 2008), such as polar environments (Rodrigues and Tiedje, 2008). Understanding how plants remain metabolically active at low temperatures could provide insights into stress adaptation.

Cold and temperate marine environments are inhabited by organisms of the same genus, suggesting specific adaptation processes. Several barriers inherent to permanently cold environments that could impart severe physiochemical restrictions on essential aspects of cell function include intracellular ice formation, changes in membrane fluidity, macromolecular interactions, and enzyme kinetics (Piette et al., 2011; Rodrigues and Tiedje, 2008). Cold-adapted, or cold-acclimated organisms, have thus employed different approaches to survive at lower temperatures (Rodrigues and Tiedje, 2008). For instance, in bacteria, loss of membrane fluidity is counteracted by variations in the lipid composition of their membranes. Bacteria avoid loss of membrane fluidity at cold temperatures by synthesizing unsaturated and branched fatty acids (Russell, 1983). Several studies have reported the importance of cold shock proteins, exopolysaccharides, and membrane modifications for cold adaptation in bacteria (Tribelli and López, 2018). Guy et al. (2008) categorized properties that could contribute to stress tolerance into five groups of metabolites that function "(1) as osmolytes to modify cellular water relations and reduce cellular dehydration; (2) as compatible solutes to stabilize enzymes, membranes, and other cellular components; (3) as chelating agents to neutralize or sequester potentially toxic levels of metals and inorganic ions; (4) in the retailoring of membrane lipid composition to optimize the liquid/crystalline physical structure [...], and (5) as energy sources" (Guy et al., 2008).

When grown in bacteria-free (axenic) conditions or in the absence of the necessary microbiome, green seaweeds such as Ulvales lose their usual shape (Wichard, 2015). As a result, plantlets proliferate in an undifferentiated and callus-like morphotype. These malformations are partly or entirely rescued by complementing the culture medium with two marine bacteria, *Maribacter* sp. strain MS6 and *Roseovarius* sp. strain MS2, forming a tripartite community (Spoerner et al., 2012) (Fig. 1A). Consequently, algal growth and morphogenesis promoting factors (AGMPF) released by those bacteria (such as thallusin released by *Maribacter* sp.) can ensure algal development (Alsufyani et al., 2020; Ghaderiardakani et al., 2019; Grueneberg et al., 2016). These observations imply that the alga and its associated bacteria, i.e. the entire holobiont, need to react to a specific stressful situation in an orchestrated action (Dittami et al., 2016; Ghaderiardakani et al., 2020).

In this study, we compared the stress responses of the Mediterranean *U. mutabilis* and the Antarctic *U. bulbosa* (both cultured) using a warm-cold temperature shift experiment to identify potential LMWCs ( $< 200\text{ Da}$ ) functioning as cold stress adaptation factors (CSAF). These potential cryoprotectants are often compatible solutes that accumulate to high intracellular concentrations either through *de novo* biosynthesis or uptake from the environment to mitigate thermal and osmotic stress. These solutes include amino acids and derivatives, polyols and sugars, methylamines, and methylsulfonium compounds with multiple functions, including stabilizing macromolecules (Yancey, 2005). For example, algae collected in polar regions often have higher compatible solutes levels than eulittoral species collected from tropical and temperate regions (Bischoff et al., 1994; Karsten et al., 1990a). The axenic Antarctic sea-ice diatom, *Nitzschia lecoointei* produces different amounts of 2,3-dihydroxypropane-1-sulfonate (DHPS), glycine betaine (GBT), and dimethylsulfoniopropionate (DMSP) at  $-1\text{ }^{\circ}\text{C}$  and  $4\text{ }^{\circ}\text{C}$  and at salinities of 32‰ and 41‰, and the effect of temperature is stronger than that of salinity (Dawson et al., 2020). DMSP is of interest because it performs a variety of ecological and physiological functions. DMSP can be detected by marine bacteria and is used as a chemoattractant (Kessler et al., 2018; Seymour et al., 2010). Further, it is important in the

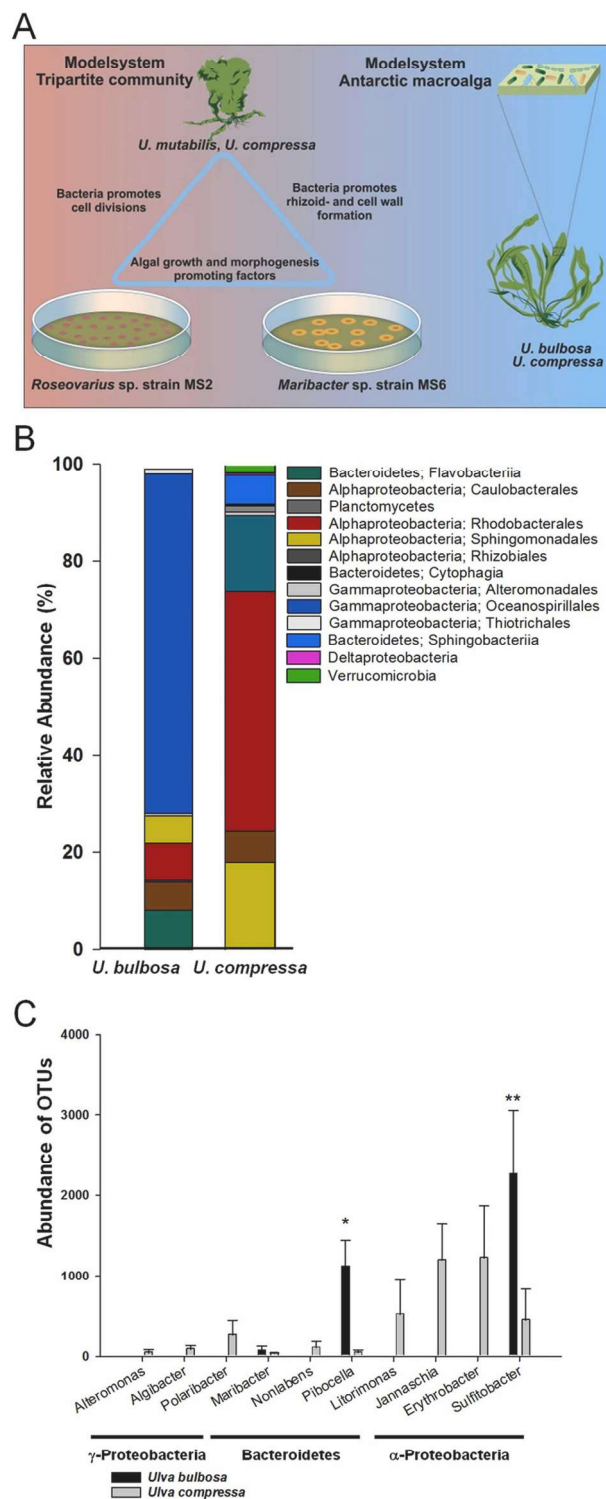


**Fig. 1.** (A) The reductionist holobiont model system *Ulva mutabilis*–*Roseovarius* sp.–*Maribacter* sp. (left side) and the Antarctic species *Ulva bulbosa* with its associated microbiome (right side) were used to identify changes in the metabolite profile under thermal stress. (B) The microbiological communities associated with *Ulva* on a taxonomic level are shown based on the abundant operational taxonomic units (OTUs) in 16S rRNA gene amplicon libraries from *U. compressa* and *U. bulbosa* samples. (C) The enrichment of selected bacterial genera in *U. compressa* and *U. bulbosa* was estimated based on the abundance of OTUs. Mean  $\pm$  standard deviation is shown ( $n = 3$ ). Significant differences between *Ulva* species are indicated by the asterisk (\*  $P \leq 0.05$ , \*\*  $P \leq 0.01$ ,  $n = 3$ ).

pathogenesis of algae (Garren et al., 2014) and bacterial-algal symbiosis (Kessler et al., 2018), and it functions as an antifreeze osmolyte in several algae exposed to salinity variations (Edwards et al., 1987). Since DMSP released by *U. mutabilis* attracts *Roseovarius* sp., which provides AGMPF for the growth of *Ulva*, DMSP production is a key factor in cross-kingdom interactions under stress conditions. Overall, both AGMPF and compatible solutes are indispensable for facilitating communication between macroalgae and bacteria within the chemosphere where the organisms interact (definition by Alsufyani et al., 2017).

To investigate the cold adaptability of the green seaweeds, two experimental designs were used with two different long-time cultured *Ulva* species—one collected from Antarctica (*U. bulbosa*) and the other from the Mediterranean Sea (*U. mutabilis* recently reclassified in *U. compressa*)—to elucidate their metabolic responses to cold stress.

First, we tested the hypothesis that a cold-adapted (i.e., high cold acclimation capacity) holobiont and a warm-adapted (i.e., low cold acclimation capacity) holobiont produce different LMWCs when exposed to low temperatures.

Second, the well-established reductionist, tripartite model system of *U. mutabilis* and its two associated essential bacteria (Wichard, 2022), *Roseovarius* sp. and *Maribacter* sp., was investigated to determine the LMWCs when the tripartite community was exposed to low temperatures and to distinguish the production of compatible solutes between *Ulva* and its bacteria (Fig. 1A).

For metabolomic analysis, hydrophilic interaction liquid chromatography coupled to electrospray ionization mass spectrometry (HILIC-ESI-MS) was applied. In addition, the microbiome of *U. bulbosa* was analyzed for AGMPF producing bacteria and compared with the non-cultured strain of *U. compressa*.

## 2. Methods

### 2.1. Algae and bacteria

The developmental mutant "slender" (mating type mt+) strain of *U. mutabilis* was propagated from unmated gametes derived from lab-grown parthenogenetic gametophytes. It has been demonstrated that *U. mutabilis*, collected initially by B. Føyn in the Ria Formosa (Portugal) in 1952 (Føyn, 1958), and *U. compressa* are conspecific (Steinhagen et al., 2019). The cultivar is referred to as *U. mutabilis* throughout this publication.

The cold-adapted strain *U. bulbosa* (strain AWI #1002) was collected in Antarctica in 1986 and cultivated at 5 °C at the Alfred Wegener Institute (AWI, Bremerhaven, Germany). In the case of *U. mutabilis*, the identity of the strain was confirmed using PCR with *tufA* (forward: GGNGCNGCNCAATGGAYGG, reverse: CCTTCNCGAATMG-CRAAWCGC; (Famà et al., 2002) and *petA* primers (forward: TGAA-CACGAGCTGGGTTTTG, reverse: TCCACGTGAACCAAATGGAC (Cai et al., 2021)). Further phylogenetic analysis is necessary to taxonomize *U. bulbosa* (strain AWI #1002).

*U. bulbosa* and *U. mutabilis* gametophytes were cultured in sterile Nunc™ cell culture plastic flasks with gas-permeable screw caps (Thermo Fisher Scientific, Dreieich, Germany) containing 100 mL *Ulva* Culture Medium (UCM) under standard growth conditions, including a 17/7 h light/dark cycle with the illumination of approximately 80 μmol photons m<sup>-2</sup> s<sup>-1</sup> provided using 50% GroLux and 50% day-light fluorescent tubes (Stratmann et al., 1996). Both species can grow efficiently at 18 °C. Depending on the experiment, the species were shifted to 5 °C or 2 °C for further cultivation.

Axenic cultures of *U. mutabilis* were prepared according to the approach described by Califano et al. (2018) and subsequently inoculated with the morphogenesis-inducing bacterial strains *Roseovarius* sp. (GenBank EU359909) and *Maribacter* sp. (GenBank EU359911) (Alsufyani et al., 2017; Califano and Wichard, 2018; Spoerner et al., 2012). After inoculation, the final calculated optical density of bacteria was

OD<sub>600</sub> = 1.0 × 10<sup>-4</sup>. The bacteria were cultured in marine broth at 18 ± 1.0 °C (Roth, Karlsruhe, Germany).

### 2.2. Microbiome analysis of *Ulva bulbosa* and *Ulva compressa*

The DNeasy PowerSoil Pro Kit (Qiagen, Germany) was used to extract the microbial metagenomic DNA, following the manufacturer's protocol without damaging the thallus of *Ulva*. Next, 16S V4 amplicon sequencing of the microbial community was performed on the Illumina MiSeq (2 × 300 bp) using the 515 F-Y "new EMP" (GTGY-CAGCMGCCGCGGTAA) and 806RB "new EMP" (GGAC-TACNVGGGTWCTAAT) primer pair (LGC Genomics GmbH, Germany). After inline barcode demultiplexing and clipping of sequencing adapters from the 3' ends of reads, the data was processed using the Mothur software package (read pair joining, quality filtering, alignment against Silva 16S reference, denoising, chimera removal) (Schloss et al., 2009). Operational taxonomic units (OTUs) were picked using Mothur (clustering of aligned sequences at the 97% identity level and taxonomy classification against the Silva reference database), and a BLAST search of OTUs against the Silva database of the 16S domain was performed (Califano et al., 2020). Different to the cultivated *U. bulbosa*, *U. compressa* (strain RFU #81) was collected in the Ria Formosa (Faro, Portugal) for microbiome analysis, and a portion of the thallus, including the rhizoid, was frozen without further cultivation (Alsufyani et al., 2014; Grueneberg et al., 2016). Microbiome analyses were performed in triplicate. The entire dataset can be retrieved from NCBI (National Center for Biotechnology Information) through the BioProject ID PRJNA828511 (BioSample Accession Numbers, *U. compressa*: SAMN27670879-SAMN27670881; *U. bulbosa*: AWI #1002: SAMN27670882-SAMN27670884).

### 2.3. Temperature treatment

Two experimental designs were carried out with a (i) complete and a (ii) designed microbiome:

- (i) To compare *U. bulbosa* and *U. mutabilis*, strains were grown with their microbiomes, which had evolved over decades (> 30 years for *U. bulbosa* and > 70 years for *U. mutabilis*), and cultivated for 14 days at 5 °C ± 1.0 °C and 18 °C ± 1.0 °C. *U. bulbosa* was cultivated at 18 °C for three life cycles prior to starting the temperature shift.
- (ii) Axenic gametes of *U. mutabilis* were cultivated together with *Roseovarius* sp. and *Maribacter* sp. in UCM at 18 ± 1.0 °C. Individuals of ~1 cm in length (n = 40) were transferred to bottles with UCM and maintained at 2 ± 0.5 °C and 18 ± 1.0 °C. Algae were harvested during their growing phase (Wichard and Oertel, 2010). All experiments were performed in triplicate.

### 2.4. Extraction protocols

The algal tissues were quickly dried with a paper towel, collected in plastic tubes (Sarstedt, Germany), and frozen with liquid nitrogen. The tissues were lyophilized (Lyophilizer: Christ Martin Alpha 1–2 LO Plus) for approximately 20 h at – 50 °C and 0.001 mbar. The freeze-dried biomass (weighing 13–21 mg) was transferred to 1.5 mL plastic tubes (Eppendorf, Germany). Two metal beads were added to each tube, and the cells were disrupted for 1 min using a TissueLyser II (Qiagen). Cold methanol (1 mL) was added to extract the metabolites after the addition of internal standards [4 μL of 100 μM D<sub>6</sub>DMSP (dimethylsulfoniopropionate) and 4 μL of 4 μM D<sub>3</sub>-ectoine ((4S)–2-methyl-3,4,5,6-tetrahydropyrimidine-4-carboxylic acid)] (Fenizia et al., 2020; Gebser and Pohner, 2013). The mixture was treated in an ultrasonic bath for 1 min and subsequently centrifuged at 1500×g for 5 min. The extraction was repeated once to verify that the first extraction was exhaustive.

## 2.5. Mass spectrometry analysis

### 2.5.1. Liquid chromatography coupled to mass spectrometry

High performance liquid chromatography (HPLC) was performed using a SeQuant ZIC®-HILIC analytical peak column (5  $\mu\text{m}$ , 150  $\times$  2.1 mm, SeQuant, Umeå, Sweden) equipped with a SeQuant ZIC®-HILIC guard column (5  $\mu\text{m}$ , 2.1  $\times$  20 mm). Analytical separation and quantification of LMWCs ( $\leq 200$  Da) were conducted on a Dionex Ultimate 3000 HPLC system linked to Q Exactive Orbitrap Mass Spectrometer (Thermo Fisher Scientific). Mass measurements were performed using the electron ionization-positive mode. Mass/charge ratios ranging from 70 to 200  $m/z$  were recorded with a mass resolution of  $R = 70,000$  at  $m/z$  200.

For high-resolution mass spectrometry (HRMS) coupled to a HILIC column, 50  $\mu\text{L}$  of the methanol extract was diluted with 150  $\mu\text{L}$  acetonitrile/water (9:1, v/v). The injection volume was 2  $\mu\text{L}$ . For separation, the eluent contained high-purity water spiked with 2% acetonitrile and 0.1% formic acid (solvent A) and 90% acetonitrile with 10% water and 5 mM ammonium acetate (solvent B) (Fenizia et al., 2020; Spielmeier et al., 2011). The flow rate was set to 0.6  $\text{mL min}^{-1}$ , and a linear gradient was used for separation with 100% solvent B (2 min), 60% B (11 min), 20% B (11.8 min), 20% B (14.9 min), 100% B (15 min), and 100% B (18 min). The column was maintained at 25  $^{\circ}\text{C}$ . Before running the samples, the HPLC was conditioned by repeatedly running blanks.

### 2.5.2. Data processing and metabolite profiling

Peak picking, deconvolution, and metabolite identification was achieved using Compound Discoverer 3.2 (Thermo Fisher Scientific). Peak detection was conducted using a tolerance of 30% for intensity, a signal-to-noise threshold of 5, and a mass tolerance of 5 ppm. The lowest possible peak intensity was set at 100,000. For all tools used for spectrum similarity searches, the mass tolerance was set to 5 ppm. Features that were also identified in blank samples were removed. Pooled quality control samples (QC) were used to compensate for time-dependent batch effects during analysis (Dunn et al., 2011). Raw data were compared with open data repositories (ChemSpider, KEGG) within Compound Discoverer (CD) using the program's default settings and an untargeted metabolomics workflow.

To discover further significant changes between features ( $m/z$ ) observed during the warm-cold temperature shift experiment, a canonical analysis of principal coordinates (CAP) was used to conduct multivariate data analysis to visualize differences in the feature assemblages (i.e., compounds) (Alsufyani et al., 2017; Anderson and Willis, 2003; Anderson and Robinson, 2003). The main coordinates (PCo) were computed from the Bray–Curtis similarity matrix, and potential overparameterization was avoided by selecting the number of PCo axes ( $m$ ) that maximized the groups' leave-one-out allocation success. The square root was used to transform the data, and column (variable) sums were applied to normalize it.

To identify important metabolites from the mass spectrometric data, a false-positive rate (FDR) correction was performed, coupled with a two-tailed t-test ( $P < 0.05$ ). Following this analysis, univariate statistical tests were completed using MetaboAnalyst 5.0 (Chong et al., 2019) to explore significant differences in intensities of metabolites in the raw data. Treatments were compared by analysis of variance (one-way ANOVA) at  $\alpha = 0.05$  after verifying homoscedasticity and normal distribution of the data. A post-hoc Fisher's LSD test ( $P < 0.05$ ) revealed the treatments between which the metabolites exhibited significant differences. Furthermore, volcano plots were utilized to display the univariate analysis results for each LMWC with adjusted  $P < 0.05$  and a fold-change larger than two. Statistical analyses in MetaboAnalyst were repeated by Tukey's multiple comparisons test calculating adjusted  $P$  values using Prism v.7.00 (GraphPad Software, USA) to ensure accuracy.

### 2.5.3. Identification and quantification of selected compounds

Candidate compounds were detected by comparison with

commercially accessible reference standards and co-injections. Ectoine and DMSP were quantified by adding synthesized labelled standards (Fenizia et al., 2020). An external calibration curve with five calibration standards was performed in triplicate (Deicke et al., 2013) to measure the concentration of the metabolites normalized to the dry weight (DW) of the extracted thallus. A linear regression model was calculated, plotted, and validated with SigmaPlot ver. 14 (Systat, Germany) and GraphPad Prism v.7.00. According to the calibration method, the limit of detection and quantification was determined for all candidate compounds (Reichenbacher and Einax, 2011) with a relative standard deviation (RSD)  $< 8.2\%$  (Table 2). Repeated extraction with methanol did not increase the amount of any analyte.

## 3. Results and discussion

### 3.1. Algal growth and morphogenesis promoting bacteria found independently of *Ulva* origin

Unlike *U. mutabilis*, the essential bacteria required for the growth and morphogenesis of *U. bulbosa* have yet to be identified (Wichard, 2015). Therefore, the microbiome analysis aimed to determine whether potential AGMPF releasing bacteria can be found independently of *Ulva*'s origin. The complete microbiome of *U. bulbosa* (strain AWI #1002) was first analyzed for the AGMPF producing bacteria and compared with the microbiome of *U. compressa* (strain RFU #81) (Alsufyani et al., 2014), collected in the Mediterranean Sea (Ria Formosa, Portugal), where *U. mutabilis* was originally found (Føyn, 1958). The microbiomes differed significantly from one another (Fig. 1B). While the Mediterranean species was primarily associated with  $\alpha$ -Proteobacteria and Bacteroidetes, as previously reported (Califano et al., 2020; Friedrich, 2012), the microbiome of *U. bulbosa* was dominated by  $\gamma$ -Proteobacteria and Bacteroidetes. The number of OTUs (41) of the cultivated *U. bulbosa* was strongly reduced compared to the number of OTUs (251) obtained from the non-cultivated *U. compressa*, which is typical for the selection process in algal-bacteria interactions and has been described previously (Califano et al., 2020; van der Loos et al., 2021). Importantly, the genera *Maribacter* and *Sulfitobacter*, which are essential AGMPF producers, were associated with both species (Fig. 1C).

### 3.2. Determination of cryoprotectant compatible solutes

The systematic examination of zwitterionic substances and highly polar metabolites was accomplished using a ZIC-HILIC separation process combined with highly sensitivity MS analysis. Comparison with reference standards led to the detection of ten cryoprotectant candidates previously identified in studies involving both *Ulva* species (Fig. 2). Amino acids, sulfonates, zwitterions, and singly-charged ions were detected. Ectoine, DMSP, cysteinolic acid, and proline were the major compatible solutes. These are commonly employed by microbes and phytoplankton as stress protectants (Fenizia et al., 2020). Ectoine synthesis and uptake provides a considerable degree of osmotic stress tolerance which can provide protection against extreme temperatures. Compatible solutes improve cryopreservation in different organisms, e. g., a combination of proline and ectoine protects human endothelial cells against cryopreservation damage (Fenizia et al., 2020; Sun et al., 2012).

### 3.3. Different stress responses of *Ulva* holobionts from the Mediterranean Sea and Antarctica

To explore the cellular metabolic responses of a temperate and a cold-adapted species, cultures of *U. mutabilis* (Ria Formosa, Portugal) and *U. bulbosa* (Polar region, Antarctica) were subjected to a temperature shift from 18  $^{\circ}\text{C}$  to 5  $^{\circ}\text{C}$  simultaneously in the first experiment. After 14 days of incubation, *Ulva* biomass was harvested, extracted, and analyzed by HILIC-HR-ESI-MS. CD revealed 30 LMWCs with mass/

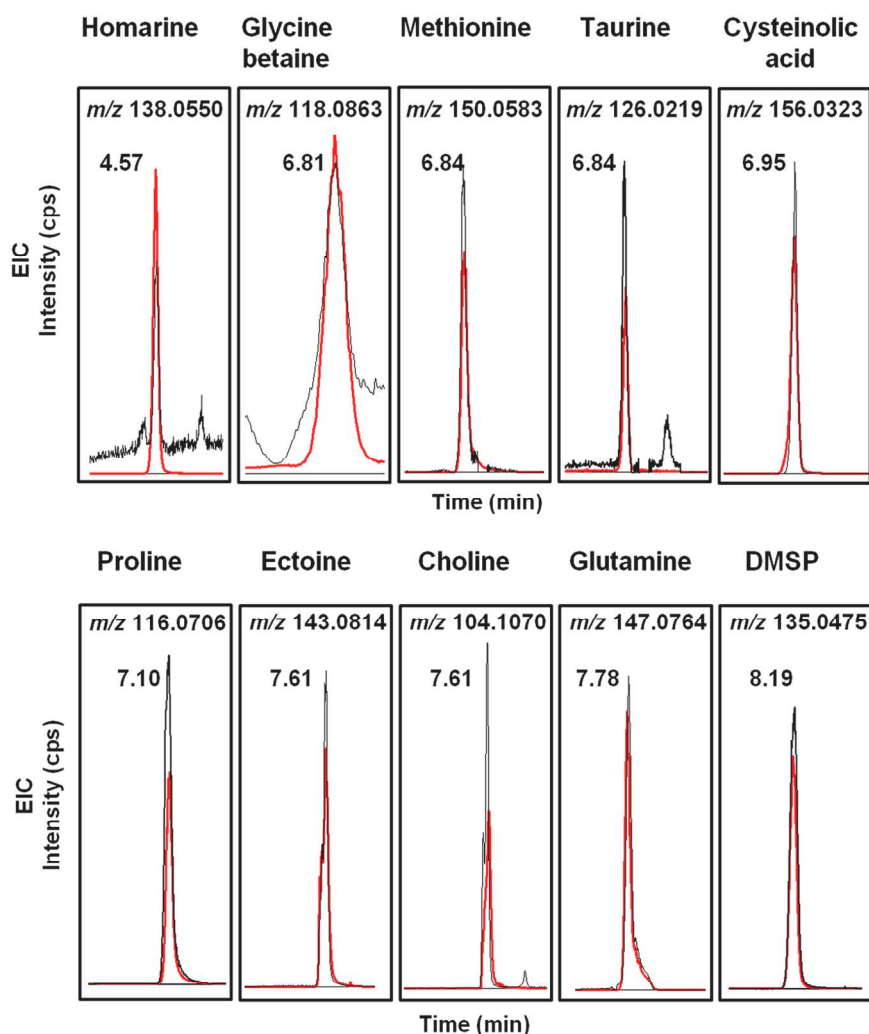


**Fig. 2.** Low molecular weight compounds identified by comparing the HILIC-ESI-MS chromatograms to the analytical reference standards (red lines). The extracted ion trace chromatograms (EIC, black line) of the  $m/z$  values  $[M + H]^+$  for all metabolites (except choline  $[M]^+$ ) detected in the methanol extract of the *Ulva mutabilis* tissue are shown. The EICs matched the reference standards (red line).  $m/z$ : Mass/charge ratios.

change ratios ranging from 70 to 200  $m/z$  after applying background corrections (Table 1). Although CD identified many new features, only a few compounds, such as DMSP, taurine, and glycerol, were clearly characterized and confirmed by reference standards (Fig. 2, Table 1).

Principal analysis of coordinates (PCo) for the 30 identified features demonstrated two distinct groups under cold treatment. The plots indicate that *U. mutabilis* and *U. bulbosa* were separated in both PCo1 and PCo2 after cold treatment, suggesting differences in the metabolic profile of *Ulva* samples influenced by both temperature and species. In contrast, *U. mutabilis* and *U. bulbosa* were not distinctly separated on the PCo plot at 18 °C (Fig. 3A), which emphasizes their similar metabolic profiles in temperate conditions. For supervised discriminant analysis, three groups were defined: (i) *U. bulbosa* at 5 °C, (ii) *U. mutabilis* at 5 °C, and (iii) one combined group of algae grown at 18 °C. CAP analysis of the a priori groups revealed that metabolite profiles significantly differed between the two species depending on the temperature (Eigenvalues: 0.9309 for axis 1 and 0.9225 for axis 2) (Fig. 3B). Using the "leave-one-out" allocation approach, cross-validation between the a priori groups resulted in one misclassification. CAP calculated the correlation coefficient  $r$  (cutoff:  $|r| > 0.5$ ) between each sample and the canonical axes to identify essential biomarkers.

Following multivariate analysis, a one-way ANOVA was used to prove whether the metabolites differed substantially across treatments. Eighteen metabolites out of 30 were identified as being significantly

different, with an FDR-adjusted  $P$ -value  $< 0.05$  (Table 1). Among the most significantly upregulated metabolites, some are well-known as compatible solutes, such as taurine (a sulfur-containing  $\beta$ -amino acid) and DMSP (Fig. 3C).

Although taurine concentrations (UM and UB in 18 °C) differ significantly between the two species (one-way ANOVA with Tukey posthoc test,  $P < 0.05$ ), box plots reveal a species-specific increase in DMSP and taurine concentrations in *U. mutabilis* and *U. bulbosa*, respectively. Apart from DMSP and taurine, the upregulated features #20 and #15 under cold conditions in *U. mutabilis* and *U. bulbosa* were conspicuous (Fig. 3B, C). The basic concentration of #15 differs significantly ( $P < 0.05$ ) between the two *Ulva* at 18 °C as well. Fisher's least significance difference test for post hoc comparisons revealed differences in metabolite abundance between the *Ulva* species at different temperatures. Future investigations will identify other substances that are only listed as sum formulas in Table 1.

In summary, the metabolic profiles of *U. mutabilis* and *U. bulbosa* in cold conditions are dissimilar, suggesting that these two holobionts respond to cold stress differently due to differences in algal metabolism (intrinsic) and microbiomes (extrinsic). It is still under discussion how the associated and stress-adapted microbiomes can help the host adapt to environmental stresses through the production and subsequent secretion of chemical metabolites (Ghaderiardakani et al., 2020).



**Table 1**

Identification of 30 features in *U. mutabilis* (UM) and *U. bulbosa* (UB) following a One-way ANOVA. Metabolites were considered significant if the FDR adjusted *P* value was < 0.05. Fisher's LSD post hoc test indicates significant differences (*P* < 0.05) between the comparisons (ns = not significantly different; n.d. not determined) (Note: retention times vary slightly from batch to batch within this study.).

No. #	<i>m/z</i> [M+H] <sup>+</sup> measured	RT [min]	Compound (identified)	Formula [M]	Significance <i>P</i> -value	FDR adjusted <i>P</i> -value	UB-5 °C vs UB-18 °C	UB-18 °C vs UM-18 °C	UM-5 °C vs UM-18 °C	UM-5 °C vs UB-5 °C
Identification						One way ANOVA				
						Fisher's LSD post hoc comparison				
1	135.0472	8.40	DMSP	C5H10O2S	1.98E-02	3.30E-02	ns	ns	< 0.05	ns
2	156.0323	7.09	Cysteinolic acid	C3H9NO4S	5.89E-04	8.11E-03	< 0.05	ns	< 0.05	< 0.05
3	157.0293	8.58		n.d.						
4	145.0495	7.12		C6H8O4	2.93E-03	8.71E-03	< 0.05	ns	< 0.05	ns
5	145.0494	7.14		C6H10O5	3.55E-03	8.71E-03	< 0.05	ns	< 0.05	ns
6	85.0283	7.14		C4H4O2	1.89E-03	8.11E-03	< 0.05	ns	< 0.05	ns
7	127.0388	7.13		C6H6O3	3.59E-03	8.71E-03	< 0.05	ns	< 0.05	ns
8	138.0219	6.99		C3H7NO3S	1.22E-03	8.11E-03	ns	ns	< 0.05	< 0.05
9	97.0283	7.13		C5H4O2	1.81E-03	8.11E-03	< 0.05	ns	< 0.05	ns
10	180.0866	7.10		C6H15NO6	1.24E-02	2.32E-02	< 0.05	ns	< 0.05	ns
11	159.0252	8.51		n.d.						
12	158.0281	7.08		n.d.	1.48E-03	8.11E-03	ns	ns	< 0.05	< 0.05
13	180.0865	7.13		C6H13NO5	8.87E-03	1.78E-02	< 0.05	ns	< 0.05	ns
14	160.0344	8.01		C6H10NPS	7.67E-03	1.64E-02	ns	ns	< 0.05	< 0.05
15	123.0553	3.84		C6H6N2O	2.38E-03	8.71E-03	< 0.05	< 0.05	ns	< 0.05
16	192.0866	7.98		C7H13NO5						
17	99.0439	7.13		C5H6O2	1.22E-03	8.11E-03	< 0.05	ns	< 0.05	ns
18	109.0283	7.09		C6H4O2	3.77E-03	8.71E-03	< 0.05	ns	< 0.05	ns
19	165.1134	8.01		C8H12N4						
20	189.087	2.68		C7H12N2O4	1.88E-02	3.30E-02	ns	ns	ns	< 0.05
21	93.0546	6.15	Glycerol	C3H8O3						
22	163.06	6.15		C6H10O5						
23	121.0318	7.70		C4H8O2S	3.02E-03	8.71E-03	< 0.05	ns	< 0.05	ns
24	178.1337	8.10		C10H15N3						
25	85.0284	6.15		C4H4O2						
26	151.0352	2.03		C3H6N2O5						
27	144.0477	8.13		C6H9NO5						
28	126.0218	6.91	Taurine	C2H7NO3S	3.50E-04	8.11E-03	< 0.05	< 0.05	ns	< 0.05
29	104.0706	8.04		C4H9NO2						
30	161.1283	8.02		C7H16N2O2						

### 3.4. Metabolite profiling of the tripartite community *Ulva mutabilis* under cold stress at 2 °C

To reduce the effect of non-essential bacteria for growth and development of *U. mutabilis*, the cold stress experiment was repeated with the tripartite community (*U. mutabilis*–*Roseovarius* sp.–*Maribacter* sp.; Fig. 1A) under more stringent conditions at 2 °C in the second experiment. Following cultivation at 18 ± 1 °C and 2 ± 0.5 °C for 14 days, the volcano plot of the identified features revealed significant differences between the metabolic profiles of *Ulva* grown under standard conditions and that grown in the cold (Fig. 4A). Among the 66 features detected in *U. mutabilis* (Table S1), 20 LMWCs were significantly different (18 upregulated and only 2 downregulated) between the two temperature treatments (Fig. 4A). As only three compounds, namely DMSP, proline, and glutamine, were identified by CD (Table S1), a targeted analysis was used to complement the exploratory approach (Fig. 4B) because additionally known candidate molecules were expected (Fig. 2).

### 3.5. Targeted analysis of cold stress-dependent changes in cryoprotectants

We performed a complementary experiment to determine the temperature stress-related production of the ten candidate compounds: DMSP, taurine, cysteinolic acid, ectoine, choline, homarine, glycine betaine, proline, glutamine, and methionine, under xenic and axenic conditions. The production of all compounds except homarine and methionine were upregulated following a temperature shift from 18 °C to 2 °C in the tripartite community of *U. mutabilis* (Fig. 4B). All substances were quantified in the low micromolar range with an operating range of one order of magnitude identified in one chromatographic run (Fig. 2) with a low relative standard deviation (RSD% from 2.5 to 8.2) and a low limit of quantification of the analytical process (Tables 2 and

3).

The concentrations of the analytes, normalized to dry weight (DW), ranged over several orders of magnitude from 7.4 × 10<sup>-4</sup> mg g<sup>-1</sup> (taurine) to 10.97 mg g<sup>-1</sup> (DMSP; Table 3). The increases following cold treatment were highly statistically significant (*P* < 0.001, Fig. 4B) for DMSP (3.5-fold increase), cysteinolic acid (9.5-fold increase), choline (1.4-fold increase), glycine betaine (13.4-fold increase), and proline (24.9-fold increase). In contrast, the increases in taurine and ectoine were of lower significance (*P* < 0.05) due to the variance of the data. At 18 °C, proline, glutamine, and glycine betaine concentrations were below the quantification limit. Proline (6.55 ± 1.53 mg g<sup>-1</sup> DW) and DMSP (10.97 ± 2.58 mg g<sup>-1</sup> DW) may be the most potentially beneficial metabolites in *Ulva*'s cold adaption process, as reported for various bacteria and sea-ice algae under high-osmolarity and colder growth conditions (Brill et al., 2011; Dawson et al., 2020; Götz et al., 2018).

DMSP has been proposed as a cryoprotectant in several green macroalgae (Karsten et al., 1992). In our study, DMSP concentration increased from 3.07 ± 0.47–10.97 ± 2.58 mg g<sup>-1</sup> DW following the shift to cold temperature, which is comparable to previously reported increases from approximately 1.3 to 37.5 mg g<sup>-1</sup> DW in green macroalgae collected from various latitudes. Those collected from polar regions had the highest DMSP concentration (Van Alstyne and Puglisi, 2007), whereas DMSP concentration was low (0.04 mg g<sup>-1</sup> DW) in the tropical chlorophyte *Ulva conglobata* (Bischoff et al., 1994). As the concentration of DMSP in *U. lactuca* increased significantly with latitude, Van Alstyne and Puglisi (2007) concluded that the concentration of compounds depends on environmental factors (e.g., light, temperature, day length) that change with latitudes. In this context, previous studies revealed that the cellular concentration of DMSP also increases with light intensity in various green macroalgal species (Karsten et al., 1990b, 1992).

Our findings support the hypothesis that DMSP production is

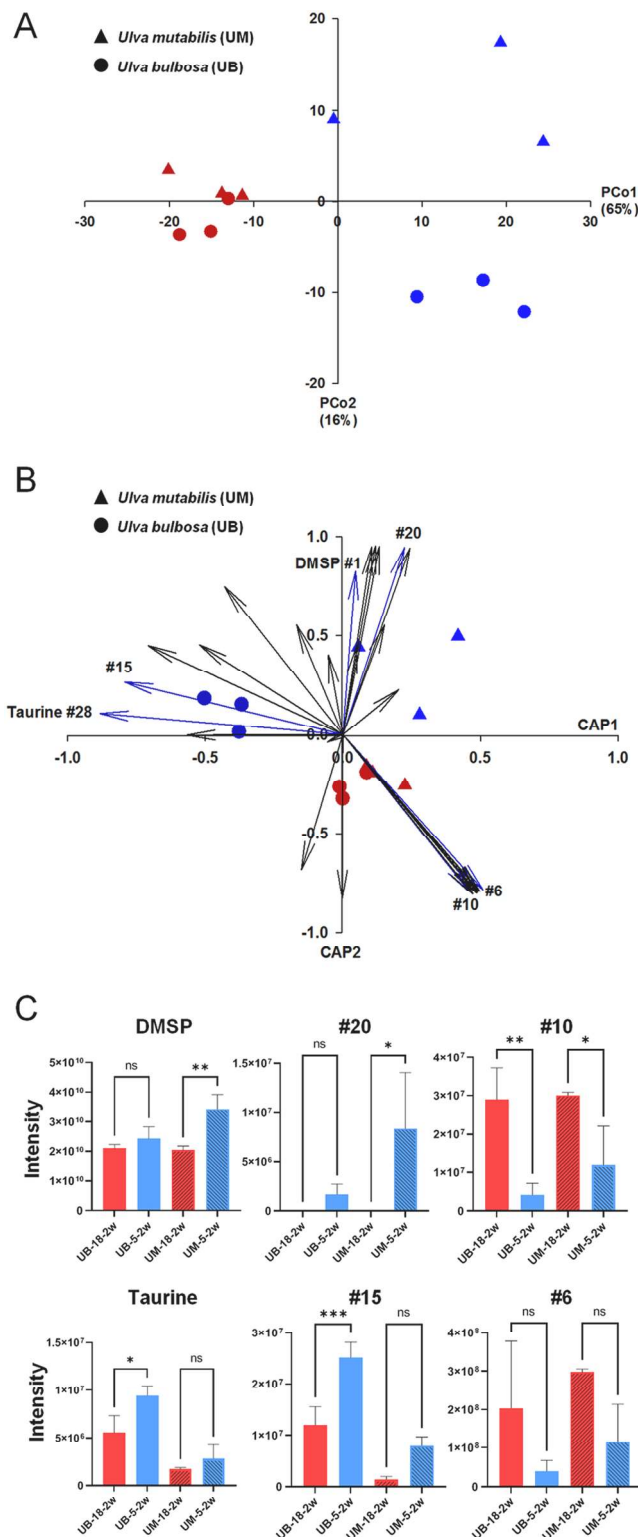


**Fig. 3.** Species-dependent cold stress response of the holobiont *Ulva*: (A) Multivariate data analysis of the mass spectrometric data upon HILIC-ESI-MS measurements. The score plot was obtained from principal coordinates analysis (PCoA) of the untargeted metabolite profiling of *Ulva mutabilis* (triangle) and *Ulva bulbosa* (circle) cultivated at  $18 \pm 1.0$  °C (red color) and  $5 \pm 1.0$  °C (blue color). (B) The first two canonical axes of the CAP analysis demonstrate the separation based on the *Ulva* species affected by the cold. Scaled vectors of the *m/z* features were significant, separating the groups for the correlation coefficient  $|r| > 0.5$  (correlation of the *m/z* features with the two CAP axes). The numbers refer to the order of features identified using Compound Discoverer software (CD) listed in Table 1. (C) Bar graphs demonstrate the species-specific significant increase in DMSP and taurine in cold-stressed *U. mutabilis* (UM) and *U. bulbosa* (UB), respectively, after two weeks (2w) of temperature treatment. There are also several unknown features (e.g., #20 and #15 are increased, and #10 and #6 are decreased). One-way ANOVA was followed by Tukey's post-hoc to indicate the significant differences (ns  $P > 0.05$ , \* $P \leq 0.05$ , \*\*\* $P \leq 0.001$ ,  $n = 3$ ).

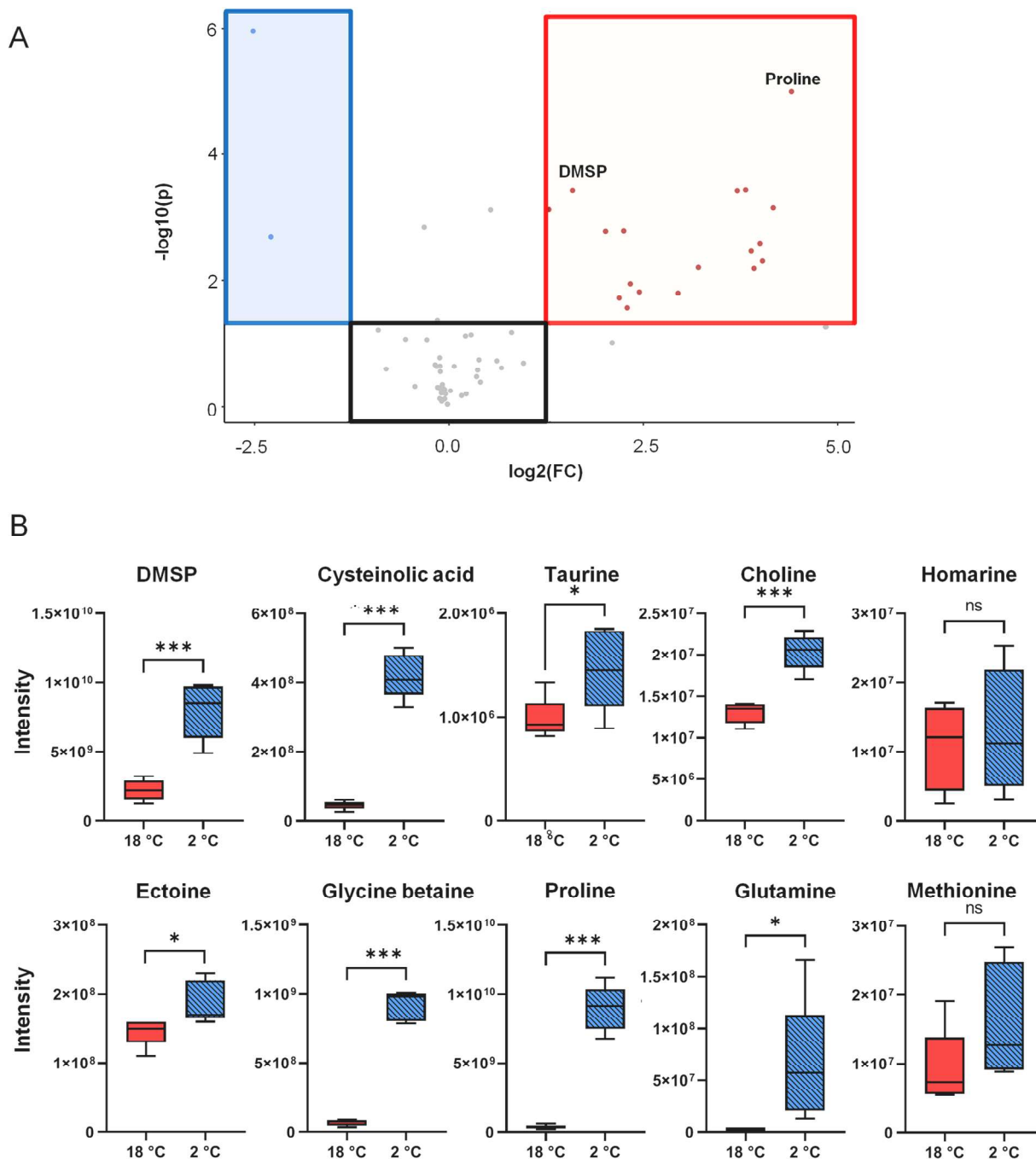


**Fig. 4.** Metabolite production in the tripartite community of *Ulva mutabilis* upon cold stress. (A) Volcano plot illustrates the 20 *m/z* features (i.e., metabolites) that were significantly altered in *U. mutabilis* due to a temperature shift from  $18 \pm 1.0$  °C to  $2 \pm 0.5$  °C. The rosa dots represent features with of statistical significance *P* less than 0.05 and a fold-change greater than 2-fold. Proline and DMSP are marked as examples. The greater the distance between the feature's coordinates and (0,0), the more significant the feature is. (B) Box plots illustrate the intensity changes in 10 selected cryoprotectants within the *U. mutabilis* metabolomic profile at 18 °C in comparison with their intensity at 2 °C. ANOVA followed by Tukey's post-hoc test was used to determine the significant differences (ns  $p > 0.05$ , \*  $p \leq 0.05$ , \*\*\*  $p \leq 0.001$ ,  $n = 3$ ).

temperature-dependent. Interestingly, the increased DMSP concentration was not associated with an increased production of its precursor methionine, which did not vary in response to temperature changes (Fig. 3C). This observation is consistent with our previous findings that a temperature-sensitive methyltransferase regulates DMSP production (De Clerck et al., 2018). Care must be taken when comparing values that have been normalized to dry weight or fresh weight. It has been estimated that the drying process causes a loss of up to 75% of the total DMSP yield (Bischoff et al., 1994; Bucciarelli et al., 2021).

Taurine content almost doubled (1.8-fold) in *U. bulbosa* upon shifting

the temperature from 18 °C to 5 °C. Taurine, a sulfur-containing  $\beta$ -amino acid, is produced from cysteine and released with no further degradation. Sulfonates are prevalent in marine algae, which may explain the extensive abundance of sulfonate-degrading bacteria in the marine ecosystem (Scholz et al., 2021). While only taurine traces were generally detected in plants, seaweeds can contain relatively high concentrations (Terriente-Palacios and Castellari, 2022). In Rhodophyta, the concentration of taurine was approximately 0.08% of DW (Scholz et al., 2021). Oxidative stress regulation was suggested to be the primary function of taurine. According to Jong et al. (2012),  $\beta$ -alanine-mediated

**Table 2**

Calibration parameters for those compatible solutes quantified in the thallus of *Ulva mutabilis* using the calibration method.

Compound	Working range	Limit of detection LOD	Limit of quantification LOQ	Rel. standard deviation RSD
Proline	5–50 $\mu\text{M}$	1.5 $\mu\text{M}$	5.4 $\mu\text{M}$	8.2%
Glutamine	1–16 $\mu\text{M}$	0.28 $\mu\text{M}$	1.01 $\mu\text{M}$	3.9%
DMSP	12.5–100 $\mu\text{M}$	2.6 $\mu\text{M}$	9.2 $\mu\text{M}$	3.5%
Taurine	6.25–50 nM	2.8 nM	9.4 nM	6.5%
Methionine	0.2–1 $\mu\text{M}$	0.1 $\mu\text{M}$	0.5 $\mu\text{M}$	2.5%
Glycine	0.5–5 $\mu\text{M}$	0.14 $\mu\text{M}$	0.5 $\mu\text{M}$	5.3%
betaine				
Ectoine	2.5–50 nM	2.9 nM	9.9 nM	5.0%

**Table 3**

Quantification of the compatible solutes per dry weight (DW) biomass of *Ulva mutabilis*.

Compound (mg/g DW)	18 °C	2 °C
Proline	< LOQ	$6.55 \pm 1.53$
Glutamine	< LOQ	$0.055 \pm 0.002$
Methionine	$1.5 \times 10^{-3} \pm 1.4 \times 10^{-4}$	$2.6 \times 10^{-3} \pm 9.2 \times 10^{-4}$
DMSP	$3.07 \pm 0.47$	$10.97 \pm 2.58$
Taurine	$7.4 \times 10^{-4} \pm 2.4 \times 10^{-4}$	$1.89 \times 10^{-3} \pm 4.5 \times 10^{-4}$
Glycine betaine	< LOQ	$1.78 \times 10^{-2} \pm 2.7 \times 10^{-3}$
Ectoine	$4.04 \times 10^{-2} \pm 6.9 \times 10^{-3}$	$5.4 \times 10^{-2} \pm 7.2 \times 10^{-3}$

taurine depletion reduces electron transport, resulting in increased mitochondrial superoxide production (Jong et al., 2012). This important observation could explain the role of taurine as a significant compound in stress regulation. In our experiments, taurine concentration was significantly affected by temperature in *U. bulbosa* but not in *U. mutabilis*, emphasizing the difference in responses of these two *Ulva* species to temperature stress. Moreover, taurine has the potential to be an important carbon source for heterotrophic bacterial growth. (Clifford et al., 2019). Therefore, algae-derived taurine may assist the metabolism of the algae-associated microbial community.

Cysteinolic acid, another sulfur amino acid, was elevated in *U. mutabilis* (9.5-fold) after the temperature shift, but the concentration of cysteinolic acid was below the limit of quantification. It has well

recognized physiological antioxidant activity and osmoregulatory effects and is a member of the class of marine sulfonates that are often produced by algae and metabolized by bacteria. The high content of D-cysteinolic acid has been reported in *Ulva* sp. (Ito, 1963). The content of cysteinolic acid in the diatom *Thalassiosira weissflogii* rose dramatically in response to short- and long-term ambient salinity changes (Fenizia et al., 2021). Similarly, cysteinolic acid concentration changed significantly under cold stress in *U. mutabilis* (Fig. 4B).

Proline concentration increased sharply by 24.9% following the temperature shift, whereas methionine concentration did not change (Fig. 4B). The accumulation of proline in plants exposed to abiotic stress is a well-documented and conserved response in most vegetal species. In our experiments, proline concentration in *U. mutabilis* had the highest fold change of any metabolite studied. Similarly, proline accumulated (to 6.48 mg g<sup>-1</sup> DW; 9.8-fold increase) in *U. fasciata* exposed to elevated salinity (Lee and Liu, 1999). Proline was also detected at high concentrations (4-fold increase) in response to decreased temperature (−1 °C vs. 4 °C) in the polar diatom, *N. lecontei* (Dawson et al., 2020). This change is similar to the 4.5-fold increase in proline concentration seen in *Fragilariopsis cylindrus*, a highly common psychrophilic diatom, while encased in newly formed sea ice and subjected to increasing external salinities and lower temperatures. In the face of these challenges, *F. cylindrus* growth is temporarily inhibited and only resumes after a prolonged period of acclimatization, during which proline accumulates in the cell (Krell et al., 2007). Proline, a cyclic amino acid, has thus emerged as a significant component of a typical algal physiological response to various abiotic stresses. Proline can stabilize sub-cellular structures, scavenge free radicals, and inhibit lipid peroxidation in the plant (Kaur and Asthir, 2015) and human cells (Sun et al., 2012). Free proline may be thus an indicator of cold-hardening and stress biomarkers in *Ulva*.

Under cold stress conditions the concentration of glutamine, also a proxy for its precursor glutamate, was increased by 20.6-fold in *U. mutabilis*. Glutamate is a precursor of several metabolites such as proline, arginine, and histidine, and it is involved in multiple responses such as those in response to pathogen resistance and abiotic stress (e.g., cold, heat, and drought) (Gawryluk et al., 2019; Qiu et al., 2020).

Glycine betaine, which increased 13.4-fold after exposure to cold stress, is widely considered an effective protectant to alleviate the negative effects of stressful environments on plants. Addition of

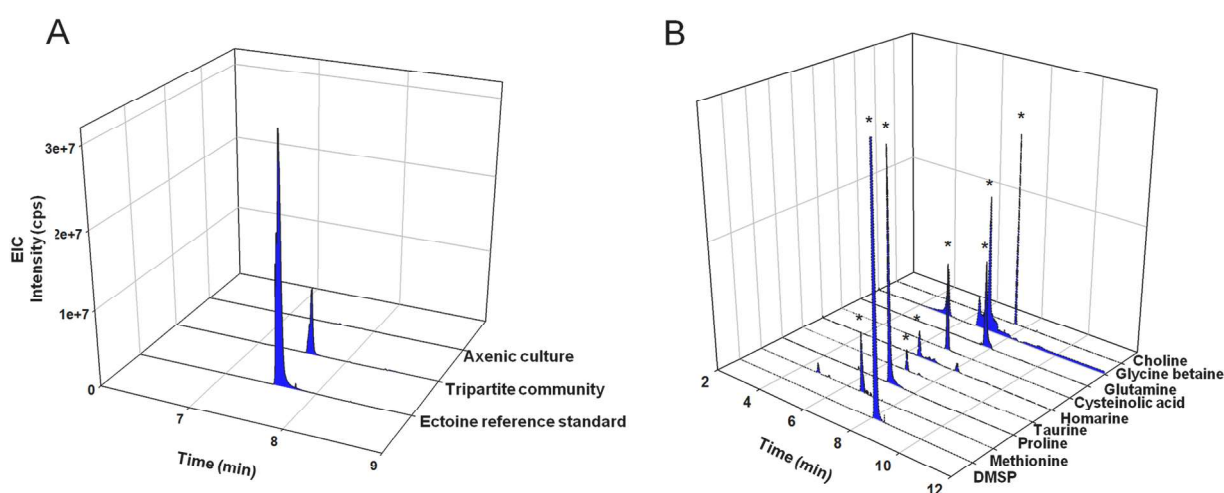


**Fig. 5.** Analysis of the tripartite community and axenic cultures of *Ulva mutabilis* for cold response candidate compounds. Extracted ion trace chromatograms (EIC) of the molecule ions  $[M+H]^+$  of the candidate compounds obtained by HILIC-ESI-MS analysis are shown. (A) Detection and structural elucidation of ectoine ( $m/z$  143.0814 for  $[M+H]^+$ ) in *U. mutabilis* co-cultured with bacteria. Ectoine was not detected in the absence of bacteria, providing further support for the bacterial origin of ectoine. Samples were collected from *U. mutabilis* tissues cultured at 5 °C for 14 days. (B) Analysis of axenic cultures: Except for ectoine, all selected metabolites were detected in axenic cultures of *U. mutabilis* (asterisks indicate the relevant peaks).

exogenous glycine betaine to cultures of the microalga *Chlorella sorokiniana* at low suboptimal temperatures improved photosynthesis by increasing the expression of genes encoding RuBisCo (Wang et al., 2016). Consistent with the current study's findings, glycine betaine concentration doubled at 41‰ salinity compared to 32‰ salinity when grown at 4 °C in the Antarctic diatom *N. lecointei*.

Choline, the precursor to glycine betaine, rose in quantity in response to temperatures below zero, although at a significantly lower intracellular concentration than that of glycine betaine (Dawson et al., 2020). The concentration of homarine, the other nitrogen-content compatible solute, did not change in *U. mutabilis* under cold stress.

### 3.6. Source of the cryoprotectants and bacterial contribution to cold adaptation

The candidate compounds were examined in axenic algae to determine whether *Ulva* or the associated microbiome had produced the solutes within the holobiont. Ectoine was the only compound not detected in axenic cultures of *U. mutabilis* at 18 °C or 5 °C (Fig. 5A), showing that it is produced exclusively by the bacteria associated with the holobiont. It has previously been shown that ectoine could be used as a biomarker to identify *Roseovarius* sp. MS2 in the algal rhizoidal zone (Vallet et al., 2021). In contrast, axenic algae had large amounts of metabolites such as cysteinolic acid, DMSP, and choline (Fig. 5B) which indicates intrinsic production (Fenzia et al., 2021; Kessler et al., 2018). The low bacterial density within the tripartite community (Fig. 1A) also explains the low concentration of ectoine ( $4.04 \times 10^{-2} \pm 6.9 \times 10^{-3}$  mg g<sup>-1</sup> DW).

Bacteria possess properties that allow biofilm formation on various *Ulva* species and promote their growth and morphogenesis (Ghaderiardakani et al., 2017; Marshall et al., 2006; Wichard, 2015). *Ulva* development is thus entirely dependent on AGMPFs provided by specific bacteria such as *Roseovarius* sp. and *Maribacter* sp. (Ghaderiardakani et al., 2019; Spoerner et al., 2012). While xenic germlings survive at 2 °C, axenic gametes of *U. mutabilis* die at temperatures < 5 °C (data not shown). Thus, it is tempting to assume that *Roseovarius* sp. contributes not only AGMPFs but also cold stress adaptation factors for growth. However, the constant requirement for bacterial morphogens makes it challenging to distinguish the effects of bacterial and algal processes on cold adaptation. In future studies, quantification of bacterial morphogens and cryoprotectants in the *Ulva* environment, experiments on ectoine uptake, and fitness measurements of *Ulva* seedlings will shed light on the ecophysiological role of cryoprotectants.

## 4. Conclusion

Warm-cold temperature shifts affect various morphological, cytological, physiological, and biochemical traits in plants. Plants acclimated to harsh ecosystems such as polar regions should retain strategies to cope with severe stresses. Metabolic profiling of *Ulva* tissues of two different species collected from Antarctica and the Mediterranean Sea enabled the identification of unknown markers and specific cryoprotectants that alleviate temperature stresses. *U. bulbosa* and *U. mutabilis* reacted differently to the temperature shift from 18 °C to 5 °C by increasing the production of taurine and DMSP, respectively, among many other (unknown) metabolites. The production of compounds was triggered in the Mediterranean *U. mutabilis* due to the cold stress; however, in the case of DMSP, the level of production was lower than expected from species of cold regions (Van Alstyne and Puglisi, 2007). Future studies are required to investigate the correlation between DMSP,

taurine, and proline production and changes in the growth rate of *U. mutabilis* during cold acclimation. Furthermore, when compared to freshly collected specimens, the long-term captivity of the studied cultures may have some effects on the biochemical inheritance.

Our study is limited to a small number of molecules that still need to be characterized to assign them to biosynthetic pathways and signal transduction chains. Future studies of *Ulva* species, which were freshly collected from the polar region, will help us further understand the cold adaptation process compared to the model system *U. mutabilis*.

Despite the several existing hypotheses regarding the microbiome's contribution to host response to environmental factors (e.g. their potential role in host resilience to stress), there is little evidence to support these hypotheses. Phycological experiments using the tripartite system and metabolomics approaches can be used to understand the contribution of microbiome composition to holobiont adaptation processes in future studies. Axenic cultures of *U. bulbosa* should be supplemented with morphogenetic compounds to reproduce algal development independent of the microbiome to distinguish the effects of morphogens on the metabolome and transcriptome from the innate cold stress response.

### CRediT authorship contribution statement

**Fatemeh Ghaderiardakani:** Methodology, Investigation, Formal analysis, Validation, Visualization, Writing – original draft. **Linda Langhans:** Investigation. **Valentin B. Kurbel:** Investigation. **Simona Fenzia:** Investigation, Validation. **Thomas Wichard:** Conceptualization, Methodology, Supervision, Formal analysis, Validation, Data curation, Funding acquisition, Writing – review & editing.

### Declaration of Competing Interest

The authors declare that they have no known competing financial interests or personal relationships that could have appeared to influence the work reported in this paper.

### Acknowledgements

We thank Georg Pohnert (Friedrich-Schiller Universität Jena) for his outstanding support and Inka Bartsch (Alfred-Wegener-Institute [AWI], Bremerhaven, Germany) for providing us with valuable cultures of the AWI culture collection. The *Ulva compressa* strain was collected as part of the European Union's Seventh Framework Programme ASSEMBLE (NUMBER: 227799), with the great support of Aschwin H. Engelen (Center of Marine Sciences, Faro, Portugal).

### Funding

This work was supported by the Deutsche Forschungsgemeinschaft (DFG, German Research Foundation) in the framework of the priority program (SPP 1158) "Antarctic Research with comparative investigations in Arctic ice areas" (424256657, FG, and TW) and by the International Max Planck Research School Exploration of Ecological Interactions with Molecular Techniques (SF).

### Appendix A. Supporting information

Supplementary data associated with this article can be found in the online version at [doi:10.1016/j.envexpbot.2022.104913](https://doi.org/10.1016/j.envexpbot.2022.104913).

## References

- Alsufyani, T., Engelen, A.H., Diekmann, O.E., Kuegler, S., Wichard, T., 2014. Prevalence and mechanism of polyunsaturated aldehydes production in the green tide forming macroalgal genus *Ulva* (Ulvales, Chlorophyta). *Chem. Phys. Lipids* 183, 100–109.
- Alsufyani, T., Weiss, A., Wichard, T., 2017. Time course exo-metabolomic profiling in the green marine macroalga *Ulva* (Chlorophyta) for identification of growth phase-dependent biomarkers. *Mar. Drugs* 15, 14.
- Alsufyani, T., Califano, G., Deicke, M., Grueneberg, J., Weiss, A., Engelen, A.H., Kwantes, M., Mohr, J.F., Ulrich, J.F., Wichard, T., 2020. Macroalgal–bacterial interactions: identification and role of thalassin in morphogenesis of the seaweed *Ulva* (Chlorophyta). *J. Exp. Bot.* 71, 3340–3349.
- Anderson, M., Willis, T., 2003. Canonical analysis of principal coordinates: a useful method of constrained ordination for ecology. *Ecology* 84, 511–525.
- Anderson, M.J., Robinson, J., 2003. Generalized discriminant analysis based on distances. *Aust. N. Z. J. Stat.* 45, 301–318.
- Becker, B., Marin, B., 2009. Streptophyte algae and the origin of embryophytes. *Ann. Bot.* 103, 999–1004.
- Bischoff, B., Karsten, U., Daniel, C., Kuck, K., Xia, B., Wiencke, C., 1994. Preliminary assessment of the beta-dimethylsulfoloniopropionate (DMSP) content of macroalgae from the tropical island of Hainan (Peoples-Republic-of-China). *Aust. J. Mar. Freshw. Res.* 45, 1329–1336.
- Brill, J., Hoffmann, T., Bleisteiner, M., Bremer, E., 2011. Osmotically controlled synthesis of the compatible solute proline is critical for cellular defense of *Bacillus subtilis* against high osmolarity. *J. Bacteriol.* 193, 5335–5346.
- Bucciarelli, E., Stiger-Pouvreau, V., Connan, S., 2021. A new protocol using acidification for preserving DMSP in macroalgae and comparison with existing protocols. *J. Phycol.* 57, 689–693.
- Cai, C., Gu, K., Zhao, H., Steinhagen, S., He, P., Wichard, T., 2021. Screening and verification of extranuclear genetic markers in green tide algae from the Yellow Sea. *PLoS One* 16, e0250968.
- Califano, G., Wichard, T., 2018. Preparation of axenic cultures in *Ulva* (Chlorophyta). In: Reddy, C. (Ed.), *Protocols for Macroalgae Research*. CRC Press, Boca Raton, pp. 159–171.
- Califano, G., Kwantes, M., Abreu, M.H., Costa, R., Wichard, T., 2020. Cultivating the macroalgal holobiont: Effects of integrated multi-trophic aquaculture on the microbiome of *Ulva rigida* (Chlorophyta). *Front. Mar. Sci.* 7–52.
- Chong, J., Wishart, D.S., Xia, J., 2019. Using MetaboAnalyst 4.0 for comprehensive and integrative metabolomics data analysis. *Curr. Protoc. Bioinform.* 68, e86.
- Clifford, E.L., Varela, M.M., De Corte, D., Bode, A., Ortiz, V., Herndl, G.J., Sintes, E., 2019. Taurine is a major carbon and energy source for marine prokaryotes in the north atlantic ocean off the Iberian peninsula. *Microb. Ecol.* 78, 299–312.
- Dawson, H.M., Heal, K.R., Boysen, A.K., Carlson, L.T., Ingalls, A.E., Young, J.N., Helmig, D., Arrigo, K., 2020. Potential of temperature-and salinity-driven shifts in diatom compatible solute concentrations to impact biogeochemical cycling within sea ice. *Elem.: Sci. Anthr.* 8.
- De Clerck, O., Kao, S.M., Bogaert, K.A., Blomme, J., Foflonker, F., Kwantes, M., Vancaester, E., Vanderstraeten, L., Aydogdu, E., Boesger, J., Califano, G., Charrier, B., Clewes, R., Del Cortona, A., D'Hondt, S., Fernandez-Pozo, N., Gachon, C.M., Hanikenne, M., Lattermann, L., Leliaert, F., Liu, X.J., Maggs, C.A., Popper, Z.A., Raven, J.A., Van Bel, M., Wilhelmsson, P.K.I., Bhattacharya, D., Coates, J.C., Rensing, S.A., Van der Straeten, D., Vardi, A., Sterck, L., Vandepoel, K., Van de Peer, Y., Wichard, T., Bothwell, J.H., 2018. Insights into the evolution of multicellularity from the sea lettuce genome. *Curr. Biol.* 28, 2921–2933.
- Deicke, M., Bellenger, J.-P., Wichard, T., 2013. Direct quantification of bacterial molybdenum and iron metallophores with ultra-high-performance liquid chromatography coupled to time-of-flight mass spectrometry. *J. Chromatogr. A* 1298, 50–60.
- Delaux, P.-M., Séjalon-Delmas, N., Bécard, G., Ané, J.-M., 2013. Evolution of the plant–microbe symbiotic ‘toolkit’. *Trends Plant Sci.* 18, 298–304.
- Dittami, S.M., Duboscq-Bidot, L., Perennou, M., Gobet, A., Corre, E., Boyen, C., Tonon, T., 2016. Host–microbe interactions as a driver of acclimation to salinity gradients in brown algal cultures. *ISME J.* 10, 51–63.
- Dunn, W.B., Broadhurst, D., Begley, P., Zelena, E., Francis-McIntyre, S., Anderson, N., Brown, M., Knowles, J.D., Halsall, A., Haselden, J.N., Nicholls, A.W., Wilson, I.D., Kell, D.B., Goodacre, R., The Human Serum Metabolome, C., 2011. Procedures for large-scale metabolic profiling of serum and plasma using gas chromatography and liquid chromatography coupled to mass spectrometry. *Nat. Protoc.* 6, 1060–1083.
- Edwards, D.M., Reed, R.H., Chudek, J.A., Foster, R., Stewart, W.D.P., 1987. Organic solute accumulation in osmotically-stressed *Enteromorpha intestinalis*. *Mar. Biol.* 95, 583–592.
- Famà, P., Wysor, B., Kooistra, W.H.C.F., Zuccarello, G.C., 2002. Molecular phylogeny of the genus *Caulerpa* (caulerpales, Chlorophyta) inferred from chloroplast tufa gene. *J. Phycol.* 38, 1040–1050.
- Fenizia, S., Thume, K., Wirgenings, M., Pohnert, G., 2020. Ectoines from bacterial and algal origin is a compatible solute in microalgae. *Mar. Drugs* 18, 42.
- Fenizia, S., Weissflog, J., Pohnert, G., 2021. Cysteinolic acid is a widely distributed compatible solute of marine microalgae. *Mar. Drugs* 19.
- Field, K.J., Pressel, S., Duckett, J.G., Rilmington, W.R., Bidartondo, M.I., 2015. Symbiotic options for the conquest of land. *Trends Ecol. Evol.* 30, 477–486.
- Føyn, B., 1958. Über die Sexualität und den Generationswechsel von *Ulva mutabilis*. *Arch. Protistenk* 102, 473–480.
- Friedrich, M.W., 2012. Bacterial communications on macroalgae. In: Wiencke, C., Bischof, K. (Eds.), *Seaweed Biology*. Springer, Heidelberg.
- Fürst-Jansen, J.M.R., de Vries, S., de Vries, J., 2020. Evo-physio: on stress responses and the earliest land plants. *J. Exp. Bot.* 71, 3254–3269.
- Garren, M., Son, K., Raina, J.-B., Rusconi, R., Menolascina, F., Shapiro, O.H., Tout, J., Bourne, D.G., Seymour, J.R., Stocker, R., 2014. A bacterial pathogen uses dimethylsulfoloniopropionate as a cue to target heat-stressed corals. *ISME J.* 8, 999–1007.
- Gawryluk, R.M.R., Tikhonenkov, D.V., Hehenberger, E., Husnik, F., Mylnikov, A.P., Keeling, P.J., 2019. Non-photosynthetic predators are sister to red algae. *Nature* 572, 240.
- Gebser, B., Pohnert, G., 2013. Synchronized regulation of different zwitterionic metabolites in the osmoadaptation of phytoplankton. *Mar. Drugs* 11, 2168–2182.
- Ghaderiardakani, F., Coates, J.C., Wichard, T., 2017. Bacteria-induced morphogenesis of *Ulva intestinalis* and *Ulva mutabilis* (Chlorophyta): a contribution to the lottery theory. *FEMS Microbiol. Ecol.* 93, fix094.
- Ghaderiardakani, F., Califano, G., Mohr, J.F., Abreu, M.H., Coates, J.C., Wichard, T., 2019. Analysis of algal growth-and morphogenesis-promoting factors in an integrated multi-trophic aquaculture system for farming *Ulva* spp. *Aquac. Environ. Interface* 11, 375–391.
- Ghaderiardakani, F., Quartino, M.L., Wichard, T., 2020. Microbiome-dependent adaptation of seaweeds under environmental stresses: a perspective. *Front. Mar. Sci.* 7, 575228.
- Götz, F., Longnecker, K., Kido Soule, M.C., Becker, K.W., McNichol, J., Kujawinski, E.B., Sievert, S.M., 2018. Targeted metabolomics reveals proline as a major osmolyte in the chemolithoautotroph *Sulfurimonas demitricans*. *MicrobiologyOpen* 7, e00586.
- Grueneberg, J., Engelen, A.H., Costa, R., Wichard, T., 2016. Macroalgal morphogenesis induced by waterborne compounds and bacteria in coastal seawater. *PLoS One* 11, e0146307.
- Guy, C., Kaplan, F., Kopka, J., Selbig, J., Hincha, D.K., 2008. Metabolomics of temperature stress. *Physiol. Plant* 132, 220–235.
- Ito, K., 1963. Distribution of D-cysteinolic acid in marine algae. *Bull. Jpn. Soc. Sci. Fish.* 29, 771–775.
- Jong, C.J., Azuma, J., Schaffer, S., 2012. Mechanism underlying the antioxidant activity of taurine: prevention of mitochondrial oxidant production. *Amino Acids* 42, 2223–2232.
- Karsten, U., Wiencke, C., Kirst, G.O., 1990a. The beta-dimethylsulfoloniopropionate (DMSP) content of macroalgae from Antarctica and Southern Chile. *Bot. Mar.* 33, 143–146.
- Karsten, U., Wiencke, C., Kirst, G.O., 1990b. The effect of light intensity and daylength on the beta dimethylsulfoloniopropionate DMSP content of marine green macroalgae from Antarctica. *Plant Cell Environ.* 13, 989–994.
- Karsten, U., Kirst, G., Wiencke, C., 1992. Dimethylsulfoloniopropionate (DMSP) accumulation in green macroalgae from polar to temperate regions: interactive effects of light versus salinity and light versus temperature. *Polar Biol.* 12, 603–607.
- Kaur, G., Asthir, B., 2015. Proline: a key player in plant abiotic stress tolerance. *Biol. Plant.* 59, 609–619.
- Kessler, R.W., Weiss, A., Kuegler, S., Hermes, C., Wichard, T., 2018. Macroalgal–bacterial interactions: role of dimethylsulfoloniopropionate in microbial gardening by *Ulva* (Chlorophyta). *Mol. Ecol.* 27, 1808–1819.
- Krell, A., Funck, D., Plettner, I., John, U., Diekmann, G., 2007. Regulation of proline metabolism under salt stress in the psychrophilic diatom *Fragilariopsis cylindrus* (Bacillariophyceae). *J. Phycol.* 43, 753–762.
- Lee, T.-M., Liu, C.-H., 1999. Correlation of decreased calcium contents with proline accumulation in the marine green macroalga *Ulva fasciata* exposed to elevated NaCl contents in seawater. *J. Exp. Bot.* 50, 1855–1862.
- Marshall, K., Joint, I., Callow, M.E., Callow, J.A., 2006. Effect of marine bacterial isolates on the growth and morphology of axenic plantlets of the green alga *Ulva linza*. *Microb. Ecol.* 52, 302–310.
- Ohama, N., Sato, H., Shinozaki, K., Yamaguchi-Shinozaki, K., 2017. Transcriptional regulatory network of plant heat stress response. *Trends Plant Sci.* 22, 53–65.
- Piette, F., D’Amico, S., Mazzucchelli, G., Danchin, A., Leprince, P., Feller, G., 2011. Life in the cold: a proteomic study of cold-repressed proteins in the Antarctic bacterium *Pseudomonas haloplanktis* TAC125. *Appl. Environ. Microbiol.* 77, 3881–3883.
- Qiu, X.-M., Sun, Y.-Y., Ye, X.-Y., Li, Z.-G., 2020. Signaling role of glutamate in plants. *Front. Plant Sci.* 10, 1743.
- Reichenbacher, M., Einax, J.W., 2011. Validation of method performance. *Challenges in Analytical Quality Assurance*. Springer, pp. 206–212.
- Rensing, S.A., 2018. Great moments in evolution: the conquest of land by plants. *Curr. Opin. Plant Biol.* 42, 49–54.
- Rodrigues, D.F., Tiedje, J.M., 2008. Coping with our cold planet. *Appl. Environ. Microbiol.* 74, 1677–1686.
- Russell, N.J., 1983. Adaptation to temperature in bacterial membranes. *Biochem. Soc. Trans.* 11, 333–335.
- Schloss, P.D., Westcott, S.L., Ryabin, T., Hall, J.R., Hartmann, M., Hollister, E.B., Lesniewski, R.A., Oakley, B.B., Parks, D.H., Robinson, C.J., 2009. Introducing mothur: open-source, platform-independent, community-supported software for describing and comparing microbial communities. *Appl. Environ. Microbiol.* 75, 7537–7541.
- Scholz, S., Serif, M., Schleheck, D., Sayer, M.D., Cook, A.M., Küpper, F.C., 2021. Sulfoquinovose metabolism in marine algae. *Bot. Mar.* 64, 301–312.
- Seymour, J.R., Simó, R., Ahmed, T., Stocker, R., 2010. Chemoattraction to dimethylsulfoloniopropionate throughout the marine microbial food web. *Science* 329, 342–345.
- Spielmeier, A., Gebser, B., Pohnert, G., 2011. Dimethylsulfide sources from microalgae: Improvement and application of a derivatization-based method for the determination of dimethylsulfoloniopropionate and other zwitterionic osmolytes in phytoplankton. *Mar. Chem.* 124, 48–56.

- Spoerner, M., Wichard, T., Bachhuber, T., Stratmann, J., Oertel, W., 2012. Growth and thallus morphogenesis of *Ulva mutabilis* (Chlorophyta) depends on a combination of two bacterial species excreting regulatory factors. *J. Phycol.* 48, 1433–1447.
- Steinhagen, S., Barco, A., Wichard, T., Weinberger, F., 2019. Conspecificity of the model organism *Ulva mutabilis* and *Ulva compressa* (Ulvophyceae, Chlorophyta). *J. Phycol.* 55, 25–36.
- Stratmann, J., Paputsoglu, G., Oertel, W., 1996. Differentiation of *Ulva mutabilis* (Chlorophyta) gametangia and gamete release are controlled by extracellular inhibitors. *J. Phycol.* 32, 1009–1021.
- Sun, H., Glasmacher, B., Hofmann, N., 2012. Compatible solutes improve cryopreservation of human endothelial cells. *Cryo Lett.* 33, 485–493.
- Terriente-Palacios, C., Castellari, M., 2022. Levels of taurine, hypotaurine and homotaurine, and amino acids profiles in selected commercial seaweeds, microalgae, and algae-enriched food products. *Food Chem.* 368, 130770.
- Tribelli, P.M., López, N.I., 2018. Reporting key features in cold-adapted bacteria. *Life* 8, 8.
- Vallet, M., Kaftan, F., Grabe, V., Ghaderiadekani, F., Fenizia, S., Svatoš, A., Pohnert, G., Wichard, T., 2021. A new glance at the chemosphere of macroalgal-bacterial interactions: in situ profiling of metabolites in symbiosis by mass spectrometry. *Beilstein J. Org. Chem.* 17, 1313–1322.
- Van Alstyne, K.L., Puglisi, M.P., 2007. DMSP in marine macroalgae and macroinvertebrates: distribution, function, and ecological impacts. *Aquat. Sci.* 69, 394–402.
- van der Loos, L.M., D'Hondt, S., Willems, A., De Clerck, O., 2021. Characterizing algal microbiomes using long-read nanopore sequencing. *Algal Res.* 59, 102456.
- Wang, Y., He, B., Sun, Z., Chen, Y.-f., 2016. Chemically enhanced lipid production from microalgae under low sub-optimal temperature. *Algal Res.* 16, 20–27.
- Wichard, T., 2015. Exploring bacteria-induced growth and morphogenesis in the green macroalga order Ulvales (Chlorophyta). *Front. Plant Sci.* 6, 86.
- Wichard, T., 2022. From model organism to application: Bacteria-induced growth and development of the green seaweed *Ulva* and the potential of microbe leveraging in algal aquaculture. *Seminars in Cell & Developmental Biology*. <https://doi.org/10.1016/j.semcdb.2022.04.007>. In press.
- Wichard, T., Oertel, W., 2010. Gametogenesis and gamete release of *Ulva mutabilis* and *Ulva lactuca* (Chlorophyta): regulatory effects and chemical characterization of the “swarming inhibitor”. *J. Phycol.* 46, 248–259.
- Yancey, P.H., 2005. Organic osmolytes as compatible, metabolic and counteracting cytoprotectants in high osmolarity and other stresses. *J. Exp. Biol.* 208, 2819–2830.

## Supplementary Material for

### **Metabolite profiling reveals new insight into the cold adaptation of the green macroalga *Ulva* (Chlorophyta) isolated from the Mediterranean and Antarctic regions**

Fatemeh Ghaderiardakani<sup>1</sup>, Linda Langhans<sup>1</sup>, Valentin Kurbel<sup>1</sup>, Simona Fenizia<sup>1,2</sup>, Thomas Wichard<sup>1\*</sup>

<sup>1</sup> Institute for Inorganic and Analytical Chemistry, Friedrich Schiller University Jena, Lessingstraße 8, 07743, Jena, Germany

<sup>2</sup> Max Planck Institute for Chemical Ecology, Hans-Knoll-Strasse 8, 07745 Jena, Germany

\* Corresponding author: Thomas Wichard, [thomas.wichard@uni-jena.de](mailto:thomas.wichard@uni-jena.de)



**Table S1: Identification of 66 features in *U. mutabilis* and biomarkers for changes in the metabolism upon the warm-cold temperature shift.**

Feature #	$m/z$ [M+H] <sup>+</sup> measured	RT [min]	Compound	Formula	<i>P</i> -value	Up/down regulated at 2°C
1	135.0474	8.16	DMSF	C5H10O2S	3.70E-04	up
2	116.0705	6.54	L-Proline	C5H9NO2	9.91E-06	up
3	118.0862	6.29	Glycine betaine	C5H11NO2	7.37E-04	up
4	85.0284	7.02		C4H4O2	6.30E-03	up
5	127.0389	7.03		C6H6O3	3.42E-03	up
6	130.0499	7.99		C5H7NO3		
7	163.0601	7.02		C6H10O5	3.62E-04	up
8	145.0495	7.02		C6H8O4	3.73E-04	up
9	162.1123	6.58		C7H15NO3	2.72E-02	up
10	97.0284	7.03		C5H4O2	4.84E-03	up
11	180.0866	7.02		C6H13NO5	2.54E-03	up
12	99.0440	7.02		C5H6O2	6.93E-04	up
13	90.0549	7.65		C3H7NO2	1.58E-02	up
14	189.1233	7.24		C8H16N2O3	1.52E-02	up
15	88.0757	4.90		C4H9NO	1.91E-02	up
16	149.0631	6.49		C6H12O2S	1.63E-03	up
17	147.0763	7.99		C5H10N2O3		
18	147.1128	11.10		C6H14N2O2	6.08E-03	up
19	110.0270	7.39		C2H7NO2S	1.13E-02	up
20	123.0553	8.58		C6H6N2O	1.65E-03	up
21	130.1590	2.90		C8H19N		
22	122.0964	3.25		C8H11N		
23	105.0699	6.34		C8H8		
24	132.1019	5.87		C6H13NO2		
25	101.0709	6.88		C4H8N2O		
26	138.0913	3.25		C8H11NO		
27	130.0863	6.40		C6H11NO2	1.10E-06	down
28	80.0494	2.13		C5H5 N		
29	167.0927	4.76		C7H10N4O		
30	83.0603	4.08		C4H6N2		
31	87.0917	3.99		C4H10N2		
32	103.0865	7.52		C4H10N2O		
33	117.0659	3.78		C4H8N2O2		
34	115.0865	3.62		C5H10N2O		
35	188.0706	5.83		C1 H9NO2		
36	156.1384	3.58		C9H17NO		
37	104.1069	7.42		C5H13NO		
38	159.0764	3.65		C6H10N2O3		
39	175.1157	6.94		C9H18OS		
40	144.0808	6.36		C10H9N		
41	143.0815	7.08		C6H10N2O2		
42	154.1226	3.08		C9H15NO		
43	87.0553	4.87		C3H6N2O		
44	108.0807	3.41		C7H9N		
45	140.0819	4.74		C6H9N3O		
46	117.1023	5.22		C5H12N2O		
47	145.0718	7.72		C4H8N4O2		
48	120.0655	7.96		C4H9NO3		
49	183.0916	3.12		C12H10N2		
50	182.0812	5.41		C9H11NO3	2.00E-03	down
51	145.1461	10.77		C8H18NO		
52	128.1182	7.44		C6H13N3		
53	169.0761	3.25		C11H8N2		

<b>54</b>	139.0978	7.76	C6H10N4
<b>55</b>	90.0913	7.45	C4H11NO
<b>56</b>	146.1175	3.40	C7H15NO2
<b>57</b>	127.0726	7.48	C3H6N6
<b>58</b>	121.0318	6.33	C4H8O2S
<b>59</b>	173.0921	3.35	C7H12N2O3
<b>60</b>	175.1078	7.27	C7H14N2O3
<b>61</b>	145.1084	7.43	C5H12N4O
<b>62</b>	160.0969	4.73	C7H13NO3
<b>63</b>	150.1124	7.46	C6H15NO3
<b>64</b>	160.1331	8.61	C8H17NO2
<b>65</b>	102.0914	7.43	C5H11NO
<b>66</b>	174.1488	8.61	C9H19NO2



### 3 Discussion

Since the CLAW hypothesis was proposed, the volatile compound dimethylsulfide (DMS) has been considered the missing key to connecting the sulfur cycle of marine and terrestrial environments, and the zwitterionic sulfonium compound dimethylsulfoniumpropionate (DMSP) as its primary precursor.

DMSP is indeed one of the most abundant organosulfur compounds on the Earth and in the aquatic ecosystem. It is a secondary zwitterionic metabolite produced in large amounts by marine algae and bacteria, where it carries out important intra- and extra-cellular functions. Moreover, it is a key component of the global geochemical sulfur cycle mainly with relevant ecological implications<sup>37,59,98-100</sup>. Despite the globally recognized environmental importance of DMSP and its structurally related and derived compounds<sup>32</sup>, the functional analysis and molecular characterization of these sulfur-derived metabolites have not been fully elucidated yet, as they require high-level bioassays and analytical techniques. Some high-throughput techniques have been used in the course of this work to investigate characteristics of zwitterionic metabolites and their ecological implications, opening new windows to the marine networks and providing plenty of avenues for future research.

#### ***Novel insights into DMSP ecology and the marine sulfur cycle***

Aquatic chemical ecology covers, among others, biotic interactions between marine algae and microorganisms. Small molecules play a central role in the organization of aquatic ecosystems and in the regulation of interactions of living organisms, where chemical cues mediate intraspecific and interspecific interactions<sup>101</sup>.

In this context, our research focused on the key metabolite DMSP, which is involved in marine biogeochemical context as well as in algal and bacterial interactions. The recent molecular characterization of *dsyB*, a DMSP biosynthetic gene found in several bacterial taxa, shed new light on the microbial contribution to oceanic DMSP production and its conversion into DMS<sup>32,59</sup>. Indeed, marine bacteria use two competing catabolic pathways to either incorporate both carbon and sulfur from DMSP, thus building-up bacterial biomass (demethylation pathway), or to take only carbon up (cleavage pathway), whereas sulfur is released as climatically active DMS (**Publication 1**). Environmental factors behind the preferential use of one

pathway instead of the other are not fully elucidated yet, highlighting an important gap of knowledge in the microbial contribution to biogeochemical cycles.

Almost two decades ago, the “DMSP Availability Hypothesis” and the “Bacterial Switch” were introduced to explain the preferential conditions leading to the exclusion of one pathway instead of the other<sup>64,102</sup>. While the first hypothesis considered the external DMSP concentration as a decisional factor, the second highlighted a bacterial control on the preferred expression of one of the two pathways<sup>102</sup>; however, both of them have been considered, to date, only hypothetical and lacking direct evidence.

To fill this gap of knowledge, by using engineered fluorescent reporter strains of the bacterium *Ruegeria pomeroyi* DSS-3, in our work (**Publication 1**), carried out in collaboration with the research group led by Professor Stocker from the Swiss Federal Institute of Technology (ETH) in Zürich, we introduced a single-cell, time-resolved method to measure DMSP degradation pathway expression, coupled with Ultra-High Performance Liquid Chromatography (UHPLC) and High-Resolution Mass Spectrometry (HRMS), to measure the expression and activity of the two competing DMSP catabolic pathways used by marine bacteria to transform DMSP and to highlight bacterial responses to different DMSP concentrations (**Publication 1**).

From our findings, we reported higher DMSP concentrations in microscale hotspots than in bulk seawater, demonstrating that DMSP concentrations, relevant for bacterial DMS production and release into the atmosphere, are found in microscale DMSP hotspots rather than in bulk seawater.

Thus, with our work we provided proof that external DMSP concentrations control the relative expression of the demethylation/cleavage pathway, and that the high DMSP concentrations found in microscale hotspots will direct towards the cleavage degradation pathway, increasing the DMS production and contribute to the global sulfur cycle, thus providing novel insights on the environmental determinants involved in global climate and biogeochemical cycles

### ***Inter- and intra-specific interactions in aquatic chemical ecology***

In addition to their contribution to the biogeochemistry of the sulfur cycle, DMSP and its metabolic product DMS play central roles in algal biotic interactions. Due to their interconnected evolutionary history, algae and

bacteria are tightly bound by a mutualistic relationship, beneficial for both (**Publication 2**).

To deepen the importance of the algal-associated microbial community and to have a new glance at the mutualistic interaction between bacteria and macroalgae, we focused on the green macroalga *Ulva mutabilis* (*U. mutabilis*) and its two bacterial symbionts, *Roseovarius* sp. MS2 and *Maribacter* sp. MS6 which releases Algal Growth and Morphogenesis Promoting Factors (AGMPFs).

Although experimental data on microbial community dynamics are available and studies on these interactions are a central active area of current research<sup>103,104</sup>, until now most of the research works focused on the analysis of the abundance and composition of bacterial strains on the algae<sup>105,106</sup>, without supplying any detail related to nor their physical localization or the distribution, within the chemosphere, of the metabolites involved in this mutualistic exchange.

To address this challenge, we performed a comparative metabolomic analysis in the phycosphere of the macroalga *U. mutabilis*. We took advantage of imaging technologies with high sensitivity and spatial resolution. Atmospheric pressure scanning microprobe matrix-assisted laser desorption/ionization high-resolution mass spectrometry (AP-SMALDI-HRMS) was used to identify and localize low-molecular-weight polar compounds that characterize the symbiosis between the macroalga and its associated bacteria (**Publication 2**).

Our results demonstrate that the chemosphere of *U. mutabilis* changes according to the presence or absence of the related symbiotic bacterium, and therefore the specific metabolites can lead to bacterial localization in proximity to the alga. In particular, a first difference was observed in the *U. mutabilis* phenotype, as in presence of the symbiotic species, the algal germlings formed a rhizoidal zone, for substrate attachment, and a thallus zone. Metabolomic analysis with matrix deposition (MALDI-HRMS) and matrix-free analysis (LDI-HRMS) of the two sections and the entire alga germlings showed metabolic differences between xenic and axenic cultures, while tissue sections showed higher similarity. In particular, among the relevant metabolites, choline has been identified in the axenic culture of *U. mutabilis*: this metabolite is the precursor of the membrane constituent phosphatidylcholine<sup>107,108</sup>, therefore its accumulation in axenic cultures might compensate for the absence of thalusin, a bacterial morphogen that induces cell wall and rhizoid formation.

While choline was a useful marker of a symbiont-free algal culture, the zwitterionic metabolite ectoine, widely distributed throughout halophilic and halotolerant bacteria<sup>109-111</sup>, was detected exclusively in presence of *Roseovarius* sp., thereby acting as a marker for the localization and identification of rhizoid algal tissue in bacterial symbiosis within the tripartite community. Thanks to the results obtained, we highlighted the central roles that the physical proximity, as well as the type of excretion products, play in the mutualistic interactions between algae and bacteria, thus providing new tools to investigate symbiotic mechanisms in aquatic ecosystems (**Publication 2**).

### ***Ecological relevance of zwitterionic metabolites***

Although several protective properties have been attributed to a wide range of zwitterionic molecules<sup>16,17,112</sup>, there is a lack of information on the chemical and ecological functions of these pivotal metabolites. Moreover, the double-charged structure of these molecules makes their analysis and quantification tricky.

Important and relevant contributions in the field have been enabled by the introduction, by Spielmeyer and Pohnert<sup>85</sup>, of an ultra-high performance liquid chromatography (UHPLC) method that allows the separation and direct determination of phytoplankton-derived zwitterionic compounds, thus expanding knowledge on the structural and functional diversity of these metabolites.

Thereby, besides DMSP, other sulfur-containing small organic molecules, shown in the figure below (Fig. 6), like gonyol, dimethylsulfonioacetate (DMSA), and dimethylsulfoxoniumpropionate (DMSOP), as well as nitrogen-containing zwitterionic metabolites, including glycine betaine (GBT), have been discovered (Fig. 6) and their ecological role has been studied in marine organisms, including phytoplankton and bacteria<sup>63,112</sup>.

Despite the important advances in the analysis and characterization of small metabolites produced by marine algae, the Total Ion Current (TIC), obtained from the chromatographic analysis of methanol extracts of the dinoflagellate *Prorocentrum minimum*, suggests that, besides some previously identified zwitterionic compounds, several highly polar small metabolites are still uncharacterized<sup>85</sup>(Fig. 6).

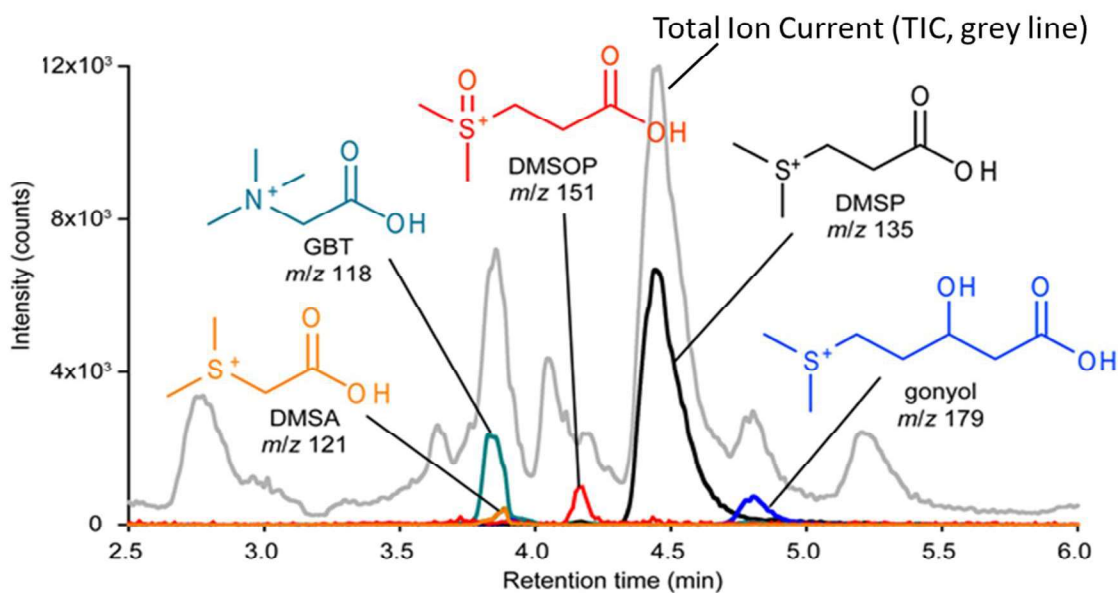


**Figure 6:** Chromatographic profile of zwitterionic metabolites from a *P. minimum* extract, separated using UHPLC-HRMS. The total ion current is shown in grey. From Thume et al., (2018).<sup>62</sup>

The assumption that small organic, likely zwitterionic metabolites, are included is supported by the extraction protocol, which allows obtaining only polar metabolites from the entire algal extract, and on the analytical conditions, as the chromatographic column used for the study is designed to retain and separate polar and hydrophilic compounds, as discussed in the next paragraphs. Therefore, by refining the chromatographic method introduced by Spielmeyer and Pohnert<sup>85</sup>, and by using high-resolution mass spectrometry, we perform an in-depth investigation of the “zwitter-metabolome” of marine diatoms to identify and quantify unknown components and reveal their ecological relevance.

### ***Ecological importance of compatible solutes for marine organisms***

Environmental salinity and temperature shifts are two key stressors to overcome for marine species<sup>113,114</sup> and can exert a high evolutionary selection. In this view, osmo- and thermoregulation are crucial aspects of the growth and life cycle of marine species. Hence, marine living organisms need to develop adaptation mechanisms to keep the intracellular osmotic pressure greater than the extracellular one and their body temperatures within narrow limits<sup>5,16,115,116</sup>.

Because marine micro-organisms, including algae, do not have any intrinsic mechanism to actively regulate the direction of water fluxes and to keep



their cellular temperatures, independent from the external environment, the achievement of proper cellular hydration and their survival to extreme temperatures relies on the physiological capabilities to compensate for these changes<sup>116,117</sup>. Among the physiological responses, the synthesis of organic zwitterionic compatible solutes, their import, accumulation and release have a central role in the survival of the species<sup>16,17,111</sup>.

### ***Novel zwitterionic compatible solutes by marine phytoplankton***

To evaluate and expand the knowledge of the osmoregulatory properties of algal-derived zwitterionic metabolites, we took advantage of optimized experimental and analytical procedures to perform an in-depth analysis of the diatoms' "zwitter-metabolome" (**Publication 3**). Ultra-High-Pressure Liquid Chromatography and High-Resolution Mass Spectrometry (UHPLC-HRMS) technologies were used to mine for highly polar unknown metabolites, potentially involved in osmoregulation, and therefore with compatible solute properties. Up-regulation under increased salinity was selected as a criterion in a metabolic profiling approach. In our screening of the zwitter-metabolome of marine phytoplankton, we initially focused on the two marine diatoms *Phaeodactylum tricornutum* and *Thalassiosira weissflogii*, both well-established model organisms for ecological studies. The genome of *Phaeodactylum tricornutum* was fully sequenced in 2008<sup>118</sup>. Since then, many studies have been conducted, providing the basis for comparative genomic studies<sup>119</sup>, biological informations and interpretations of the ecological success of these organisms<sup>120</sup>.

The diatom *Thalassiosira weissflogii*, on the other hand, is also considered a model organism, being one of the few diatoms identified that does not directly produce quantifiable amounts of DMSP, but it can take it up from the external medium<sup>121</sup>. It can be, thus, useful to investigate the physiological role of cellular DMSP, offering the opportunity to test both DMSP-free and DMSP-enriched cultures of the same algal strain<sup>122,123</sup>. In addition, *T. weissflogii* has been previously used to study acclimation to hyposalinity with a reported detailed transcriptomic and physiologic survey of the response to this stress factor<sup>124,125</sup>. Moreover, it served as a model organism for the investigation of algal responses to other types of environmental stress, such as seawater acidification, temperature and light changes and anoxia<sup>126,127</sup>.

For our purpose, osmoadaptation experiments were performed on xenic and axenic strains of the diatoms *T. weissflogii* and *P. tricornutum*, grown

at normal (35 PSU) and high (50 PSU) salinity, inducing both a short-term stress, where a solution of NaCl was added 24 h before the extraction, and a long-term stress, where algae were grown in a high salinity medium (**Publication 3, Publication 4**). The salinity range was selected according to previous studies on osmoregulation and it is within the salinity span of sea water<sup>125</sup>.

Our approach of combining a ZIC-HILIC chromatographic separation protocol with HRMS allowed us to get more insights into the ecological role of DMSP. In addition, by performing osmoadaptation experiments on microalgal stock cultures, we could identify, characterize and quantify novel zwitterionic metabolites involved in algal defence mechanisms against environmental salinity and temperature changes, providing new insights on the ocean network and dynamics.

### ***Osmoregulation in marine diatoms: novel algal-derived compatible solutes***

An in-depth analysis of the UHPLC-HRMS chromatographic profiles obtained from methanol extracts of the two selected diatoms, we encountered in two metabolites whose identities, according to the mass spectra and fragmentation patterns, were most likely attributable to ectoine and cysteinolic acid. Both these molecules were already known either, in the case of ectoine, as abundant and characteristic osmolyte of aerobic heterotrophic eubacteria, or, this is the case for cysteinolic acid, as a major sulfonic compound and sulfur reservoir of brown algae<sup>32,128-130</sup>. Both these molecules have never been mentioned to be involved in physiological responses to salt stress in marine algae. With this work, we demonstrate their wide spread in aquatic environments and their contribution to the osmoregulation of halophilic marine organisms, thus granting the survival of different species and their life cycle.

#### ***Ectoine***

The spectrometric and spectroscopic analyses of the extracts of xenic cultures of *P. tricornutum* and *T. weissflogii* lead us to the identification of one of the most predominant metabolites visible in the chromatograms of the two algal species.

Through the analysis of the fragmentation pattern, its comparison with several online databases (i.e., METLIN, MassBank of North America, MetaboLights) and bioinformatic software (i.e., Sirius v4.0.1,

CSI:FingerID)<sup>131,132</sup>, as well as coelution and matching MS/MS data with the corresponding synthetic standard, we confirmed the identity of ectoine, a bacterial metabolite that belongs to the class of heterocyclic amino acids and partially hydrogenated pyrimidine derivatives<sup>109,117,133</sup>. Ectoine, 2-methyl-1,4,5,6-tetrahydropyrimidine-4-carboxylic acid, was isolated, for the first time, in 1985 in the halophilic phototrophic sulfur bacterium *Halorhodospira halochloris*, originally named *Ectothiorhodospira halochloris*, hence the name ectoine<sup>133</sup>.

The biosynthesis and natural occurrence of this metabolite were initially considered to be rare and limited as specialized microbial osmoprotectant in halophilic bacteria responding to high salinity<sup>109,117</sup>. Given the ability of microalgae to take up mainly bacterial-derived zwitterionic metabolites from the external environment to overcome adverse conditions<sup>121</sup>, we investigated whether the presence of this metabolite in the algal methanol extracts was imputable either to an algal biosynthetic activity or an up-take mechanism.

To answer this question, methanol extracts from both xenic and axenic cultures of the diatoms were analyzed and compared, to conclude that, in addition to other main metabolites such as glycine betaine, ectoine was present in both the analyzed cultures. Because lower, although still significant concentrations were detected in axenic cultures of the diatom *P. tricornutum*, we investigated further the fully sequenced genome of diatom *P. tricornutum*. We looked for genes associated with ectoine biosynthesis<sup>117,134</sup>, finding out that two out of three homologs of the bacterial genes involved in its biosynthetic pathway are also present in the genome of this alga, pointing towards a dual origin of this metabolite in the algae, from both biosynthesis and external uptake (**Publication 3**).

Once the algal origin of this metabolite was confirmed, we verified the osmoregulatory function of this metabolite, through its quantification in cultures of *T. weissflogii* grown at different salinities<sup>125</sup>. Indeed, we observed a significant increase of ectoine intracellular concentration after an induced salinity shift, of 3.5- and 1.6-fold respectively in xenic and axenic cultures grown for 24h at high salinity levels (50 PSU), and this increase was of 11- and 4.8-fold after an induced long-term stress. The amount of ectoine produced by the diatom in xenic conditions is three orders of magnitude higher in comparison with the axenic cultures, highlighting the importance of the microbial community associated with the diatoms (**Publication 3**).

In 2011, Spielmeyer et al.<sup>121</sup> already demonstrated that the diatom *T. weissflogii* does not produce quantifiable amounts of DMSP, but also showed the ability of this diatom to take this metabolite up from the external environment to compensate for this lack. Aware of this particular behaviour, we evaluated the ability of microalgae to take up extracellular (perhaps of bacterial origin) ectoine. Thus, we performed an incubation experiment by adding the correspondent labeled ectoine (D3-ectoine), synthesized in our laboratory, to axenic cultures of *T. weissflogii*, grown at physiological and high salinity levels (**Publication 3**).

All the methanol extracts containing the algal intracellular metabolites showed an excess of the D3-ectoine compared to the correspondent unlabeled form of this metabolite. The highest uptake took place in those cultures grown at physiological salinity level (35 PSU), when the diatom production rate of ectoine is low. This result highlights the ability of *T. weissflogii* to import this metabolite from the external medium, reducing its energetically costly biosynthetic activity<sup>32</sup>. Based on this evidence, the higher ectoine content found in xenic cultures has to be linked to the diatom uptake of the bacterial-derived ectoine from the external medium. Due to this import system, *T. weissflogii* increases the intracellular ectoine content by adding the bacterial-derived metabolite to the own intracellular pool, thus becoming a natural sink of ectoine (**Publication 3**).

These results confirm the importance and demonstrate the substantial contribution of the algal-associated microbial community to the increase of the intracellular content of ectoine in marine algae.

Living organisms either modify their cell sizes to adapt and counteract external salinity changes<sup>112</sup>, or, keeping their original cell sizes and volumes, they modify the intracellular composition and concentration of organic osmolytes. By measuring the cell volumes of the diatom *T. weissflogii* right before the extraction at the end of the exponential growth phase, we did not observe any difference in the cell size between the three salinity treatments: hence, we suggest that the mechanism adopted by the diatom to overcome the environmental osmotic stress condition is only based on a variation of intracellular osmolyte concentration (**Publication 3**).

A different behaviour and adaptation to salinity changes has been observed in the other model organism *P. tricornutum*, which, in contrast to most other diatoms, actually increases its cellular volume by 20.6% according to the modification of the external salinity. For this reason, higher intracellular concentrations were not observed, as they were compensated by the

changes in the cellular volume: thus, the compensation with acquired ectoine can be considered, indirectly, as a means of adaptation for this diatom as well (**Publication 3**).

### ***Ectoine vs other metabolites investigated***

In addition to ectoine, in our survey of zwitterionic metabolites with compatible solute properties, chromatographic profiles of both *T. weissflogii* and *P. tricornutum* showed the nitrogen-containing zwitterions glycine betaine and homarine, while the sulfur-containing metabolite DMSP was only detected in *P. tricornutum*.

For our study, the identities of both these metabolites were verified through co-injection with corresponding synthetic standards and, for a proper quantification, a calibration curve of each standard, followed by a comparison of its peak area with the peak area of the correspondent analytes was performed (**Publication 3**).

Glycine betaine (GBT) is a nitrogen-derived zwitterionic metabolite. Although the biosynthesis of this compound relies on nitrogen availability, which is a limiting factor in aquatic ecosystem<sup>135</sup>, GBT is a highly abundant and widespread compound among marine organisms. It has been previously reported as an osmoregulator produced by several algae<sup>112,136</sup> and bacterial species<sup>137,138</sup>.

The osmoadaptation experiment performed on the diatom *T. weissflogii* showed physiological intracellular levels of this metabolite between 0.3-0.4 pmol/cell, values that increase 0.5- and 2-folds, reaching almost 1 and 1.2 pmol/cell, respectively, during the short- and long-term salt stress experiments in both axenic and xenic cultures. This result indicates the alga-dependent regulation of this metabolite, whose production is not linked to algal-microbial interactions, but rather to environmental salinity (**Publication 3**).

### ***Homarine***

Homarine, also referred to as N-methyl picolinic acid<sup>136</sup>, is also a nitrogen-derived metabolite, already encountered among algal-compatible solutes in the previous studies<sup>112,136</sup>. Homarine occurs in several marine invertebrates<sup>136</sup> and it has recently been found in the ubiquitous marine cyanobacterium *Synechococcus*<sup>139</sup>; nevertheless, this metabolite has not been frequently detected among marine algae besides the red macroalga *Trichocarpus crinitus*<sup>136,140</sup>, where it was identified, and , as a minor

component, in the microalgae *Emiliana huxleyi*<sup>85</sup>, and *Platymonas subcordiformis*<sup>136</sup> while never described, prior our study, in diatoms (**Publication 3**).

Although our analysis and quantification of zwitterionic organic metabolites in axenic cultures of *T. weissflogii* confirmed glycine betaine as a major and widespread metabolite, thanks to our results we added homarine as a major metabolite in the non-DMSP-producer diatom *T. weissflogii*. Indeed, at physiological salinity conditions (35 PSU), homarine intracellular concentrations in axenic cultures of *T. weissflogii* were 2-times higher compared to the xenic ones, indicating an almost exclusive algal-derived synthesis of this metabolite. At 50 PSU, no significant differences between xenic and axenic cultures have been detected, suggesting that already after short-term stress this metabolite reaches its highest concentration (**Publication 3**).

Nevertheless, compared to the physiological salinity conditions, the osmoregulatory properties of this metabolite are confirmed by an increase of the intracellular concentration in xenic cultures of 3.9- and 3.5-fold after the short- and long-treatment respectively. In axenic conditions, instead, a 1.5-fold increase was observed only after the short-term experiment, suggesting that homarine responds quickly to the salinity shift, reaching its highest concentration within 24h of incubation in a high-osmotic medium (**Publication 3**).

## ***Major biogenic organic sulfur compounds in the ocean***

### ***Cysteinolic acid***

The model organism that we mainly analyzed during this research work (**Publication 4**) is a diatom, *T. weissflogii*, which does not produce the abundant metabolite DMSP and therefore has to rely on other molecules with similar properties to compensate for this lack.

Our in-depth analysis of the zwittermetabolome of this marine microalga led to the identification of an additional highly polar sulfur metabolite, cysteinolic acid, and therefore we investigated on its ecological characteristics. We questioned its compatible solute properties and mined for changes in the abundance of this metabolite in the cultures of the diatom *T. weissflogii*, grown in hyperosmotic culture medium. The UHPLC-HRMS profile of cysteinolic acid showed a characteristic sulfur isotope pattern and its molecular ion was among the up-regulated masses in the

LC-MS profile. Through the analysis of the fragmentation pattern and by comparison with online databases and bioinformatic software<sup>131,132</sup>, we attributed the identity of this metabolite to cysteinolic acid and verified it by co-injection with the correspondent commercially available standard.

Cysteinolic acid is a zwitterionic chiral aminosulfonate beneficial to microorganisms and their surrounding environment, stimulating chemotaxis, supporting carbon and sulfur demands and contributing to the energy requirement of heterotrophs<sup>39,141</sup>.

Sulfonates have been of recent increasing interest, in particular since the C3-sulfonate 2,3-dihydroxypropane1-sulfonate (DHPS) has been identified in the microbial food web and resulted to be an abundant diatom and coccolithophore intracellular metabolite, where it is accumulated up to millimolar range, comparable to the main metabolite DMSP, suggesting sulfonates as central players in the environment. This class of metabolites contributes substantially not only to the global carbon and sulfur cycles<sup>130</sup>, but also to the osmoregulation of aquatic species, as studies showed that accumulation of DHPS, alongside other osmolytes like DMSP and proline, is regulated by salinity in the diatom *T. pseudonana* and in the chemoautotrophic bacterium *Sulfurimonas denitrificans*, widespread in marine environments<sup>39,130,142</sup>..

Cysteinolic acid, as DHPS, is a C3-sulfonate, isolated for the first time in 1957 in the red alga *Polysiphonia fastigiata* by Wickberg and colleagues<sup>143</sup>, expanding the sulfonates class which was limited to taurine and its derivatives. The presence of this metabolite was also reported in terrestrial soil and marine environments<sup>39,144</sup>. It was detected in brown algae and in the diatom *Navicula pelliculosa*<sup>145</sup>, but its identification and quantification were so far based on indirect measurements. Here, we performed an in-depth analysis of the fragmentation pattern through bioinformatic software and by comparison with online databases. The identity of cysteinolic acid was verified and confirmed by co-injection with the corresponding synthetic standard (**Publication 4**).

Because of the osmoregulatory properties of the C3-sulfonate DHPS, we verified the contribution of cysteinolic acid to the intracellular osmotic balance in marine diatoms through osmoadaptation experiments performed on both xenic and axenic cultures of *T. weissflogii*. Our results showed a 2-fold increase in the intracellular concentration of this compound when short-term stress is induced in xenic cultures of the diatom, compared to the concentration at physiological seawater salinity

level (35 PSU), and a 2.4-fold increase after the long-term stress. At 35 PSU, instead, the intracellular content of cysteinolic acid was 1.5-fold higher in axenic conditions compared to the xenic and did not increase significantly during the short-term experiment, while a 2.6-fold increase was observed during the long-salinity treatment (**Publication 4**). The higher amount of this compound in axenic cultures compensates for the lower amount of ectoine, which is mainly supplied by bacteria and therefore reaches lower intracellular concentrations in axenic cultures. Because cysteinolic acid concentrations are higher in axenic conditions, it is reasonable to consider its consumption or conversion by associated bacteria in xenic cultures, resulting in a lower algal intracellular amount.

These results support the contribution of the microbial community to the regulation of algal physiology and highlight the presence of a coupled microbial metabolic network between eukaryotic phytoplankton (sulfonate producers) and heterotrophic bacteria (sulfonate consumers, ectoine producers) (**Publication 4**).

### ***Survey of ectoine and cysteinolic acid among different algal species and comparison with other compatible solutes***

Several algal species showed diversity in distribution and abundances of zwitterionic metabolites<sup>112</sup>, which play a specific role in several environmental conditions. Due to the importance of DMSP and of its recently discovered sulfoxonium derivative, DMSOP, we also included DMSP- and DMSOP- in our analysis. Taking advantage of a former quantitative survey of zwitterionic metabolites in different algal species<sup>62</sup>, we investigated on the distribution of and abundances of previously described zwitterionic metabolites<sup>112</sup> and the latest discovered ectoine and cysteinolic acid among the same organisms, and compared them to DMSP and DMSOP (**Publication 4**).

Interestingly, both ectoine and cysteinolic acid were detected in all the investigated algae and their amounts were always in the same order of magnitude as the main metabolite DMSP (fmol/cell), and three orders of magnitude higher in comparison to the most recently identified DMSOP. Only in the dinoflagellate *P. minimum*, where, DMSOP is more abundant, both ectoine and cysteinolic acid were two orders of magnitudes higher than DMSOP instead of three (**Publication 4**). Based on these results, the zwittermetabolome of this alga could be updated compared to the



chromatographic profile previously published by Thume<sup>62</sup> by adding both cysteinolic acid and ectoine (Fig.7).

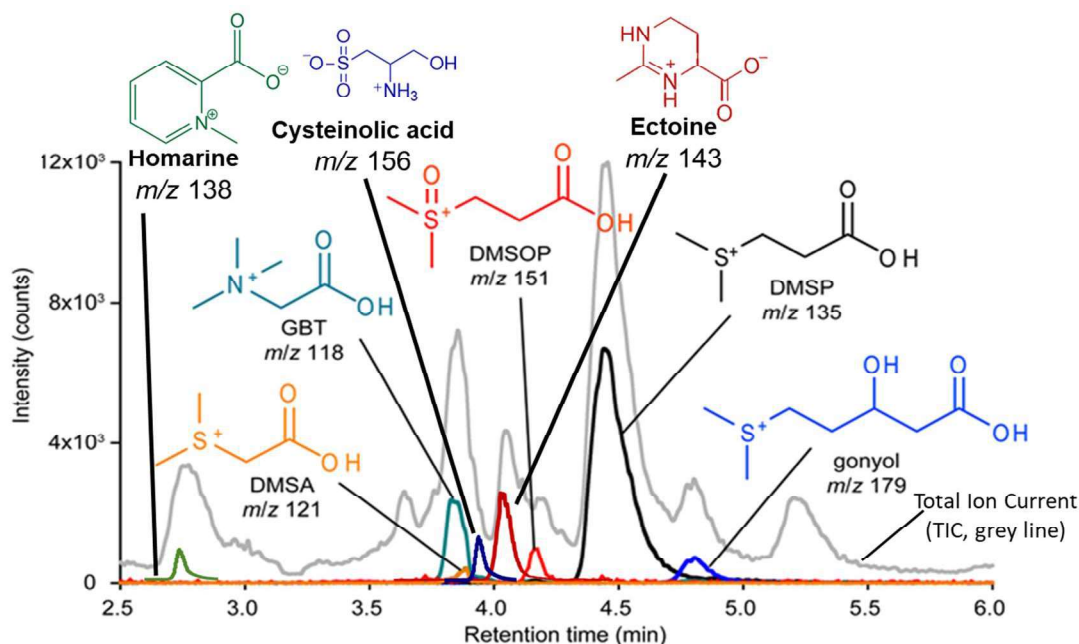


**Fig.7:** Updated chromatographic profile (since Thume, 2018<sup>62</sup>) of zwitterionic metabolites from *P. minimum* methanol extract, separated using UHPLC-HRMS. The total ion current is shown in grey.

Cysteinolic acid was the most abundant metabolite in the dinoflagellate *Amphidinium carterae* and it is widespread among all the analyzed algal species, where its concentrations are in the same range of DHPS, considered the most abundant sulfonate in marine organisms<sup>68</sup>.

Hence, through our research, we added a new algal metabolite to the sulfonate family and confirmed eukaryotic phytoplankton as major producers of this class of metabolites. Taking into account that the annual DMSP turnover is estimated at around 109 tons/year<sup>60</sup>, the similar concentration of these two metabolites in marine algae suggests a massive and important contribution of ectoine and cysteinolic acid to ecological sulfur, nitrogen, and carbon turnover (**Publication 4**).

### ***Algal adaptation to thermal stress***

In addition to the salinity, the ocean is susceptible to other climatic factors and abiotic stresses, such as ultraviolet radiations, nutrient deficiency, heavy metals, and temperature fluctuations<sup>146</sup>. Research focused on the impact of high temperatures on marine organisms. Notably in the context of global warming, and studies on heat stress might answer some fundamental questions related to terrestrial and marine plant evolution<sup>147-</sup>

<sup>150</sup>. On the other hand, 85% of terrestrial environments and 90% of Earth's oceans have permanently a temperature equal to or lower than 5°C<sup>151</sup>; understanding how marine organisms cope with these low temperatures will provide new information on their stress adaptation mechanisms.

In the first part of this dissertation, we highlighted the importance and the ability of compatible solutes in the osmoregulation and osmoadaptation of marine organisms to sea water salinity shifts. Besides their osmoregulatory properties, compatible solutes have also been demonstrated to be involved in cryoprotection, when the decrease in temperature may alter the intracellular ionic concentrations after partial freezing of the cellular water<sup>16,152</sup>. We expanded our analysis and included marine green macroalgae together with phytoplankton species. The genus *Ulva*, which comprises a large number of species that are widely distributed around the world, is considered a model organism to study algal growth, development, and morphogenesis<sup>153</sup>. Hence, we investigated on the temperature tolerance of the two algal species, the Mediterranean *Ulva mutabilis*, and the Antarctic *Ulva bulbosa*. A warm-cold temperature shift was used to evaluate the cryoprotectant activities of several zwitterionic compatible solutes, including the latest identified ectoine and cysteinolic acid (**Publication 5**).

The first experiment was performed to evaluate the different responses of the cold-adapted and the warm-adapted holobiont to low temperatures exposition: xenic strains of *U. bulbosa* and *U. mutabilis* were hence subjected to a temperature shift from 18 °C to 5 °C. An untargeted metabolomic analysis revealed significant low-molecular-weight compounds, among which the well-known zwitterionic metabolites DMSP and taurine.

In addition, the analysis of cryoprotectant-compatible solutes showed proline, ectoine and cysteinolic acid as major components during the temperature stress experiment. It was striking that taurine concentrations were significantly different between the two species and increased in *U. bulbosa*, while a DMSP increase was more evident in *U. mutabilis*, suggesting a species-specific response to cold stress. This response might derive from differences in algal metabolism and the associated microbiome.

To reduce effects from non-essential bacteria, a second analysis was performed, taking into account the tripartite community *U. mutabilis* – *Roseovarius sp.* – *Maribacter sp.* subjected to a stronger temperature shift,

from 18°C to 2°C. In this case, a targeted metabolomic approach was applied and we showed that several zwitterionic compatible solutes were up-regulated after the temperature shift. Among the identified compounds, the intracellular concentrations of latest discovered ectoine and cysteinolic acid increased significantly in *U. mutabilis*: here, cysteinolic acid, which has been previously reported in *Ulva* sp., showed a 9.5-fold increase, while ectoine up-regulation was lower, but still significant.

Our study confirms that both ectoine and cysteinolic acid are widespread among micro- and macro-algae, where they act as compatible solutes. Next to their osmoregulatory characteristics, ectoine and cysteinolic acid also exhibit cryoprotectant properties in marine organisms, contributing to algal adaptation mechanisms adopted to survive temperature changes (**Publication 5**).

## 4 Conclusions and Outlook

Applications of LC-MS techniques in the field of chemical ecology lead to significant advancement in the identification and quantification of highly polar phytoplankton metabolites, key mediators of physiological and ecological interactions. In this context, DMSP is a central player in marine ecosystems and a pivotal osmotically active metabolite. Previous investigations on this compound mainly focused on its role as major precursor of the volatile DMS and principal component of the sulfur and carbon fluxes through phytoplankton and bacterioplankton. This work provides the first evidence that external DMSP concentrations regulate the bacterial utilization of this metabolite and define the fate of sulfur in the ocean and in the environment. The development and application of a single-cell, time-resolved method to measure DMSP degradation pathway expression, coupled with LC-MS based analysis, show that while lower external DMSP levels (nanomolar scale) induce the cleavage pathway, micromolar concentrations trigger the expression of the microbial demethylation pathway.

DMSP availability in the ocean is also directly linked to external environmental factors, including salinity and temperature.

Although everyone is aware of the high salinity levels characterizing seawater and open oceans, the dramatic effects of climate change on the ocean salinity composition and the entire ecosystem are yet underestimated.

Our work extends the current knowledge about the physiological roles of compatible solutes and the importance of their biosynthesis, accumulation and excretion by aquatic organisms to face and overcome environmental stress conditions.

The refined extraction protocols and LC-MS methods used in this work now enable the detection and quantification of two novel phytoplankton-derived zwitterionic molecules, ectoine and cysteinolic acid. As the intracellular concentrations of these metabolites are in the same millimolar range as the main zwitterionic compatible solute DMSP, it can be argued that they are key players in aquatic ecosystems and contribute substantially to global sulfur and carbon cycles, thus influencing the climate. Our results also show significant positive correlations of ectoine and cysteinolic acid with increasing seawater salinity, supporting the hypothesis that both these metabolites play pivotal roles in the osmoregulation of marine algae.

Moreover, we demonstrate that diatoms synthesize and take up bacterial-derived ectoine, thus acting as a sink of this metabolite, useful to fulfill cellular functions.

In axenic cultures, the lower amounts of ectoine are balanced by higher concentrations of cysteinolic acids, denoting physiological compensatory mechanisms between these compatible solutes.

Cryoprotectant properties of these two metabolites were also evaluated in this study: our results show that, together with other well-known zwitterions like DMSP and taurine, intracellular contents of cysteinolic acid and ectoine increase during the temperature shift, thus contributing to algal adaptation to thermal stress.

Moreover, in the model organism *Ulva mutabilis*, ectoine acts as a marker for the localization and the identification of rhizoid algal tissue within the tripartite community, made up of the green macroalga and its two symbiotic bacteria *Roseovarius* sp. and *Maribacter* sp.

Our results highlight the importance of physical proximity on mutualistic interactions between algae and bacteria, thus providing new tools to investigate symbiotic mechanisms in aquatic ecosystems.

In conclusion, our investigation on phytoplankton-derived zwitterionic metabolites highlighted two new key players involved in the osmoregulation, thermotolerance and interactions of marine organisms, which are at the root of biodiversity.

These results are only a small piece of the puzzle: there is still so much to discover and understand. The LC-MS based analytical methods used in this work revealed that marine algae produce many other, yet unknown, polar metabolites. Their structures, physiological and environmental functions have not yet been characterized, thus the methods proposed in this study represent an additional tool for further investigations, opening new perspectives and providing plenty of avenues for future research.

## 5 References

- 1 Costanza, R. The ecological, economic, and social importance of the oceans. *Ecological Economics*, **1999**, *31*, 199-213, doi:10.1016/s0921-8009(99)00079-8.
- 2 Snelgrove, P. V. An ocean of discovery: biodiversity beyond the census of marine life. *Planta Med*, **2016**, *82*, 790-799, doi:10.1055/s-0042-103934.
- 3 Canedo-Arguelles, M., Kefford, B. & Schafer, R. Salt in freshwaters: causes, effects and prospects - introduction to the theme issue. *Philos Trans R Soc Lond B Biol Sci*, **2018**, *374*, doi:10.1098/rstb.2018.0002.
- 4 Williams, P. D. *et al.* The role of mean ocean salinity in climate. *Dynamics of Atmospheres and Oceans*, **2010**, *49*, 108-123, doi:10.1016/j.dynatmoce.2009.02.001.
- 5 Kirst, G. O. Osmotic Adjustment in Phytoplankton and MacroAlgae. In *Biological and Environmental Chemistry of DMSP and Related Sulfonium Compounds* (eds Kiene, R.P., Visscher, P.T., Keller, M.D., & Kirst, G.O.), **1996**, Springer US 121-129, doi:10.1007/978-1-4613-0377-0\_11.
- 6 Smyth, K., Elliott, M. Effects of changing salinity on the ecology of the marine environment. in *Stressors in the marine environment*, **2016**, 161-174, doi:10.1093/acprof:oso/9780198718826.003.0009.
- 7 Fofonoff, N. P. Physical properties of seawater: a new salinity scale and equation of state for seawater. *Journal of Geophysical Research*, **1985**, *90*, doi:10.1029/JC090iC02p03332.
- 8 Millero, F. J. *et al.* The composition of Standard Seawater and the definition of the Reference-Composition Salinity Scale. *Deep Sea Research Part I: Oceanographic Research Papers*, **2008**, *55*, 50-72, doi:10.1016/j.dsr.2007.10.001.
- 9 Duxbury, A. C., Byrne, R. H. & Mackenzie, F. T. Seawater, **2022**, Encyclopædia Britannica, Inc., <https://www.britannica.com/science/seawater>.
- 10 Sverdrup, H. U., Johnson, M. W. & Fleming, R. H. *The Oceans, Their Physics, Chemistry, and General Biology.*, **1942**, *c1942*, New York: Prentice-Hall.
- 11 Hauton, C. Effects of salinity as a stressor to aquatic invertebrates. In *Stressors in the marine environment* (ed Solan, M.W., N.), **2016**, Oxford University Press 3-24, doi:10.1093/acprof:oso/9780198718826.003.0001.
- 12 Whiteley, N. M. & Mackenzie, C. L. Physiological responses of marine invertebrates to thermal stress. In *Stressors in the marine environment* (ed Solan, M.W., N., Eds), **2016**, Oxford University Press 56-72, doi:10.1093/acprof:oso/9780198718826.003.0004.
- 13 Kultz, D. Molecular and evolutionary basis of the cellular stress response. *Annu Rev Physiol*, **2005**, *67*, 225-257, doi:10.1146/annurev.physiol.67.040403.103635.

- 14 Dubyak, G. R. Ion homeostasis, channels, and transporters: an update on cellular mechanisms. *Adv Physiol Educ*, **2004**, *28*, 143-154, doi:10.1152/advan.00046.2004.
- 15 Fernandez-Reiriz, M. J., Navarro, J. M. & Labarta, U. Enzymatic and feeding behaviour of *Argopecten purpuratus* under variation in salinity and food supply. *Comp Biochem Physiol A Mol Integr Physiol*, **2005**, *141*, 153-163, doi:10.1016/j.cbpb.2005.04.020.
- 16 Welsh, D. T. Ecological significance of compatible solute accumulation by micro-organisms: from single cells to global climate. *FEMS Microbio. Rev.*, **2000**, *24*, 263-290, doi:10.1111/j.1574-6976.2000.tb00542.x.
- 17 Yancey, P. H. Organic osmolytes as compatible, metabolic and counteracting cytoprotectants in high osmolarity and other stresses. *J Exp Biol*, **2005**, *208*, 2819-2830, doi:10.1242/jeb.01730, doi:10.1242/jeb.01730.
- 18 DiBartola, S. P. Chapter 3 - Disorders of Sodium and Water: Hyponatremia and Hyponatremia. In *Fluid, Electrolyte, and Acid-Base Disorders in Small Animal Practice (Third Edition)* (ed Dibartola, S.P.), **2006**, W.B. Saunders 47-79, doi:10.1016/B0-72-163949-6/50006-0.
- 19 Yancey, P. H. *et al.* Betaines and dimethylsulfoniopropionate as major osmolytes in Cnidaria with endosymbiotic dinoflagellates. *Physiol Biochem Zool*, **2010**, *83*, 167-173, doi:10.1086/644625.
- 20 Erdmann, N. & Hagemann, M. Salt Acclimation of Algae and Cyanobacteria: A Comparison. In *Algal Adaptation to Environmental Stresses*. (eds Rai, L.C. & Gaur, J.P.), **2001**, Springer, Berlin, Heidelberg., doi:10.1007/978-3-642-59491-5\_11.
- 21 Morgan, E. A. *et al.* Effects of temperature stress on ecological processes. In *Stressors in the Marine Environment: Physiological and ecological responses; societal implications*, **2016**, Oxford University Press, doi:10.1093/acprof:oso/9780198718826.003.0012.
- 22 Sen, B. *et al.* Relationship of Algae to Water Pollution and Waste Water Treatment. In *Water Treatment* (eds Walid, E. & Rezaul Kabir, C.), **2013**, IntechOpen, doi:10.5772/51927.
- 23 Fogg, G. E. Algal Adaptation to Stress — Some General Remarks. In *Algal Adaptation to Environmental Stresses: Physiological, Biochemical and Molecular Mechanisms* (eds Rai, L.C. & Gaur, J.P.), **2001**, Springer Berlin Heidelberg 1-19, doi:10.1007/978-3-642-59491-5\_1.
- 24 Scholz, B. & Liebezeit, G. Compatible solutes in three marine intertidal microphytobenthic Wadden Sea diatoms exposed to different salinities. *European Journal of Phycology*, **2012**, *47*, 393-407, doi:10.1080/09670262.2012.720714.

- 25 Hare, P. & Cress, W. Metabolic implications of stress-induced proline accumulation in plants. *Plant Growth Regulation*, **1997**, *21*, doi:10.1023/A:1005703923347.
- 26 Bohnert, H. J. e. a. A genomics approach towards salt stress tolerance. *Plant Physiology and Biochemistry*, **2001**, *39*, doi:10.1016/S0981-9428(00)01237-7.
- 27 Brown, A. D. & Simpson, J. R. Water relations of sugar-tolerant yeasts: the role of intracellular polyols. *Journal of General Microbiology*, **1972**, *72*, 589-591, doi:10.1099/00221287-72-3-589
- 28 Bisson, M. A. & Kirst, G. O. Osmotic acclimation and turgor pressure regulation in algae. *Naturwissenschaften*, **1995**, *82*, 461-471, doi:10.1007/BF01131597.
- 29 Roberts, M. F. Organic compatible solutes of halotolerant and halophilic microorganisms. *Saline Syst*, **2005**, *1*, 5, doi:10.1186/1746-1448-1-5.
- 30 DasSarma, S. & DasSarma, P. Halophiles, **2017**, eLS, doi:10.1002/9780470015902.a0000394.pub4.
- 31 Sanz-Luque, E. *et al.* Understanding nitrate assimilation and its regulation in microalgae. *Front Plant Sci*, **2015**, *6*, 899, doi:10.3389/fpls.2015.00899.
- 32 Moran, M. A. & Durham, B. P. Sulfur metabolites in the pelagic ocean. *Nature reviews. Microbiology*, **2019**, *17*, 665-678, doi:10.1038/s41579-019-0250-1.
- 33 Yancey, P. H. Compatible and counteracting solutes: protecting cells from the Dead Sea to the deep sea. *Science Progress*, **2004**, *87*, 1-24, doi:10.3184/003685004783238599.
- 34 Tang, K. Chemical Diversity and Biochemical Transformation of Biogenic Organic Sulfur in the Ocean. *Frontiers in Marine Science*, **2020**, *7*, doi:10.3389/fmars.2020.00068.
- 35 Canfield, D. E. & Farquhar, J. Animal evolution, bioturbation, and the sulfate concentration of the oceans. *PNAS*, **2009**, *106*, doi:10.1073/pnas.0902037106.
- 36 Kiene, R. P. *et al.* Dimethylsulfoniopropionate and methanethiol are important precursors of methionine and protein-sulfur in marine bacterioplankton. *Applied and environmental microbiology*, **1999**, *65*, doi:10.1128/AEM.65.10.4549-4558.1999.
- 37 Ksionzek, K. B. *et al.* Dissolved organic sulfur in the ocean: Biogeochemistry of a petagram inventory. *Science*, **2016**, *354*, 456-459, doi:10.1126/science.aaf7796.
- 38 Sunda, W., Kieber, D. J., Kiene, R.P., Huntsman, S. An antioxidant function for DMSP and DMS in marine algae. *Nature*, **2002**, *418*, 317-320, doi:10.1038/nature00851.
- 39 Williams, B. T. & Todd, J. D. A day in the life of marine sulfonates. *Nat Microbiol*, **2019**, *4*, 1610-1611, doi:10.1038/s41564-019-0576-5.



- 40 Wang, R., Gallant, E. & Seyedsayamdost, M. R. Investigation of the Genetics and Biochemistry of Roseobacticide Production in the Roseobacter Clade Bacterium *Phaeobacter inhibens*. *mBio*, **2016**, *7*, e02118, doi:10.1128/mBio.02118-15.
- 41 Haas, P. The liberation of methyl sulphide by seaweed. *Biochemical Journal*, **1935**, *29*, doi:10.1042/bj0291297.
- 42 Challenger, F. & Simpson, M. I. Studies on biological methylation; a precursor of the dimethyl sulphide evolved by *Polysiphonia fastigiata*; dimethyl-2-carboxyethylsulphonium hydroxide and its salts. *J Chem Soc.* , **1948**, *3*, doi:10.1039/jr9480001591.
- 43 Lovelock, J., Maggs, R. & Rasmussen, R. Atmospheric Dimethyl Sulphide and the Natural Sulphur Cycle. *Nature* **1972**, *237*, doi:10.1038/237452a0.
- 44 Liss, P. Take the Shuttle - from Marine Algae to Atmospheric Chemistry. *Science*, **1999**, *285*, doi:10.1126/science.285.5431.12.
- 45 Charlson, R. J. *et al.* Oceanic phytoplankton, atmospheric sulphur, cloud albedo and climate. *Nature*, **1987**, *326*, 655-661, doi:10.1038/326655a0.
- 46 Quinn, P. K. & Bates, T. S. The case against climate regulation via oceanic phytoplankton sulphur emissions. *Nature*, **2011**, *480*, 51-56, doi:10.1038/nature10580.
- 47 Kloster, S. *et al.* Response of dimethylsulfide (DMS) in the ocean and atmosphere to global warming. *Journal of Geophysical Research: Biogeosciences*, **2007**, *112*, doi:10.1029/2006JG000224.
- 48 Shaw, D. K., Sekar, J. & Ramalingam, P. V. Recent insights into oceanic dimethylsulfoniopropionate biosynthesis and catabolism. *Environmental microbiology*, **2022**, *24*, 2669-2700, doi:10.1111/1462-2920.16045.
- 49 Yoch, D. C. Dimethylsulfoniopropionate: its sources, role in the marine food web, and biological degradation to dimethylsulfide. *Applied and environmental microbiology*, **2002**, *68*, 5804-5815, doi:10.1128/aem.68.12.5804-5815.2002.
- 50 Gypens, N. & Borges, A. V. Increase in dimethylsulfide (DMS) emissions due to eutrophication of coastal waters offsets their reduction due to ocean acidification. *Frontiers in Marine Science*, **2014**, *1*, doi:10.3389/fmars.2014.00004.
- 51 Lana, A. *et al.* An updated climatology of surface dimethylsulfide concentrations and emission fluxes in the global ocean. *Global Biogeochem. Cy.*, **2011**, *25*, doi:10.1029/2010gb003850.
- 52 Gwinn, J. K., Robertson, A. & Kiene, R. P. Effect of Salinity on DMSP Production in *Gambierdiscus belizeanus* (Dinophyceae). *J Phycol*, **2019**, *55*, 1401-1411, doi:10.1111/jpy.12923.
- 53 Dickson, D. M., Jones, R. G. W. & Davenport, J. Steady state osmotic adaptation in *Ulva lactuca*. *Planta* **1980**, *150*, doi:10.1007/BF00582360.

- 54 Kettles, N. L., Kopriva, S. & Malin, G. Insights into the regulation of DMSP synthesis in the diatom *Thalassiosira pseudonana* through APR activity, proteomics and gene expression analyses on cells acclimating to changes in salinity, light and nitrogen. *PLoS One*, **2014**, *9*, e94795, doi:10.1371/journal.pone.0094795.
- 55 Giordano, M., Norici, A. & Hell, R. Sulfur and phytoplankton: acquisition, metabolism and impact on the environment. *New Phytol.*, **2005**, *166*, 371-382, doi:10.1111/j.1469-8137.2005.01335.x.
- 56 Gage, D. A. *et al.* A new route for synthesis of dimethylsulphonioacetate in marine algae. *Nature*, **1997**, *387*, doi:10.1038/43160.
- 57 Summers, P. S. *et al.* Identification and Stereospecificity of the First Three Enzymes of 3-Dimethylsulfonylpropionate Biosynthesis in a Chlorophyte Alga. *Plant Physiology and Biochemistry*, **1998**, *116*, doi:10.2307/4278101.
- 58 Curson, A. R. J. *et al.* DSYB catalyses the key step of dimethylsulfonylpropionate biosynthesis in many phytoplankton. *Nat Microbiol*, **2018**, *3*, 430-439, doi:10.1038/s41564-018-0119-5.
- 59 Curson, A. R. *et al.* Dimethylsulfonylpropionate biosynthesis in marine bacteria and identification of the key gene in this process. *Nat. Microbiol.*, **2017**, *2*, doi:10.1038/nmicrobiol.2017.9.
- 60 Curson, A. R. *et al.* Catabolism of dimethylsulphonylpropionate: microorganisms, enzymes and genes. *Nature reviews. Microbiology*, **2011**, *9*, 849-859, doi:10.1038/nrmicro2653.
- 61 Moran, M. A. *et al.* Genomic insights into bacterial DMSP transformations. *Ann Rev Mar Sci*, **2012**, *4*, 523-542, doi:10.1146/annurev-marine-120710-100827.
- 62 Thume, K., Gebser, B., Chen, L., Meyer, N., Kieber, D. J., Pohnert, G. The metabolite dimethylsulfoxonium propionate extends the marine organosulfur cycle. *Nature*, **2018**, *563*, 412-415, doi:10.1038/s41586-018-0675-0.
- 63 Bullock, H. A., Luo, H. & Whitman, W. B. Evolution of Dimethylsulfonylpropionate Metabolism in Marine Phytoplankton and Bacteria. *Front Microbiol*, **2017**, *8*, 637, doi:10.3389/fmicb.2017.00637.
- 64 Kiene, R. P., Linn, L. J. & Bruton, J. A. New and important roles for DMSP in marine microbial communities. *Journal of Sea Research*, **2000**, *43*, 209-224, doi:10.1016/S1385-1101(00)00023-X.
- 65 Zhang, X. H. *et al.* Biogenic production of DMSP and its degradation to DMS-their roles in the global sulfur cycle. *Sci China Life Sci*, **2019**, *62*, 1296-1319, doi:10.1007/s11427-018-9524-y.
- 66 Alcolombri, U. *et al.* MARINE SULFUR CYCLE. Identification of the algal dimethyl sulfide-releasing enzyme: a missing link in the marine sulfur cycle. *Science* **2015**, *348*, doi:10.1126/science.aab1586.

- 67 Yost, D. M. & Mitchelmore, C. L. Dimethylsulfoniopropionate (DMSP) lyase activity in different strains of the symbiotic alga *Symbiodinium microadriaticum*. *Marine Ecology Progress Series*, **2009**, *386*, 61-70, doi:10.3354/meps08031.
- 68 Durham, B. P. *et al.* Sulfonate-based networks between eukaryotic phytoplankton and heterotrophic bacteria in the surface ocean. *Nat. Microbiol.*, **2019**, *4*, 1706-1715, doi:10.1038/s41564-019-0507-5.
- 69 Kertesz, M. A. Riding the sulfur cycle - metabolism of sulfonates and sulfate esters in Gram-negative bacteria. *FEMS Microbiology Reviews*, **2000**, *24*, doi:10.1111/j.1574-6976.2000.tb00537.x.
- 70 Volkova, P. Y. & Geras'kin, S. A. 'Omic' technologies as a helpful tool in radioecological research. *J Environ Radioact*, **2018**, *189*, 156-167, doi:10.1016/j.jenvrad.2018.04.011.
- 71 Baudino, S., Lucas, C. & Smadja, C. Omics in Chemical Ecology. In *Chemical Ecology* (eds Bagnères, A.G. & Hossaert-Mckey, M.), **2016**, 117-137, doi:10.1002/9781119329695.ch6.
- 72 Gubb, E. & Matthiesen, R. Introduction to Omics. in: *Methods in Molecular Biology*. In *Bioinformatic Methods in Clinical Research* Vol. 593 (ed Matthiesen, R.), **2010**, Humana Press, doi:10.1007/978-1-60327-194-3\_1.
- 73 McColl, E. R. *et al.* The Age of Omics-Driven Precision Medicine. *Clinical Pharmacology & Therapeutics*, **2019**, *106*, doi:10.1002/cpt.1532.
- 74 Rochfort, S. Metabolomics Reviewed: A New "Omics" Platform Technology for Systems Biology and Implications for Natural Products Research. *Journal of Natural Products*, **2005**, *68*, doi:10.1021/np050255w
- 75 Schmidt, C. Metabolomics Takes Its Place as Latest Up-and-Coming "Omic" Science. *Journal of the National Cancer Institute*, **2004**, *96*, 732-734, doi:10.1093/jnci/96.10.732.
- 76 Oliver, S. G. *et al.* Systematic functional analysis of the yeast genome. *Trends in Biotechnology*, **1998**, *16*, doi:10.1016/S0167-7799(98)01214-1.
- 77 Vaidyanathan, S. & Goodacre, R. Metabolome and Proteome Profiling for Microbial Characterization. In *Metabolic Profiling: Its Role in Biomarker Discovery and Gene Function Analysis* (eds Harrigan, G.G. & Goodacre, R.), **2003**, Springer US 9-38, doi:10.1007/978-1-4615-0333-0\_2.
- 78 Mitchell, S., Holmes, E. & Carmichael, P. Metabonomics and medicine: the Biochemical Oracle. *Biologist (London)*, **2002**, *49*, 217-221.
- 79 Macel, M., Van Dam, N. M. & Keurentjes, J. J. B. Metabolomics: the chemistry between ecology and genetics. *Molecular Ecology Resources*, **2010**, *10*, 583-593, doi:10.1111/j.1755-0998.2010.02854.x.
- 80 Ryan, D. & Robards, K. Metabolomics: The Greatest Omics of Them All? *Analytical Chemistry*, **2006**, *78*, 7954-7958, doi:10.1021/ac0614341.

- 81 Bundy, J. G., Davey, M. P. & Viant, M. R. Environmental metabolomics: a critical review and future perspectives. *Metabolomics*, **2009**, *5*, 3-21, doi:10.1007/s11306-008-0152-0.
- 82 Bayona, L. M., de Voogd, N. J. & Choi, Y. H. Metabolomics on the study of marine organisms. *Metabolomics*, **2022**, *18*, 17, doi:10.1007/s11306-022-01874-y.
- 83 Hay, M. E. Marine Chemical Ecology: Chemical Signals and Cues Structure Marine Populations, Communities, and Ecosystems. *Annual Review of Marine Science*, **2009**, *1*, 193-212, doi:10.1146/annurev.marine.010908.163708.
- 84 Kuhlisch, C. & Pohnert, G. Metabolomics in chemical ecology. *Natural Product Reports*, **2015**, *32*, 937-955, doi:10.1039/C5NP00003C.
- 85 Spielmeier, A., Pohnert, G. Direct quantification of dimethylsulfoniopropionate (DMSP) with hydrophilic interaction liquid chromatography/mass spectrometry. *J Chromatogr B* **2010**, *878*, 3238-3242, doi:10.1016/j.jchromb.2010.09.031.
- 86 Smith, G. C. *et al.* Methodology for Analyzing Dimethyl Sulfide and Dimethyl Sulfoniopropionate in Seawater Using Deuterated Internal Standards. *Analytical Chemistry*, **1999**, *71*, 5563-5568, doi:10.1021/ac990211q.
- 87 Gage, D. A. & Hanson, A. D. Characterization of 3-Dimethylsulfoniopropionate (DMSP) and its Analogs with Mass Spectrometry. In *Biological and Environmental Chemistry of DMSP and Related Sulfonium Compounds* (eds Kiene, R.P., Visscher, P.T., Keller, M.D., & Kirst, G.O.), **1996**, Springer US 29-44, doi:10.1007/978-1-4613-0377-0\_3.
- 88 Gorham, J. Separation of plant betaines and their sulphur analogues by cation-exchange high-performance liquid chromatography. *Journal of Chromatography A*, **1984**, *287*, 345-351, doi:10.1016/S0021-9673(01)87710-4.
- 89 Zhang, J. *et al.* Capillary electrophoretic analysis of dimethylsulfoniopropionate in sugarcane and marine algal extracts. *Talanta*, **2005**, *66*, 244-248, doi:10.1016/j.talanta.2004.11.019.
- 90 Sánchez-Hernández, L. *et al.* Determination of betaines in vegetable oils by capillary electrophoresis tandem mass spectrometry - application to the detection of olive oil adulteration with seed oils. *Electrophoresis*, **2011**, *32*, 1394-1401, doi:10.1002/elps.201100005.
- 91 Wiesemeier, T. & Pohnert, G. Direct quantification of dimethylsulfoniopropionate (DMSP) in marine micro- and macroalgae using HPLC or UPLC/MS. *Journal of Chromatography B*, **2007**, *850*, 493-498, doi:10.1016/j.jchromb.2006.12.023.
- 92 Li, C., Hill, R. W. & Jones, A. D. Determination of betaine metabolites and dimethylsulfoniopropionate in coral tissues using liquid chromatography–time-of-flight mass spectrometry and stable isotope-labeled internal standards. *Journal of Chromatography B*, **2010**, *878*, 1809-1816, doi:10.1016/j.jchromb.2010.05.014.

- 93 Hao, Z., Xiao, B. & Weng, N. Impact of column temperature and mobile phase components on selectivity of hydrophilic interaction chromatography (HILIC). *Journal of Separation Science*, **2008**, *31*, 1449-1464, doi:10.1002/jssc.200700624.
- 94 Jandera, P. & Hájek, T. Mobile phase effects on the retention on polar columns with special attention to the dual hydrophilic interaction–reversed-phase liquid chromatography mechanism, a review. *Journal of Separation Science*, **2018**, *41*, 145-162, doi:10.1002/jssc.201701010.
- 95 Alpert, A. J. Hydrophilic-interaction chromatography for the separation of peptides, nucleic acids and other polar compounds. *Journal of Chromatography A*, **1990**, *499*, 177-196, doi:10.1016/S0021-9673(00)96972-3.
- 96 Buszewski, B. & Noga, S. Hydrophilic interaction liquid chromatography (HILIC)--a powerful separation technique. *Anal Bioanal Chem*, **2012**, *402*, 231-247, doi:10.1007/s00216-011-5308-5.
- 97 Sentkowska, A. & Biesaga, M. Evaluation of ZIC-HILIC columns for the analysis of flavonols. *Current Topics in Analytical Chemistry*, **2012**, *9*, 49-55.
- 98 Keller, M. D., Bellows, W. K. & Guillard, R. R. L. Dimethyl Sulfide Production in Marine Phytoplankton. In *Biogenic Sulfur in the Environment ACS Symposium Series*, **1989**, 167-182, doi:10.1021/bk-1989-0393.ch011.
- 99 Stefels, J. *et al.* Environmental constraints on the production and removal of the climatically active gas dimethylsulphide (DMS) and implications for ecosystem modelling. *Biogeochemistry*, **2007**, *83*, 245-275, doi:10.1007/s10533-007-9091-5.
- 100 Deng, X. *et al.* Eco-chemical mechanisms govern phytoplankton emissions of dimethylsulfide in global surface waters. *Natl Sci Rev*, **2021**, *8*, nwaa140, doi:10.1093/nsr/nwaa140.
- 101 Poulin, R. X. *et al.* Aquatic Chemical Ecology—A Focus on Algae. In *Comprehensive Natural Products III* (eds Liu, H.-W. & Begley, T.P.), **2020**, Elsevier 244-267, doi:10.1016/B978-0-12-409547-2.14684-0.
- 102 Simó, R. Production of atmospheric sulfur by oceanic plankton: biogeochemical, ecological and evolutionary links. *TRENDS in Ecology & Evolution*, **2001**, *16*.
- 103 Cooper, M. B. & Smith, A. G. Exploring mutualistic interactions between microalgae and bacteria in the omics age. *Curr Opin Plant Biol*, **2015**, *26*, 147-153, doi:10.1016/j.pbi.2015.07.003.
- 104 Widderich, N., Czech, L., Elling, F. J., Konneke, M., Stoveken, N., Pittelkow, M., Riclea, R., Dickschat, J. S., Heider, J., Bremer, E. Strangers in the archaeal world: osmostress-responsive biosynthesis of ectoine and hydroxyectoine by the marine thaumarchaeon *Nitrosopumilus maritimus*. *Environmental microbiology*, **2016**, *18*, 1227-1248, doi:10.1111/1462-2920.13156.

- 105 Selvarajan, R. *et al.* Distribution, Interaction and Functional Profiles of Epiphytic Bacterial Communities from the Rocky Intertidal Seaweeds, South Africa. *Sci Rep*, **2019**, *9*, 19835, doi:10.1038/s41598-019-56269-2.
- 106 Tujula, N. A. *et al.* Variability and abundance of the epiphytic bacterial community associated with a green marine Ulvacean alga. *ISME J*, **2010**, *4*, 301-311, doi:10.1038/ismej.2009.107.
- 107 Sato, N. *et al.* Diverse pathways of phosphatidylcholine biosynthesis in algae as estimated by labeling studies and genomic sequence analysis. *Plant J*, **2016**, *87*, 281-292, doi:10.1111/tpj.13199.
- 108 Hirashima, T. *et al.* Evolution of the Phosphatidylcholine Biosynthesis Pathways in Green Algae: Combinatorial Diversity of Methyltransferases. *J Mol Evol*, **2018**, *86*, 68-76, doi:10.1007/s00239-017-9826-4.
- 109 Pastor, J. M. *et al.* Ectoines in cell stress protection: uses and biotechnological production. *Biotechnol Adv*, **2010**, *28*, 782-801, doi:10.1016/j.biotechadv.2010.06.005.
- 110 Leon, M. J. *et al.* Compatible Solute Synthesis and Import by the Moderate Halophile *Spiribacter salinus*: Physiology and Genomics. *Front Microbiol*, **2018**, *9*, 108, doi:10.3389/fmicb.2018.00108.
- 111 Imhoff, J. F. *et al.* Osmotic Adaptation and Compatible Solute Biosynthesis of Phototrophic Bacteria as Revealed from Genome Analyses. *Microorganisms*, **2020**, *9*, doi:10.3390/microorganisms9010046.
- 112 Gebser, B. & Pohnert, G. Synchronized regulation of different zwitterionic metabolites in the osmoadaptation of phytoplankton. *Mar. Drugs*, **2013**, *11*, 2168-2182, doi:10.3390/md11062168.
- 113 Pinsky, M. L., Selden, R. L. & Kitchel, Z. J. Climate-Driven Shifts in Marine Species Ranges: Scaling from Organisms to Communities. *Annual Review of Marine Science*, **2020**, *12*, 153-179, doi:10.1146/annurev-marine-010419-010916.
- 114 Cuthbert, R. N. *et al.* Emergent effects of temperature and salinity on mortality of a key herbivore. *Journal of Sea Research*, **2021**, *177*, 102126, doi:10.1016/j.seares.2021.102126.
- 115 Fogg, G. E. X. *Algal Adaptation to Environmental Stresses Physiological, Biochemical and Molecular Mechanisms.*, (Springer-Verlag 2001).
- 116 Dawson, H. M. *et al.* Potential of temperature- and salinity-driven shifts in diatom compatible solute concentrations to impact biogeochemical cycling within sea ice. *Elem Sci Anth*, **2020**, *8*, doi:10.1525/journal.elementa.421.
- 117 Czech, L., Bremer, E. With a pinch of extra salt—Did predatory protists steal genes from their food? *PLoS Biol*, **2018**, *16*, doi:10.1371/journal.pbio.2005163.g001.
- 118 Bowler, C. *et al.* The *Phaeodactylum* genome reveals the evolutionary history of diatom genomes. *Nature*, **2008**, *456*, 239-244, doi:10.1038/nature07410.

- 119 Martino, A. D. *et al.* Genetic and phenotypic characterization of *Phaeodactylum tricornutum* (Bacillariophyceae) accessions. *Journal of phycology*, **2007**, *43*, 992-1009, doi:10.1111/j.1529-8817.2007.00384.x.
- 120 Yang, M. *et al.* Genome Annotation of a Model Diatom *Phaeodactylum tricornutum* Using an Integrated Proteogenomic Pipeline. *Mol Plant*, **2018**, *11*, 1292-1307, doi:10.1016/j.molp.2018.08.005.
- 121 Spielmeyer, A., Gebser, B., Pohnert, G. Investigations of the uptake of dimethylsulfonylpropionate by phytoplankton. *Chembiochem : a European journal of chemical biology*, **2011**, *12*, 2276-2279, doi:10.1002/cbic.201100416.
- 122 Petrou, K. & Nielsen, D. A. Uptake of dimethylsulphonylpropionate (DMSP) by the diatom *Thalassiosira weissflogii*: a model to investigate the cellular function of DMSP. *Biogeochemistry*, **2018**, *141*, 265-271, doi:10.1007/s10533-018-0507-1.
- 123 Theseira, A. M., Nielsen, D. A. & Petrou, K. Uptake of dimethylsulphonylpropionate (DMSP) reduces free reactive oxygen species (ROS) during late exponential growth in the diatom *Thalassiosira weissflogii* grown under three salinities. *Marine Biology*, **2020**, *167*, doi:10.1007/s00227-020-03744-4.
- 124 Bussard, A. *et al.* Physiological adjustments and transcriptome reprogramming are involved in the acclimation to salinity gradients in diatoms. *Environmental microbiology*, **2017**, *19*, 909-925, doi:10.1111/1462-2920.13398.
- 125 Garcia Lagunas, N. *et al.* Effect of salinity on growth and chemical composition of the diatom *Thalassiosira weissflogii* at three culture phases. *Latin American Journal of Aquatic Research*, **2012**, *40*, 435-440, doi:10.3856/vol40-issue2-fulltext-18.
- 126 Li, F. *et al.* Physiological and biochemical responses of *Thalassiosira weissflogii* (diatom) to seawater acidification and alkalization. *ICES Journal of Marine Science*, **2019**, *76*, 1850-1859, doi:10.1093/icesjms/fsz028.
- 127 Kamp, A. *et al.* Response of the Ubiquitous Pelagic Diatom *Thalassiosira weissflogii* to Darkness and Anoxia. *PLOS ONE*, **2013**, *8*, e82605, doi:10.1371/journal.pone.0082605.
- 128 Weinisch, L., Kuhner, S., Roth, R., Grimm, M., Roth, T., Netz, D. J. A., Pierik, A. J., Filker, S. Identification of osmoadaptive strategies in the halophile, heterotrophic ciliate *Schmidingerothrix salinarum*. *PLoS Biol*, **2018**, *16*, doi:10.1371/journal.pbio.2003892.
- 129 Harding, T. *et al.* Osmoadaptive Strategy and Its Molecular Signature in Obligately Halophilic Heterotrophic Protists. *Genome Biol Evol*, **2016**, *8*, 2241-2258, doi:10.1093/gbe/evw152.
- 130 Durham, B. P. *et al.* Cryptic carbon and sulfur cycling between surface ocean plankton. *PNAS*, **2015**, *112*, 453-457, doi:10.1073/pnas.1413137112.

- 131 Dührkop, K. *et al.* SIRIUS 4: a rapid tool for turning tandem mass spectra into metabolite structure information. *Nature Methods*, **2019**, *16*, 299-302, doi:10.1038/s41592-019-0344-8.
- 132 Dührkop, K. *et al.* Searching molecular structure databases with tandem mass spectra using CSI:FingerID. *Proceedings of the National Academy of Sciences*, **2015**, *112*, 12580-12585, doi:10.1073/pnas.1509788112.
- 133 Galinsky, E. A., Pfeiffer, H. P. & Trüper, H. G. 1,4,5,6-Tetrahydro-2-methyl-4-pyrimidinecarboxylic acid. *European Journal of Biochemistry*, **1985**, *149*, doi:10.1111/j.1432-1033.1985.tb08903.x.
- 134 Reshetnikov, A. S. *et al.* Chapter Two - Genes and Enzymes of Ectoine Biosynthesis in Halotolerant Methanotrophs. In *Methods in Enzymology* Vol. 495 (eds Rosenzweig, A.C. & Ragsdale, S.W.), **2011**, Academic Press 15-30, doi:10.1016/B978-0-12-386905-0.00002-4.
- 135 Keller, M. D. *et al.* Production of glycine betaine and dimethylsulfonylpropionate in marine phytoplankton. II. N-limited chemostat cultures. *Marine Biology*, **1999**, *135*, 249-257, doi:10.1007/s002270050622.
- 136 Dickson, D. M. J. & Kirst, G. O. The role of  $\beta$ -dimethylsulphonylpropionate, glycine betaine and homarine in the osmoacclimation of *Platymonas subcordiformis*. *Planta*, **1986**, *167*, 536-543, <http://www.jstor.org/stable/23377964>.
- 137 Smith, L. T. *et al.* Osmotic control of glycine betaine biosynthesis and degradation in *Rhizobium meliloti*. *Journal of Bacteriology*, **1988**, *170*, doi:10.1128/jb.170.7.3142-3149.1988
- 138 Miller, K. J., Zelt, S. C. & Bae, J.-H. Glycine betaine and proline are the principal compatible solutes of *Staphylococcus aureus*. *Current Microbiology*, **1991**, *23*, doi:10.1007/bf02091971.
- 139 Heal, K. R. *et al.* Marine Community Metabolomes Carry Fingerprints of Phytoplankton Community Composition. *mSystems*, **2021**, *6*, e01334-01320, doi:10.1128/mSystems.01334-20.
- 140 Blunden, G. *et al.* Extraction, Purification and Characterisation of Dragendorff-positive Compounds from Some British Marine Algae. **1981**, *24*, 451-456, doi:doi:10.1515/botm.1981.24.8.451.
- 141 Levine, N. M. Putting the spotlight on organic sulfur. *Science (New York, N.Y.)*, **2016**, *354*, doi:10.1126/science.aai8650.
- 142 Gotz, F. *et al.* Targeted metabolomics reveals proline as a major osmolyte in the chemolithoautotroph *Sulfurimonas denitrificans*. *Microbiologyopen*, **2018**, *7*, e00586, doi:10.1002/mbo3.586.
- 143 Wickberg, B. Isolation of 2-L-amino-3-hydroxy-1-propane sulfonic acid from *Polysiphonia fastigiata*. *Acta Chem. Scand.*, **1957**, *11*, 506-511, doi:10.3891/acta.chem.scand.11-0506.



- 144 Burchill, L. & Williams, S. J. Chemistry and biology of the aminosulfonate cysteinolic acid: discovery, distribution, synthesis and metabolism. *Organic & biomolecular chemistry*, **2022**, *20*, 3043-3055, doi:10.1039/d2ob00362g.
- 145 Busby, W. F. & Benson, A. A. Sulfonic acid metabolism in the diatom *Navicula pelliculosa*. *Plant and Cell Physiology*, **1973**, *14*, 1123-1132, doi:10.1093/oxfordjournals.pcp.a074951.
- 146 Kaur, M. *et al.* Abiotic stress in algae: response, signaling and transgenic approaches. *Journal of Applied Phycology*, **2022**, *34*, 1843-1869, doi:10.1007/s10811-022-02746-7.
- 147 Xu, S. Y. & Weng, J. K. Climate change shapes the future evolution of plant metabolism. *Advanced Genetics*, **2020**, *1*, e10022, doi:10.1002/ggn2.10022.
- 148 Dahl, T. W. & Arens, S. K. M. The impacts of land plant evolution on Earth's climate and oxygenation state – An interdisciplinary review. *Chemical Geology*, **2020**, *547*, 119665, doi:10.1016/j.chemgeo.2020.119665.
- 149 Fürst-Jansen, J. M. R., de Vries, S. & de Vries, J. Evo-physio: on stress responses and the earliest land plants. *Journal of Experimental Botany*, **2020**, *71*, 3254-3269, doi:10.1093/jxb/eraa007.
- 150 Ohama, N. *et al.* Transcriptional Regulatory Network of Plant Heat Stress Response. *Trends in Plant Science*, **2017**, *22*, 53-65, doi:10.1016/j.tplants.2016.08.015.
- 151 Rodrigues, D. F. & Tiedje, J. M. Coping with Our Cold Planet. *Applied and environmental microbiology*, **2008**, *74*, 1677-1686, doi:10.1128/AEM.02000-07.
- 152 Mazur, P. Survival of Fungi after Freezing and Desiccation. In *The Fungal Population: An Advanced Treatise* Vol. 3 (eds Ainsworth, G.C. & Sussman, A.S.), **1968**, Academic Press, doi:10.1016/B978-1-4832-2744-3.50020-1.
- 153 Wichard, T. *et al.* The green seaweed *Ulva*: a model system to study morphogenesis. *Front Plant Sci*, **2015**, *6*, 72, doi:10.3389/fpls.2015.00072.



## Erklärungen

### Selbstständigkeitserklärung

Ich erkläre, dass ich die vorliegende Arbeit selbstständig und unter Verwendung der angegebenen Hilfsmittel, persönlichen Mitteilungen und Quellen angefertigt habe.

Pisa (Italy),

Simona Fenizia

### **Erklärung zu den Eigenanteilen des Promovenden sowie der weiteren Doktoranden/Doktorandinnen als Koautoren an den Publikationen und Zweitpublikationsrechten bei einer kumulativen Dissertation**

Für alle in dieser kumulativen Dissertation verwendeten Manuskripte liegen die notwendigen Genehmigungen der Verlage („Reprint Permissions“) für die Zweitpublikation vor. Die Koautoren der in dieser kumulativen Dissertation verwendeten Manuskripte sind sowohl über die Nutzung, als auch über die oben angegebenen Eigenanteile der weiteren Doktoranden/Doktorandinnen als Koautoren an den Publikationen und Zweitpublikationsrechten bei einer kumulativen Dissertation informiert und stimmen diesem zu. Die Anteile des Promovenden sowie der weiteren Doktoranden/Doktorandinnen und Koautoren an den Publikationen und Zweitpublikationsrechten bei einer kumulativen Dissertation sind der jeweiligen Publikation vorangestellt.

Name der Promovenden	Datum	Ort	Unterschrift
Simona Fenizia	26/01/2023	Pisa (Italy)	



**Einverständniserklärung des Betreuers**

Ich bin mit der Abfassung der Dissertation als publikationsbasiert, d.h. kumulativ, einverstanden und bestätige die vorstehenden Angaben.

Name Betreuer	Datum	Ort	Unterschrift
Prof. Dr. Georg Pohnert	23.1.23	Jena	

Name Betreuer	Datum	Ort	Unterschrift
Prof. Dr. Jonathan Gershenzon	27.01.23	Jena	



## Curriculum vitae

### Personal data

Name: Simona Fenizia  
Email: [simona.fenizia@libero.it](mailto:simona.fenizia@libero.it)  
ResearchGate: [https://www.researchgate.net/profile/Simona\\_Fenizia](https://www.researchgate.net/profile/Simona_Fenizia)  
ORCID: <https://orcid.org/0000-0002-3592-9368>

### Education

06/2021 – ongoing      Research Fellow in Clinical Physiology  
Institute of Clinical Physiology, Italian National  
Research Council Pisa, Italy

02/2017- 05/2021      PhD in Analytical Chemistry  
Max Planck Institute for Chemical Ecology, Jena,  
Germany  
Institute for Inorganic and Analytical Chemistry,  
Friedrich Schiller University, Jena.

Supervisors: Prof. Dr. Georg Pohnert, Institute of  
Inorganic and Analytical Chemistry, Friedrich Schiller  
University, Jena;  
Prof. Dr. Jonathan Gershenzon, Dept. of  
Biochemistry, Max Planck Institute for Chemical  
Ecology, Jena.

07/2016      Licensed to practice as professional pharmacist

03/2016      M.Sc. in Pharmaceutical Chemistry and  
Technology, University Federico II of Naples, Italy.  
Thesis project: “Isolation and structural  
elucidation of bioactive secondary metabolites  
from the marine sponge *Agelas nakamura*”.

Supervisors: Prof. Dr. Alfonso Mangoni, University  
Federico II, Naples, Italy; Dr. Marie-Lise Bourguet-  
Kondracki, Director UMR 7245 CNRS, Muséum  
National d’Histoire Naturelle, Paris, France.

### Scholarship / Trainings

06/2021 – ongoing	Research grant, Italian National Research Council
02/2020 – 11/2020	Friedrich Schiller University Scholarship project 081021/36; project 081021/37
02/2017 – 02/2020	International Max Planck Research School scholarship "The Exploration of Ecological Interactions with Molecular and Chemical Techniques", Max Planck Institute for Chemical Ecology, Jena, Germany
02/2015 – 07/2015	Erasmus Placement Traineeship grant National Museum of Natural History, Paris, France
09/2014 – 02/2015	Trainee for graduation thesis project Department of Natural Products Chemistry, Faculty of Pharmacy, University "Federico II", Naples, Italy
06/2013 – 12/2013	Trainee before degree Pharmacy "Autolino", Avellino, Italy

### Publications

- Cornuti S., Chen S., Lupori L., Finamore F., Carli F., Samad M., Fenizia S., *et al.* (2023). "Brain histone beta-hydroxybutyrylation couples metabolism with gene expression". *Cellular and Molecular Life Sciences* 80 (1). doi: 10.1007/s00018-022-04673-9. PMID: 36607453.
- Ghaderiardakani F., Langhans L., Kurbel V.B., Fenizia S., Wichard T. (2022). "Metabolite profiling reveals insights into the species-dependent cold stress response of the green seaweed holobiont *Ulva* (Chlorophyta)". *Environmental and Experimental Botany* 104913. doi: 10.1016/j.envexpbot.2022.104913
- Fenizia S., Weissflog J., Pohnert G. (2021). "Cysteinolic Acid Is a Widely Distributed Compatible Solute of Marine Microalgae". *Marine Drugs* 19(12), 683. doi: 10.3390/md19120683
- Vallet M., Kaftan F., Grabe V., Ghaderiardakani F., Fenizia S., Svatos A., Pohnert G., Wichard T. (2020). "A new glance at the chemosphere of macroalgal-bacterial interactions: In situ profiling of metabolites in symbiosis by mass spectrometry". *Beilstein journal of organic chemistry* 17(1), 1313-1322. doi: 10.3762/bjoc.17.91



- Gao C., Fernandez V., Lee K. S., Fenzia S., Pohnert G., Seymour J., Raina J. B., Stocke R. (2020). "Single-cell bacterial transcription measurements reveal the importance of dimethylsulfoniopropionate (DMSP) hotspots in ocean sulfur cycling". *Nature Communications* 11, 1942. doi: 10.1038/s41467-020-15693-z
- Fenzia S., Thume K., Wirgenings M., Pohnert G. (2020). "Ectoine from bacterial and algal origin is a compatible solute in microalgae". *Marine Drugs* 18(1):42. doi:10.3390/md18010042
- Poulin X. R., Baumeister T. U. H., Fenzia S., Pohnert G., Vallet M. (2019). "Aquatic Chemical Ecology - A focus on Algae", in *Comprehensive Natural Products III: Chemistry and Biology*. doi: 10.1016/B978-0-12-409547-2.14684-0

### Presentations

- XVI MaNaPro & XI ECMNP meeting, Peniche, Portugal: "With a little help from my friends - Ectoine, a compatible solute in microalgae from bacteria". (2019, poster presentation)
- XVIII International Max Planck Research School Symposium, Dornburg, Germany: "Novel zwitterionic metabolites from marine diatoms". (2019, oral presentation)
- VII International Conference on Microbial Communication for Young Scientists, Jena, Germany. "Identification, physiological and ecological function of zwitterionic metabolites in marine diatoms". (2018, oral presentation)
- II International Summer School of Natural Products "Luigi Minale and Ernesto Fattorusso", Naples, Italy. "Zwitterionic metabolites: signals and resources". (2017, oral presentation)



## Acknowledgements

*“It always seems impossible, until it’s done”. This quote from Nelson Mandel effectively sums up my PhD journey, which started with an unexpected letter of acceptance from the International Max Planck Research School, jointly organized by one of the most prestigious research institutions, the Max Planck Society, and a top ranked university, the Friedrich Schiller University. That seemed actually impossible. Instead, here we are, at the last steps before the “Finish line” towards new great challenges. During these years there have been many challenges, but from each of them I have learned a lesson. I have learned, or better, I have tried to learn, perhaps in vain but with all my efforts, a new language (not the easiest one!), improve my English and try not to forget my own completely; I have learned about new cultures and traditions; I have learned how to manage my own work, how to organize myself better, how to face fears, accept my limitations and defeats, to get back up, try new paths, recognize my strengths. It has been an incredible journey, made even more incredible by all the people I’ve traveled with, and to whom all my thanks go.*

*I cannot, of course, refrain from thanking my supervisor, Georg Pohnert. You gave me the opportunity to embark on this journey, you believed in me, glimpsed abilities and potential that most likely I was not aware of, allowing me to join a group of excellence and offering me all possible means to be able to give my best. You supported me, advised me and entrusted me with tasks and responsibilities that made me grow, and become more and more independent. I am so grateful, thank you for all this.*

*In the same way, I want to thank my second supervisor, Professor Jonathan Gershenzon: thank you for always being helpful, for all the suggestions, ideas that came from other points of view and opened new horizons. Thank you for always welcoming me into*

*your study and making me comfortable, asking me how I was, how I was doing in my new work environment, for every "whatever you need, I'm here". Thank you for the wonderful IMPRS symposiums organized, days of pure science, days where you breathed research, where you appreciated the work, the passion, the motivational drive of a huge working group, which I was honoured to be a part of. I had the opportunity to work with and be mentored by two top scientists in the field, two supervisors to be taken as models, to hopefully be able to carry out even a small part of their principles in the future. For all this, thank you.*

*My thanks also to Thomas, thank you for the great opportunity to collaborate with you and your group, for all the advice, suggestions, nice discussions, your curiosity toward Italian life-style and the wonderful working atmosphere.*

*I thank Claudia, Angela and Sarah for their administrative support, the IMPRS and the Friedrich Schiller University for this opportunity. I thank all the former and current working group members because the work and life would have been much less interesting and fun without you.*

*A huge and special thanks to Marine, for being a friend, a confidant, as well as a wonderful colleague and a Post-doc who always bestowed valuable advice. Thank you for every moment we spent together, for all the evenings and weekends we shared, thank you for always keeping me company over my varied daily coffees. Thank you for the breakfasts we shared together, strictly with croissants from Carlos P. and espresso coffee prepared with my irreplaceable machine. "Can I have some more?" or "Shall we make a second one?" were requests that filled my heart. Thank you for trusting me, confiding in me, sometimes, in the most extreme cases, speaking in French because then you would feel better afterwards and advise me to use the same tactic, venting to*

*you in Italian. Because we both knew that being away from your own land, your own home, was anything but easy.*

*So, thank you for your Friendship, Marine.*

*In the same way, I want to thank Marino for always sharing, enjoying and appreciating my espresso coffee, for always being helpful, friendly, smiling and kind. Thank you for your patience in trying to teach me some German, even in a somewhat atypical way, but I have to admit that your "Auf den sieben Robbenklippen sitzen sieben Robbensippen..." is still printed in my mind.*

*Herzlich danke!*

*Also, thank you Alberto, for being such a nice friend, for the small trips we did together, thank you for the days together at the IMPRS symposiums, for celebrating my achievements and yours together, for reassuring and helping me in the darkest moments, for being confident and open with me, giving me your trust. Thank you for your advices, your points of view that always helped to grow and improve...because they were sincere and direct, as a true friend would. A great thank you goes also to Fatemeh, for your kindness, your help and collaboration, your availability, at work as well as in sharing some spare-time together.*

*Thank you to the Italian friends and colleagues, Emilio, Gianmaria, Davide, Emilia, with whom I was able to laugh and joke freely and feel a little more at home; to my friends in Italy, who were always waiting for me to be back in Italy for my vacations so we could spend some time together. Thank you, Maria Rosaria, Antonio, Rita: although months passed, the friendship between us is so strong that every time we got together it was as if we had seen each other a couple of days before. Thank you for your support, both from near and far, and of course thank you for being as you are, just perfect, each in your own way.*

*A big thanks goes of course to my family, to those who are close, to those who are far away...in all meanings... thanks, because you believed in me, rooted for me, and will continue to do so.*

*But the biggest, enormous, huge “thank you” goes to those who always supported me in any decision, in every new and exciting adventure, thank you mum, thank you dad. Thank you for giving me the opportunity to live this experience without making me weigh the distance, neither physical nor moral, and for being close to me in every single moment. Thank you, Francesca, thank you Ippolito, for your advice, your suggestions, for your patience that countered my anxieties. But most of all, thank you for the wonderful new entry, to you my dear goes all my love.*

*I am pretty sure someone is still missing, but my acknowledgements go to you as well.*

*Lastly, I wish myself to never lose my enthusiasm, willingness and passion to do what I enjoy, to always believe in myself and what I think is right; I wish myself to always have the strength to face new challenges and not to fear change.*

*“The most important step a person can take is always the next one” (B. Sanderson). Now it’s my turn to climb one step more: tomorrow will be a new chapter in my life.*

**“Shoot for the moon, even if you miss, you’ll land  
among the stars” (L. Brown)**

***Wish you good luck, Simona!***